TECHNISCHE UNIVERSITÄT MÜNCHEN

TUM School of Engineering and Design

Integrated Design of Advanced Flight Control Configurations and System Architectures

Thomas Stefan Lampl

Vollständiger Abdruck der von der TUM School of Engineering and Design der Technischen Universität München zur Erlangung des akademischen Grades eines

Doktors der Ingenieurwissenschaften (Dr.-Ing.)

genehmigten Dissertation.

Vorsitzender:	Prof. Dr.-Ing. Florian Holzapfel
Prüfer der Dissertation:	1. Prof. Dr.-Ing. Mirko Hornung
	2. Prof. Dr.-Ing. Frank Thielecke

Die Dissertation wurde am 02.02.2021 bei der Technischen Universität München eingereicht und durch die Fakultät für Luftfahrt, Raumfahrt und Geodäsie am 20.08.2021 angenommen.

Obstacles don't have to stop you.
If you run into a wall,
don't turn around and give up.
Figure out how to climb it,
go through it or work around it.

Michael Jeffrey Jordan

Abstract

In 2009, the aviation industry addressed the global challenge of climate change and defined ambitious goals for global air traffic (*Vision 2050*). The continuously improving system technologies of commercial transport aircraft provide a significant contribution to meet these challenging climate goals. This thesis focuses on the design and analysis of advanced flight control systems with the main goal to increase the overall aircraft efficiency. Advanced flight control systems aim to combine the technological trends of gradual electrification and the functional enhancement by additional flight control functions. The analysis of previous work revealed a lack of enabling methodologies and tools for the design and analysis of such advanced flight control systems during early aircraft design phases. This thesis contributes to close this gap and proposes a three-staged methodology. The first two stages enable a functional-driven and integrated design of advanced flight control systems. This includes the flight control configuration, the flight control system architecture and the overall system mass estimation. The third stage provides a comprehensive simulation environment for the analysis and assessment on system, aircraft and mission level, regarding secondary power requirements, engine thrust, fuel flow and (specific) fuel consumption. Furthermore, a medium-range and long-range baseline aircraft are defined to have a basis for comparison. At the end of this thesis, the methodology is applied in a demonstrating case study for a medium-range transport aircraft. In this study two advanced system technologies and different additional flight control functions are considered for the design of advanced flight control systems. The results of the developed aircraft concepts with different flight control systems show that essential technological dependencies can be calculated and displayed on mission, aircraft and system level. This allows the consideration of essential design and integration aspects at an early stage of aircraft design, enabling a holistic analysis and evaluation of advanced flight control systems, and thus provides a good basis for decision-making.

Kurzfassung

Um sich der globalen Herausforderung des Klimawandels zu stellen hat die Luftfahrtindustrie ehrgeizige Ziele für den globalen Luftverkehr definiert (*Vision 2050*). Einen wesentlichen Beitrag zur Erreichung dieser anspruchsvollen Klimaziele leisten dabei immer effizientere Flugzeugsysteme sowie neue Systemtechnologien und -konzepte. Diese Arbeit konzentriert sich auf den Entwurf und die Analyse fortschrittlicher Flugsteuerungssysteme, mit dem Hauptziel, die Gesamteffizienz bzw. die Treibstoffersparnisse von Flugzeugen zu erhöhen. Diese innovativen Flugsteuerungssysteme kombinieren die technologischen Trends der funktionalen Erweiterung, durch zusätzliche Flugsteuerungsfunktionen, und der schrittweisen Elektrifizierung von Flugzeugsystemen. Eine umfassende Analyse früherer Arbeiten ergab dabei eine Mangel an Methoden und Berechnungstools, die den Entwurf und die Analyse fortschrittlicher Flugsteuerungssysteme in frühen Phasen des Flugzeugentwurfs ermöglichen. Die vorliegende Arbeit trägt dazu bei, diese Lücke zu schließen und schlägt eine dreistufige Vorgehensweise vor. In den ersten zwei Stufen wird durch einen funktionsgetriebenen und integrierten Ansatz der (konzeptionelle) Entwurf innovativer Flugsteuerungssysteme ermöglicht, welche die Konfiguration und die Architektur des Flugsteuerungssystems sowie die Abschätzung der Gesamtsystemmasse umfassen. In der dritten Stufe der Methodik ermöglicht eine entwickelte Simulationsumgebung eine Analyse und Bewertung auf System-, Flugzeug- und Missionsebene. Darüber hinaus werden Referenzflugzeuge für die Mittel- und Langstrecke definiert, um eine Vergleichsbasis für die Auswertung und Interpretation der Ergebnisse zu haben. In einer Fallstudie für ein Mittelstreckenflugzeug wird die entwickelte Methodik mit den Berechnungs- und Analysetools angewendet. In dieser Studie werden zwei innovative Systemtechnologien und zusätzliche Flugsteuerungsfunktionen für den Entwurf und die Integration verschiedener Flugsteuerungssysteme berücksichtigt. Die Ergebnisse der Studie zeigen, dass wesentliche technologische Abhängigkeiten auf Missions-, Flugzeug- und Systemebene berechnet und dargestellt werden können. Dabei können bereits in frühen Flugzeugentwurfsphasen wesentliche Entwurfs- und Integrationsaspekte berücksichtig werden, und ermöglicht so eine ganzheitliche Analyse und Bewertung innovativer Flugsteuerungssysteme.

Contents

Nomenclature

Abbreviations

2H-2E	2 Hydraulic- 2 Electric (power circuits)	*Power system architecture*
3H	3 Hydraulic (power circuits)	*Power system architecture*
ABK	Air Brake	*Control function (FCS)*
ACP	Air Conditioning Pack	*System component (ECS)*
ACS	Air Conditioning System	*Aircraft system (ECS)*
ADHF	Adaptive Dropped Hinge Flap	*System component (FCS)*
AEA	All-Electric Aircraft	
AFC	Active Flow Control	*Control function (FCS)*
ALC	Active Load Control	*Control function (FCS)*
ALN	Aileron	*Flight control device (FCS)*
ALT	Altitude	*Aircraft altitude*
ATAX	Aircraft System Technology Analysis Tool	*Calculation tool*
AVL	Athena Vortex Lattice	*Aerodynamic calculation tool*
AVLX	Aerodynamic Vortex Lattice Calculation and Analysis Tool	*Calculation tool*
BPR	Bypass-Ratio	*Engine parameter (Turbofan)*
CAC	Cabin Air Compressor	*System component (ECS)*
CAS	Calibrated Air Speed	*Aircraft speed*
CPS	Cycles Per Second	*System activity (FCS)*
CVC	Cruise Variable Camber	*Control function (FCS)*
DFS	Differential Flap Setting	*Control function (FCS)*
DGB	Drive Gearbox	*System component (FCS)*
DMC	Direct Maintenance Costs	*Aircraft operating costs*
DMM	Domain Mapping Matrix	
DN	Droop nose	*Flight control device (FCS)*
DOC	Direct Operating Costs	*Aircraft operating costs*
DSF	Double-Slotted Flap	*Flight control device (FCS)*

DSM	Design Structure Matrix	
EASA	European Aviation Safety Agency	*Agency of the European Union*
EBHA	Electrical Backup-Hydraulic Actuator	*System component (FCS)*
ECS	Environmental Control System	*Aircraft system*
EHA	Electro-Hydrostatic Actuator	*System component (FCS)*
EIPS	Engine Ice Protection System	*Aircraft system (IPS)*
EIS	Entry into Service	*Year of airline service entry*
EMA	Electro-Mechanical Actuator	*System component (FCS)*
EPI	Engine Electrical Power Index	
FAA	Federal Aviation Administration	*National authority (USA)*
FAF	Final Approach Fix	*Mission Altitude*
FBW	Fly-By-Wire	*System technology (FCS)*
FCC	Flight Control Computer	*System component (FCS)*
FCS	Flight Control System	*Aircraft system*
FCX	Function x (general)	*Control Function (FCS)*
FHA	Functional Hazard Assessment	*Safety assessment method*
FLN	Flaperon	*Flight control device (FCS)*
FMDM	Functional Multiple Domain Matrix	
FTA	Fault Tree Analysis	*Failure analysis method*
HLC	High-Lift Control	*Control Function (FCS)*
HLCC	High-Lift Control Computer	*System component (FCS)*
IAF	Initial Approach Fix	*Altitude (Flight mission)*
IAS	Indicated Air Speed	*Aircraft speed*
IB	Inboard (wing)	
ICAO	International Civil Aviation Organization	*Agency of the United Nations*
IFE	In-Flight Entertainment	*Aircraft system (MIS)*
IPS	Ice Protection System	*Aircraft system*
ISA	International Standard Atmosphere	
KF	Krueger Flap	*Flight control device (FCS)*
KGB	Kink Gearbox	*System component (FCS)*
LED	Leading Edge Device (wing)	*High lift control system*
LD	Landing	*Flight phase (MSN)*
LDP	Lift Dump	*Control Function (FCS)*
LG	Landing Gear	*Aircraft system (MIS)*
LR	Long-Range	*Aircraft category*
LWC	Liquid Water Content	*Icing parameter (IPS)*
MAC	Mean Aerodynamic Chord	*Aircraft characteristics (wing)*

MDO	Multidisciplinary Design Optimization	
MDM	Multiple Domain Matrix	
MEA	More-Electric Aircraft	
MIS	Miscellaneous Systems	*Aircraft systems*
MLM	Maximum Landing Mass	*Aircraft parameter*
MR	Medium-Range	*Aircraft category*
MSL	Mean Sea Level	*Altitude (MSN)*
MSN	Mission	
MTOM	Maximum Take-Off Mass	*Aircraft parameter*
OB	Outboard (wing)	
OEI	One Engine Inoperative	*Failure condition*
OEW	Operating Empty Weight	*Aircraft parameter*
OPR	Overall Pressure Ratio	*Engine Parameter (SFC)*
PAX	Passengers	*Payload*
PBW	Power-By-Wire	*System (FCS)*
PCU	Power Control Unit	*System component (FCS)*
PFCC	Primary Flight Control Computer	*System component (FCS)*
PPU	Positioning Pickup Unit	*System component (FCS)*
PSSA	Preliminary System Safety Assessment	
PTC	Pitch Control	*Control function (FCS)*
RLC	Roll Control	*Control function (FCS)*
RGB	Right-angle Gearbox	*System component (FCS)*
SBK	Speed Brake	*Control function (FCS)*
SFC	Specific Fuel Consumption	*Engine parameter*
SFCC	Secondary Flight Control Computer	*System component (FCS)*
SHA	Servo-valve Hydraulic Actuator	*System component (FCS)*
SHC	Spare Holding Costs	*Aircraft operating costs (DOC)*
SL	Slat	*Flight control device (FCS)*
SPL	Spoiler	*Flight control device (FCS)*
SSF	Single-Slotted Flap	*Flight control device (FCS)*
STL	System Torque Limiter	*System component (FCS)*
TAS	True Air Speed	*Aircraft/Mission parameter*
TED	Trailing Edge Device	*System component (FCS)*
TET	Turbine Entry Temperature	*Engine parameter (SFC)*
TG	Thrust gate	*Flight control device (FCS)*
TLR	Top Level Requirements	
TO	Take-off	*Flight phase (MSN)*

TOC	Top of Climb	*Altitude (MSN)*
TOD	Top of Descent	*Altitude (MSN)*
TRL	Technology Readiness Level	
TRM	Trim Control	*Control function (FCS)*
TSF	Triple-Slotted Flap	*Flight control device (FCS)*
VLM	Vortex Lattice Method	*Numerical method (aerodynamic)*
WIPS	Wing Ice Protection System	*Aircraft system (IPS)*
WTB	Wing Tip Brake	*System component (FCS)*
YWC	Yaw Control	*Control function (FCS)*

Latin Symbols

a	Acceleration (aircraft)	$\frac{m}{s^2}$
A	Cross-section, surface area	m^2
c	Specific heat capacity	$-$
$c, \bar{c}$	Surface chord (local), average chord	m
C	Coefficient	$-$
f	Factor, ratio	$-$
h	Flight altitude	m, ft
k	Induced drag factor	$-$
l	Length	m
$\dot{m}$	Mass flow rate	$\frac{kg}{s}, \frac{lbs}{min}$
M	Moment	Nm
Ma	Mach number	$-$
Nu	Nusselt number	$-$
p	Pressure	Pa
P	Power (electric, hydraulic)	W
Pr	Prandtl number	$-$
$\dot{q}$	Heat flux density	$\frac{W}{m^2}$
$\dot{Q}$	Heat flow rate	W
R	Ratio, factor	$-$
Re	Reynolds number	$-$
$S\bar{c}$	Second moment of area	m^4
T	Temperature	$°C, K$
v, V	Speed, velocity	$\frac{m}{s}, kt$

Greek Symbols

α	Angle of attack	deg, rad
β	Prandtl-Glauert (compressibility) factor	$-$
γ	Flight path angle, Adiabatic index	$-$
$\delta, \hat{\delta}$	Deflection, maximum deflection	deg, rad
η	Efficiency	$-$
κ	Compression temperature function	$-$
λ	Taper ratio (wing) Thermal conductivity	$-$ $\frac{W}{mK}$
Λ	Aspect ratio (wing)	$-$
μ	Stagnation temperature ratio	$-$
ρ	Density	$\frac{kg}{m^3}$
φ	Wing sweep	deg, rad
Φ	Non-dimensional turbine entry temperature	$-$

Indices

$+, -$	Positive, negative (deflection)
0	Zero, Standard, Basic
∞	Ambient (air)
ac	Aircraft
act	Actuator, actuation system
af	Airfoil
aw	Adiabatic wall
add	Additional
b	Bleed air
bal	Balanced
$basic$	Basic (thrust, SFC, fuel flow)
$bleed$	Bleed air (engine offtakes)
c	Compressor, compression
con	Conduction
$conv$	Convection
cs, CS	Control Surface
cyc	cyclic
d, D	Drag (2D, 3D)
des	Design
$dist$	Distribution system

$elec$	Electrical
eng	Engine(s)
$evap$	Evaporation
f	Fan (engine)
$flap$	Flap (high-lift control system)
$fresh$	Fresh air
$fuel$	Fuel, Fuel flow
G	Gas generator (engine core)
gen	Electrical Generator
$heat$	Heat, heating
$hinge$	Hinge moment, line
hyd	Hydraulic (system)
ice	Ice, icing
$idle$	Idle thrust (engine)
i	Inlet (engine)
kin	Kinetic (heating)
l, L	Lift (2D, 3D)
LWC	Liquid Water Content
met	Metabolism
mix	Mix, mixing
n	Nozzle (engine)
p	Pressure
ps	Parting strip area ratio
pmp	Hydraulic pump
ram	Ram air
$rated$	Rated thrust, power (engine)
rec	Recirculation, recovery
ref	Reference
$sens$	Sensible heating
$shaft$	Shaft power (engine offtakes)
$spec$	Specific
sun	Sun, solar
$surf$	Surface to protect from ice
sys	Systems
t	Turbine
th	Thermal
$vent$	Ventilation

w	Water
wet	Wetted area
$wing$	Wing

List of Figures

List of Tables

1 Introduction

In 2009, the aviation industry – including airlines, aircraft manufacturers, air navigation service providers and airports worldwide – addressed the global challenge of climate change and defined three ambitious goals[1] for air transport. Figure 1.1 schematically illustrates the climate goals of global air transport until 2050, considering a continuous rate of growth[2]. In general, the overall efficiency improvements are achieved by increased aircraft efficiency, enhanced operations, and optimized air traffic management. However, over the last decades, most of the improvements in fuel efficiency was achieved by aircraft technology improvements (International Civil Aviation Organization (ICAO), 2010, p. 68). This trend will not change for the near future, as the exact level of contributions of alternative fuels is very uncertain[3]. Consequently, improved and innovative aircraft technologies can be seen as the *basement* of all contributions to reduce the environmental impact of global air transport and to achieve these ambitious goals.

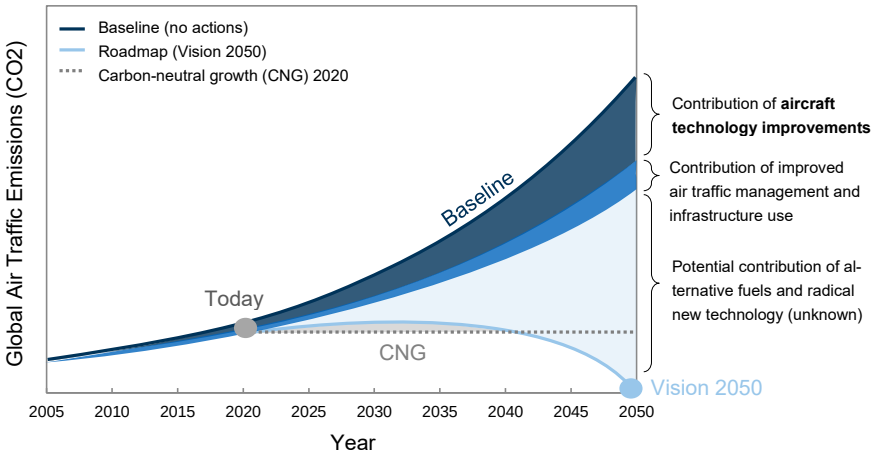

Figure 1.1 Schematic illustration of global air traffic emission trends from 2005 to 2050 and the emission reduction roadmap of the aviation industry (based on IATA (2013, p. 8) and ICAO (2013, p. 24, 2016, p. 18)).

[1] The aviation industry defined three goals to reduce the emissions of global air transport: (1) An average improvement in fuel efficiency of 1.5% per year from 2009 to 2020; (2) A cap on net aviation CO2 emissions from 2020 (carbon-neutral growth) (3) A reduction in net aviation CO2 emissions of 50% by 2050, relative to 2005 levels. (IATA, 2013, p. 1)

[2] Historical data showed significant growth rates of the air transport industry, despite the worldwide crisis in the past. Furthermore, almost all important forecasts assume a doubling of the worldwide revenue passenger kilometers over the next 20 years. (Randt, 2016, pp. 1-2)

[3] According to ICAO (2016, p. 18), an increased use of alternative jet fuels *"[…] would require high availability of bioenergy feedstocks, the production of which is significantly incentivized by price or policy mechanisms"*. In addition, the 100% replacement of alternative fuel jet would require a complete shift to biofuel production and substantial expansion of the agricultural sector. This would need substantial policy support and is therefore associated with great uncertainty.

1.1 Motivation

In general, the overall aircraft efficiency is closely linked to *engine efficiency*, *aircraft aerodynamics* and *aircraft weight*. The gradual development of more efficient and reliable turbofan engines led to a significant increase in engine efficiency and the specific fuel consumption (SFC) decreased by approximately 30% over the last 50 years (Torenbeek, 2013, p. 59). At the same time, the introduction of supercritical airfoils, winglets, multidisciplinary wing design and advanced high-lift control devices, improved the overall aerodynamic efficiency. Aircraft weight savings was primarily achieved by the use of composite materials, increased use of electronics and electrical systems. Besides the trend towards higher BPR turbofan engines[4], two other major technological trends emerged over the last two decades: *More-Electric Aircraft* and the *Functional Enhancement* of the Flight Control System (FCS).

More-Electric Aircraft. The first trend that can be observed is the growing use of electrical power and the reduction of hydraulic or pneumatic systems. This is also clearly visible by the significant increase of the Engine Electrical Power Index (EPI)[5] over the last 10 years, see Figure 1.2. In comparison, only a small increase of rated electrical generator power could be observed in the 1980s and 1990s. In 2011, Boeing took a radical step in electrification and introduced the 787 as the first commercial transport aircraft with a bleed-less system architecture (Sinnet, 2007). The latest introduced Airbus A380 (EIS 2007) and A350 (2014) show a smaller increase in rated electrical generator power. However, Airbus introduced a 2H-2E (2 hydraulic and 2 electrical) power system architecture in addition to electrical actuators for flight control surfaces (Bossche, 2006; Criou, 2007). For this reason, these aircraft can also be described as the first generation of MEA.

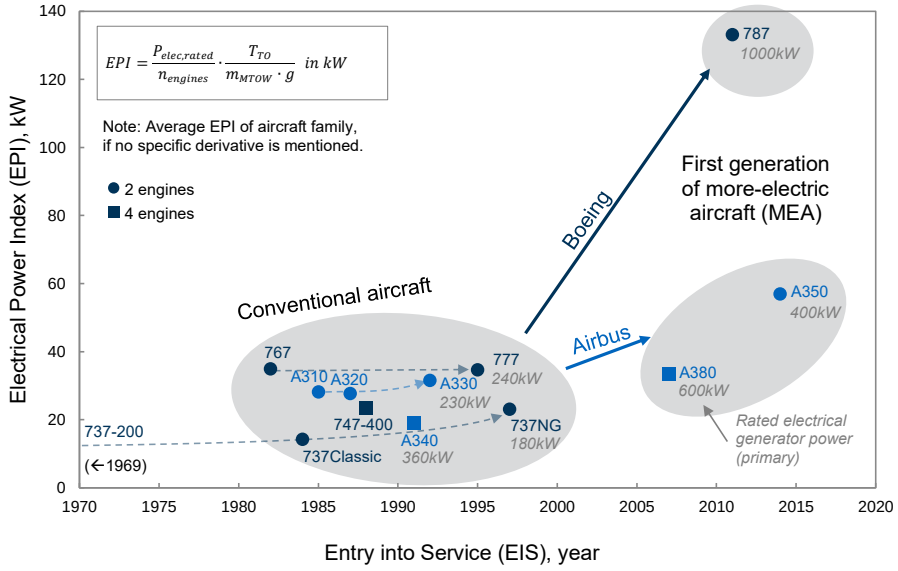

Figure 1.2 Evolution of the rated electrical generator power of commercial transport aircraft over the last 50 years (Airbus and Boeing).

[4] Today, modern transport aircraft use the 5th generation of turbofans (BPR > 10) or the geared turbofan (BPR > 12).

[5] The Engine Electrical Power Index (EPI) (see definition in Figure 1.2) considers the rated electrical generator power $P_{elec,rated}$, the number of engines $n_{engines}$, maximum takeoff thrust T_{TO} and the maximum takeoff weight m_{MTOW} of the aircraft. This enables the comparison, regardless of the aircraft size and engine configuration.

According to various research studies (e.g. Tagge *et al.*, 1985; Jones, 1999; Botten *et al.*, 2000; Cutts, 2002), MEA enables improvements in fuel consumption, system installation and maintenance. In addition, electronics and electrical systems lead to enhanced safety and increased reliability.

Functional Enhancement. The second trend is the functional enhancement of the FCS by additional flight control functions. During the last decades, the FCS of commercial transport aircraft were steadily optimized, and a plateau in terms of possible benefits at aircraft level was reached. Conventional FCS are generally knowledge-based designs with mono-functional flight control devices[6], and are often limited to small and local improvements under high effort (Recksiek, 2009, p. 51; Reckzeh, 2014, p. 5). For that reason, the functional enhancement of the FCS is of major interest to enable further improvements in overall aircraft performance or efficiency. The trend of functional enhancement is clearly visible for the trailing-edge devices of the high-lift control system: Even though the complexity of the trailing-edge flaps were reduced, additional control functions were integrated, see Figure 1.3. For example, multifunctional trailing-edge devices of the Airbus A350 (EIS 2014) additionally provide the Cruise Variable Camber (CVC) function for aerodynamic improvements or the Differential Flap Setting (DFS) function for wing load control.

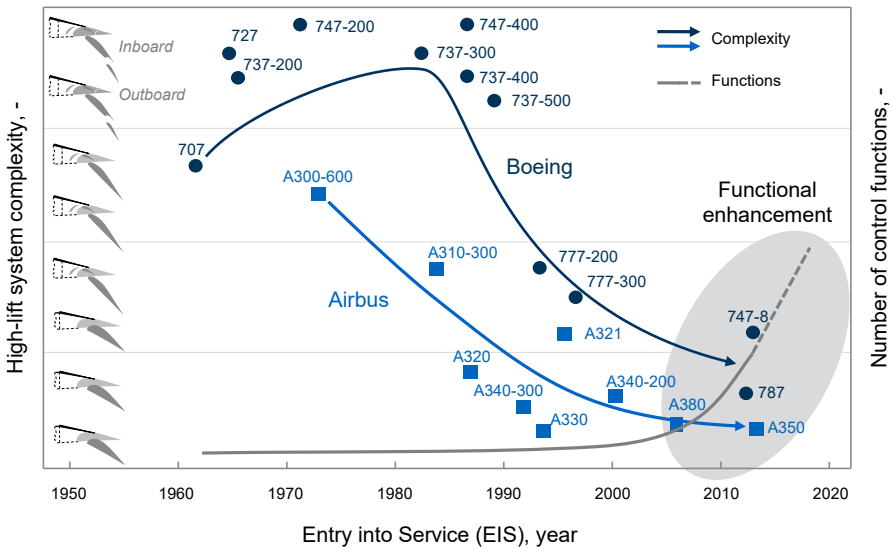

Figure 1.3 Evolution of high-lift system trailing-edge devices of commercial transport aircraft over the last 50 years, regarding complexity[7] and number of control functions (Airbus and Boeing).

Another example, but not yet implemented on commercial transport aircraft, is the use of Active Flow Control (AFC) systems to improve the aerodynamic performance of local areas at the wing, airframe or different flight control devices (e.g. Brunet *et al.*, 2013; Ciobaca and Wild, 2013; Lengers, 2014; Reckzeh, 2014). More details on advanced technologies and further examples are presented in section 2.3.4 *Advanced Technologies and Concepts*.

[6] In this work, flight control devices are surfaces, movables, or technologies which provide or support flight control functions.

[7] The high-lift system complexity of the Airbus A350 is reduced (cf. Figure 1.3), considering the single flap and low complex hinge-mechanism solution of the Advanced Dropped Hinge Flap (ADHF). Nevertheless, additional spoiler downward deflection for gap control and the required installation of Differential Gear Boxes (DGB) to enable Differential Flap Settings (DFS) consequently increased the complexity of the high-lift control *actuation system architecture*.

The review of technological trends provides the following major findings: First, the number of electronics and electrical systems are increasing, resulting in a higher demand of electrical generator power. Furthermore, the increased use of electrical systems leads to considerable changes of the power generation and distribution systems, with great impact on other aircraft systems. Second, the functional enhancement of the FCS increases the design space and enables multifunctional solutions. In addition, low complex solutions are targeted, to keep the system weight, installation and maintenance costs as low as possible. Summarized, the integrated and multidisciplinary design of multifunctional flight control devices[8] along with the electrification of the system architecture is of major interest for future FCS of commercial transport aircraft. In addition to improvements in overall efficiency of the aircraft, including fuel consumption, installation and maintenance costs, considerable advantages are expected in reliability and safety.

Previous Work. Several research studies present advanced technologies or concepts for innovative FCS concepts. However, only few studies show *how* advanced FCS with enabling technologies can be considered and integrated into early aircraft design phases. The following review of previous work considers ideas, methodologies and concepts for the design and analysis of *advanced* flight control configurations or architectures, considering functional enhancement and more-electric systems.

Reckzeh (2014) presented a first idea of a functional-driven design approach for advanced FCS. The intent of this top-down approach is to provide a transition from a *knowledge-based design* to a *functional-driven design*, to increase the overall design space and to enable multifunctional concepts, as illustrated in Figure 1.4. The required setup of an integrated, multidisciplinary design process and the development of validated tools are seen as key challenges of this design approach (Reckzeh, 2014, p. 5).

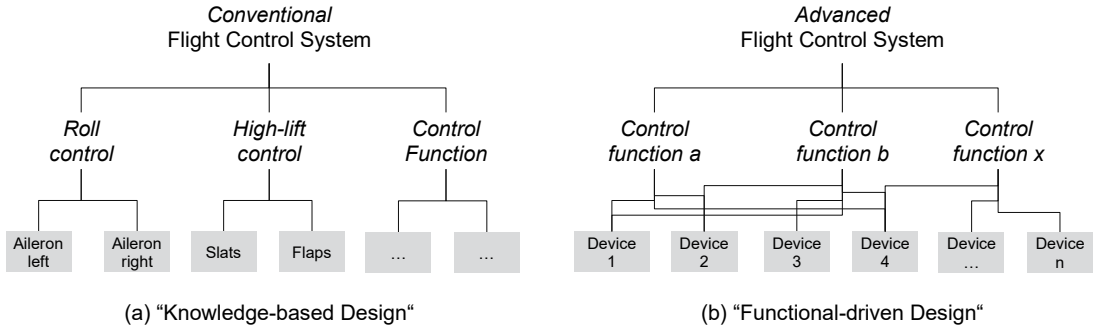

Figure 1.4 Functional breakdown of a conventional (left) and an advanced flight control system with multifunctional flight control devices (right) (based on Reckzeh (2014, p. 5)).

Bauer *et al.* (2007) developed a discrete optimization algorithm to find an optimal FCS architecture regarding minimum system weight in early aircraft design phases, while fulfilling the safety constraints. However, this approach requires defined flight control configurations and is limited to conventional (knowledge-based) FCS designs.

[8] Multifunctional flight control devices provide multiple flight control functions, either by multifunctional design or by multifunctional use.

Kreitz *et al.* (2015) suggest a simulation-driven methodology to support the preliminary design and assessment of innovative flight control system architectures. This approach requires a complex nonlinear simulation model of the aircraft, including a defined flight control configuration, for the analysis of the handling quality and flight performance.

Chakraborty *et al.* (2015) presented a requirements-driven methodology for MEA for the analysis and assessment of aircraft systems in early aircraft design phases. In this work, two different electrical actuation architectures for one flight control configuration (layout) are sized and analyzed on aircraft and mission level. The methodology enables the rapid assessment of different flight control actuation systems, regarding system weight and mission fuel burn.

Akoto *et al.* (2017) apply a stochastic clustering algorithm to derive potential system architectures for the preliminary design of novel high-lift control actuation system, considering multifunctional requirements of flight control devices. This approach is based on a functional design structure matrix with focus on interacting functions of the actuation system and components. However, this approach requires a defined arrangement of the flight control devices and allocation of functions, which considerably limits the design space.

Cai *et al.* (2017) presented a system-level assessment of different architectures for high-lift systems consisting of trailing-edge devices with AFC. The integration and performance analysis of the AFC system in addition to the system-level assessment is based on the subsystem sizing methodology of Chakraborty (2015). The results show that the power requirements of the AFC system (pressurized air, total mass flow) significantly influence the performance improvements and the design of the system architecture. In conclusion, the authors confirmed the necessity of a multidisciplinary design framework to consider all interdependencies and influences.

Garriga *et al.* (2017) presented such a modelling framework which enables the comparison and trade-off study for system architectures of MEA. In a case study of a full-electric primary flight control system with EHAs and EMAs, they demonstrated the capability to evaluate the aircraft-level impact of different system architectures, based on changes in engine power-offtakes, system weight and fuel consumption.

Summary. The analysis of the most relevant work on the design of advanced FCS revealed the following findings: The design of advanced FCS requires an integrated and multidisciplinary design process and the development of supporting tools. Additionally, a functional-driven design approach is recommended to increase the design space and enable multifunctional solutions. However, most of the presented methods focus only on the system architecture and do not consider functional enhancement of the flight control configurations, including the arrangement and functional allocation of flight control devices. Furthermore, the applied development and analysis tools are often tailored to one type of technology under investigation and prevents the analysis and assessment of other types of technologies or concepts.

1.2 Objectives

The integration of new technologies and concepts for future aircraft is preceded the comprehensive and multidisciplinary concept studies in early aircraft design phases. Thus, following main activities are indispensable for advanced aircraft design (based on Torenbeek, 2013, pp. 6–7):

- Identification of key technologies and concepts for future aircraft in addition to research and development to increase the Technology Readiness Level (TRL).
- Conduction of pre-conceptual and conceptual design studies for future aircraft concepts in a highly multidisciplinary design environment.
- Tool development for aircraft sizing, performance analysis, weight predictions and optimization techniques, to enable the analysis and comparison of different technologies in order to have a basis for decisions in early aircraft design phases.

Research Questions. Driven by the need of continuous development of advanced technologies, inspired by recent technological trends and the idea of a functional-driven design of future FCS, the following two ***research questions*** arise:

Question 1 What methodology is required to enable the design and analysis of advanced FCS with new technologies and concepts during early aircraft design phases?

Question 2 How can we analyze and assess the impact of such advanced FCS at aircraft and system level, independently from applied technologies and system concepts?

Research Objectives. Based on the review of technological trends and previous work in addition to the needs of advanced aircraft design, following key ***objectives*** must be achieved in order to answer the research questions adequately:

Objective 1 Provide a method to support the shift from a *knowledge-based design* to a *functional-driven design* of advanced flight control systems.

Objective 2 Enable an *integrated design* of advanced flight control systems, including the design of the flight control configuration and system architecture.

Objective 3 Development of a *simulation framework for technology analysis* and assessment of new system technologies or concepts applicable for advanced flight control systems.

According to the research questions and the key objectives, the overarching goal of this thesis is to develop a methodology for the integrated design of advanced flight control configuration and system architectures, and enable their analysis and assessment in early aircraft design phases.

1.3 Organization of the Thesis

The focus of this work is on the early aircraft design phases of commercial transport aircraft that are certified according to CS-25[9] or FAR-25[10] regulations. Nevertheless, the developed methodology and calculation tools may be applied for other aircraft configurations. The thesis is organized in four parts as illustrated in Figure 1.5.

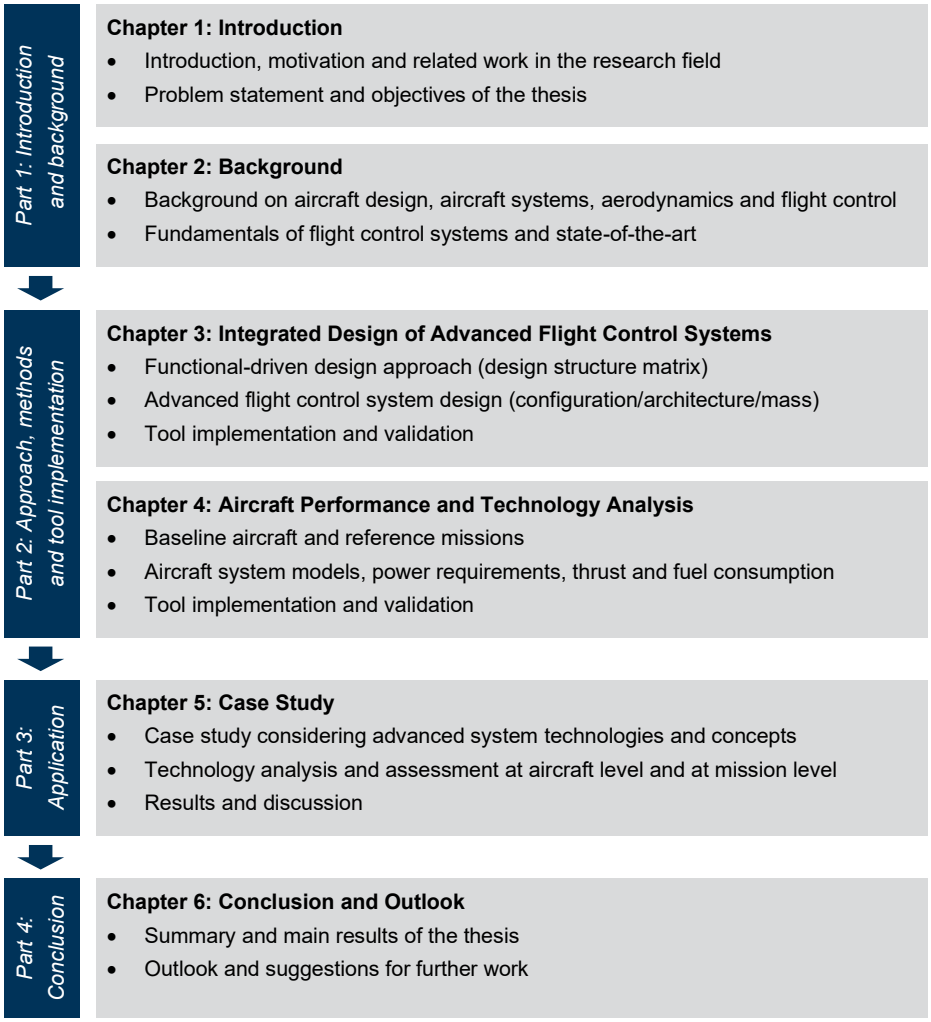

Figure 1.5 Overview and structure of the thesis.

Part 1: Introduction and Background. The first part describes the motivation and objectives of the thesis and provides helpful background information within the research fields of aircraft design, aircraft systems and flight control. In addition, the fundamentals and state-of-the-art transport aircraft flight control systems are presented, including an overview of promising advanced technologies and concepts for future FCS.

[9] European Aviation Safety Agency (EASA) (2018): *Certification Specifications and Acceptable Means of Compliance for Large Aeroplanes CS-25.*

[10] Federal Aviation Administration (FAA) (2019): *Federal Aviation Regulations (FAR) Part 25 - Airworthiness Standards: Transport Category Airplanes.*

Part 2: Approach, methods and tool implementation. The second and main part of the thesis focuses on the overall, integrated design methodology with three major steps. The first two steps of the methodology, the functional-driven design approach and the advanced flight control system design method, are presented in *Chapter 3,* whereas the last step for aircraft performance and technology analysis is shown in *Chapter 4*. Within the functional-driven design approach, the potential design space is explored, and several concepts of advanced FCS can be derived. This approach aims to fulfill ***Objective 1,*** to enable and support the shift from a *knowledge-based design* to a *functional-driven design* of FCS. The design of advanced FCS represents the second step of the integrated design methodology. The preliminary design of the configuration considers preliminary design rules in addition to aerodynamic calculation results. Following this, the redundant FCS architecture is designed on the basis of defined design rules, distribution logics for actuators and power supply, and defined technological assumptions. Finally, the total mass for the found FCS configuration and architecture is calculated, using different mass estimation methods. This design method enables the integrated design of advanced FCS and drives to fulfill ***Objective 2.*** The last step of the overall design methodology is the simulation framework for aircraft system technology analysis. To achieve that, the framework has to consider aircraft aerodynamics, aircraft systems and system architectures in addition to engine technologies to calculate the fuel flow and the fuel consumption of the aircraft. Therefore, a parameterized mission with typical altitude and speed profile of commercial transport aircraft is defined. On basis of aircraft-level functions, simplified system models of the Environmental Control System (ECS), the Ice Protection System (IPS) and the Flight Control System (FCS) are derived. Whereas the power requirement estimations of all other, miscellaneous aircraft systems (MIS), e.g. galleys, avionics, and fuel systems, are mainly based on data from literature or are estimated. This method enables the analysis and assessment of new system technologies and concepts on aircraft and mission level, meant to fulfill ***Objective 3.***

Part 3: Application. In this part, the integrated design methodology and the implemented tools are applied in a case study. The study considers commercial transport aircraft with an advanced high-lift control system architecture and multifunctional trailing-edge flaps. The results of the concept aircraft are compared to the results of the baseline aircraft. Finally, the integration of an advanced trailing-edge flap with active flow control is analyzed. The case study should demonstrate the applicability of the methodology and the developed tools in early aircraft design phases.

Part 4: Conclusion. At the end of the thesis there is a brief summary and discussion of the major results. Based on the key findings and the achieved results, the contribution of the work in the field of research will be analyzed and evaluated. Finally, this part ends with an outlook and recommendations for further research.

2 Background

The Flight Control System (FCS) of transport aircraft is an essential and safety-critical system with strong physical interaction with airframe and structure, and significant information-based integration into avionics and mission systems (cf. Figure 2.12). Furthermore, the FCS is situated in a multidisciplinary design framework, with several requirements, specifications and constraints. For this reason and with the intention of an integrated design of advanced FCS, a holistic systems-view of the aircraft is required. As a result, all influences or factors which may affect the FCS design can be taken into account. Accordingly, good knowledge about the overall aircraft design, aircraft aerodynamics and performance in addition to overall aircraft system architectures is essential.

This chapter provides the relevant background in the required fields of research in context of this thesis. The first subchapter *2.1 Aircraft Design and Aircraft Systems* generally describes the conceptual and preliminary aircraft design phases and gives an overview of state-of-the-art aircraft systems. Furthermore, the trends, technologies, and challenges of More-Electric Aircraft (MEA) are explained. In the second subchapter *2.2 Aircraft Aerodynamics and Performance* the governing equations to calculate the aircraft aerodynamics and performance are explained. Afterwards, the Vortex Lattice Method (VLM) is introduced, which is applicable in early aircraft design phases to calculate aircraft aerodynamics. The third subchapter *2.3 Flight Control Systems* starts with the definition of the system boundary and required terms, regarding the design and development of FCS configurations and architectures. Afterwards, the principles of flight control, state-of-the-art flight control configurations and system architectures in addition to the overall requirements and design aspects are examined. Finally, enabling technologies for advanced FCS are reviewed.

2.1 Aircraft Design and Aircraft Systems

The aircraft development and design process starts with the analysis of market (customer) requirements for answering the question *why* – rather than *how* – a new aircraft will be developed (Torenbeek, 2013, p. 7). Together with the research of enabling technologies and the consideration of airworthiness certification rules, the Top-Level Requirements (TLRs) can be defined within this pre-conceptual design phase. The found set of design characteristics, definitions and constraints is the starting point of the aircraft design and development process. The overall development process is subdivided into configuration design, detail design (including manufacturing and testing), and service engineering, see Figure 2.1a.

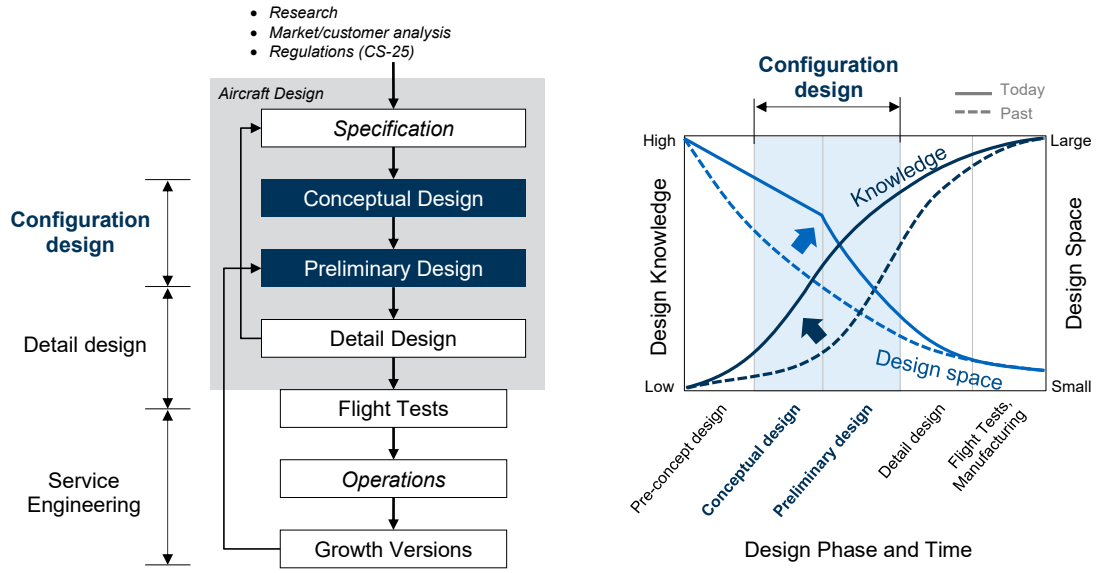

(a) Aircraft design and development (Torenbeek, 2013, p. 8, modified)

(b) Available knowledge and design space (based on Schrage *et al.* (1991))

Figure 2.1 The aircraft design and development process (left) and the available knowledge and design space during the aircraft design process (right).

The aircraft design process can be broken down into *conceptual design*, *preliminary design* and *detail design*. The conceptual and preliminary design is also referred to as *Aircraft Configuration Design* (cf. *2.1.1*). The configuration design ends with the so-called *design freeze* of the most promising aircraft configuration. Subsequently, after a successful go-ahead approval of the management, the construction, manufacturing and testing starts. Further major events during this phase are the first flight and the type certification. With the first deliveries of the aircraft to the customers, the service engineering (or product support) starts. During this phase, a lot of data and information is gathered, which leads to engineering modifications to continuously improve the aircraft (Torenbeek, 1982, p. 4).

In 1991, the AIAA Technical Committee on MDO observed for the traditional aircraft design approach, that the short conceptual design phase "*with unequal distribution of disciplines*[11] *does not allow use of the design freedom to improve quality and integrate disciplines for optimization*" (Schrage *et al.*, 1991). For this reason, the committee recommended a reorganized design process to increase the available knowledge and the design space in early aircraft design phases as it is illustrated in Figure 2.1b. This approach has become standard for highly complex and multidisciplinary design projects. Consequently, the early aircraft design phases are very challenging: Due to the large design space and little available knowledge at the beginning, a lot of parameter studies and tradeoffs have to be done within a multidisciplinary design framework (characteristics, definitions, and constraints). Subsequently, during early aircraft design stages, low to medium fidelity tools of different disciplines are required, which enable the free variation of parameters, constraints and objectives (Torenbeek, 2013, p. 214). This early phase of the design process is in focus of this work, where the integrated design methodology and developed tools are applied.

[11] General disciplines are aerodynamics, propulsion, structures, controls, manufacturing, supportability, costs.

2.1.1 Aircraft Configuration Design

The principle aim of the aircraft configuration design is to obtain the required information in order to decide whether the aircraft concept will be technically feasible and also economical (Torenbeek, 1982, p. 5). The configuration design process is divided into conceptual and preliminary design, as illustrated in Figure 2.2. Starting with a set of initial design specifications, first aircraft concepts are iteratively developed. The *conceptual design* is characterized by a large design space. To find promising aircraft concepts, a great number of iterative design changes and tradeoff studies have to be performed. In a next step, the most promising aircraft concept is selected, and an initial baseline aircraft is defined.

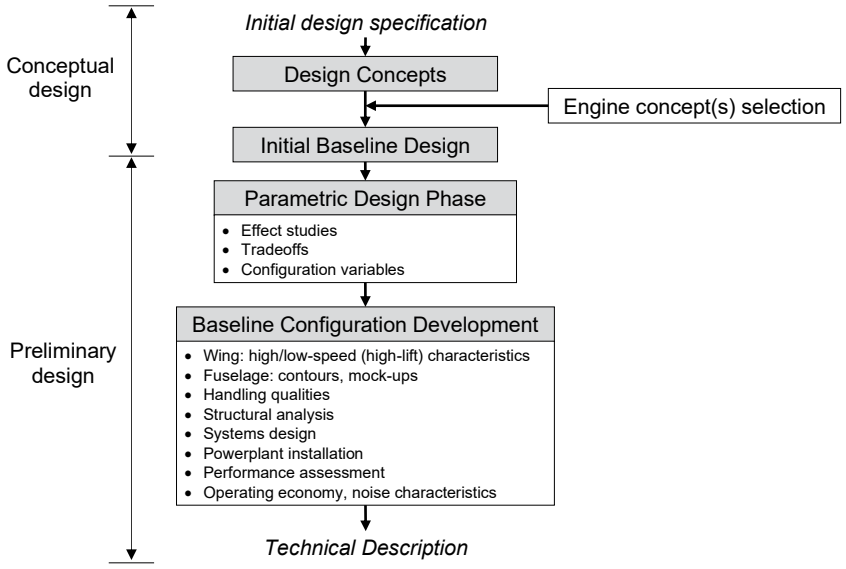

Figure 2.2 The aircraft configuration design process (Torenbeek, 1982, p. 5).

The *preliminary design* starts with the parametric design phase, where several design variants of the initial baseline design are derived and developed. At the end of this phase, a baseline configuration will be chosen for further development. During the conceptual design and early preliminary design, low to medium fidelity design tools are used. Thus, the focus is less on the absolute accuracy of the applied methods, but more on the comparability and differentiability of the design variants among themselves (Torenbeek, 1982, p. 8). Nevertheless, the applied methods or tools should provide results with sufficient accuracy[12] and reasonable computation time, depending on the level of detail. The objective of the baseline configuration development is to further develop the baseline aircraft to a certain depth of detail. During this phase, observed errors, which were made during the earlier phases due to lack of data or low accuracy, are iteratively corrected – affecting the overall aircraft design and all involved disciplines (Torenbeek, 1982, pp. 8–9). Finally, if the baseline aircraft configuration is regarded as sufficiently mature and all essential requirements are fulfilled, the preliminary design phase finishes with the design freeze (Torenbeek, 1982, p. 9)

[12] Typical level of accuracies in conceptual and early preliminary aircraft design are in the range of 5-15%, depending on the discipline and available level of detail (in comparison to the final, optimized design).

The main objective during the conceptual and early aircraft design is to specify the design concept at the main component level, and only sometimes include aircraft systems (Torenbeek, 2013, p. 9). Nevertheless, it is suggested to consider and investigate the potential of new (system) technologies in early design phases, as these technologies may have a large effect on the overall aircraft design and aircraft performance. Accordingly, conceptual studies with detailed analysis and assessment of advantages and disadvantages of new system technologies and concepts are necessary (Torenbeek, 2013, p. 11).

2.1.2 Aircraft Systems

Today's transport aircraft are equipped with many different interacting aircraft systems[13], which are essential for reliable and safe operation. To operate these aircraft systems, the engine has to provide secondary power throughout the full mission. The overall power of the aircraft is generally provided by the aircraft engines[14] and can be divided into primary power (propulsion) and secondary power (non-propulsion), see Figure 2.3. The primary power produces the necessary thrust, whereas the secondary power is required to supply the onboard distributed aircraft systems. The main aircraft systems, regarding large secondary power or safety requirements, can be grouped as the Environmental Control System (ECS), the Ice Protection System (IPS), and the Flight Control System (FCS). Further, important aircraft systems are avionics, fuel system, landing gear and braking system, thrust reverser, lighting, galleys, and in-flight entertainment, which are summarized as Miscellaneous Systems (MIS).

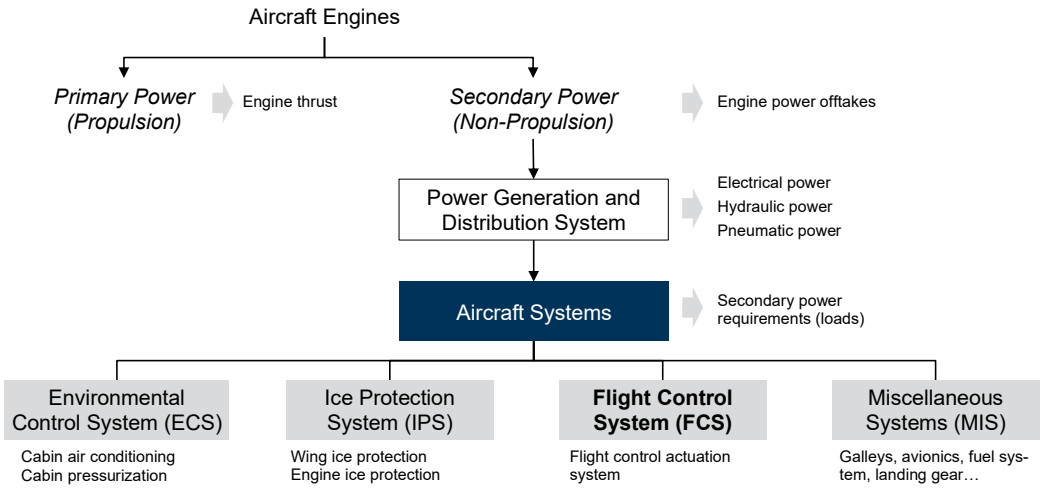

Figure 2.3 Schematic overview of the aircraft secondary power architecture, with the power generation, distribution systems and the aircraft systems.

In general, each aircraft system has to fulfill different functions during the whole flight or dedicated flight phases. For example, the ECS has the main functions of air conditioning and cabin pressurization, and operates throughout the full mission. Whereas the IPS has the main function of protecting critical surfaces of the aircraft from ice formation. In contrast to the ECS, the IPS is

[13] Aircraft systems are also known as general systems, utility systems, or subsystems.

[14] Other onboard power sources are the Auxiliary Power Unit (APU) and the Ram Air Turbine (RAT). The APU is a conventional gas turbine engine that provides electrical and bleed-air power (optional) during ground operations or as backup power during flight. The RAT is the heart of the aircraft's emergency power system and activated when all engines or main generators failed.

only active if the aircraft is operating in icing conditions. Typical short-term operating aircraft systems are landing gear actuation and the setting of the high-lift system devices. A comprehensive overview of functional analysis and typical operation schedules of aircraft systems is presented in the work of Liscouët-Hanke (2008, pp. 30–34).

Today's transport aircraft provide three different forms of secondary power: *electrical power*, *hydraulic power* and *pneumatic power*. The electrical and hydraulic power are generated by mechanical power offtakes from the engines, to drive the electrical generator and the hydraulic pumps. Additionally, bleed air from the engine compressor is extracted and regulated (temperature and pressure reduction), before it is used as pneumatic power for various systems. A major advantage of bleed air is the easy availability of high-pressure air from the engine (Moir and Seabridge, 2008, p. 240). However, the low efficiency and the difficulty of the detection of leaks are major drawbacks (Rosero *et al.*, 2007, p. 3). Hydraulic systems are effective, high-density power systems and are very robust. Drawbacks are the heavy and inflexible piping, and the potential of leakage of the hydraulic fluid. Electrical systems have the advantage of relatively flexible and light-weight infrastructure[15] with lower maintenance costs. A major drawback is the relatively low power density compared to hydraulic power systems (Rosero *et al.*, 2007, p. 3).

In a study published by Slingerland and Zandstra (2007), the performance of the turbofan engine of a commercial transport aircraft is evaluated for bleed air offtakes and electric power offtakes. In a first study, the two types of power offtakes are compared in an exergy[16] analysis during design point operation and over the full flight cycle, with following results:

- Engine power offtakes have a significant effect on the performance of turbofan engine and should be limited as much as possible.
- During design point operation of the engine, electrical power offtakes lead to larger performance losses than the extraction of bleed air.
- Also, over the full flight mission, the use of bleed air is more efficient and has some major advantages, especially during cruise and ground idling[17].

In another study they included a generic subsystem model – a bleed-air powered and an electrically powered Environmental Control System (ECS) – to estimate the secondary power requirements over the full flight cycle. The comparison of the two models showed, that the electrically powered ECS is 2% better in terms of Specific Fuel Consumption[18] (SFC). The authors concluded that this is due to the more-efficient electrical bleed air system and not by the electrical power offtakes within the engine itself. Finally, they concluded that the electrical ECS has the potential of significant improvements in SFC. Nevertheless, further potential benefits such as lower system

[15] Please note, that today's electrical actuators are approximately twice as heavy as comparable hydraulic actuators. Nevertheless, weight savings at aircraft level are possible due to light-weight infrastructure (network).
[16] Exergy is the available energy or work. This relationship is used, as the electrical power offtakes (in kW) and the extracted bleed air (in kg/s) cannot directly be compared (Slingerland and Zandstra (2007, p. 2).
[17] At maximum thrust, bleed air reduces the engine pressure and rotational speeds. Furthermore, bleed air increases the stall margin to run the engines safer and more efficient during ground idling (Slingerland and Zandstra (2007, p. 8).
[18] In this work, unless otherwise defined, the Specific Fuel Consumption (SFC) is equal to the Thrust Specific Fuel Consumption (TSFC).

weight or less system complexity also must be investigated. (Slingerland and Zandstra, 2007, pp. 9–11)

The trend of modern turbofan engines shows increasing Bypass Ratio (BPR) and decreasing overall fuel consumption. However, the penalty in SFC relative to the engine power offtakes significantly increases (Giannakakis *et al.*, 2011, pp. 1027–1028), see Figure 2.4.

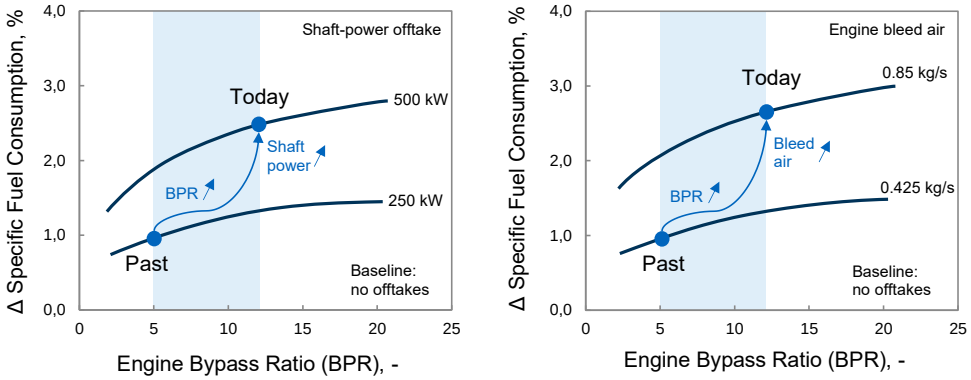

Figure 2.4 Specific Fuel Consumption (SFC) penalty due to shaft-power offtakes (left) and bleed-air extraction (right) from a turbofan engine with different Bypass Ratios (BPR) (data from Giannakakis *et al.* (2011)).

The comparison between the past and today show small increases in SFC for higher BPR and large increases for higher secondary power requirements. Furthermore, a slight divergence of the two curves of different power requirements can be observed for increasing BPR. This confirms the findings by Hunt *et al.* (1995, pp. 7–8) of increasing fuel consumption due to bleed-air offtakes of an engine with higher BPR.

The results show that a simple replacement of systems or the introduction of new technologies without considering a system model is not enough to estimate the overall impact at system level or at aircraft level. Independently from the type of power systems, all power offtakes have a direct impact on the engine and accordingly influences the fuel consumption, depending on the engine technology, thrust settings, and overall secondary power requirements.

So far, the design and characteristics of aircraft systems were of minor significance during early aircraft design phases. Often an aircraft system is considered as a simplified mass or layout (Liscouët-Hanke, 2008, p. 6), or only a basic idea of the system and its functionality exists (Lammering, 2014, p. 10). Liscouët-Hanke (2008, p. 6) identified two aspects, why the aircraft systems were of minor significance so far: First, the power generation and distribution systems has not changed significantly, and the aircraft systems were predictable by extrapolation. Second, the fuel consumption due to secondary power (without considering the changes in mass and drag) is in the range of 1-5% of the fuel consumption required to produce thrust. However, the aircraft systems contribute significantly (around 30%) to the Operating Empty Weight (OEW), Direct Operating Costs (DOC), Direct Maintenance Costs (DMC), and aircraft development costs (Liscouët-Hanke, 2008, p. 6). For that reason and due to the increasing number of aircraft systems and the greater effect of secondary power offtakes on the SFC of high-BPR engines, an early consideration

of aircraft systems in addition to performance analyses on aircraft and system level is recommended.

2.1.3 More-Electric Aircraft

The trend of More-Electric Aircraft (MEA) is clearly visible in the increasing use of electrical power and the reduction of hydraulic or pneumatic systems, which lead to a notable increase in rated electrical generator power (cf. Figure 2.1). For example, the Boeing 787 has a bleed-less system architecture and a full-electrical ECS and electro-thermal wing IPS[19] (Sinnet, 2007). Smaller, but not less important changes were made by Airbus for the A380 and A350, where a more-electrical power system architecture and electrical actuators for the flight control surfaces were introduced[20] (Bossche, 2006; Criou, 2007). As illustrated in Figure 2.5a, a conventional aircraft system architecture provides three forms of power to supply the different electrical, hydraulic and pneumatic aircraft systems (loads). During the last decades, this system architecture was established as a standard for transport aircraft. However, each aircraft system has become more and more complex, and the interactions between the different systems reduced the system efficiency[21] (Rosero *et al.*, 2007, p. 3). Figure 2.5b shows the concept of the so called All-Electric Aircraft (AEA), where all aircraft systems are supplied by electrical power.

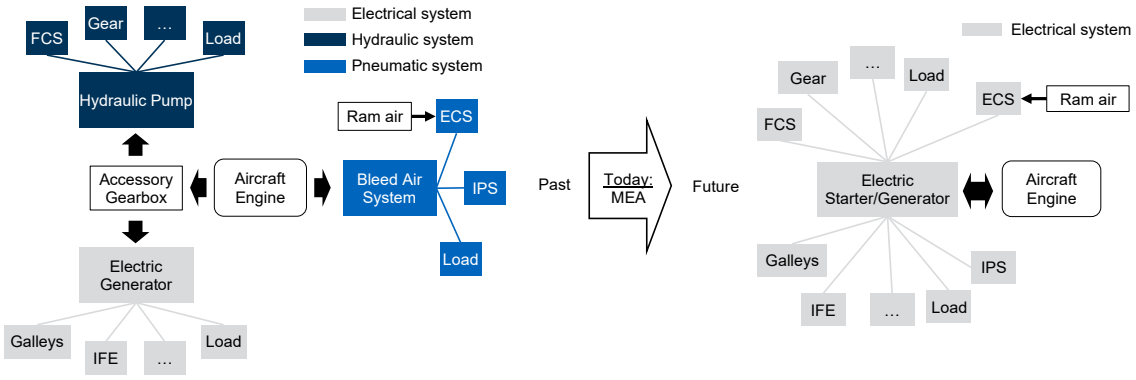

(a) Conventional system architecture (b) All-Electric Aircraft (AEA)

Figure 2.5 Schematic overview of the conventional aircraft system architecture (left) and the future All-Electric Aircraft (AEA) system architecture (right).

Actually, the MEA is seen as an intermediate step towards the AEA to reduce technological and financial risks of the aircraft development programs (Jones, 1999, p. 2; Botten *et al.*, 2000, p. 55; Cutts, 2002, p. 223). In addition, Jones (2005, p. 268) observed, that during this step-wise MEA approach "*the perceived area of major benefits has shifted from fuel efficiency to that of reliability and maintenance gains for electric-powered systems*".

[19] The Engine IPS (EIPS) at the cowling (inlet) of the B787 is still supplied by the locally available engine-bleed air.
[20] The Airbus aircraft generation before the A380 had three independent hydraulic power circuits (3H).
[21] Here, the system efficiency considers the system performance, production, installation, maintainability, and flexibility.

On the basis of major research studies on MEA or AEA over the last 30 years[22], following main benefits at *aircraft level* can be summarized:

- Improvements in fuel consumption
- Overall weight reduction
- Improvements in system installation and maintenance
- Predictive maintenance and health monitoring
- Enhanced safety and increased reliability

The trend of MEA leads to considerable changes on aircraft system level, regarding power generation architecture and distribution, and thus has a decisive impact on the design and integration of flight control actuation systems (Botten *et al.*, 2000, p. 66). Today, the electrical signaling for FCS, known as Fly-By-Wire (FBW), is standard for commercial and military aircraft (Botten *et al.*, 2000, p. 55; Maré and Fu, 2017, pp. 860–861). The application of electric actuators and Power-By-Wire (PBW) actuation, especially for safety-critical systems, does not work in the straightforward replacement of hydraulic actuators with electric actuators (Maré and Fu, 2017, p. 867). Rather, it can be observed that hydraulic actuators are gradually being replaced by electrical actuators, which pragmatically follows the stepwise MEA approach. As a result, the problems and challenges of electric actuation can be gradually solved with more sophisticated technologies. In general, electric actuation shows following benefits at *system level* (Botten *et al.*, 2000, p. 56):

- Improved maintainability, due to fewer hydraulic components, fewer spares and tools, improved fault-diagnosis.
- Improved system availability and reliability: Electrical power distribution is more practical and flexible, and generally have a higher Mean Time Between Failures (MTBFs).
- Improved system safety, through dissimilar actuator power supplies and subsequent avoidance of common mode failures.
- Reduced system weight, by the replacement of entire hydraulic systems (pumps, pipes, fluid, and valve blocks) by electrical systems and components.

Besides these potential benefits, electric actuator technologies also present some significant challenges (Botten *et al.*, 2000, p. 57):

- Electrical power sources have lower specific power density compared to equivalent hydraulic power sources.
- Electric actuation has increased and localized heating effects in addition to reduced heat dissipation.
- Maintaining the required power quality: Increasing electrical loads impact the power supply quality, due to distortions of the high-power controllers.

[22] The first research studies on MEA/AEA were conducted by NASA, Lockheed, Boeing, and the US Airforce, which were published by Hoffman *et al.* (1985); Tagge *et al.* (1985); Cronin (1990); Weimer (1993). An overview of the Totally Integrated More Electric Systems (TIMES) project of an UK aerospace consortium is published by Cutts (2002). A summary of the Power Optimized Aircraft (POA) project (half funded by the EU) is given by Faleiro (2006). Furthermore, Jones (2005); Rosero *et al.* (2007) provide a good (historical) overview of the MEA/AEA initiative.

Taken into account that the time scale for the full replacement of mechanical signaling with FBW lasted more than two decades[23], the PBW has just started to be used for modern transport aircraft, and significant improvements can be expected in the future (Maré and Fu, 2017, p. 867). Regarding electrical actuation for flight control, more details and characteristics of the different types of (electric) actuators are presented in subchapter *2.3.3 System Architecture and Actuation*.

2.2 Aircraft Aerodynamics and Performance

This section starts with an introduction of the basic aerodynamic forces and moments of an aircraft in addition to governing equations. Based on this, the basics of aircraft flight physics are presented, assuming a simplified point mass model. Finally, the principles of the different modelling methods for aircraft aerodynamics used in this thesis are briefly explained.

2.2.1 Aerodynamic Forces and Moments

The main aerodynamic forces acting on a wing or aircraft are lift L, drag D and the pitching moment M. In general, the forces are described in the aerodynamic axis systems as illustrated in Figure 2.6. The lift acting on the aircraft is perpendicular to the direction of flight and the free-stream velocity V_∞, whereas the drag is the aerodynamic force acting in direction of the airflow. The pitching moment about the lateral axis (y_a) results due to the total aerodynamic force acting at a distance to the aircraft reference point (e.g. center of gravity). Other corresponding aerodynamic moments to mention are the rolling moment about the longitudinal axis (x_a) of the aircraft and the yawing moment about the vertical axis (z_a).

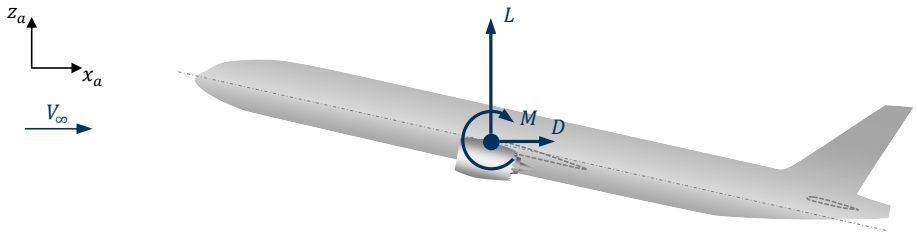

Figure 2.6 Aerodynamic forces and the resulting pitching moment acting on the aircraft.

The coefficients to describe the lift, drag and pitching moment are defined in Equations (2.1)-(2.3). These coefficients are dimensionless quantities to describe the aerodynamic characteristics of a wing or aircraft with the reference wing area S_{ref} and a reference wing chord c_{ref}. In general, the Mean Aerodynamic Chord (MAC, $\bar{c}$) of the reference wing is used as the reference chord.

$$C_L = \frac{L}{q_\infty \cdot S_{ref}} \tag{2.1}$$

$$C_D = \frac{D}{q_\infty \cdot S_{ref}} \tag{2.2}$$

$$C_M = \frac{M}{q_\infty \cdot S_{ref} \cdot c_{ref}} \tag{2.3}$$

[23] Airbus introduced the first digital fly-by-wire FCS for the A320 in 1988 (EIS), but with remaining mechanical signaling for yaw damper, rudder actuators and for the THS (as backup). With the introduction of the Airbus A380 20 years later, the last mechanical backup signaling for THS was removed (full fly-by-wire) (Maré and Fu (2017, p. 861).

The dynamic pressure q_∞ is defined in Equation (2.4) where ρ is the air density and V_∞ the flow speed of the wing (or aircraft) relative to the air. The lift generated by an airfoil (2D wing section) arises due to the pressure distribution on the top and bottom of the airfoil contour. This pressure distribution can be described by the defined pressure coefficient c_P in Equation (2.5).

$$q_\infty = \frac{1}{2} \cdot \rho \cdot V_\infty^2 \tag{2.4}$$

$$c_P = \frac{p - p_\infty}{q_\infty} \tag{2.5}$$

The total drag of a finite wing can be divided into zero-lift drag C_{D0} (lift-independent) and the induced drag C_{Di} (lift-dependent), see Figure 2.7. The zero-lift drag arise due to skin-friction forces and pressure forces, which also include the interference forces of the combined components (e.g. wing and body). A third drag element is due to compressibility effects (wave drag) varying with the Mach number, but is neglected within this thesis. Based on empirical analysis, the drag of subsonic transport aircraft can be estimated by a symmetric parabolic drag polar, see Equation (2.6). The sum of the profile or zero-lift drag[24] C_{D0} and the induced drag C_{Di}, associated with lift kC_L^2, represents a good approximation of the overall drag coefficient.

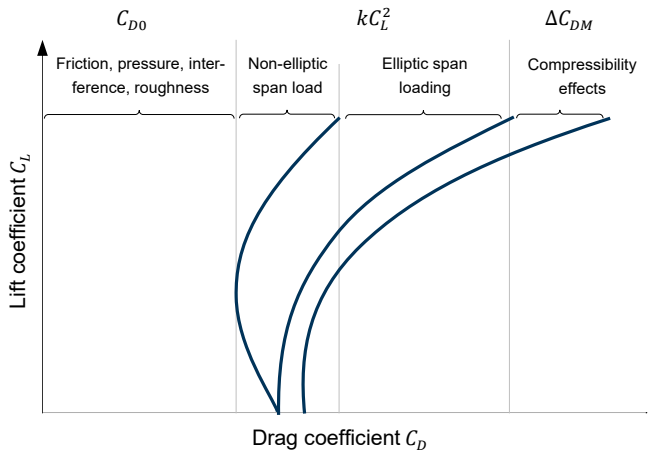

Figure 2.7 Typical drag polar and the different types of drag of a subsonic transport aircraft (Bowes, 1974, p. 4).

The induced drag factor k is calculated with Equation (2.7), where e is the efficiency or Oswald factor[25], and Λ is the wing aspect ratio. The Oswald efficiency accounts for the non-elliptic lift distribution, the increase of profile drag of the wing, and other configuration items producing induced drag (also varying with the lift coefficient) (Bowes, 1974, p. 4; Torenbeek, 1982, p. 148).

[24] Due to the general case of a non-symmetric aircraft drag polar, the real drag C_D for $C_L = 0$ is slightly higher than the (fictitious) zero-lift drag coefficient.

[25] According to Torenbeek (1982, p. 149) and Bertin and Smith (1994, p. 198), typical values for transport aircraft of the Oswald factor are between 0.6 and 0.9.

$$C_D = C_{D0} + C_{Di} = C_{D0} + kC_L^2 \tag{2.6}$$

$$k = \frac{1}{\pi \cdot e \cdot \Lambda} \tag{2.7}$$

The defined drag polar in Equation (2.6) can be used for all subsonic flight conditions of the aircraft in clean configuration. During low-speed phases with extended high-lift devices and landing gear during take-off and landing, separate and modified drag polars have to be used, see Equation (2.8). The additional drag elements $\Delta C_{D,TO}$ and $\Delta C_{D,LD}$ due to the aircraft configuration – including the flap setting and the landing gear (extended or retracted) – have to be estimated separately.

$$C_D = \begin{cases} C_{D0} + kC_L^2 & ,clean\ configuration \\ C_{D0} + k_{TO}C_L^2 + \Delta C_{D,TO} & ,takeoff\ configuration \\ C_{D0} + k_L C_L^2 + \Delta C_{D,LD} & ,landing\ configuration \end{cases} \tag{2.8}$$

Good estimation methods of the single drag elements for various configurations, which are applicable in early aircraft design phases, are presented in the book of Howe (2010, Chapter 6, pp. 139-164).

In general, transport aircraft use high-lift control systems, consisting of leading-edge and trailing-edge devices on the wing, to keep the speed in reasonable limits during takeoff and landing. The typical effects of deployed high-lift control devices on the lift curve are illustrated in Figure 2.8.

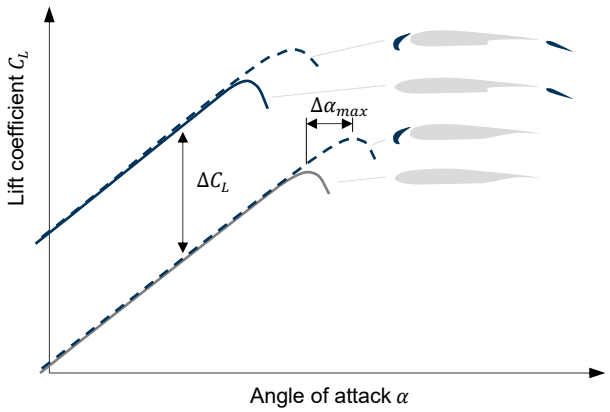

Figure 2.8 Typical effects of leading-edge and trailing-edge devices on the lift curve of the aircraft (Dam, 2002, p. 103).

The leading-edge device increases the maximum possible angle of attack α_{max}, and thus the possible maximum lift. Whereas a deployed trailing-edge device shifts the lift curve upwards and decreases the required angle of attack to reach higher lift coefficients. A semi-empirical methodology to calculate the lift and drag increments due to flap deflection is presented by Torenbeek (1982, pp. 525–565).

2.2.2 Aircraft Stability and Flight Mechanics

Commercial transport aircraft have to fulfill certain requirements in terms of stability and controllability, which are defined in the standards and regulations of the European Aviation Safety Agency (EASA) or the Federal Aviation Administration (FAA). For example, in paragraph CS 25.171 it is generally defined, that "*the aeroplane must be longitudinally, directionally and laterally stable in accordance with the provisions of CS 25.173 to 25.177. In addition, suitable stability and control feel (static stability) is required in any condition normally encountered in service, if flight tests show it is necessary for safe operation*" (European Aviation Safety Agency (EASA), 2018, p. 1-B-21). Furthermore, in paragraph CS 25.143, certain requirements on the controllability and maneuverability (handling qualities) of an aircraft are defined.

During a typical flight mission, the aircraft is most of the time in a stationary or quasi-stationary condition, in which the forces and moments do not change significantly with time. Furthermore, the aircraft is in (trimmed) equilibrium, when the sum of all forces and moments about the various axes equals zero. In general, the aircraft stability is divided into static and dynamic stability. The static stability of an aircraft is defined as the initial tendency to restore the original equilibrium state after a disturbance again. Whereas the dynamic stability defines the motion following after a disturbance of the equilibrium state of the aircraft. In order to have a dynamically stable aircraft, the motion must be positively damped to converge[26]. For a typical transport aircraft, the aerodynamic damping of the longitudinal motion is primarily achieved by the horizontal tail, and of the lateral motion by the vertical tail and the wing. (Torenbeek, 2014, pp. 339–341)

The study of flying qualities or aircraft characteristics is an extensive and complicated discipline within the aircraft design process (Torenbeek, 2014, p. 333). Therefore, it is often acceptable to linearize the equations of motion by using simplifications and approximations, especially for conventional, subsonic transport aircraft in early aircraft design phases. For the basic analysis of the aircraft during different flight phases, the aircraft can be simplified as a point-mass model and quasi-steady flight. The general forces acting on the aircraft are lift L, drag D, aircraft weight W, and thrust T. The following Equations (2.9) and (2.10) describe the general motion of an aircraft in symmetric flight in the aerodynamic axis system. The predominant thrust angle $\Delta\alpha_T$ is assumed to be very small and can be neglected. Consequently, the thrust line varies with the angle of attack α. The forces F_x are components of the external force in flightpath direction, whereas the forces F_z are perpendicular to the flightpath. Furthermore, m is the aircraft mass, dV/dt represents the tangential acceleration and the term $V\ d\gamma/dt$ represents the centripetal acceleration (due to changes of the flightpath angle).

$$\sum F_x = m \cdot \frac{dV}{dt} = T \cdot cos(\alpha) - D - W \cdot sin(\gamma) \qquad with\ W = m \cdot g \tag{2.9}$$

$$\sum F_z = -m \cdot V \cdot \frac{d\gamma}{dt} = -T \cdot sin(\alpha) - L + W \cdot cos(\gamma) \tag{2.10}$$

[26] Positively damped means, that the deviation from the equilibrium condition is reduced continuously with time.

The flightpath is defined by the flightpath angle γ and the aircraft weight W is calculated with the aircraft mass m and the gravitational acceleration g. For steady flight conditions, where the flightpath angle γ is constant ($d\gamma/dt = 0$), and without any acceleration ($dV/dt = 0$), the general equations of motion simplify to Equations (2.11) and (2.12).

$$T \cdot cos(\alpha) - D - W \cdot sin(\gamma) = 0 \tag{2.11}$$

$$T \cdot sin(\alpha) + L - W \cdot cos(\gamma) = 0 \tag{2.12}$$

The resulting balance of forces in flightpath direction and perpendicular to the flightpath respectively are illustrated in Figure 2.9. In general, during steady flight – e.g. level ($\gamma = 0$), climb ($\gamma > 0$), and descent ($\gamma < 0$) – the angle of attack is near or equal zero, and the thrust vector acts essentially in the direction of flight. With the useful assumption of $\alpha \approx 0$, the Equations (2.9) and (2.10) can be further simplified.

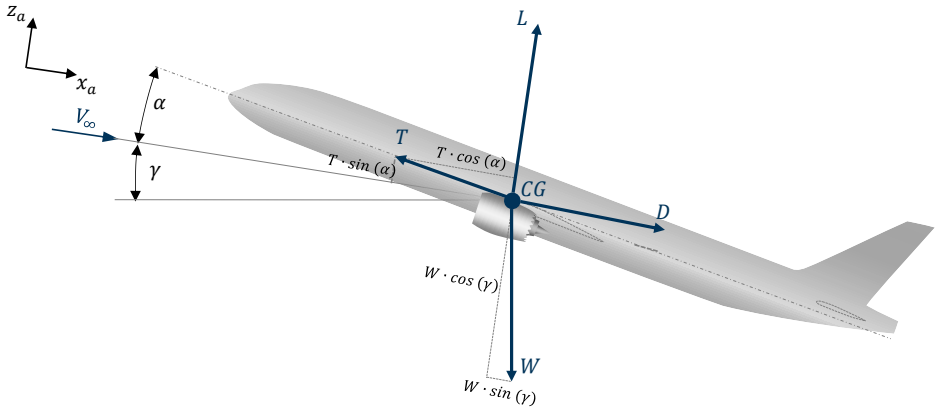

Figure 2.9 Definitions of the angle of attack α, the flightpath angle γ, and the aerodynamic forces.

If the aircraft is in trimmed equilibrium, all moments acting on the aircraft about the center of gravity (CG) are in equilibrium, and the resulting pitching moment $C_{M,CG}$ is zero. Following conditions for static stability of an aircraft can be defined, see Equations (2.13) and (2.14) (Torenbeek, 2014, p. 359).

$$\frac{dC_{M,CG}}{d\alpha} = \frac{dC_{M,CG}}{dC_L} < 0 \qquad with \ \frac{dC_L}{d\alpha} > 0 = const. \tag{2.13}$$

$$C_{M,L=0} > 0 \tag{2.14}$$

The first condition (2.13) for static stability, defines the tendency of the aircraft to restore the equilibrium by a nose-down pitching moment after positive disturbance of the angle of attack ($\Delta\alpha > 0$), or a nose-up pitching moment after a negative disturbance ($\Delta\alpha < 0$), respectively. The second condition (2.14), implies that an aircraft can only maintain a stable equilibrium with positive lift, if the zero-lift moment $C_{M,L=0}$ is tail-down. (Torenbeek, 2014, p. 359)

The slope of the moment curve, also known as the *stability margin*, can be determined for a given location of the neutral point x_{NP} of the aircraft with Equation (2.15)[27], where $\bar{c}$ is the MAC of the reference wing.

$$-\frac{dC_M}{\partial C_L} = \frac{x_{NP} - x_{CG}}{\bar{c}} \tag{2.15}$$

The stability margin is positive for a stable aircraft. This means, for a longitudinal static stability, the position of the center of gravity must always be forward of the neutral point. According to Torenbeek (2014, p. 367), for a conventional subsonic aircraft, a stability margin of at least 5 to 10% of the MAC is desirable.

2.2.3 Aerodynamic Modelling

In this thesis, several aerodynamic modelling methods are used or combined for rapid aircraft or wing configuration analysis, suitable within early aircraft design. This section intends to provide a brief overview of different modelling methods for aircraft aerodynamics and points out the capabilities and limitations of each.

Vortex-Lattice Method (VLM). The vortex-lattice method (VLM) is a numerical method for the calculation of incompressible flow over finite wings. VLM is an enhancement of the Prandtl's classical lifting-line theory to predict the aerodynamic properties of a finite wing. In the following, to understand the basics and limitations of the VLM, a brief overview of the foundations of incompressible flow over airfoils and finite wings is given. The Laplace-Equation (2.16) describes the condition of an inviscid, incompressible and irrotational flow, defined as the velocity potential Φ (*potential flow theory*) (Schlichting and Truckenbrodt, 1967, p. 50). Since this flow is governed by the linear Laplace's equation, a complicated flow pattern for an irrotational and incompressible flow can be added by a number of elementary flows[28] that are also irrotational and incompressible (Bertin and Smith, 1994, pp. 73–77).

$$\nabla^2\Phi = \frac{\partial^2\Phi}{\partial x^2} + \frac{\partial^2\Phi}{\partial y^2} + \frac{\partial^2\Phi}{\partial z^2} = 0 \qquad with\ \Phi = \Phi(x, y, z) \tag{2.16}$$

The aerodynamic consideration of a wing could be generally split into the study of a wing section or airfoils (2D) and the study of the modifications of the properties for a finite wing (3D) (Anderson, 2011, p. 297). To solve the Equation (2.16) of the flow over an airfoil (2D), two sets of boundary conditions have to be applied (Anderson, 2011, p. 225): the *infinity boundary conditions* and the *wall boundary conditions*. The first set of boundary conditions describe the flow pattern in all direction far away from the airfoil (infinity) to approach the uniform freestream conditions. The second set describes the wall tangency condition of the velocity vector. This means, that the contour of the airfoil (top and bottom) is a streamline of the flow (Bertin and Smith, 1994, p. 77).

[27] The larger the static stability margin, the more stable the aircraft. Or, if the center of gravity shifts backwards (in direction of the neutral point), the stability margin decreases.

[28] An overview and combination of elementary flows (uniform flow, source flow, doublet flow, vortex flow) is given in Schlichting and Truckenbrodt (1967, pp. 54–71), Bertin and Smith (1994, pp. 78–84) or Anderson (2011, pp. 227–248).

Based on these fundamental definitions, complex flows around lifting surfaces can be synthesized by vortex flow in combination with other superimposed elementary flows, which enables the calculation of finite lift (Schlichting and Truckenbrodt, 1967, p. 72; Anderson, 2011). The vortex flow is described by circulation Γ, which specifies the strength of the vortex flow. According to the *Kutta-Joukowski theorem*, the resulting lift L' (per unit span) over an airfoil is directly proportional to the circulation around the airfoil, see Equation (2.17) (Bertin and Smith, 1994, p. 97).

$$L' = \rho_\infty \cdot V_\infty \cdot \Gamma \tag{2.17}$$

To calculate the aerodynamic characteristics of airfoils, a vortex sheet formed of side-by-side vortex filaments, is distributed over the airfoil contour. For thin airfoils, the distributed vortices on top and bottom of the airfoil can be approximated by a single vortex sheet distributed on the camber-line of the airfoil. Additionally, the Kutta condition is applied, which results in a flow leaving smoothly at the trailing-edge (Anderson, 2011, pp. 312–316). However, this vortex sheet method is limited to airfoils or infinite wings.

The incompressible flow over finite wings (3D) consequently leads to a three-dimensional flow, due to the flow around the wing tips from the high-pressure region (bottom) to the low-pressure region (top). This leads to a flow in spanwise-direction and thus to a curvature of the streamlines over the top and bottom of the wing, see Figure 2.10a-b. The resulting trailing wing-tip vortices of the wing induces small downward velocity components w_i at the wing itself, see Figure 2.10c. This phenomenon is called downwash, which results in a smaller, effective angle of attack α_e at a local wing section (airfoil). In addition to this, induced drag D_i arises, as there is a component of the local lift vector in the direction of the infinite flow V_∞.

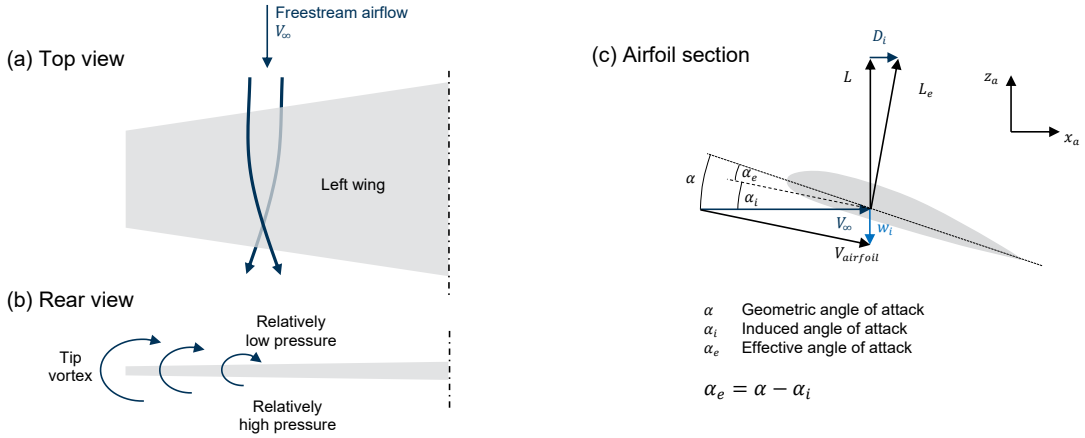

Figure 2.10 Schematic of a finite wing with three-dimensional flow (left) and the downwash effect on the local flow over an airfoil section (right) (based on Bertin and Smith (1994, p. 237 and p. 241).

Prandtl's classical lifting-line theory was the first practical method to calculate the aerodynamic properties of a finite wing and represents the fundamentals of the numerical VLM (Anderson,

2011, p. 404). In the lifting-line theory, the finite wing is replaced by an infinite number of horseshoe vortices[29] along the so-called lifting line; leading to a continuous distribution of the circulation (vortex strength) $\Gamma(y)$, and thus to induced velocities in arbitrary points by each vortex filament, according to the Biot-Savart Law (Bertin and Smith, 1994, p. 261). The main results of the lifting-line theory for a wing with finite span b are given by the following Equations (2.18)-(2.21). The total lift of the wing is calculated by integration of the continuous circulation distribution function $\Gamma(y)$ in spanwise direction, see Equation (2.18) and (2.19).

$$L = \rho_\infty \cdot V_\infty \cdot \int_{-\frac{b}{2}}^{\frac{b}{2}} \Gamma(y) dy \tag{2.18}$$

$$C_L = \frac{2}{V_\infty \cdot S_{ref}} \cdot \int_{-\frac{b}{2}}^{\frac{b}{2}} \Gamma(y) dy \tag{2.19}$$

The induced drag and induced drag coefficient are generally calculated analogue to the lift with considering the induced angle α_i and the assumption of $\sin(\alpha_i) \approx \alpha_i$ for small angles, see Equations (2.20) and (2.21).

$$D_i = \rho_\infty \cdot V_\infty \cdot \int_{-\frac{b}{2}}^{\frac{b}{2}} \Gamma(y) \alpha_i(y) dy \tag{2.20}$$

$$C_{D,i} = \frac{2}{V_\infty \cdot S_{ref}} \cdot \int_{-\frac{b}{2}}^{\frac{b}{2}} \Gamma(y) \alpha_i(y) dy \tag{2.21}$$

The lifting-line theory gives reasonable results for straight wings, but is inappropriate for swept wings or wings with complex geometries. In this case, the more sophisticated Vortex Lattice Method (VLM) is more suitable. The VLM superimpose a finite number of horseshoe vortices of different vortex strength Γ_n (*circulation*). Therefore, the lifting surface is divided into a number of panels in spanwise and chordwise direction (*lattice*). In each panel of the lattice a horseshoe vortex is placed on the quarter-line and a *control point* is placed at three-quarter-chord location of the panel. This principle is schematically illustrated in Figure 2.11. At any control points of the panels, the flow-tangency condition[30] is applied and a system of linear equations results. This set of linear equations with the unknown strengths Γ_n of each horseshoe vortex can be solved, and finally the total lift, induced drag and pitching moment of the aircraft can be calculated.

[29] A horseshoe vortex consists of a bound vortex and two free-trailing vortices downstream of the wing to infinity. This is due to the Helmholtz's theorem, that a vortex filament cannot end in the fluid, see Bertin and Smith (1994, pp. 238–239) and Anderson (2011, pp. 404–405).

[30] Note: The normal component of the induced velocity of all panel vortices are equal to the normal component of the freestream velocity and the resulting normal component of the velocity at the control point is zero. This fulfills the wall boundary condition and the airfoil/surface contour (top and bottom) is treated as streamline of the flow.

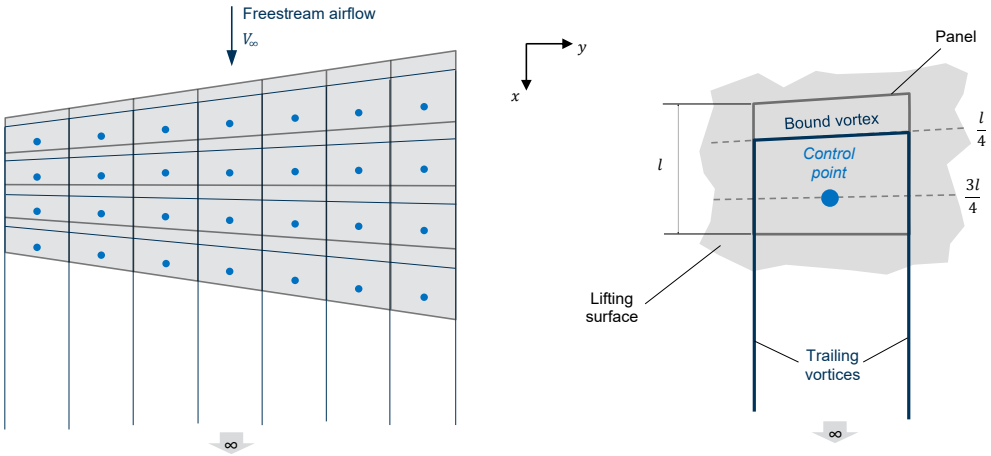

(a) Vortex-lattice system of a wing (top view) (b) Detail: Single horseshoe vortex

Figure 2.11 Schematic of a lifting surface with a typical vortex-lattice system (left) and details of a single panel with horseshoe vortex and control point (right).

Athena Vortex Lattice (AVL). Based on the presented background of VLM, the Athena Vortex Lattice[31] (AVL) tool used in this thesis can be introduced. AVL is based on an extended, linear VLM and can calculate the 3D aerodynamics of finite-wing configurations. In addition to this, it is possible to consider flight control surfaces and deflections at the leading edge and trailing edge of lifting surfaces (e.g. wings). AVL shows good aerodynamic results within the linear region of the lift slope. The calculation results include the total forces and moments, derivatives of forces and moment coefficients with respect to freestream, rotation and control deflections. In addition, Trefftz-plane[32] analysis of lift-distribution, induced drag and downwash are possible. Furthermore, trim calculations for different constraints can be performed (Drela and Youngren, 2017a).

AVL is widely used in the community and validated. Recent examples of studies including transport aircraft wings and AVL are listed below:

- The German Aerospace Center (DLR) calculated the aerodynamic loads with AVL for an early wing mass estimation method. The aerodynamic results of a transport aircraft with deflected trailing edge devices show good accordance to the results of a high-fidelity CFD calculation. (Dorbath *et al.*, 2012)
- In a work conducted at NASA Langley Research Center, AVL is used in a semi-empirical approach to calculate the 3D aerodynamics of a transport aircraft in high-lift configuration; the results were successfully validated with experimental data. (Olson, 2015)
- In another work at NASA, 3D aerodynamic results of AVL and experimental data of transport aircraft wing show good agreement. (Fujiwara and Nguyen, 2015)

For the aerodynamic calculation of fuselages or engine nacelles, the Slender-Body Theory (SBT) can be used. SBT can be applied where the variation of the body dimensions in flight direction (airflow direction) is small and only small perturbation of the (axial) velocity are assumed and

[31] AVL is freely available online at: https://web.mit.edu/drela/Public/web/avl/ (last accessed in November 2018).
[32] A plane, located downstream, far behind the wing ($x \to \infty$) and perpendicular to the wake, is a so called *Trefftz-plane*.

consequently neglected (Thomas and Nerney, 1976) [33]. In AVL, bodies are modelled via superposition of the elementary flows of sources and doublets, and the resulting forces and moments are consistent with SBT. Nevertheless, as the experience is relatively limited, the modelling and results of bodies should be done with caution (Drela and Youngren, 2017b).

2.3 Flight Control Systems

The Flight Control System (FCS) has a strong physical interaction with airframe and structure, and significant information-based integration into avionics and mission systems. Accordingly, the FCS can be divided into *configuration* and *architecture*, as illustrated in Figure 2.12 (Lampl *et al.*, 2017c). The configuration describes the layout of the FCS, including the type, allocation and positioning of flight control devices. Also, the kinematics and support, fairings, and airframe integration aspects are associated to the configuration. The architecture represents the heart and brain of the FCS and defines the number of the flight control computers and their assignment to dedicated flight control devices. Also, linkage, actuation and redundant distribution of the power supply is attributed to the architecture.

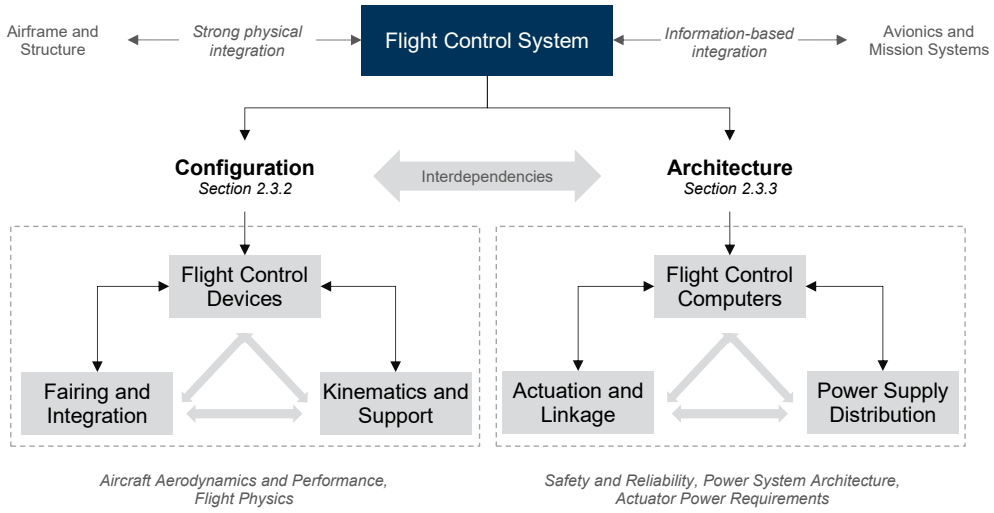

Figure 2.12 Breakdown of a flight control system into configuration and architecture with strong interdependencies at system level and sub-system level.

Today's commercial transport aircraft have full fly-by-wire (FBW) flight control systems with automatic control features, envelope protections, and control laws for safety enhancement. Since the FCS is a safety critical system, very stringent dependability requirements in terms of safety and availability must be considered and the design of hardware and software should be fault-tolerant (Brière and Traverse, 1993). For commercial transport aircraft, dedicating standards and regulations are defined in CS-25 (European Aviation Safety Agency (EASA), 2018) and FAR 25 (Federal Aviation Administration (FAA), 2019).

[33] Thomas and Nerney (1976) successfully combined the vortex-lattice theory and the slender-body theory for the analysis of wing-body configurations and suggested further extensions of that method.

2.3.1 Principles of Flight Control

The main task of the FCS of commercial transport aircraft is the directional control of the aircraft around the longitudinal, lateral, and vertical axes. Further important tasks are high-lift control during low speed phases and trim control. The flight control devices for directional control (e.g. aileron, elevator, and rudder) are flight-critical and continuously activated to maintain safe attitude and trajectory control of the aircraft. The high-lift control devices at the wing leading-edge and trailing-edge are classified as less critical from the standpoint of safe flight control (Raymond and Chenoweth, 1993, p. 9), nevertheless they are essential for the sizing, performance and efficiency of transport aircraft[34]. Figure 2.13 shows the flight control configuration of the Airbus A320 with typical flight control devices and dedicated flight control functions. Most flight control devices on the aircraft – ailerons, slats, flaps, rudder, and elevator – fulfill only a single control function. In contrast, the spoilers on the wing fulfill or support several functions[35]: air brake, roll control, lift dump, active load control.

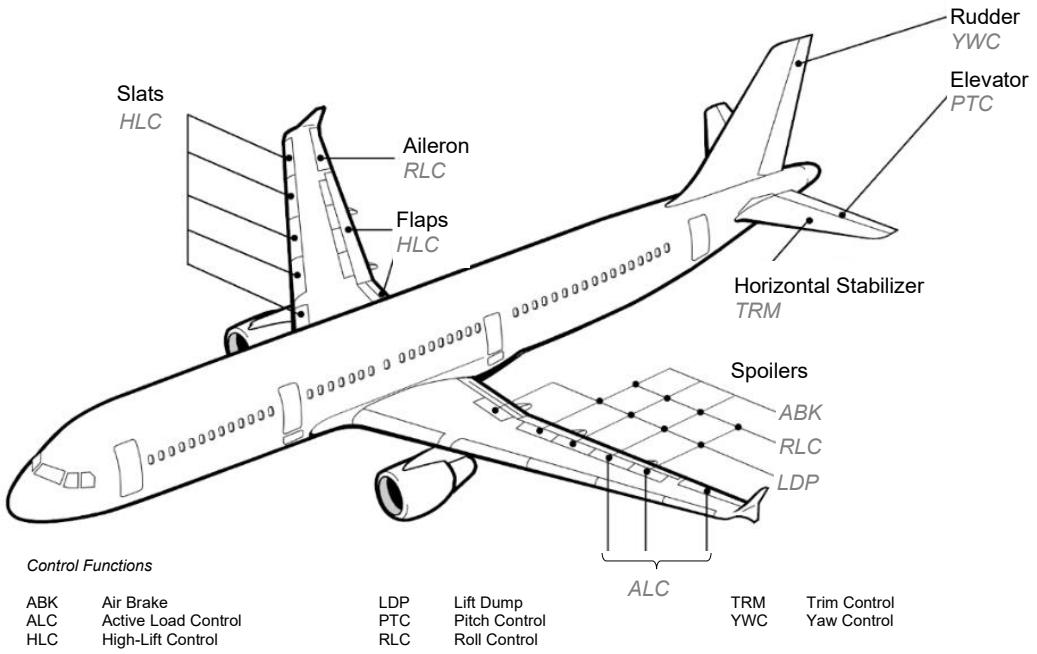

Figure 2.13 Overview of the flight control configuration with dedicated functions of the Airbus A320.

The flight control functions can be classified as flight-critical or less-critical control functions to enable a safe flight. Table 2.1 gives an overview of the basic flight control functions and the corresponding flight control devices in addition to the required characteristics. In this work, all movables, control surfaces and technologies which are providing or supporting flight control functions are defined as *flight control devices*.

[34] In the literature, flight-critical control devices are generally referred to as *primary flight controls*. Whereas less flight-critical or non-flight-critical control devices are generally referred to as *secondary flight controls*. However, in this work and the presented design methodology, this distinction is of minor importance.

[35] Accordingly, spoilers are *multifunctional* flight control devices *by multifunctional use*.

Table 2.1 Overview of basic flight control functions and typical flight control devices.

Flight Control Function(s)	Flight Critical	Control Device(s)	Location	Characteristics
Roll control (RLC)	yes	Ailerons	Wing (L/R)	Unsymmetrical (L/R) deflections up/down
Pitch control (PTC)	yes	Elevators	Empennage	Symmetrical (L/R) deflections up/down
Yaw control (YWC)	yes	Rudder	Empennage	Deflections left/right
Trim (TRM)	no	Horizontal stabilizer	Empennage	Move (rotate) up/down, discrete positions
High-lift control (HLC)	no	Leading-edge (slats) Trailing-edge (flaps)	Wing (L/R)	Fowler motion/deflections down, defined positions (settings) only
Airbrake (ABK) *Lift Dump (LDP)*	no	Spoiler	Wing (L/R)	Coordinated (L/R) deflections up

The simplified, electrically signaled flight control system illustrated in Figure 2.14 shows the system boundaries of the defined flight control *configuration* and the system *architecture* (cf. Figure 2.12). Within the system architecture, the Flight Control Computers (FCCs) interpret the pilot inputs and electrical signals command the actuation system to actuate the flight control devices as necessary. The actuation system is supplied by the power generation and distribution system, providing electrical, hydraulic and pneumatic power. The resulting aircraft response due to actuated flight control devices is monitored by several sensors and air data probes, which provide a feedback to the flight control computers and to the pilot or autopilot. Summarized, the main purpose of the FCS architecture is to translate the commands of the pilots or autopilot into a demand for power to drive the actuators of the flight control devices.

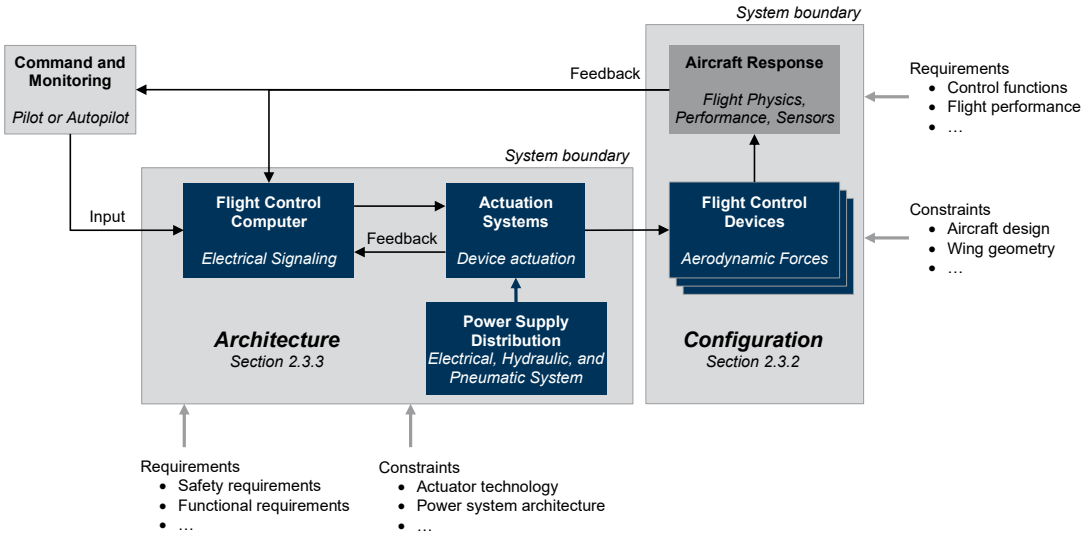

Figure 2.14 Simplified schematic of a flight control system with defined system boundaries of the architecture and configuration.

The top-level design drivers of the FCS are safety, structural limitations, flight envelope, and flight performance of the aircraft. In addition, many different requirements at system level must be considered. Constraints for the flight control configuration design arise primarily from the aircraft and wing geometry. Whereas available actuator technologies and the aircraft power system architecture restrict the FCS architecture design space.

2.3.2 Flight Control Configuration and Devices

The flight control configuration defines the allocation and positioning of different flight control devices, including the required kinematics and integration aspects (cf. Figure 2.13). In general, the selection, arrangement and sizing of the flight control devices on the wing is directly influenced by the overall wing design[36] in addition to the required flight performance and handling qualities of the aircraft during certain flight phases. For commercial transport aircraft, the flight control devices are typically located at the wing and the empennage[37].

Figure 2.15 shows the flight control configurations of the Airbus A350 and the Boeing 777 in comparison. The roll control function of the Boeing 777 is primarily fulfilled by an outboard aileron and an inboard flaperon, with optional support of the spoilers. Furthermore, the wing configuration (area, camber) can be modified by the extendable high-lift control devices at the leading and trailing edge – supported by drooped ailerons and flaperons – to generate the necessary lift during low speed phases. In comparison, the flight control configuration on the A350 wing is similar. However, the configuration mainly differs in two points: First, the roll control architecture is completed by four segmented ailerons at the outboard of the wing and the spoiler (supportive function) and there are no inboard flaperons (or ailerons). Second, the high-lift control system features a droop nose at the wing leading edge, and Advanced Dropped Hinge Flaps (ADHF) at the inboard and outboard trailing edge, which are simple, low complex solutions. For both, the A350 and B777, the pitch and yaw control function are enabled by a single rudder at the vertical stabilizer and two independently moving elevators (left and right) on the Trimmable Horizontal Stabilizer (THS) (not shown in the figure).

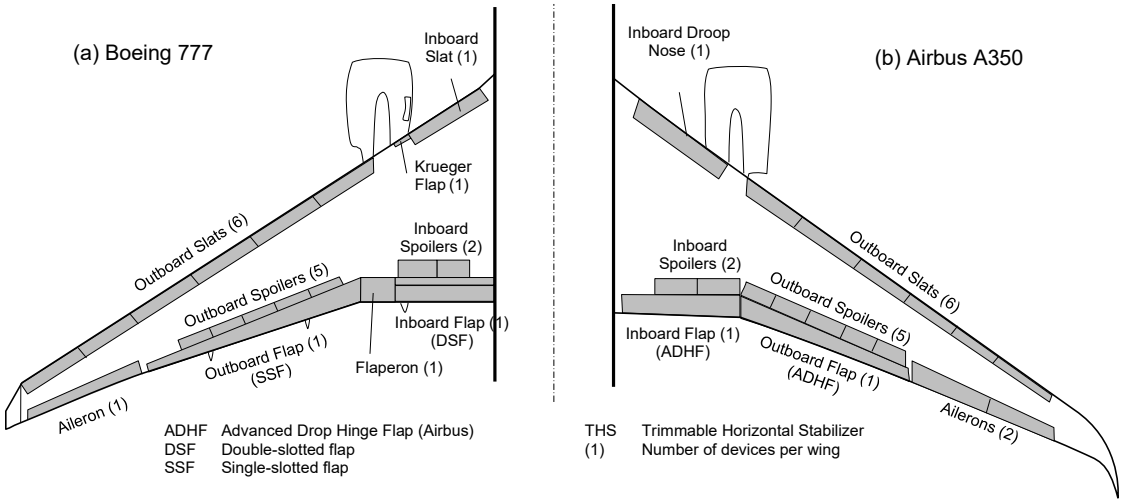

Figure 2.15 Flight control configurations of the Boeing 777 and the Airbus A350 (wing only).

[36] The overall wing design (e.g. area, sweep, aspect ratio …) of transport aircraft is primarily driven by the required flight performance during cruise (cruise speed and altitude) (Reckzeh (2003, p. 109)).

[37] For example, the regional jet British Aerospace BAe 146 (since 1993 Avro RJ) features two large control surfaces at the rear of the fuselage which are used as airbrakes, enabling steeper approach angles if required (Velupillai (1981)). Another example is an extendable flap on top of the fuselage of a fighter, which is used as an airbrake (e.g. Eurofighter Typhoon, McDonnell Douglas F/A-18 Hornet).

The flight control configurations of modern airliners are very similar due to the typical aircraft design consisting of a fuselage, swept wing and an empennage with a horizontal and vertical stabilizer. That's why the (wing) flight control configurations of recent airliners are very similar and innovative solutions or new technologies are generally introduced on system or device level. Nevertheless, the segmentation and combination of different types of flight control devices lead to several configuration options. Table 2.2 gives an overview of the flight control configurations on the wing of recent transport aircraft of Airbus and Boeing. The flight control devices are located at the wing's leading and trailing edge, and on top of the wing. A substantial part of the wing is used for the high-lift control system. As mentioned in the introduction, high-lift control systems consists of relatively large and heavy control devices, with complex kinematic requirements (e.g. fowler motion[38]). Typical high-lift control devices[39] used on airliners are the slat, Krueger flap, and droop nose at the wing leading edge, and Single-Slotted Flap (SSF), Double-Slotted Flap (DSF) and Advanced Dropped Hinge Flap (ADHF) at the wing trailing edge. To minimize the drag, aerodynamic fairings cover the relatively large flap-panel linkages and supports. Consequently, the main design tradeoff is to find a low complexity high-lift system with good aerodynamic performance.

Table 2.2 Overview of the wing flight control configuration of Airbus and Boeing aircraft (selection).

	Aircraft Data		Wing Data		Leading-Edge Devices*		Trailing-Edge Devices*		Wing Top Devices*	
Aircraft Type	EIS (year)	MTOM (kg)	Area (m²)	Span (m)	IB	OB	IB	OB	IB	OB
Airbus										
A310-300	1985	150000	219.0	43.90	1 SL	2 SL	1 DSF, 1 TG	1 SSF, 1 ALN	2 SPL	5 SPL
A320-200	1987	73500	122.4	33.91	1 SL	4 SL	2 SSF	1 SSF, 1 ALN	1 SPL	4 SPL
A321-200	1996	89000	126.4	33.91	1 SL	4 SL	1 DSF	1 DSF, 1 ALN	1 SPL	4 SPL
A330-300	1992	230900	363.1	60.30	1 SL	6 SL	1 SSF	1 SSF, 2 ALN	1 SPL	5 SPL
A340-600	2002	368000	439.4	63.45	1 SL	6 SL	1 SSF	1 SSF, 2 ALN	1 SPL	5 SPL
A350-900	2014	268000	432.1	64.75	2 DN	6 SL	1 ADHF	1 ADHF, 2 ALN	2 SPL	5 SPL
A380-800	2007	569000	846.0	79.75	2 DN	6 SL	1 SSF	2 SSF, 3 ALN	2 SPL	8 SPL
Boeing										
737-800	1998	79002	124.6	35.8	2 KF	4 SL	1 DSF, 1 TG	1 DSF, 1 ALN	1 SPL	5 SPL
747-400	1988	396830	525.0	62.3	3 KF	11 KF	1 TSF, 1 FLN	1 TSF, 1 ALN	2 SPL	4 SPL
747-8	2012	447696	554.0	68.4	2 KF	11 KF	1 DSF, 1 FLN	1 SSF, 1 ALN	2 SPL	4 SPL
757-300	1999	122470	185.3	38.05	1 SL	4 SL	1 DSF, 1 TG	1 DSF, 1 ALN	2 SPL	4 SPL
767-300	1986	156489	283.3	47.57	1 SL	5 SL	1 DSF, 1 FLN	1 SSF, 1 ALN	2 SPL	4 SPL
777-300ER	2004	351535	436.8	64.8	1 SL	6 SL	1 DSF, 1 FLN	1 SSF, 1 ALN	2 SPL	5 SPL
787-8	2011	227930	377.0	60.12	1 SL	5 SL	1 SSF, 1 FLN	1 SSF, 1 ALN	3 SPL	4 SPL

ADHF	Advanced Drop Hinge Flap	IB	Inboard (wing)	TG	Thrust Gate	* All shown device numbers are per wing side	
ALN	Aileron	KF	Krueger Flap	TSF	Triple-Slotted Flap		
DN	Droop Nose	OB	Outboard (wing)	SPL	Spoiler		
DSF	Double-Slotted Flap	SL	Slat				
FLN	Flaperon	SSF	Single-Slotted Flap				

[38] The fowler motion describes the rearward and downward extension of a flap panel, increasing the area and camber of the wing.

[39] A comprehensive review of different high-lift control system designs of subsonic airliners, including the characteristic functions and design criteria of possible leading-edge and trailing-edge devices can be found in the report of Rudolph (1996).

The design space for the flight control configuration is generally limited due to several distances and gaps by design, as illustrated in Figure 2.16. Additionally, the chordwise extensions of the high-lift devices are limited by the location of the front-spar and rear-spar (wing stiffness and fuel tank volume). Typical values for the chord of leading-edge devices are 15-20% of the local wing chord, and 25-35% of the local wing chord for trailing-edge devices (Torenbeek, 2013, pp. 346–347).

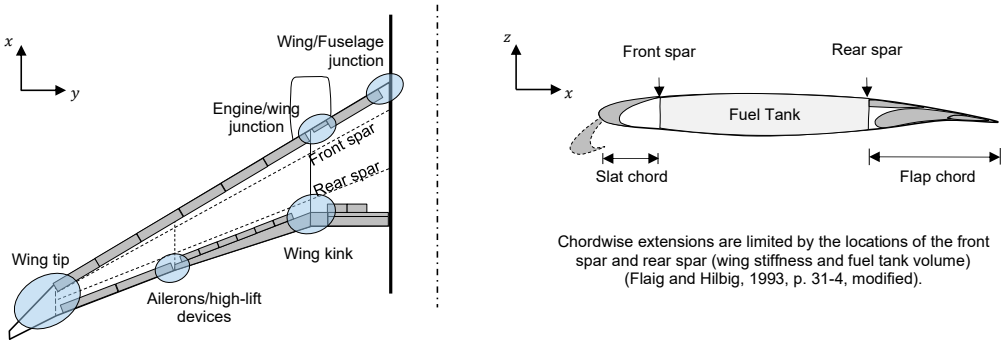

Figure 2.16 General constraints and limitations of the flight control configuration on the wing.

Summarized, the study of existing flight control configurations and devices has revealed the following main design aspects, constraints and limitations:

- At the wing trailing-edge the ailerons and high-lift control system have to share the available space alongside the span.
- The required performance for roll control and the geometric constraints of the wing, mostly defines the (minimum) size of the main roll control devices. For a first guess, it is recommended to allocate about one third of the wing trailing edge for the roll control devices (ailerons). The remaining space is available for the outboard and inboard high-lift trailing-edge devices. Additionally, span-wise discontinuities of the high-lift control devices should be avoided, to achieve maximum aerodynamic efficiency.
- The spoilers are generally located on top of the wing and in front of the trailing-edge devices of the high-lift control system.
- The design problem at the leading edge is reduced to the sizing, segmentation and the selection of the type of leading-edge devices of the high-lift control system, as they are the only flight control devices at the wing leading edge[40].
- Additionally, strakes at the engine nacelles or small Krueger-flaps at the engine pylon can locally improve the flow pattern behind the engine/wing-junction.

Summarized it can be said that the final flight control configuration should be *"[…] understood as the best achievable compromise between the requirements from all interacting disciplines, which has to be developed in an iterative design process"* (Reckzeh, 2003, p. 109).

[40] Nevertheless, it should be considered that the maneuverability of the aircraft should be available as long as possible during low-speed phases. In general, this is achieved by continuously reducing the wing angle of incidence towards the wing tip (washout), which should keep the ailerons at the outboard of the wing effective. The aerodynamic performance of the leading-edge devices should not counteract that effect.

2.3.3 System Architecture and Actuation

The FCS architecture, in terms of number of actuators, distribution of the power supply and Flight Control Computer (FCC), is primarily driven by safety considerations (Traverse *et al.*, 2004, p. 193; Goupil, 2011, p. 524). The fault tolerance and fault detection are key points in the design of FCS architectures to withstand single or multiple failures, while maintaining the necessary level of safety (Goupil, 2011, p. 524). For example, the complete loss of power supply for the flight control actuation systems should be extremely improbable (failure rate $< 10^{-9}$ per flight hour). For that reason, a minimum of three independent power sources for the actuation of the flight control devices fulfilling flight-critical control functions are required, considering the current reliability of secondary power generation and distribution systems (Bossche, 2006, p. 2).

In general, there are different philosophies regarding the fly-by-wire FCS architecture of different manufacturers[41]. To understand the main design principles of the FCS architectures, the Airbus A320 should again serve as a representing example, see Figure 2.17 and Figure 2.18. The electrical signaling of the actuators is done over two primary flight control computers (PFCC) and three secondary flight control computers (SFCC), with a defined reconfiguration order for automatic management following a failure. The signals for the high-lift control systems are provided by two high-lift control computers (HLCC). Each FCC controls and monitors the assigned actuators, or the drive systems of the high-lift control systems, respectively. The evolution of Airbus fly-by-wire FCC from the A320 to the A350 show slightly different numbers and notations of the FCC. Nevertheless, the principle of the configuration of primary and secondary FCC remains the same (Moir and Seabridge, 2008, p. 39; Lammering and Weber, 2013, p. 131).

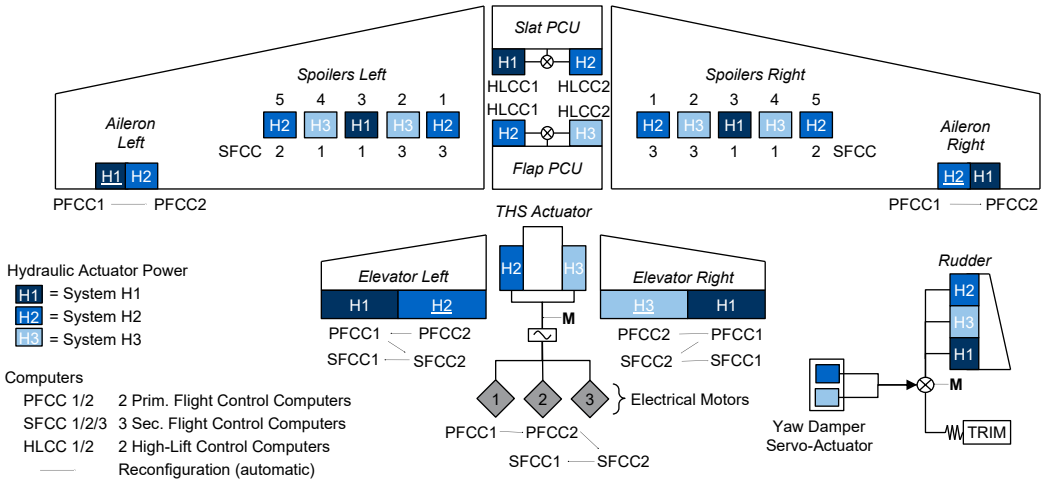

Figure 2.17 Flight control system architecture of the Airbus A320 (Wild, 1990, p. 112).

The three redundant hydraulic systems[42] provide hydraulic power to the servo-valve controlled hydraulic actuators (SHA). The defined distribution of the hydraulic systems and assignment of the actuators to the flight control devices still enables a safe operation of the FCS in the case of a

[41] Lammering and Weber (2013) give a good overview and brief explanation of the main differences between the Airbus, Boeing, and Liebherr-Aerospace approach for the fly-by-wire FCS architecture design.

[42] Usually, the hydraulic systems are defined as Blue, Green, and Yellow (Airbus) or Left, Center, and Right (Boeing). In this study, a more general notation is used and the hydraulic systems are defined as H1, H2, and H3.

failure of one or two hydraulic systems. The main flight control devices responsible for flight-critical control functions are actuated by two (aileron, elevator) or three actuators (one-part rudder). The spoilers are each actuated by a single actuator. The slats and flaps of the high-lift control system are powered over two central Power Control Units (PCUs) and a mechanical transmission shaft system.

The main design requirements of the high-lift system architecture of commercial transport aircraft is to assure synchronous setting[43] and to avoid asymmetric flap and slat deflections. Consequently, conventional system architectures with central PCUs and mechanical transmission shaft were established (cf. Figure 2.18). The PCUs consist of two hydraulic motors and are supplied by the hydraulic power circuits H1, H2 or H3. Drive Gear Boxes (DGB) and Rotary Actuators (RA), driven by the mechanical transmission shaft, extend and retract the slats and flaps. Additionally, right-angle gearboxes and kink gearboxes at the wing kink are necessary for larger direction changes of the transmission shaft (not shown in the figure). Wing Tip Brakes (WTB) prevent asymmetric operation, runaway or overspeed of the high-lift control devices. Asymmetric operation is detected by Position Pick-up Units (PPU) at the wing tips, which are also used for system monitoring.

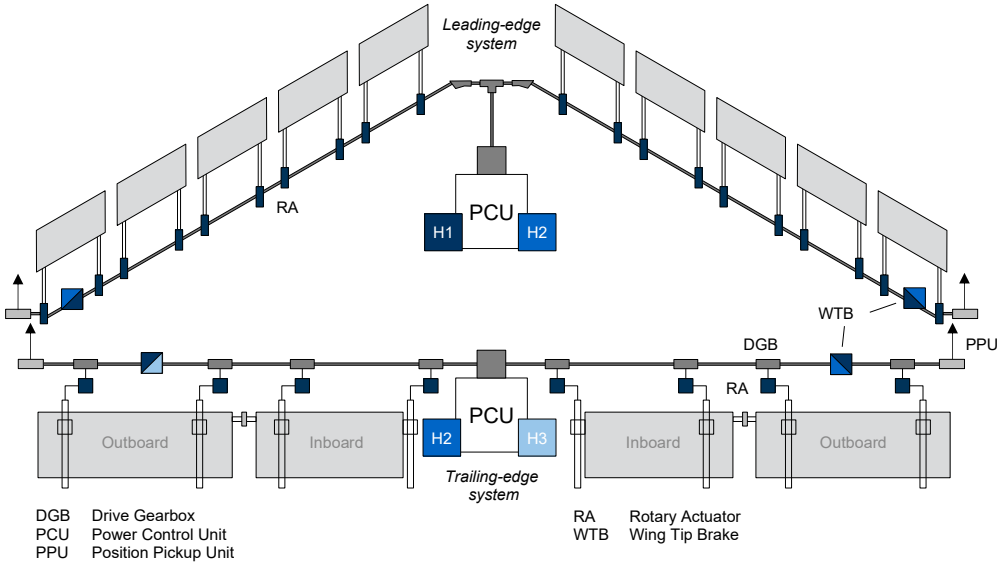

Figure 2.18 High-lift control system architecture of the Airbus A320 (Wild, 1990, p. 117).

According to Recksiek (2009, p. 51), this type of architecture requires high design-engineering and installation effort, and prohibits functional flexibility. Further improvements regarding functional enhancement, system mass, maintenance costs, and assembly are expected by high-lift control systems with distributed electrical actuation (Bennett *et al.*, 2005; Recksiek, 2009; Lampl *et al.*, 2017a).

[43] According to CS25.701a: *"Unless the aeroplane has safe flight characteristics with the flaps or slats retracted on one side and extended on the other, the motion of flaps or slats on opposite sides of the plane of symmetry must be synchronised by a mechanical interconnection or approved equivalent means."* (European Aviation Safety Agency (EASA)).

In recent years, the actuation for aerospace applications made significant steps forward, due to the extensive introduction of electrical technologies. The application of electric actuation technologies, also for safety-critical FCS, offers new opportunities and enables performance improvements at aircraft and system level (Maré and Fu, 2017, p. 857). However, while the electrical signaled actuators or Fly-By-Wire (FBW) is well established for modern transport aircraft[44], the use of Power-by-Wire (PBW) for FCS actuation just started to appear[45].

Today, four different types of actuators are generally used for flight control actuation on modern transport aircraft, see Figure 2.19 and Table 2.3. The actuators mainly differ in type of power supply and actuation drive unit. The default actuator used is the Servo-valve Hydraulic Actuator (SHA), see Figure 2.19a. The SHA is electrically signaled, which are processed by the Actuator Control Electronics (ACE) to command the servo valve, which controls the power to move the hydraulic ram. This allows a sophisticated interface between the electrical FCS and the actuation. An evolutionary electrical development is the Electro-Hydrostatic Actuator (EHA), which combines the advantages of both electrical power (on demand) and hydraulic actuation, Figure 2.19b. The EHA is supplied by 3-phase AC power to feed the power electronics. The power electronics drives a variable speed motor, which further drives a local hydraulic pump in a self-contained unit.

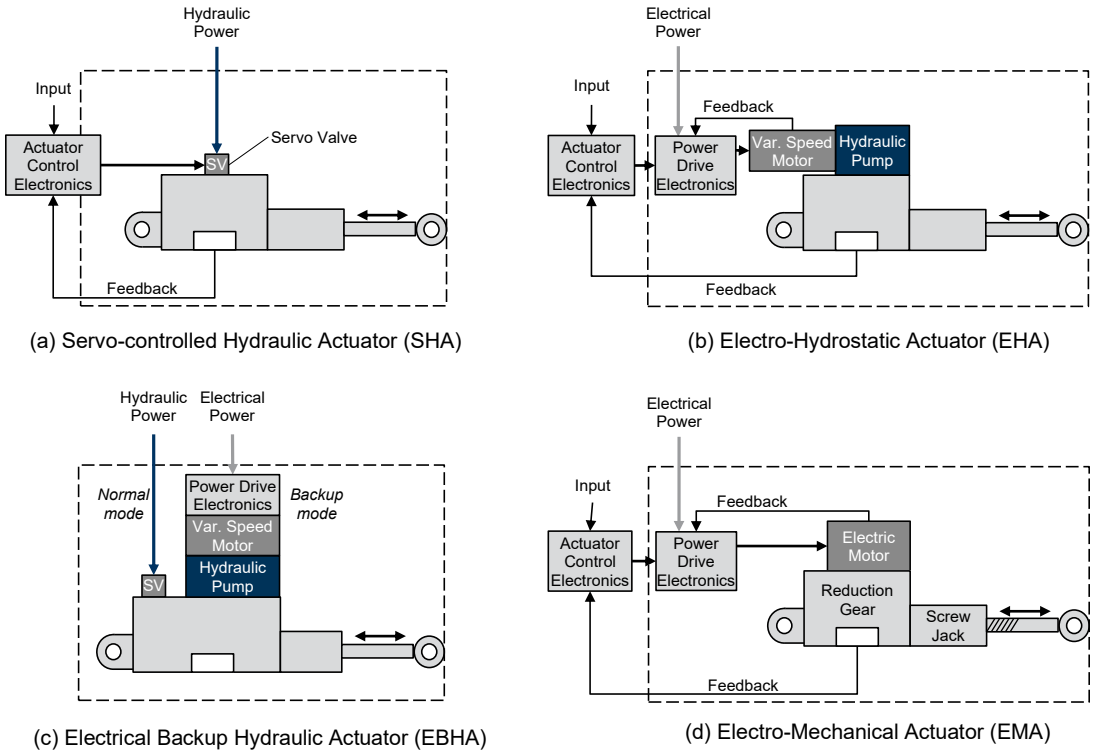

Figure 2.19 Schematics of different actuator types used for flight control actuation of modern transport aircraft (Moir and Seabridge, 2008, pp. 31–33 and p. 44).

[44] The first electrical flight control system (analog, full-authority system for all flight controls, mechanical back-up system) for civil transport aircraft was installed on the Concorde in 1969. In 1988, the first full (digital) fly-by-wire system was introduced by Airbus with the A320.

[45] The Airbus A380 (EIS 2007) and the Airbus A350 (EIS 2015) are the only commercial transport aircraft which are partly using electrically powered actuators (EHA and EBHA) for flight controls.

The Electrical Backup Hydraulic Actuator (EBHA) combines the features of a conventional SHA (primary) and an EHA (backup), see Figure 2.19c. The EBHA has the same performance as an SHA in the hydraulic (normal) mode, but a reduced deflection rate in the electrical (backup) mode. The EMA directly converts the electric energy into mechanical motion. Therefore, the electro-hydraulic actuator of the EHA is replaced by an electric motor and a gearbox to move a screwjack actuator, see Figure 2.19d. The biggest disadvantage of the EMA is a certain single-point failure leading to a mechanical jam. According Botten *et al.* (2000, p. 57), the use of additional devices to reduce or avoid this failure mode increases complexity, weight and costs. For these reasons, EMAs are still not used for flight-critical applications of commercial transport aircraft.

Table 2.3 Overview of the main flight control actuator types of modern transport aircraft (based on Moir and Seabridge (2008, p. 34)).

Actuator Type	Power Source	Drive Unit	Actuation	Flight Controls
Servo-valve Hydraulic Actuator (SHA)	Hydraulic System	Hydraulic fluid (SV controlled)	Hydraulic actuator	Aileron, Elevator, Rudder, Spoiler
Electro-Hydrostatic Actuator (EHA)	Electrical System	Electric motor + hydraulic pump	Hydraulic actuator	Aileron, Elevator, Rudder, Spoiler
Electrical Backup Hydraulic Actuator (EBHA)	Hyd. (primary) Elec. (backup)	Hydraulic fluid (SV) Electric motor + hydraulic pump	Hydraulic actuator	Aileron, Elevator, Rudder, Spoiler
Electro-Mechanical Actuator (EMA)	Electrical System	Electric motor + gearbox	Ballscrew actuator	THS, Slats, Flaps, Spoiler

SV Servo Valve
THS Trimmable Horizontal Stabilizer

The distribution and assignment of power sources to the actuators is another key element of a fault-tolerant FCS architecture. As mentioned above, a complete loss of the power supply for the flight control actuation should be extremely improbable. Consequently, different power sources or distribution systems are required, to provide the necessary level of redundancy. Figure 2.20 shows common power generation and distribution architectures of recent transport aircraft. The architectures are either defined as 3H (3 hydraulics networks) or as 2H-2E (2 hydraulic and 2 electrical networks) architectures. In addition, a minimum of three independent power systems are required to fulfill the safety requirements of the flight control actuation system. All shown aircraft, except for the Boeing 787[46], have a pneumatic power system using bleed-air. With respect to a possible integration of future Active Flow Control (AFC) systems, the presence of a bleed-air system for pressurized air supply could be also relevant.

According to Bossche (2006, p. 3) there are several benefits of the 2H-2E arrangement, compared to the conventional 3H architecture: The number of power sources for flight control actuation is increased from three to four, which increases the redundancy and provides an additional margin of safety. Additionally, the dissimilarity in the power sources provides further protection against

[46] The Boeing 787 (EIS 2008) has a bleed-less system architecture, with fully electrical Environmental Control System (ECS) and Wing Ice Protections System (WIPS). Nevertheless, the Engine Ice Protection System (EIPS) is still supplied by the locally available bleed air.

common failures (e.g. maintenance errors). Furthermore, electrical power is more flexible, regarding routing, segregation, and the capability of isolation and reconfiguration. Other benefits are improvements of MTBF, better dispatch reliability, and resulting overall weight savings on aircraft and system level[47].

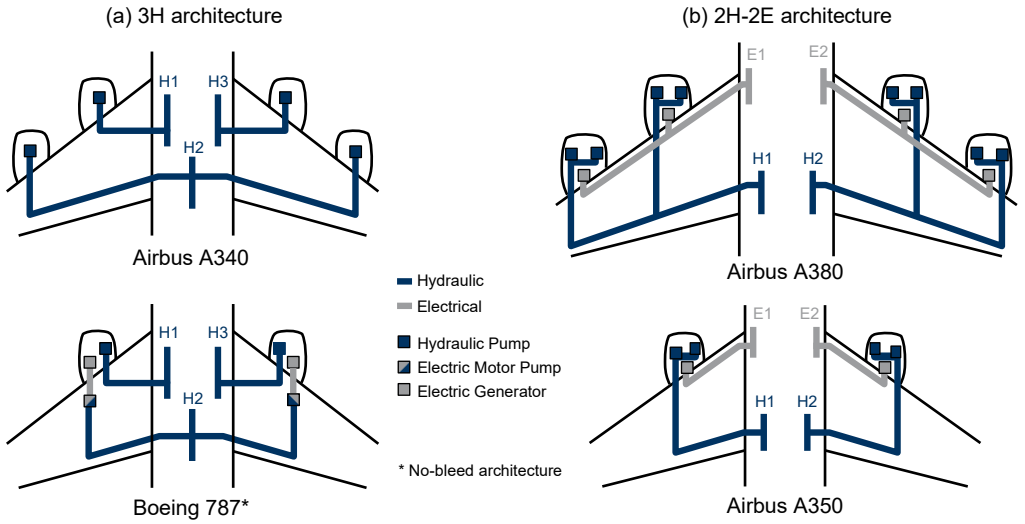

Figure 2.20 Primary power generation and distribution system of transport aircraft: 3 hydraulic power circuits (3H, left) and 2 hydraulic and 2 electrical power circuits (2H-2E, right).

Based on the study of state-of-the-art of FCS architectures and relevant work, following architectural design aspects and principles can be derived: The FCS architecture is primarily driven by safety considerations. Consequently, to enable a fault-tolerant design of the FCS architecture the principle techniques of redundancy, dissimilarity and segregation are required. Redundancy is the multiplication of flight critical components or functions of the safety-critical system with the intention of increasing reliability of the system (backup or fail-safe). Redundancy within the FCS design enables the capability of reconfiguration[48], which is a key point for a fault tolerant system. Dissimilarity increases the robustness to common-mode faults by using dissimilar hardware and/or dissimilar software, with the objective to tolerate an unknown design error of the system. An example for dissimilarity is the application of different types of actuators for the same control surface. Installation segregation is applied for critical systems/components and hydraulic/electrical routes, to avoid the loss of several functionalities due to a single failure (e.g. engine burst)[49].

In summary, to find a suitable FCS architecture in early aircraft design phases, a wealth of information needs to be considered, including safety and functional requirements in addition to technological constraints of actuators, power generation and distribution systems.

[47] Although an EMA is about twice as heavy as a comparable SHA, weight savings on aircraft/system level are possible, if required power generation and distribution systems are considered.

[48] According to Goupil (2011, p. 524), reconfiguration of hardware or software is defined as the automatic management following a failure.

[49] As this thesis aims on the integrated design in in early aircraft design phases with limited available system details, the focus is on hardware redundancy and dissimilarity. In general, installation segregation – including the routing of electrical and hydraulic lines – is dedicated to the detail design phase.

2.3.4 Advanced Technologies and Concepts

During the last decades, the flight control configurations – including the flight control devices – were optimized, and a plateau in terms of possible benefits at aircraft level were reached (cf. Figure 1.3). For that reason, the functional enhancement (e.g. DFS, CVC) of the FCS and the gradual electrification (e.g. PBW) of the FCS is of major interest to further improve the overall aircraft performance or efficiency, while minimizing the environmental impact.

In 1984, Hilbig and Wagner were among the first to present the idea of "*variable wing camber control*" for aerodynamic improvements of commercial transport aircraft and to achieve a better operational flexibility. The concept was to use the already existing high-lift control devices and ailerons on the wing to provide the requisite camber variation. Figure 2.21 illustrates the principal effects of the variable camber during cruise. The variable camber curve represents the envelope of a number of camber positions, by varying the deflection of the trailing-edge devices (fowler travel). At the design point, an aerodynamic efficiency improvement of about 3% is achieved. Moreover, the maximum lift-to-drag ratio is shifted to higher values of the lift coefficient. Summarized, this functional enhancement by variable wing camber enables the potential to further increase the overall aircraft weight (allowing to stretch the aircraft) and/or extending the design range (Hilbig and Wagner, 1984, pp. 243–248).

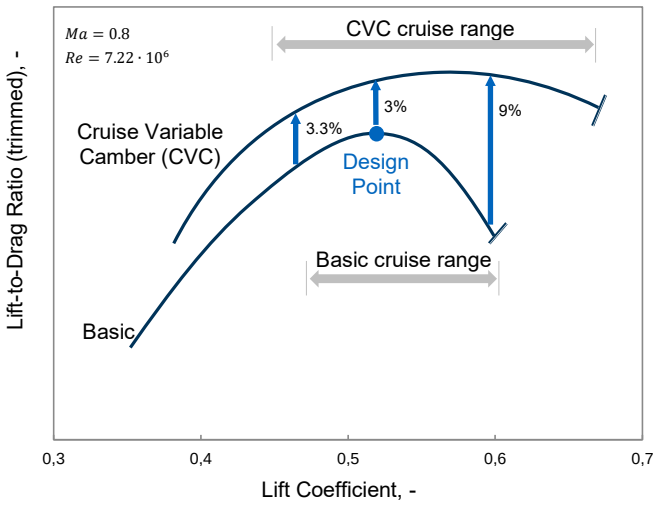

Figure 2.21 Principle effects and aerodynamic improvements of the Cruise Variable Camber (CVC) function on the lift-to-drag ratio of the aircraft (Hilbig and Wagner, 1984, p. 245).

In the beginning of the 1990s, the variable camber for adaptive wings were still subject of research. However, as the methods of predicting wing flexibility, wing loading and wing twist under load became much more accurate, the predicted performance improvements of 1% by CVC "*has never been dominant compared to the additional system complexity and the related increased maintenance costs*"[50] (Concilio *et al.*, 2018, p. xlix).

[50] The quote is taken from the foreword of the book, written by Prof. Dr. Dieter Schmitt (former Vice-President, Research and Technology at Airbus in Toulouse).

Ten years later, in the project *AWIATOR*[51], so called Miniature Trailing-Edge Devices (MiniTEDs) as a part of a multifunctional FCS were investigated. The MiniTEDs are small split flaps (2% of the local chord, max. 7.5° deflection) located at the trailing-edge of the inboard and outboard trailing-edge flaps of the high-lift control system. As a case study, an A340-300 was selected, and numerical simulations and wind-tunnel experiments were conducted to explore the effectiveness of these MiniTEDs. Results show that an increase of the lift and a shift of the lift distribution towards wing root could be achieved. Nevertheless, in real cruise conditions no improvements can be expected, because the MiniTEDs lead to significant drag increase. Furthermore, a high system integration effort of the MiniTEDs into the trailing-edge flaps is stated, leading to a complex and heavy design. (Richter and Rosemann, 2012)

A similar approach was pursued by the German Aerospace Center (DLR) in the national project *Pro-HMS.* In this project, additional control surfaces (tabs) at the wing trailing-edge lead to improved aerodynamics. But in contrast to the MiniTEDs, the added tabs are much larger and distributed over the full wingspan. During low speed phases, the tabs can be deployed additionally to the high-lift control flaps. In cruise conditions, the wing camber can be adapted by small deflections of the tabs. Finally, the authors emphasize the sophisticated design problem with multiple disciplines and their strong interconnections. (Dargel *et al.*, 2002)

With the experiences and results of the Pro-HMS project, Airbus started the *HICON* project to develop innovative high-lift control system configurations for commercial transport aircraft (Kiefner *et al.*, 2009). One main objective was to reduce the highly complex systems and develop a single, but multifunctional flap design. Based on the demonstrated feasibility of the multifunctional concept, Airbus developed the Adaptive Dropped Hinge Flap (ADHF) which was first introduced on the Airbus A350 in 2014 (Reckzeh, 2014).

Characteristic for the ADHF design is the simple hinge-mechanism, including the capability of spoiler downward deflections. Summarized, the ADHF enables following control functions:

- High-lift Control (HLC): Flap deflection down (and spoiler deflection down for gap control between spoiler and flap).
- Cruise Variable Camber (CVC): Control of the wing camber with small deflections up/down (± 3°).
- Differential Flap Setting (DFS): Control of the lift distribution with differentially deployed inboard and outboard flaps.
- Other functions: Air Brake (ABK) and supportive Roll Control (RLC).

Since 2010, NASA and Boeing investigate a more advanced concept of an innovative wing shaping control technology called the Variable Camber Continuous Trailing Edge Flap (VCCTEF) (Nguyen, 2010; Nguyen *et al.*, 2015). The objective of this adaptive aeroelastic wing shaping control technology is to optimize the spanwise lift distribution by modifying the wing camber. This

[51] Aircraft Wing with Advanced Technology Operation (AWIATOR) was a technology platform project (July 2002 – June 2007) within the 5th Framework Programme of the European Commission. The main objective was to integrate advanced technologies into novel fixed wing configuration to improve the overall aircraft efficiency. Link: https://cordis.europa.eu/project/rcn/64807/factsheet/en (last accessed on March 25, 2019).

enables the aerodynamic improvement during cruise (due to reduced drag) and take-off and landing (due to enhanced lift) (Nguyen *et al.*, 2015).

Recent experimental and numerical studies successfully confirm the potential benefits of the application and integration of Active Flow Control (AFC) on the aircraft (Petz and Nitsche, 2004; Shmilovich and Yadlin, 2009; Ciobaca *et al.*, 2011; Brunet *et al.*, 2013; Lengers, 2014; Meyer *et al.*, 2014; Bauer *et al.*, 2014). One promising approach for the improvement of future transport aircraft is the use of AFC on high-lift control devices[52] (Bauer *et al.*, 2014). The idea is to increase the aerodynamic performance of a flap by re-energizing the flow on the upper flap surface to suppress separation. This allows to reduce the complexity of the flap (e.g. using an SSF instead of a more slotted flap), which goes along with the mechanical simplification of the flap-track and smaller fairings. Furthermore, the flap size can be reduced in span-wise and chord-wise direction, while maintaining the high-lift performance by means of AFC on the flap. As a result, the overall weight of the high-lift system can be significantly reduced.

The AFC concept published by Bauer *et al.* (2014) and Meyer *et al.* (2014) is a two-stage actuator system to generate the required pulsed air jets, see Figure 2.22. The pulsed air is generated by fluidic actuators, which are controlled by fluidic oscillators. Consequently, no moving parts or electrical components are required to provide high-control authority (Bauer *et al.*, 2014, p. 1307). The AFC system only needs a certain amount of pressurized air for a stabilized and robust performance[53], which can be provided by engine bleed air or electrical compressors. According to Meyer *et al.* (2014, p. 3), the flap size can be reduced by 20% in spanwise and by 30% in chordwise direction, while the maximum lift coefficient can be maintained by using AFC. Consequently, the associated weight reduction is higher than the additional system weight required for AFC.

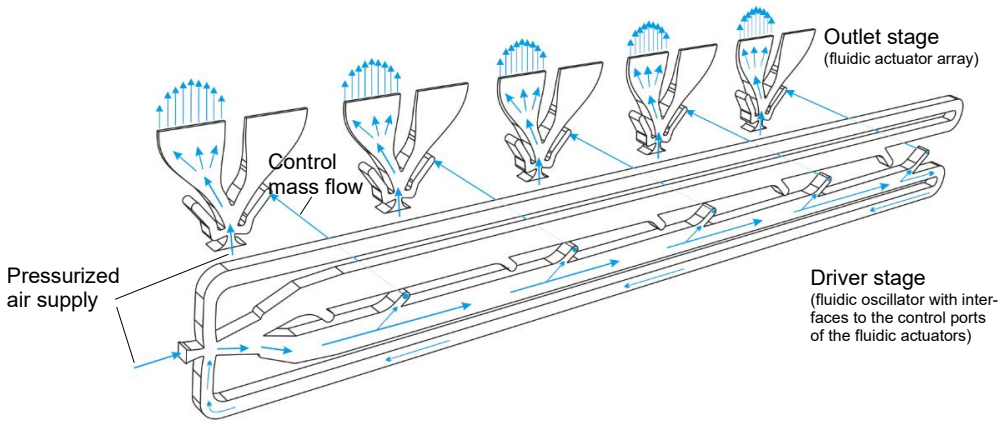

Figure 2.22 Sketch of the two-stage fluidic actuator system concept for transport aircraft applications (Meyer *et al.*, 2014, p. 4).

A study conducted by Boeing (McLean *et al.*, 1999) estimates, that a simplified high-lift system using flow control can reduce the OEW of a single-aisle aircraft by 3.3%. Most of the weight reduction comes from AFC at the trailing edge system. However, it should not be forgotten that the

[52] Other potential areas for local active flow control on commercial transport aircraft are at the engine-wing junction, at the outer area of the wing (tip), or at the vertical tail.

[53] The two-staged AFC system was successfully tested on a real-scale system test rig under normal operation or failure conditions (Lampl, 2012). The experimental results were analyzed and published by Meyer *et al.* (2014).

safety, reliability, maintenance and, in this case unneglectable, noise emissions of the AFC system are taken into account for the overall assessment. Accordingly, the multidisciplinary integration of AFC technologies, under the constraints of a commercial transport aircraft, is seen as the key challenge of this technology (Reckzeh, 2014, p. 8).

For the sake of completeness, Hybrid Laminar Flow Control (HFLC) should be briefly mentioned at this point, but will not be further discussed in this thesis. HLFC combines natural laminar flow (passive) and laminar flow control (active) for viscous drag reduction[54] by delaying the transition from laminar to turbulent flow as far as possible downstream of the chord of the surface[55]. The most promising HLFC concepts use wall suction (e.g. with a suction pump) (Torenbeek, 2013, p. 115), and was already successfully tested in flight[56]. However, comparable to the AFC concept described above, the integration of HLFC systems into commercial transport aircraft face multiple challenges regarding design, integration, operation, safety, and certification.

Various research studies (Recksiek, 2009; Bennett *et al.*, 2010; Lampl *et al.*, 2017a; Schlottbohm *et al.*, 2019) see potential benefits of a high-lift system architecture with distributed electrical drives. One main advantage of Distributed System Architecture (DSA) is the capability of an easy integration of additional control functions (e.g. DFS) (Recksiek, 2009, p. 53). In comparison to conventional high-lift systems with transmission shaft, distributed system architectures have more components acting in parallel and therefore require a certain level of redundancy and fault tolerance to meet the safety and reliability requirements (Bennett *et al.*, 2010, p. 916).

An example of a DSA for the trailing edge of the high-lift control system is shown in Figure 2.23b. For the DSA, the transmission shaft system and the centrally located PCU are removed. The two drive stations for each inboard and outboard flap are connected via a local drive shaft. This ensures a synchronous deployment of both actuators. In the case of a failure of one actuator, the other actuator can drive the flap in a degraded mode. The presented DSA is independent from the implemented actuator types due to the PBW concept. Consequently, either only EMAs, EHAs or a combination of both can be chosen for actuation.

The analysis of the DSA concepts show weight savings up to 30% and benefits in direct operating costs up to 20%, compared to the conventional system architecture (Lampl *et al.*, 2017a, p. 8). Additionally, improvements of the design-engineering, manufacturing, and assembly can be expected (Recksiek, 2009, pp. 9–10; Bennett *et al.*, 2010, pp. 915–916). Furthermore, distributed electric drive architectures fulfill both desired characteristics of innovative and advanced systems of future aircraft, by using electrical actuators (*MEA*) and enabling the integration of additional control functions (*functional enhancement*).

[54] For a given Reynolds number, the friction drag of laminar flow is lower compared to the friction drag of turbulent flow.
[55] The application of natural laminar flow on swept wings is ineffective due to the crossflow instabilities, which are the dominating factor for the laminar turbulent transition. That's why a hybrid solution is favored, to overcome the limitations by natural laminar flow, and keep the system complexity of the laminar flow control system in reasonable limits.
[56] In 1990, Boeing successfully tested an HLFC concept on a large wing section of a Boeing 757. Airbus successfully completed flight tests of an Airbus A320 with a HLFC concept on the vertical tail of an Airbus A320 in 1998. Both flight test showed promising results regarding the operation of the HLFC systems (Braslow (1999); Henke (1999)).

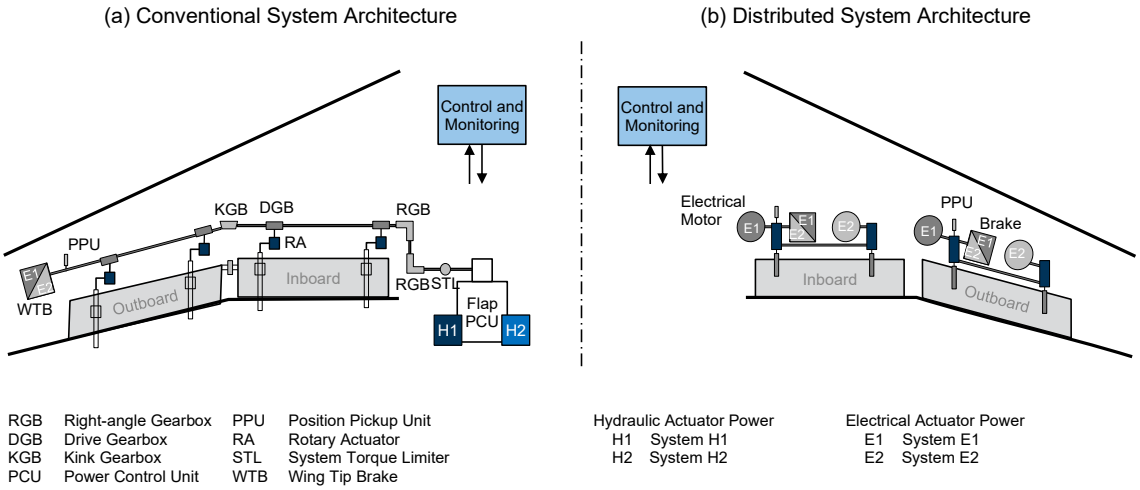

Figure 2.23 Schematics (simplified) of a conventional system architecture (left) and an electric distributed system architecture (right) for high-lift systems (Lampl *et al.*, 2017a, p. 7, modified).

Based on the presented overview of enabling technologies and concepts, an overview – analogue to the basic flight control functions is listed in Table 2.1 – of additional flight control functions, and the corresponding flight control devices is given in Table 2.4.

Table 2.4 Examples of additional flight control function and typical flight control devices at the wing.

Additional Flight Control Function(s)	Flight Critical	Control Device(s)	Characteristics
Roll control (RLC)	No	Aileron (Flaperon)	Deflections up/down
(e.g. supportive)		Spoiler	Deflections up/down
High-lift control (HLC)	No	Aileron (Flaperon)	Deflections down (droop)
(e.g. supportive)		Flap with AFC	Fluidic actuators on (e.g. pulsed jet)
Active load control (ALC)	No	Aileron	Deflections up/down
		Spoiler	Deflections up
Differential flap setting (DFS)	No	Flaps/Flaperon	Deflections down
Cruise variable camber (CVC)	No	Flaps/Flaperon	Deflections down
		Spoiler	Deflections down (for gap control)

AFC Active Flow Control

Summary. The presented technologies and concepts confirm the trends of functional enhancement and more-electric systems for commercial transport aircraft. The objective of functional enhancement is one of the main design drivers for advanced flight control *configurations*, including additional control functions (e.g. DFS, CVC) or multifunctional flight control devices (e.g. MiniT-EDs, AFC). Besides the safety aspects, the use of more-electric systems (e.g. PBW, DSA) is one of the main design drivers for the *system architectures* of advanced FCS. However, new technologies and concepts should be considered holistically in order to assess the real impact at aircraft and system level.

3 Integrated Design of Advanced Flight Control Systems

The Flight Control Systems (FCS) of today's commercial transport aircraft consist of highly optimized flight control devices, which require high effort for small and local improvements. Consequently, various research studies present new technologies and concepts for functional enhancement of the FCS to increase the aircraft efficiency or performance during certain flight phases (cf. *2.3.4 Advanced Technologies and Concepts*). In addition, a transition from a knowledge-based to a functional-driven design approach is recommended (cf. *Figure 1.4*). Beside the means of functional enhancement, the trend towards More-Electric Aircraft (MEA) leads to considerable changes at aircraft system level, and thus has a decisive impact on the FCS architecture design. In addition, more and more electrical actuators are used for flight control actuation (cf. *2.1.3 More-Electric Aircraft*). According to the recommended and reorganized aircraft design process[57] for highly complex and multidisciplinary design projects, the proposed overall methodology should be applicable in the early design phases and should enable the execution of parameter studies and their analysis (cf. *2.1 Aircraft Design and Aircraft Systems, pp. 10*).

This chapter starts with an overview of the *Overall Methodology* and a brief introduction to the main terms and definitions required for the following chapters. Afterwards the *Functional-driven Design Approach* and the *Advanced Flight Control System Design,* which represent the first two stages of the overall methodology, are described. Besides the description of the used approach and design methods, the developed design tools are presented and finally validated against the results of published work. The last stage of the overall methodology will be discussed in the following chapter *4 Aircraft Performance and Technology Analysis*.

3.1 Overall Methodology

On the basis of a comprehensive review of state-of-the-art FCS, advanced technologies and system concepts, following overall methodology was developed, see Figure 3.1. The overall objective of this methodology is to enable an *integrated design* and *analysis* of advanced FCS in early aircraft design phases. For that reason, the overall design methodology is divided into *three main stages*: The first two stages enable an integrated design of advanced FCS, whereas the third stage provides a simulation environment for the analysis and assessment. This overall methodology and the developed tools are dedicated for the early design phases of subsonic commercial transport

[57] The main objective of this reorganized design process is to increase the available knowledge and the design space in early aircraft design phases, especially during the conceptual and preliminary design phases (cf. Figure 2.1b).

aircraft. Furthermore, it is assumed that an initial idea or concept of an aircraft configuration (e.g. arrangement of fuselage, wings, and tail) already exists.

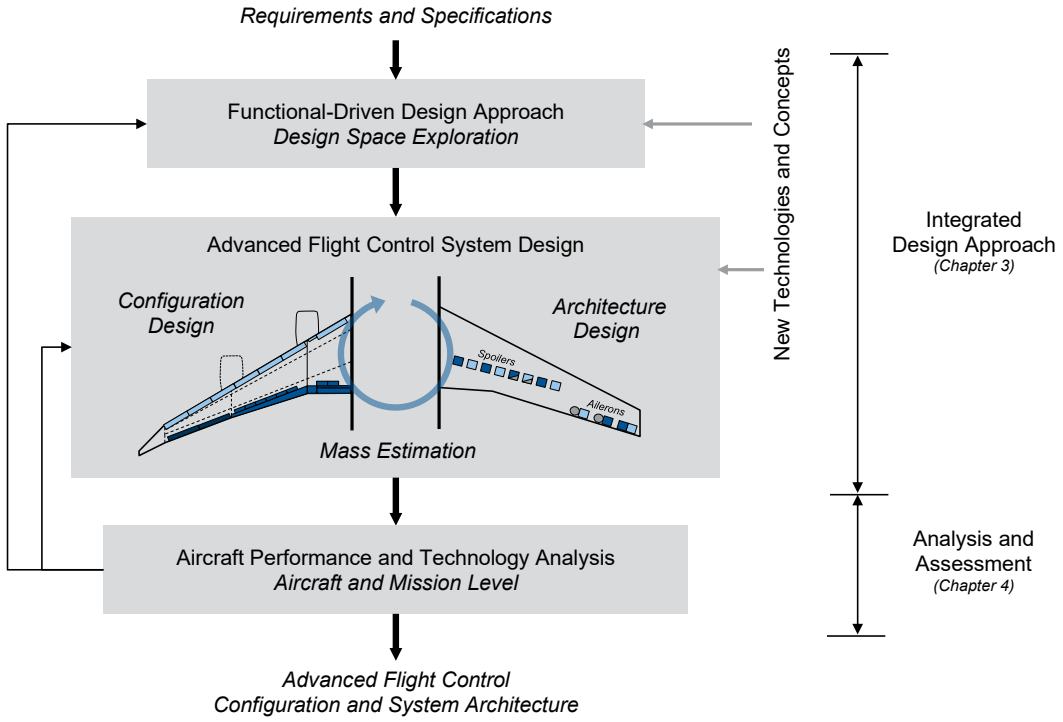

Figure 3.1 Overview of the overall methodology for the integrated design and analysis of advanced flight control systems in early aircraft design phases (top-level view).

For a better understanding of the subsequent chapters, the following terms are clearly defined and briefly described:

- *Advanced Flight Control System:* An advanced FCS integrates new technologies and concepts in addition to multifunctional flight control devices. Furthermore, electric actuators are increasingly being used for the flight control actuation system.
- *Flight Control Configuration:* The configuration describes the layout of the FCS, including the type, allocation and positioning of flight control devices, including the kinematics and support, fairings, and other integration aspects (cf. Figure 2.12).
- *Flight Control System Architecture:* The architecture defines the number of the flight control computers and their assignment to dedicated flight control devices. Additionally, the actuation, linkage and redundant distribution of the power supply is also attributed to the architecture (cf. Figure 2.12).
- *Flight Control Device:* Flight control devices are movables, surfaces or technologies which provide, support, or enable single or multiple flight control function(s). They can be actuated (activated) individually or in combination to fulfill a flight control function. In addition, depending on the flight control function(s) they have to perform, flight control devices differ in whether they are activated continuously or only intermittently during certain flight phases.

- *Flight Control Function:* A flight control function describes a defined task of the FCS which leads to a change in attitude (e.g. directional control), wing configuration (e.g. high-lift control) or aircraft performance or efficiency (e.g. cruise variable camber). The flight control function can be activated either by individual flight control devices or by the coordinated use of several control devices.

3.2 Functional-Driven Design Approach

The first step of the integrated design methodology is the functional-driven design approach, as illustrated in Figure 3.2. The objective of this approach is the transition from a knowledge-based to a functional-driven design, to explore the potential design space and to derive several solutions of advanced and multifunctional concepts (*Objective 1*). These solutions are then used as the starting point for the advanced FCS design. The development of the flight control configurations and system architectures takes place against the background of functional fulfilment at *aircraft*, *system* and *device* level. The subdivision into three levels enables the consideration of different aspects which affect the design of the flight control *configuration* or the system *architecture* (cf. Figure 2.12). Thus, flight-mechanical aspects, flight control device characteristics can, for example, be analyzed separately from integration aspects of the system architecture. However, interdependencies must still be taken into account. With regard to the methodology presented in the following, this hierarchical distinction is applied in particular to the *Functional Multiple Domain Matrix (FMDM)* and the *Function Catalog* (cf. Figure 3.2).

In order to meet the different requirements in the best possible way, a comprehensive understanding of the functions and associated design possibilities of the FCS is required. Furthermore, the potentials of different flight control configurations have to be determined. Nevertheless, possible synergies and conflict potentials are not always obvious, but must first be identified by a thorough analysis. The objective of this early identification of such conflicts and synergies is especially pursued through the functional-driven design. Thus, the approach is to examine the functions at different levels.[58] While the functional way of thinking is dominating, holistic design aspects should also be considered in this design approach. This is also true for the consideration of new technologies and concepts for the flight control configuration, where their specific integration into the system architecture and further characteristics do not have to be considered at first.[59] For that reason, the initial focus is on determining the impact of certain flight control configurations and technologies on the system architecture rather than on the design of the system architecture itself.

[58] This *differentiated approach* is illustrated in the following example: The lateral movement is highly influenced by the coupling of rolling and yaw movements. Thus, a control input regarding the longitudinal axis also requires a corrective control input regarding the vertical axis of the aircraft. The same applies in reverse order. Accordingly, on the one hand, there is a strong interaction of the functions at aircraft level regarding control around the longitudinal axis and control around the vertical axis. On the other hand, the functions at *system* and *device* level are independent, simply because of the spatial separation of the rudder (empennage) and ailerons (wing). With regard to the advanced and multifunctional design of FCS, these interrelationships are of great importance.

[59] This is illustrated by a brief example: The use of Active Flow Control (AFC) at trailing-edge devices to locally increase the aerodynamic performance has a direct impact on the system architecture design (cf. Figure 2.22): e.g. fluidic actuators have to be integrated into the system, require a control signal and are supplied by pressurized air. However, at this

The design of advanced FCS is characterized by conflicts and contradictory requirements, which can be described by the three main aspects of *safety*, *performance* and *costs*. In principle, the simultaneous optimization of each individual aspect is not possible. Rather, a solution in the form of an optimal agreement on all aspects must be found. In the same way, synergy effects (*potentials*) can be identified in many areas. To identify these potentials and synergies in addition to possible conflicts are essential objectives of this functional-driven design approach.

Figure 3.2 illustrates the developed design approach for the functional-driven design of advanced flight control configurations. The focus is in particular on the functional allocation, but also on the distribution and segmentation of flight control devices. The approach is divided into four major steps: *Requirements Engineering*, *Functional Analysis*, *Functional Synthesis*, and *Validation and Evaluation*. This systematic approach promotes transparency in evaluation and decision-making processes, which is of particular importance for multidisciplinary design processes such as the development of advanced FCS. The Functional Multiple Domain Matrix (FMDM) represents the core of the design approach and accompanies the entire development process. Furthermore, the FMDM also serves as a database, where coherences are modelled, and information is stored.

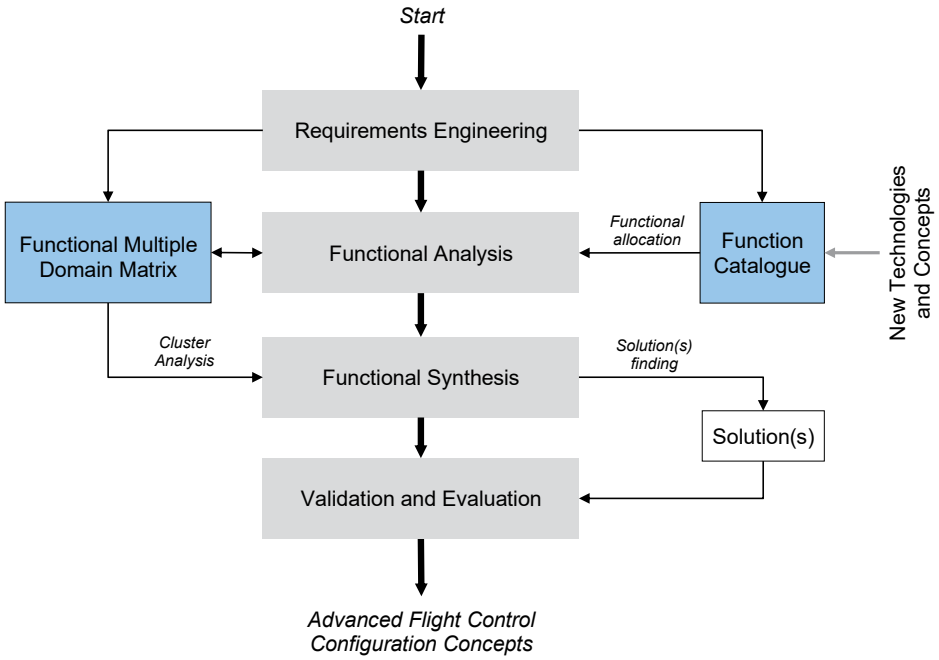

Figure 3.2 Functional-driven design approach to derive potential solutions of advanced flight control configuration concepts (Lampl *et al.*, 2017c, p. 9).

The four major steps of the approach can be run through iteratively as well as sequentially. Nevertheless, the main objective is to achieve a continuous use of the FMDM to facilitate the handling of system complexity. In the following, the individual elements and steps of the functional-driven design approach are examined in more detail.

point it is irrelevant whether the AFC system is supplied with compressed air by means of engine bleed-air or electric compressors, and if the control signal (mass flow) for the fluidic actuators is provided by fast-switching valves or a fluidic oscillator stage.

3.2.1 Requirements Engineering

A clear definition of objectives and requirements is fundamental for a successful development process. However, these must be newly determined and defined for each project. One objective of the functional-driven design approach is to integrate the requirements analysis into the development process. On the one hand this requires an exact identification of all requirements, boundary conditions and limitations and the continuous comparison with the defined goals and requirements on the other hand. This also includes adjustments and changes due to new circumstances that may arise in the course of the design process. Hence the requirements analysis can be seen as a basis to derive the functional requirements.

The basic functional requirements are primarily driven by safety and reliability aspects according to airworthiness regulations (CS-25, FAR 25). These basic requirements are directional control, trim or high-lift control of the aircraft. In contrast, additional functional requirements aim to increase the overall efficiency or performance of the aircraft. Nevertheless, a compromise must often be found between increased functionality and the resulting system complexity.

In general, the use of advanced technologies and concepts for FCS lead to new design possibilities and requirements in addition to new boundary conditions and constraints (cf. *2.3.4 Advanced Technologies and Concepts*). Figure 3.3 gives an overview of the main design aspects, technologies or concepts which enable a functional enhancement, efficiency improvement, or have a major influence on the overall FCS design. For example, aerodynamic and structural technologies have a major impact on the flight control *configuration*, whereas the aircraft power generation and distribution system has major influences on the *system architecture* of the FCS.

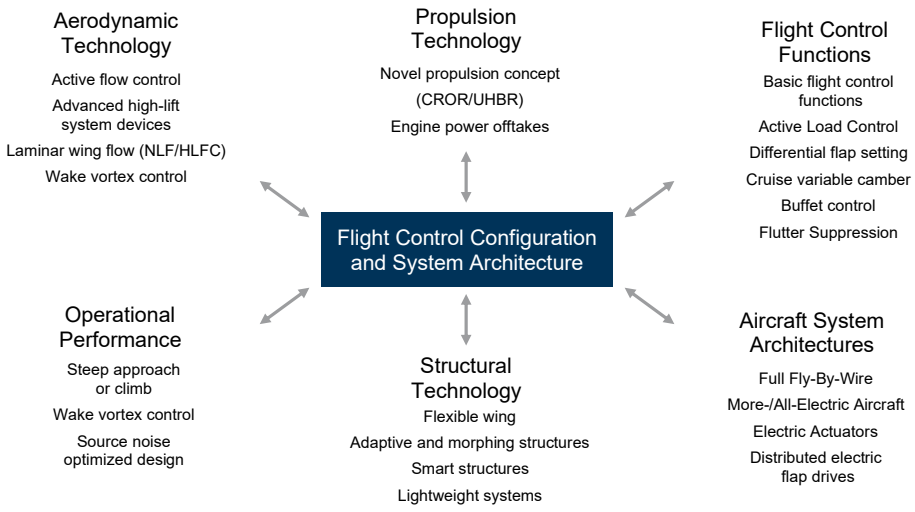

Figure 3.3 Main design aspects, technologies, and concepts regarding the design of advanced flight control systems of commercial transport aircraft (Lampl *et al.*, 2017c, p. 6).

3.2.2 Function Catalogue

In order to enable a functional-driven design of advanced FCS, the functional requirements must be known. Hence, the first step is to identify the individual functions, which can be derived from the requirement analysis and must first be determined (cf. *3.2.1 Requirements Engineering*). Each flight control function is examined with regard to its characteristics and the possible implementation into the FCS under consideration of certain design aspects. Finally, the collection and compilation of the individual documents and tables form the function catalogue.

The function catalogue describes all potential functions with their characteristics, requirements and constraints for the design process. In addition, it works as a data basis and supports a differentiated view on each level. The flight mechanical aspects are defined at aircraft level. System integration aspects as well as the coordination of flight control devices and redundancy are described at system level. On device level, the characteristics of potential flight control devices (e.g. *deflection up* and *down*, *fowler translation*, *positions*, *modes*…) are described. To get an idea of such a catalogue, an example of a specified flight control function is shown in Table 3.1. Further examples of basic and additional flight control functions (e.g. DFS and CVC) are given in the appendix (cf. *A.3 Flight Control Function Catalogue)*.

Table 3.1 Example of the specification of the high-lift control function for the function catalogue.

Flight Control Function	High-Lift Control (HLC)
Aircraft Level	
Requirements, Specifications	EASA CS-25: 25.105, 25.107, 25.109, 25.111, 25.113, 25.115, 25.117, 25.119, 25.121, 25.125, 25.701, Handling Qualities
Model, Objectives	Enable low speed phases for safe start and landing, steep climb-out, steep approach, minimum weight (low complexity), minimize start and landing distances
Parameter	Lift Coefficient, Drag Coefficient, Lift over Drag, Lift-off speed, touchdown speed, climb rate, angle of attack,
Interactions	Flight control, stability, trim
System Level	
Conventional Configuration	Leading-edge and trailing-edge control devices (slats/flaps), different positions (discrete)
Integration, Constraints	Wing design (span, elasticity, space, airfoil, wing sweep), winglets, front/rear spar (hinge line), ailerons, engines, landing gear, MTOM
Redundancy, Reconfiguration	Segmented high-lift control devices (inboard/outboard), redundant actuation and flight control computers, electronic rigging
New Technologies	Flexible (morphing) structures, active flow control, distributed electric drives…
Device Level	
Control Devices	Leading-edge devices (Krueger-Flap, Slat, Droop nose) and trailing-edge devices (single-slotted flap, double slotted flap, fowler flap)
Deflection and Motion	Different kinematics: dropped hinge, linkage, track, fowler motion: translation, rotation
Aerodynamics, Aeromechanics	Pressure distribution (airfoil, wing), reduction of suction peaks, delay of flow detachment at the outer wing (to keep ailerons effective), boundary layer control
Multifunctionality	Cruise variable camber, differential flap setting

3.2.3 Functional Multiple Domain Matrix

The Functional Multiple Domain Matrix (FMDM) represents the core of the design approach and accompanies the entire development process. In addition, a hierarchical segmentation allows a differentiated view on various design aspects of each level. Besides the usage of the FMDM for analyses, it also serves as a database, where coherences are modelled and information is stored. The FMDM is composed of the individual Multiple Domain Matrices (MDM)[60] at aircraft, system and device level, as illustrated in Figure 3.4. For each of the level, different characteristic domains are identified, which are based on the findings of the literature review in addition to the results of the analysis of the aircraft design process. The relationships between the individual domains are basically bidirectional. However, these are not considered separately in this thesis, but are understood as mutual interactions. Thus, entries in the individual matrices are exclusively the diagonal and above.

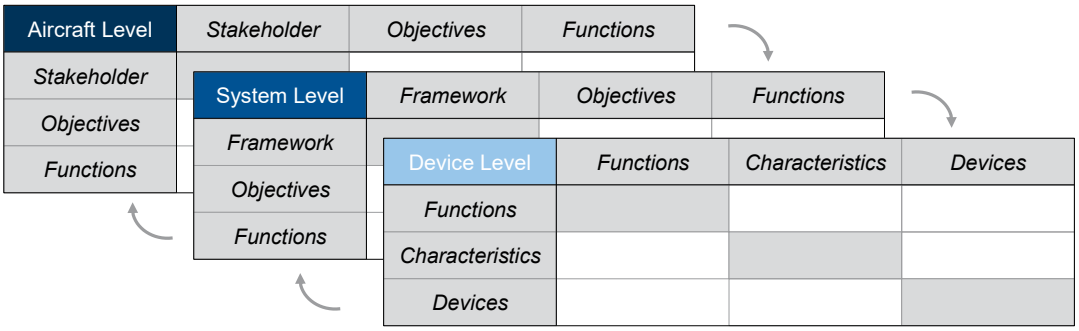

Figure 3.4 Setup of the Functional Multiple Domain Matrix (FMDM) with the hierarchical breakdown into aircraft, system and device level (Lampl *et al.*, 2017c, p. 9).

Aircraft Level. The design of the flight control system is influenced by requirements, regulations and constraints at aircraft level. Accordingly, the different expectations of stakeholders[61] must be taken into account. Based on this, individual objectives are formulated. Consequently, the domains stakeholders and objectives are assigned to the aircraft level. In order to achieve the formulated objectives, the flight control system must fulfill certain control functions at aircraft level. Hence, at aircraft level, an MDM with a diagonal of the three Domain Structure Matrices (DSMs) *Stakeholder*, *Objectives* and *Functions*. Furthermore, the MDM is completed by the corresponding Domain Mapping Matrices (DMMs) above the diagonal as illustrated in Figure 3.5a. The domains are modelled by DSMs. The DSM Stakeholder includes interactions of the different expectations and requirements of each stakeholder. Certain requirements may conflict with each other. In the same way, the different goals can be related to each other. This is investigated in the DSM Objectives. An essential element of the aircraft-level MDM are the effects and interactions of (flight control) functions. Questions such as *"How does the aircraft behave due to this flight control function?"* or *"How does a control function affect other functions or systems?"* arise and are supposed to be answered. Furthermore, aerodynamic interdependencies are primarily analyzed within the DSM Functions. The objectives at aircraft level are initially derived from the stakeholders. Further relations at aircraft level are depicted and analyzed in the corresponding DMMs (see Figure 3.5a).

[60] For some background information see section *A.2 Design Structure Matrix and Multiple Domain Matrix* in the appendix.
[61] Typical stakeholders are manufacturers, airlines, maintenance operators, aviation authorities, passengers, and airports.

In short, the MDM at aircraft level plays an important role in early aircraft design phases. This essentially affects the requirements analysis and the functional analysis. As in the entire development process, the use of the MDM should be interactive to the individual sub-processes.

(a) Multiple domain matrix at aircraft level

Aircraft Level	*Stakeholder*	*Objectives*	*Functions*
Stakeholder	Interaction of different expectations and requirements of the stakeholders	Relationships between stakeholder objectives and expectations	Relationships between functions and stakeholder expectations
Objectives		Interaction of different goals at aircraft level	Relationships between functions and objectives
Functions			Functional interaction at aircraft level

(b) Multiple domain matrix at system level

System Level	*Framework*	*Objectives*	*Functions*
Framework	Interaction of different boundary conditions at system level	Interactions between objectives and boundary conditions (framework)	Relationships between functions and boundary conditions (framework)
Objectives		Interaction of different goals at system level	Relationships between functions and objectives at system level
Functions			Functional interaction at system level

(c) Multiple domain matrix at device level

Device Level	*Functions*	*Characteristics*	*Devices*
Functions	Functional interaction at device level	Relationships between (design) characteristics and functions	Functional allocation and segmentation of the flight control devices
Characteristics		Interaction of different design characteristics at device level	Relationships between flight control devices and characteristics
Devices			Interaction of different flight control devices

Figure 3.5 Setup of multiple domain matrices at aircraft level, system and device level.

System Level. At system level, the focus is particularly on the flight control configuration and system architecture integration. Therefore, several boundary conditions have to be determined, which have a major impact on the development and design of advanced FCS. For example, the aircraft configuration and the wing design can have a major influence on the arrangement and integration of certain flight control devices (cf. Figure 2.16). Hence, besides aerodynamic and flight-mechanic characteristics also design and integration aspects regarding available space or interactions with other components and systems have to be considered. Moreover, objectives at system level are formulated while keeping in mind the aspects of overall system complexity, redundancy and reconfiguration. Analogue to the functions defined at aircraft level, individual functions are derived and analyzed at system level with focus on system integration aspects. This

part requires a high degree of system thinking[62] and is closely coupled with the *Requirements Engineering* (cf. *3.2.1*) in the beginning. The resulting DSM at system level are *Framework*, *Objectives*, and *Functions*, as illustrated in Figure 3.5b. Together with the corresponding DMMs, the interactions of specific objectives can be displayed, and hence possible conflicts and synergies highlighted. In addition, the analysis of the MDM at system level enables a first estimation of the expected overall system complexity.

Device Level. One main objective of the MDM at device level is the functional allocation and the development of several solutions using different flight control devices and combinations. For that reason, this MDM is strongly connected with the *Functional Analysis and Synthesis* (cf. *3.2.4)*. The functional performance at device level shows strong interconnections with the characteristics of the flight control devices. Hence, the focus at device level is on the selection and design of certain types of flight control devices. Accordingly, following relevant questions have to be answered: *"Which types of flight control devices are required to fulfill a certain flight control function?"*, *"What characteristics must the flight control device have in order to be able to perform a particular function?"* or "*Are there any new technologies or concepts to fulfill or support a particular flight control function?"* As a result, a MDM at device level is set up as illustrated in Figure 3.5c. The relations between the domains *Functions* and *Devices* represent the functional allocation and distribution of the flight control devices. Moreover, the different types of flight control are characterized by specific properties. This results in a DMM, which maps the relations between (flight control) *Devices* and *Characteristics* and supports the generation of alternative solutions. The third DMM represents the relations between *Functions* and *Characteristics*. In summary, for the functional allocation, the selection and design of flight control devices, a compromise has to be found to meet the corresponding (functional) requirements as well as possible.

3.2.4 Functional Analysis and Synthesis

During the development of advanced FCS, a lot of multidisciplinary requirements and constraints have to be considered. In addition, as already mentioned, a good compromise must be found between the three main aspects of safety, performance and cost. Furthermore, especially for the development of advanced FCS, another important aspect to keep in mind is system complexity. For commercial transport aircraft, a clear trend towards simplification and complexity reductions is visible (cf. Figure 1.3). Thus, system weight and costs can also be significantly reduced. However, the aerodynamic performance must be sufficient. These aspects are often contradictory and must therefore be examined in detail in parameter studies and analyses in order to find a good compromise solution.

The functional analysis and synthesis are the central and creative parts of this design approach. The main objective of the functional analysis is the functional allocation, which means the assignment of flight control functions to determined flight control devices. Whereas the generation of alternative and multifunctional solutions within in the design space, considering new technologies and concepts, are the main objectives of the functional synthesis. At this point it should be

[62] *System thinking* is the ability to take a holistic or a total systems view of the development or analysis of any system (Seabridge and Moir (2013, p. 3)).

emphasized that the functional analysis and synthesis are not unidirectional processes, but highly iterative.

Functional Analysis. The functional analysis is the link between the *Requirements Engineering* and *Functional Synthesis* to find multiple solutions. Figure 3.6 illustrates the main steps of the functional analysis. In a first step, the control functions are determined. On the basis of the comprehensive requirements analysis, the functional requirements and boundary conditions are derived. To support the determination and analysis of the characteristics of different flight control functions, a *Function Catalogue* is used (cf. 3.2.2). As mentioned above, a special feature of the function catalogue is the differentiation at aircraft, system and device level.

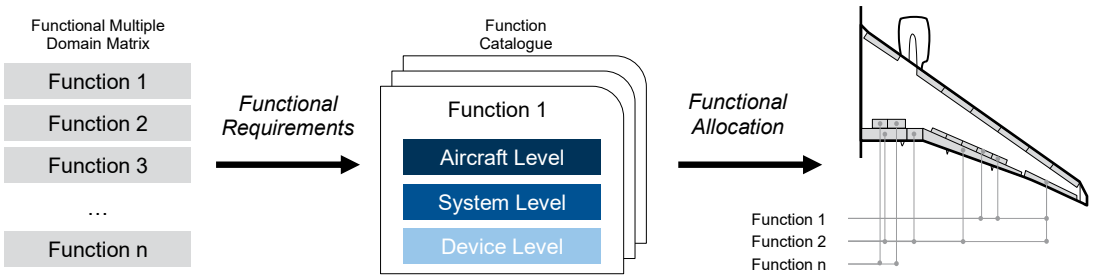

Figure 3.6 Schematic overview of the functional analysis – the link between requirements engineering and functional synthesis to find different solutions (Lampl *et al.*, 2017c).

Finally, the basic design space for further investigations is generated by allocating functions to dedicated flight control devices. The objective is not to find the best configuration, but to initially exploit the basic configuration design space. An example of allocated functions to dedicated flight control devices is illustrated in Figure 3.7. The different links between flight control device and functions symbolize *standard* and *optional* solutions[63]. Standard solutions are mainly mono-functional, whereas optional allocations target multifunctional flight control devices.

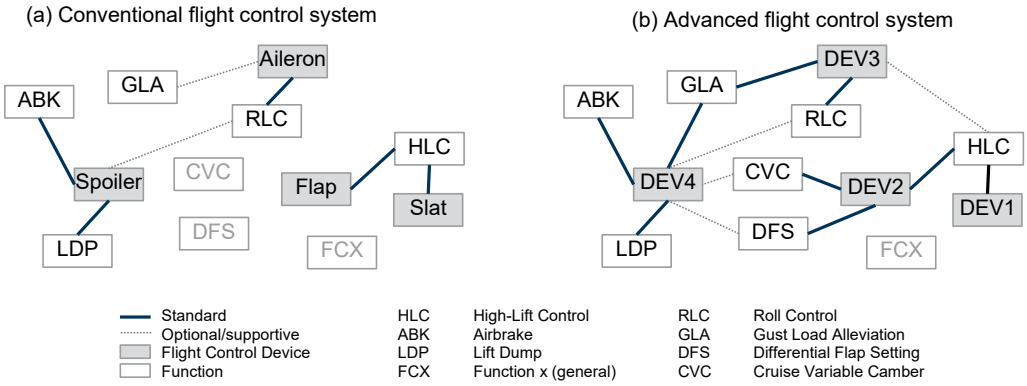

Figure 3.7 Simplified comparison of the functional allocation of a conventional (left) and of an advanced flight control system (right).

[63] This distinction between *standard* and *option* is briefly explained in the following example: Conventional flight control systems primarily use ailerons at the trailing-edge of the outboard wing for roll control and can be defined as *standard* allocation. Whereas a multifunctional use by asynchronous setting of the trailing-edge devices of the high-lift system for roll control is defined as *optional*.

In the development of the functional design space, the focus is thus on the identification of possible functional segmentation. This should initially be done independently of overall evaluations with regard to feasibility, costs, performance or system complexity.

Functional Synthesis. The objective of the functional synthesis is to find alternative solutions within the design space. This is done in close cooperation with the FMDM. Based on the aforementioned functional allocation, a cluster analysis is conducted. A cluster defines a group of elements with a lot of internal coherences and few or none external coherences. The coherences can be dependencies, synergies or conflicts. Figure 3.8 shows an exemplary cluster analysis at device level. Further cluster analyses at aircraft or system level lead to other perspectives. For example, the emphasis of effects of certain functions at aircraft level (e.g. flight mechanics) or at system level (e.g. system integration aspects). To support the analysis, a cluster algorithm[64] for optimizing assignment is recommended to provide a structured approach.

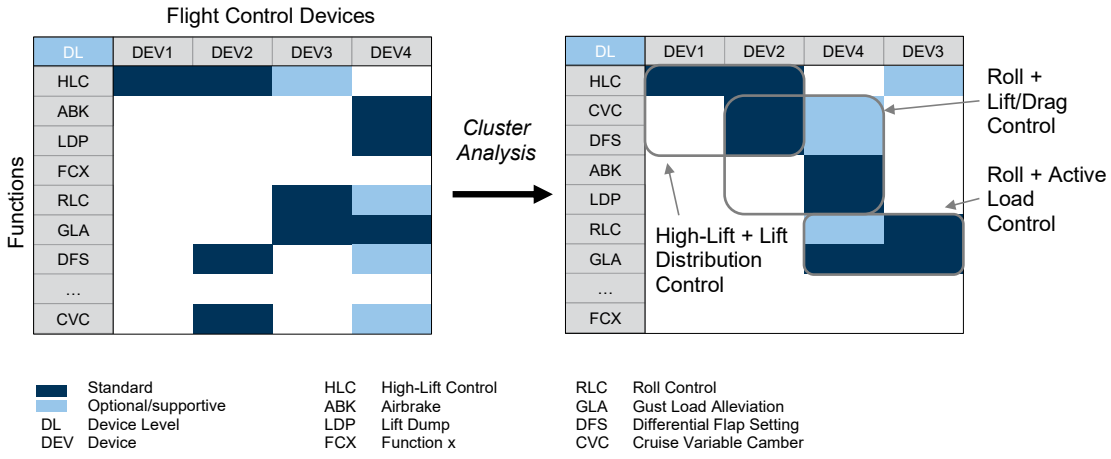

Figure 3.8 Exemplary cluster analysis of an advanced flight control system at device level (simplified).

The evaluation of alternative solutions for suitability can basically be done by qualitative or quantitative methods. Furthermore, a metric is needed to describe the characteristics numerically and to enable a comparison. If the individual characteristics are weighted differently, this is referred to as weighted scoring or utility analysis. However, a hierarchical value system is required for the utility value analysis. Table 3.2 shows an example of such a weighted point evaluation of several configurations, taking into account different characteristics at aircraft and system level. In this context, configuration does not necessarily mean the entire flight control configuration of the FCS. Configurations of individual functions, sub-areas and modules can also be evaluated. The weighting must be adjusted accordingly. In conjunction with the weighting of the individual features, this results in a utility value for each configuration. The utility value can then be used to determine a ranking of the different solution alternatives.

[64] A good example of a cluster algorithm tool can be found in the work of Thebeau (2001). This stochastic clustering algorithm has already been successfully applied in the work of Akoto *et al.* (2017) to derive potential system architectures for the preliminary design of novel high-lift control actuation systems.

Table 3.2 Example of a weighted point evaluation of alternative solutions at aircraft and system level.

		Configuration (solutions)					
	Characteristics	#1	#2	#3	#4	…	Weighting
Aircraft Level	*Safety*	3	2	1	2	…	3
	Handling Qualities	2	3	3	2	…	2
	Costs	2	2	1	3	…	2
	Efficiency Improvements	2	2	1	3	…	1
System Level	*Complexity*	2	1	1	1	…	2
	System Weight	2	1	1	3	…	2
	Redundancy	3	2	1	1	…	3
	Reconfiguration	3	2	3	1	…	2
	Integration	2	1	1	3	…	1
	Utility Value	**44**	**33**	**26**	**35**	…	

The result of the utility value analysis depends to a large extent on the selection of the individual characteristics and their weighting. This requires a comprehensive requirements analysis and an exact definition of the objectives. Additionally, must-have or exclusion criteria can be defined to be able to exclude certain concepts in advance. Finally, the ranking results are a first indication of the suitability of a solution alternative and a preselection can be conducted for a detailed validation and evaluation in advance.

3.2.5 Validation and Evaluation

In the last step of this functional-driven design approach, the solutions are preliminary validated and evaluated at aircraft and system level. Besides the functional fulfillment, the achievement of the safety requirements is essential for preliminary validation and evaluation. In addition, the solutions are to be examined and evaluated with regard to environmental impact and cost aspects. This can be done for each defined cluster or for the overall configuration concept.

A full safety assessment of the advanced FCS according to ARP4761[65] is not feasible for early aircraft design phases. However, the initial sub-process, including the general Functional Hazardous Assessment (FHA) and the Preliminary System Safety Analysis (PSSA), can still be applied. The FHA is the first step in the safety process. This method is used for the very first failure identification by the thorough evaluation of the functions. The FHA has the task of identifying and classifying individual failure cases of the FCS, which can occur at aircraft, system, and device level. The error cases are generally associated with the flight control functions of the FCS, and can be classified according to the certification regulations CS-25 (cf. Table A.2). Based on the FHA and the determined safety objectives, the PSSA is conducted, where a standard and widespread method used is the Fault Tree Analysis (FTA). Therefore, a FTA for each considered flight control function is conducted. In contrast to the FHA, which can be conducted independently from considered configurations, system architectures, system technologies and concepts, the PSSA requires not only details of the FCS design at aircraft level but also at system level. Consequently, the PSSA supports the iterative characteristic of this design approach, by constant questioning

[65] The ARP4761 describes guidelines and methods of performing the safety assessment of aircraft systems and equipment for certification of civil aircraft (SAE ARP4754A, 2010)

and analysis of the advanced FCS concepts. For the assessment of the safety validated solutions, a reasonable metric is required. This can be a similar to preliminary evaluation described for the functional synthesis, but should contain significantly more characteristics. Finally, one or more functional-driven design concepts should result for further and more detailed investigations of advanced FCS.

3.3 Advanced Flight Control System Design

Based on the results of the functional-driven design approach, the advanced FCS can be designed, which represents the second part of the overall methodology (cf. Figure 3.1). The objective is to enable an integrated design of advanced flight control configurations and system architectures[66] in addition to the overall mass estimation in the end. Consequently, the design approach is divided into three steps, as illustrated in Figure 3.9: *Configuration Design, Architecture Design,* and *Mass Estimation*. In a first step, the configuration design (layout) is defined and validated on the basis of preliminary allocation, sizing and aerodynamic calculations. In the second step, redundant flight control system architectures of a given configuration are determined. The method behind is realized by defined technological assumptions and implemented rules for redundancy, power supply distribution and reconfiguration.

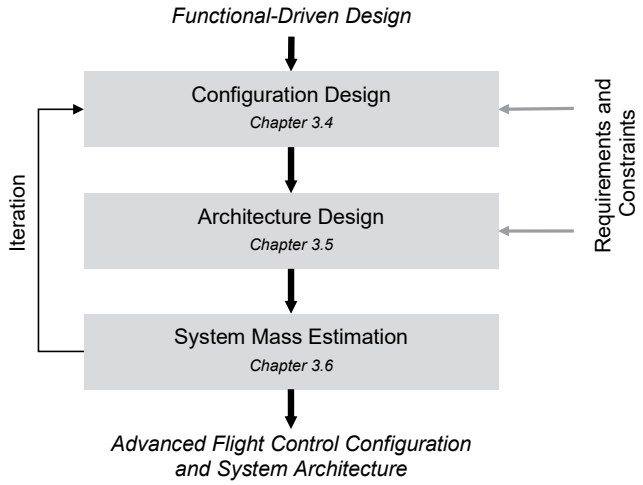

Figure 3.9 Overview of the top-level design approach for advanced flight control systems.

Finally, if a valid combination of flight control configuration and system architecture is found, the overall mass FCS is calculated in the last step. To optimize the resulting FCS design (e.g. towards minimum mass), the sizing, segmentation and distribution of the flight control devices can be iteratively modified.

[66] According to the breakdown shown in Figure 2.12, the FCS can be divided into *configuration* and *architecture* with strong interdependencies.

3.4 Flight Control Configuration Design

The configuration design method enables the design of flight control configuration, including device allocation and sizing in addition to aerodynamic calculations of an aircraft model, see Figure 3.10. Since the integrated design approach should be applicable in early aircraft design phases, only limited available geometry data can be considered. Therefore, handbook methods, semi-empirical approaches, statistical data, and vortex lattice models are used. Finally, if a valid configuration is found, the control surface loads, and hinge moments are determined for later actuation system sizing within the architecture design.

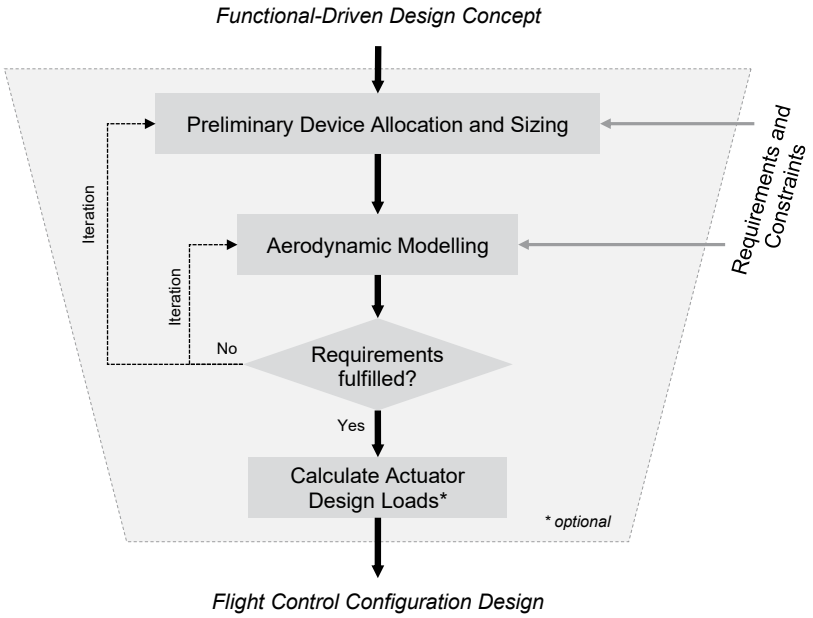

Figure 3.10 Schematic overview of the flight control system configuration design method (Lampl and Hornung, 2018).

3.4.1 Preliminary Device Allocation and Sizing

Starting point of the preliminary device allocation and sizing is the available functional-driven design concept where the functional design space and the possible functional segmentation has been identified (cf. *3.2.4 Functional Analysis and Synthesis*). However, the physical design space of the FCS configuration is very limited due to the wing design, the front and rear spar, or fuel tanks (cf. Figure 2.16). That's why the configurational designs of the FCS of recent transport aircraft are very similar and innovative solutions or new technologies are generally introduced on system or device level. Considering these limitations and constraints for the FCS configuration design, following conflicts, allocation criteria and prioritization were recognized:

The wing *leading-edge* devices of the high-lift control system are the only flight control devices at the wing leading edge. That implies, that the design problem is reduced to the sizing, segmentation and the selection of the type of leading-edge devices. Nevertheless, it should be considered that the maneuverability of the aircraft should be available as long as possible during low speed phases – by continuously reducing the wing angle of incidence towards the wing tip (washout) –

and to keep the ailerons at the outboard of the wing effective. The aerodynamic performance of the leading-edge devices should not counteract that effect. Additionally, strakes at the engine nacelles or small Krueger-flaps at the engine pylon can locally improve the flow pattern behind the engine/wing-junction.

At the wing *trailing-edge* the ailerons and high-lift control system have to share the available space alongside the span. Flight control devices on the wing upper side (spoiler) are generally located in front of the trailing-edge devices of the high-lift control system. In contrast to the high-lift control system, the required performance for roll control and the geometric constraints of the wing, mostly defines the (minimum) size of the main roll devices. For a first guess, it is recommended to allocate about one third of the wing trailing edge for roll control devices. After the minimum size of the main roll devices are defined, the remaining space at the wing trailing-edge is available for the outboard and inboard high-lift devices. Finally, after sizing and allocation of the high-lift control devices, the spoilers can be arranged.

3.4.2 Aerodynamic Modelling and Analysis

The aerodynamic modelling and analysis can be done in two steps. In the first step, the preliminary allocation of the flight control surfaces described above are considered and the initial aerodynamic performance is calculated on the basis of handbook and semi-empirical methods. In the second step, a vortex lattice model of the full aircraft is used to analyze the three-dimensional lift and drag coefficients. This approach works well for the overall aircraft aerodynamics with simple hinged control surfaces. More challenging – in the context of early aircraft design phases – is the aerodynamic modelling of different high-lift control configurations during low-speed phases. Therefore, a semi-empirical approach (Olson, 2015) can be applied to determine the low-speed aerodynamics of the aircraft. In this approach, empirical correlations for flap effectiveness, chord extension, drag and lift-coefficient increments as a function of flap deflection are combined with the characteristics of the clean airfoil. With the aerodynamic characteristics of the flapped airfoil sections, a vortex-lattice model can be set-up to calculate the three-dimensional lift and drag coefficients of the full aircraft configuration (Olson, 2015; Bunk, 2016).

A similar approach is recommended if new technologies or systems should be considered; especially if only few data are available, or the modelling is too costly for early aircraft design phases. In that case it is recommended to use the (estimated) aerodynamic performance results of the technology/concept and consider local drag and lift coefficient increments once the technology/system is activated. The modelling of additional flight control functions using AVL is limited, because complex control surface configurations or aerodynamic interactions cannot be modelled due to the linearity of the vortex lattice method. Nevertheless, the aerodynamic modelling of the Active Load Control (ALC) function of the Pro-HMS aircraft in addition to the Differential Flap Setting (DFS) was successfully demonstrated (Lampl and Hornung, 2018, p. 8, 12).

3.4.3 Calculate Actuator Design Loads

Finally, if all necessary requirements of the FCS configuration are fulfilled (after several design iterations), the design loads for the flight control device actuators can be (optionally) calculated, to have a basis for the required actuator design. The actuation design loads for hinged control

surfaces are characterized by the maximum hinge moment. Therefore, the results of the AVL model with defined control surfaces or different handbook methods can be used, depending on the type of the flight control surface and available data. However, this requires a sophisticated actuator model and details about actuator installation (e.g. level arm, kinematics), which are often not available in early phases of aircraft design. Consequently, if no detailed information or actuator model are available, the actuator mass is still considered within the parameterized mass estimation method (cf. *3.6 Mass Estimation Method*). To determine the design loads for unconventional flight control devices and actuators (e.g. fluidic actuators for active flow control), available system data and parameters must be used (if available) or a simplified system model must be set up to estimate the requirements (e.g. design pressure, max. mass flow rate).

3.4.4 Tool Implementation

The main step of aerodynamic modelling within the flight control configuration design methodology (cf. Figure 3.10) is implemented in an object-oriented programmed MATLAB®-tool, named Aerodynamic Vortex Lattice Calculation and Analysis Tool (AVLX). AVLX uses the Athena Vortex Lattice (AVL) program as a "black-box" to perform the 3D aerodynamic calculations (cf. *2.2.3 Aerodynamic Modelling, pp. 25*). All required input or output data files for AVL are generated or extracted in MATLAB® in an automated process. Furthermore, a Graphical User Interface (GUI) was developed for the easy setup, execution and analysis of multiple run cases, see Figure 3.11.

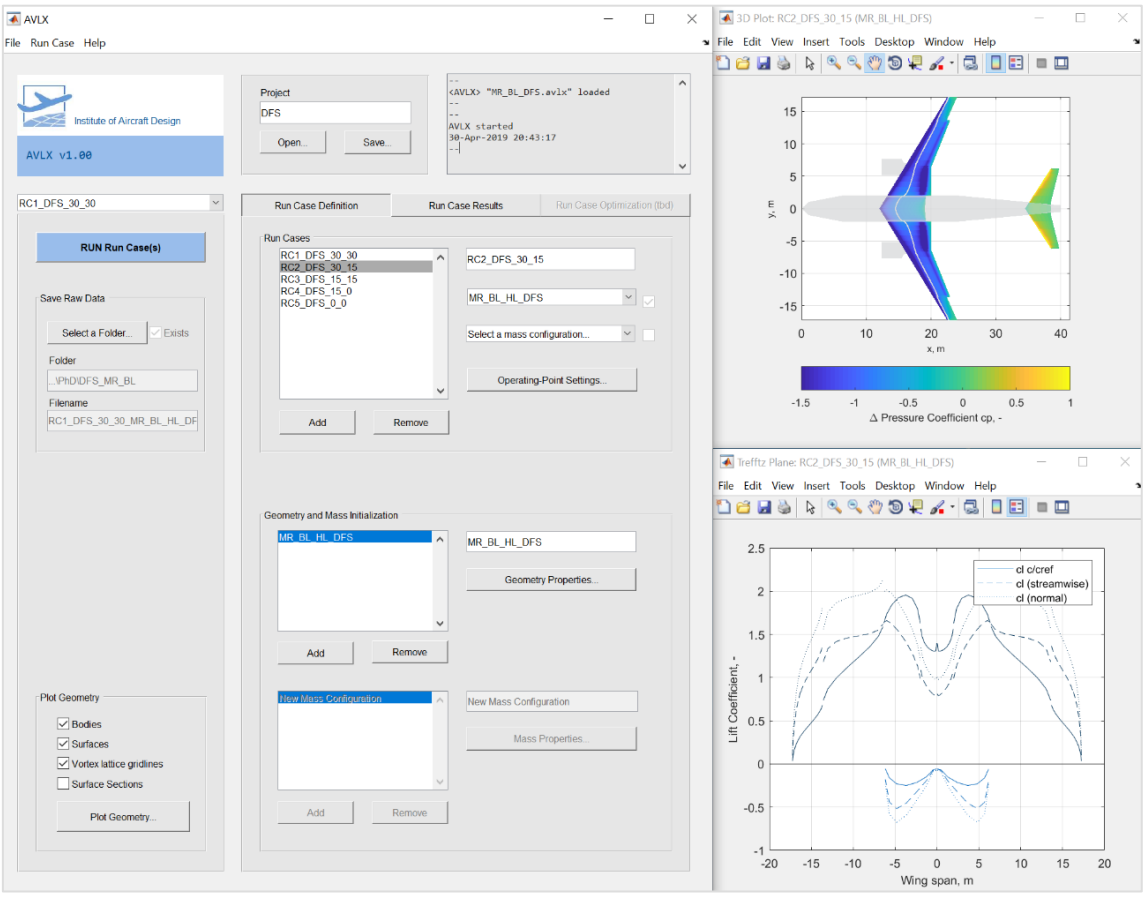

Figure 3.11 Overview of the main user interface (left) and exemplary result plots (right) of the Aerodynamic Vortex Lattice Calculation and Analysis Tool (AVLX).

Due to the modular structure of the implemented tool, all data models and functions of AVLX can be also used without the GUI, and thus further integrated into scripts or other tools. To run the aerodynamic calculation, a so-called *run case* has to be defined. A single run case is defined by an initialized geometry and a selected operating point, see Figure 3.12. The geometry properties contain general properties (e.g. reference area, reference chord), surface properties (e.g. wing and tail geometry, control surfaces) and body properties (e.g. fuselage, nacelles). The planform of the surfaces can be defined manually or by using the integrated wing surface generation tool (cf. Figure A.15). Furthermore, the implemented tool enables the parallel calculation of multiple defined run cases.

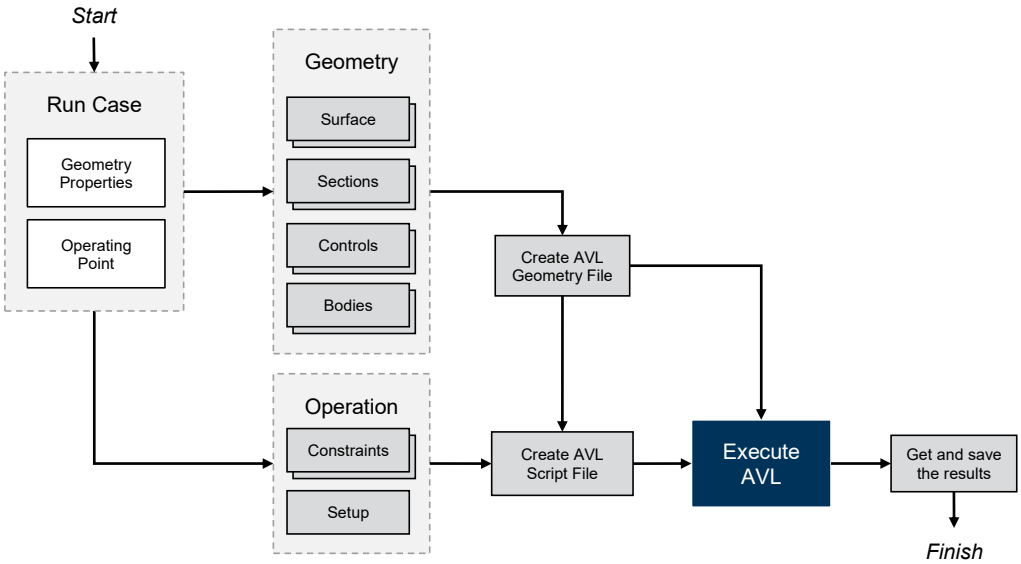

Figure 3.12 Overview of the implemented aerodynamic modelling procedure within the Aerodynamic Vortex Lattice Calculation and Analysis Tool (AVLX).

All calculation results are saved within the project. Furthermore, the raw data from AVL can be optionally saved in the project folder. In addition, AVLX provides several functions to display, analyze and plot the aerodynamic results of the run cases. For example, following main aerodynamic results are calculated and displayed by AVLX:

- Aerodynamic forces and moments
- Hinge moments
- Bending moments
- Surface and panel forces
- Stability data (derivatives)
- Plot functions (2D and 3D):
  - Lift distribution
  - Downwash angle
  - Bending moment (local)
  - Wing load
  - Pressure distribution

Further details about AVLX, including the structure of the data model behind, are given in the appendix *A.6 Data Model Structures and User Interfaces*.

3.5 Flight Control System Architecture Design

The main characteristics of the FCS architecture can be described by the FCC unit, the actuation system, and the power supply allocation. In this study, the simplified FCC unit consists of three primary and two secondary FCCs in addition to two HLCCs. The actuation system defines all actuators required for the flight control devices of the FCS configuration, including the PCUs and actuation system of the high-lift control system. The power supply distribution describes the assignment of different power sources to the actuators and PCUs. Furthermore, the main interfaces for the input of the pilot or autopilot, aircraft feedback, and for the device actuation are required. The design of the FCS architecture is mainly driven by functional and safety requirements. Whereas technological constraints and top-level aircraft system architectures restrict the design space.

The preliminary design of FCS architectures is based on a top-down approach, illustrated in Figure 3.13. The input data for the preliminary design tool is an FCS configuration, consisting of arranged flight control devices and dimensioning loads or hinge moments.

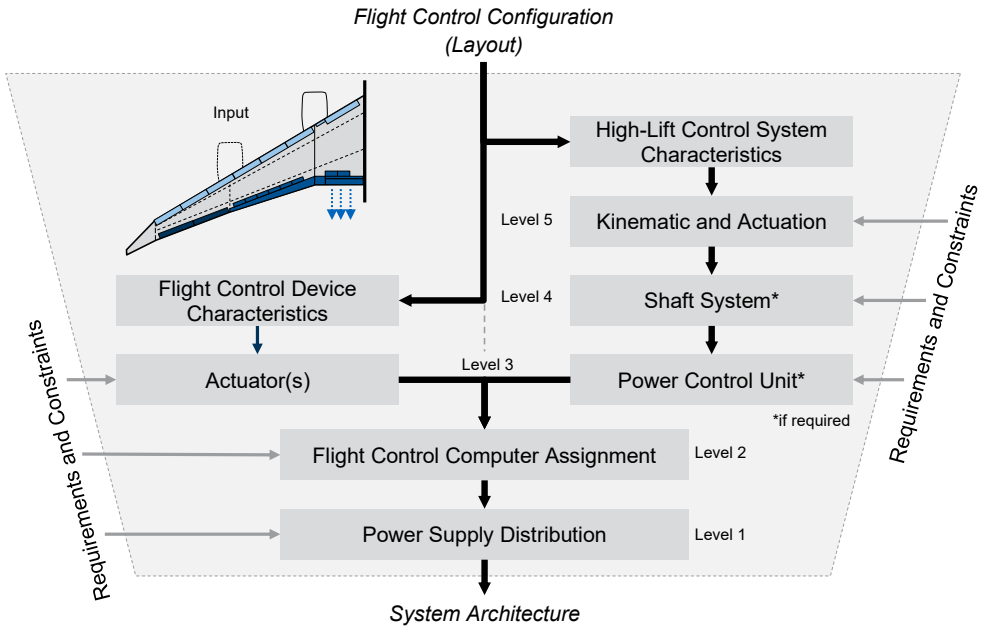

Figure 3.13 Overview of the implemented top-down approach for the preliminary design of flight control system architectures (Lampl *et al.*, 2017d).

Due to the very different design aspects of the primary flight control devices and spoilers, and the high-lift control system, the top-down approach is separated. On the one hand, the actuator types are selected and arranged to the dedicated flight control devices. On the other hand, the high-lift control system characteristics define the kinematic and actuation requirements, including the actuation system. The actuation can be a conventional transmission shaft together with a

PCU, or an innovative, distributed electrical drive system concept (cf. Figure 2.23). Afterwards, the FCCs are assigned to each flight control device per defined redundancy and reconfiguration rules. The distribution logics defines the power supply assignment to each flight control device and its actuator(s) and completes the architectural design.

3.5.1 Design Rules and Technological Constraints

Technological constraints for the FCS architecture are primarily defined by the FCS configuration and the overall aircraft system architecture (e.g. MEA, 2H-2E, no-bleed). According to the findings in the background section and the design rules published by Bauer *et al.* (2007), following main technological constraints can be defined:

Flight Control Computers

- The Flight Control Computer (FCC) Unit consists of (minimum) three PFCCs, three SFCCs and (if required) two HLCCs.
- All actuators at the same flight control device should be assigned to different FCCs.
- The actuation systems which enable flight-critical control functions should be connected to at least two different FCCs for reconfiguration.
- FCCs should be evenly distributed to have a comparable number of tasks.

Actuation System

- All actuators must be connected to the appropriate types of power source(s).
- Flight control devices, which have to fulfill one or multiple flight-critical control functions, should be actuated by at least two actuators (e.g. active-passive mode).
- It is not allowed to use EMAs for devices that have to fulfill flight-critical functions[67].

Power Supply

- Each PCU for high-lift systems (if required) is powered by two different power sources.
- All actuators at the same flight control device should have different power sources
- Power sources should be evenly distributed to have a comparable load.

Based on these technological constraints, following basic design rules for conventional FCS architectures can be derived, see Table 3.3. The main control functions are identified and classified as flight-critical or not. Afterwards, the actuators are distributed to the dedicating flight control surfaces and their control function(s). Finally, the power supply and the FCCs are assigned by defined rules. The basic design rules lead to reasonable results of conventional FCS, regardless if the aircraft provides a 3H or 2H-2E power system architecture (Lampl *et al.*, 2017d, p. 8).

[67] Due to the certain single-point failure which leads to a mechanical jam of the actuator.

Table 3.3 Design rules for conventional flight control system architectures (Lampl *et al.*, 2017d, p. 7).

Basic Flight Control Function	Flight critical	Flight Control Device(s)	Number of actuators	Power supply distribution	Flight Control Computer (FCC)	FCC Assignment
Roll control	yes	Aileron	2	Symmetrical[W]	PFCC, SFCC[B]	Enumerate
Pitch control	yes	Elevator	2	Enumerate	PFCC, SFCC[B]	Symmetrical
Yaw control	yes	Rudder (1/2)	3/2	Enum./Sym.	PFCC, SFCC[B]	Enum./Sym.
Trim	yes	THS	3	Enumerate	PFCC, SFCC[B]	Enumerate
Airbrake/lift Dump	no	Spoiler	1	Symmetrical[W]	PFCC, SFCC[A]	Symmetrical[W]
High-lift control	no	LE Flaps	1 (PCU)	Enumerate	HLCC	Enumerate
High-lift control	no	TE Flaps	1 (PCU)	Enumerate	HLCC	Enumerate

LE Leading Edge (wing)
TE Trailing Edge (wing)
THS Trimmable Horizontal Stabilizer
HLCC High-Lift Control Computer
PFCC Primary Flight Control Computer
SFCC Secondary Flight Control Computer
[A] Alternately PFCC and SFCC
[B] Backup
[W] Wing-symmetric (left/right)

Based on these basic design rules, additional design rules can be derived for advanced FCS with multifunctional flight control devices, see Table 3.4. The control devices shown in the table are examples. Nevertheless, the control functions can be fulfilled by different types of control devices collectively or individually. Accordingly, multifunctional flight control devices of advanced FCS are might be differently named[68].

Table 3.4 Design rules for advanced flight control system architectures (Lampl *et al.*, 2017d, p. 9).

Additional Flight Control Function	Control Device(s)	Control Device Characteristics	Power supply distribution	Flight Control Computer (FCC)	FCC Assignment
Roll control[S]	Flaperon Spoiler	Deflection up/down Deflection up/down	Symmetrical[W]	PFCC, SFCC[B] PFCC, SFCC[A]	Enumerate Enumerate
High-lift control[S]	Aileron Flaperon AFC[F]	Deflection down Deflection down Fluidic actuators on[P]	Symmetrical[W]	PFCC, SFCC[B]	Enumerate
Active load control	Aileron Spoiler	Deflection up/down Deflection up/down	Symmetrical[W]	PFCC, SFCC[B]	Enumerate
Differential flap setting	Flaperons/Flaps	Deflection up/down	Enumerate	HLCC	Enumerate
Cruise variable camber	Flaperons/ Flaps Spoiler	Deflection up/down Deflection down[G]	Enumerate	HLCC PFCC, SFCC[B]	Enumerate Symmetrical[W]

AFC Active Flow Control
TE Trailing Edge (wing)
HLCC High-Lift Control Computer
PFCC Primary Flight Control Computer
SFCC Secondary Flight Control Computer
[A] Alternately PFCC and SFCC
[B] Backup
[W] Wing-symmetric (left/right)

3.5.2 Tool Implementation

The approach is implemented in MATLAB® using object-oriented programming. The subsystems are defined as classes with system-specific properties (e.g. technology, interfaces and failure rates) and functions. Furthermore, within the implemented method, all technological relevant designs of the subsystems are pre-defined as objects. For example, the SHA is defined as an instance of the class *Actuator* and filled with architecture-independent properties. The specific design of each subsystem of level 3 to 5 show strong dependability to the properties and characteristics of the respectively higher-level subsystem (see Figure 3.13). Therefore, the technological constraints and the rules for the interface between two subsystems are defined in the higher-level subsystem. After subsystem level 3, the FCC assignment (level 2) and power supply distribution

[68] For example, known flight control devices with blended control functions are *flaperons* (flap and aileron functions), *tailerons* (tail and aileron functions) or *elevons* (elevator and aileron functions).

(level 1) are strongly dependent on the subsystem properties of the same level. Therefore, the interface definitions for the FCC and power supply in level 2 and 1 are defined in the object *Architecture*.

3.6 Mass Estimation Method

The parametric estimation tool calculates the total mass of the FCS configuration and architecture, including control surfaces, actuators, linkages, and wiring. The mass estimation method includes different parametric methods, which were researched and evaluated by Graiff (2016). The methods included are based on the works of Torenbeek (1982), Rudolph (1996), and Anderson *et al.* (1976). Here, the developed mass estimation method is initially limited to conventional control surfaces. However, it is assumed that if new technologies or concepts (e.g. AFC) are used, information about the system and installation masses are available[69], and can therefore also be taken into account. The mass estimation results thus provide a further parameter for the evaluation of an FCS design.

In general, the development of a mass estimation tool is hampered by the few available data and parameters in early aircraft design phases. Therefore, most methods start with a "should weigh" approach based on the technology level and are statistically expanded. For the extent of the mass estimate, the FCS are divided into panels, supports, fairings and actuation systems; each subsystem is considered separately but not independently from the others.

Overview. The existing estimation methods for flight control systems can be generally divided into two groups: The first group are directional control surfaces (aileron, spoiler, elevator, and rudder) which enable pitch, roll and yaw control. The second group considers high-lift control devices at the leading and trailing edge of the wing.

According to (Torenbeek, 2013, p. 348), the specific mass of hinged control surface panels (e.g. aileron) at the trailing edge (TE) of the wing can be calculated with the empirical Equation (3.1). The specific mass of control surface panels at the upper surface (US) of the wing (e.g. spoiler) can be calculated similar, using Equation (3.2).

$$\Omega_{CS_{TE}} = 3.0 \cdot \Omega_{ref} \cdot k_{bal} \cdot \left(\frac{S_{CS}}{S_{CS,ref}}\right)^{0.044} \tag{3.1}$$

The reference specific mass of the panel Ω_{ref} is specified by the used material. Torenbeek (2013) defines a reference specific weight of $\Omega_{ref} = 56\,N/m^2$ for the theoretical weight of two Al-alloy skins with one millimeter thickness each. However, weight reduction factors are presented for composite materials. Typical achievable reductions for composite control surface panels at the wing are in the range of 10-25%. The factor k_{bal} considers unbalanced ($k_{bal} = 1$), aerodynamically balanced (1.3) or mass balanced control surfaces (1.54). The control surface area S_{CS} denotes the

[69] For example, the study of Lampl *et al.* (2017a), distributed and electrical system architectures for high-lift control systems also provides detailed information about the system masses.

total planform behind the hinge line of the control surface in neutral position and are normalized by $S_{CS,ref} = 10m^2$.

$$\Omega_{CS_{US}} = 2.2 \cdot \Omega_{ref} \cdot \left(2 \cdot \frac{S_{CS}}{S_{ref}}\right)^{0.032} \tag{3.2}$$

Both expressions include the control structures, hinges and supports, and balance weights. If single actuator masses for the control surfaces are already available, the total required actuator mass can already be derived from the FCS architecture. Otherwise, and for a first estimation, the method provided by Anderson *et al.* (1976) can be applied, see Equations (3.3) and (3.4)[70]. Equation (3.3) considers hinged control surfaces at the trailing edge of the wing (e.g. ailerons), whereas Equation (3.4) is applied for control surfaces at the upper surface of the wing (e.g. spoilers).

$$W_{act,CS_{TE}} = 29.35 \cdot \left[2 \cdot \sum_{1}^{N} \left(k_i \cdot 2 \cdot S\bar{c}_{CS,i}\right)\right]^{0.44} \quad (\text{in } lb) \tag{3.3}$$

Where:

$S\bar{c}_{CS,i}$	Second order area moment of the control surface panel (in ft^3)
N	Number of control surface panels per wing
k_i	Number of actuators of each control surface

$$W_{act,CS_{US}} = 89 + f_{SBK} + 76.8 \cdot \sum_{i}^{N} \left(\frac{\delta_{CS,max}}{100} \cdot \left(\frac{V_{des} \cdot \cos(\lambda_{CS}) \cdot \sin(\delta_{CS,max})}{10^6} \cdot S\bar{c}_i\right)^{0.75}\right) \quad (\text{in } lb) \tag{3.4}$$

Where:

f_{SBK}	If control surface is used as a speed brake at ground: 20 (otherwise 0)
$\delta_{CS,max}$	Maximum control surface deflection (deg.) (typical value is 50 deg)
V_{des}	Design speed for control surface deployment (typical value is 295 kn)
λ_{CS}	Sweep angle of spoiler panel hinge line
$S\bar{c}_i$	Second order area moment of the control surface panel (in ft^3)

For the mass estimation of the high-lift control surfaces, Graiff (2016) suggested to use the method presented in the work of Rudolph (1996, pp. 118–122). This method is characterized by its simplicity, as the specific weight[71] (kg/m²) of different leading and trailing edge devices are given. However, the state-of-the-art high-lift control devices, such as the droop nose or the Adaptive Dropped Hinge Flap (ADHF), are missing. For that reason, relative approximations have been chosen. According to Pantelakis *et al.* (2011, p. 384), the total weight of a droop nose is approximately 66% of the weight of a conventional slat. The total weight of an ADHF is assumed to be approximately 20% less of the total weight of a conventional Single-Slotted Flap (SSF) (Torenbeek, 2013, p. 347). A complete overview of the specific weight of typical high-lift control devices are given in Table 3.5 and Table 3.6.

[70] Please note, that the input parameters of Equations (3.3) and (3.4) require imperial units (e.g. ft), and the results are expressed in pounds ($1\ lb = 0.453592\ kg$).

[71] Please note, that the specific weight is referred to the *stowed* flap area. It should also be noted that the segmentation of the high-lift control device surfaces has no impact on the weight estimate using this method.

Table 3.5 Specific weights for typical high-lift control devices at the wing leading edge of commercial transport aircraft (based on Rudolph (1996, p. 121)).

High-lift device	Krueger Flap	Krueger Flap	Slat	Slat	Droop nose
Specific weights in kg/m²	Rigid flap	Variable camber	Slave track	No slave track	Mechanical kinematic
Panels	7.3	10.3	12.2	11.4	7.5
Actuation	7.3	8.5	6.3	6.3	4.2
Total	**14.6**	**18.8**	**18.5**	**17.7**	**11.7**

Table 3.6 Specific weights for typical high-lift control devices at the wing trailing edge of commercial transport aircraft (based on Rudolph (1996, p. 119)).

High-lift device	SSF	SSF	ADHF	DSF[F]	DSF[A]	DSF[M]	TSF
Specific weights in kg/m²	Hooked track	Link-track	Hinged kinematic	Hooked track	Hooked track	Hooked track	Hooked track
Panels	13.2	13.2	10.6	14.6	17.1	23.4	26.9
Actuation	14.6	7.3	5.8	10.7	11.2	11.7	12.2
Supports	10.7	9.8	7.8	15.6	18.6	22.9	27.3
Fairing	4.9	0.5	0.4	4.9	5.6	6.3	6.8
Total	**43.4**	**30.8**	**24.6**	**45.8**	**52.5**	**64.3**	**73.2**

ADHF Adaptive Dropped Hinge Flap (ADHF)
DSF Double-Slotted Flap
SSF Single-Slotted Flap
TSF Triple-Slotted Flap

[A] Articulating vane/main configuration
[F] Fixed vane/main configuration
[M] Main/aft configuration

Wing Planform and Control Surface Model. The area of the control surfaces is essential for the applied calculation methods. Therefore, a complete parametric model of the wing and the control surfaces is required. To ensure a wider range of use, the parametric model is implemented as flexible as possible to enable the covering of different wing planforms and surface configurations. Examples of different wing and control surface models are shown in Figure 3.14.

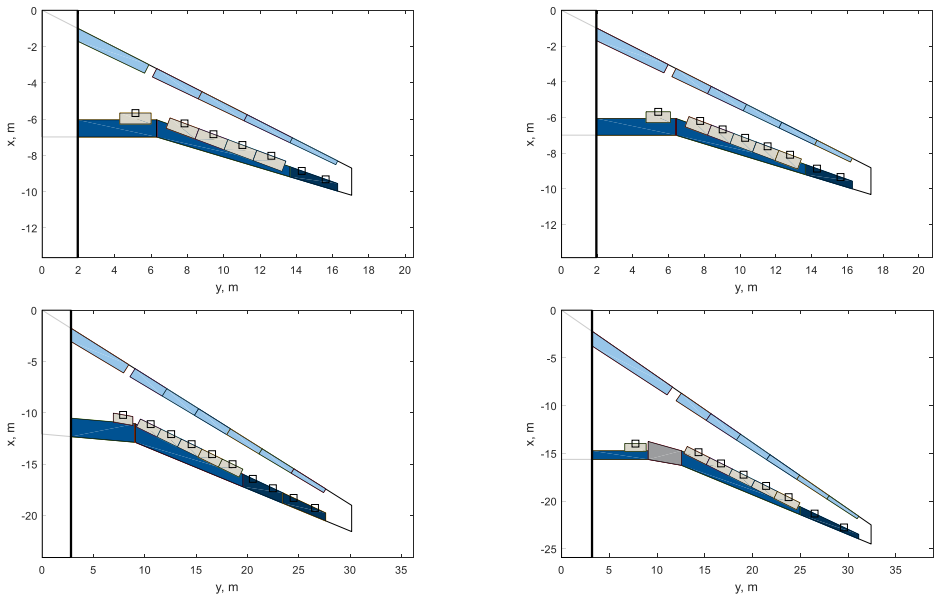

Figure 3.14 Examples of different generated wing planforms and control surface models (Lampl and Hornung, 2018, p. 9).

For a quicker and easier modelling, all surfaces were represented as polygons with straight edges in MATLAB®, which allows the definition of a simple column vector containing all the vertices coordinates. The objective of this approach is to represent the wing planform geometry and the FCS configuration as accurate as possible with the minimum amount of required input parameters. The number of required parameters to model the wing are kept within a reasonable amount, and only those strictly necessary for an accurate and effective modelling are needed as input. The main parameters required for the geometric definition of the wing are based on the work by Platz (1999). Nevertheless, some adaptions and simplifications are necessary to integrate the method in the mass estimation tool. The following main parameters and definitions are required for the *wing planform model*:

- Wingspan and wing area
- Wing sweep at 25% chord
- Wing taper ratio
- Wing chord at the fuselage and wing tip
- Relative wing kink position
- Sweep angle of inboard trailing-edge
- Span of the thrust gate (if required)

One important step of the *control surface modeling* is the determination of the relative wing-span position of the control surface. If it is located before the wing kink/first engine, the control surface is assigned to the inboard wing, otherwise to the outboard wing. This definition allows the application of simplified rules[72].

Summary. Based on the overall design and mass results, the flight control configuration and system architecture design can now be further analyzed, evaluated, or iteratively optimized. Therefore, the results of the integrated design approach (*Stage 1* and *Stage 2,* cf. Figure 3.1*)* serve as an input for a comprehensive analysis and assessment on system, aircraft, and mission level (*Stage 3*, see next Chapter *4 Aircraft Performance and Technology Analysis*).

[72] For example, all outboard control devices have constant chords relatively to the local wing chord. Furthermore, the inboard trailing-edge devices and spoilers have a constant chord. Further details on the wing planform and control surface models are explained in the work of Graiff (2016).

4 Aircraft Performance and Technology Analysis

After the procedure for the integrated design of advanced flight control configurations and system architecture was shown in the previous chapter, this chapter now presents the development and implementation of the Aircraft System Technology Analysis Tool (ATAX[73]). The simulation tool ATAX enables the analysis and assessment of new system technologies and concepts on system, aircraft, and mission level (*Objective 3*), representing the last part of the overall methodology (cf. Figure 3.1). ATAX uses a model-based approach to determine the secondary power requirements of the aircraft systems. Moreover, an engine performance model is implemented, combined with a method to calculate the impact of engine power-offtakes on the overall Specific Fuel Consumption (SFC). In addition, a medium-range (MR) and long-range (LR) aircraft and the associated mission profiles are defined in this work in order to have a baseline configuration for later comparison. In the end of this chapter, the validation of the tools (models) and selected results are presented and discussed.

4.1 Baseline Aircraft Models

To calculate the performance and power requirements of a commercial transport aircraft, a lot of specific aircraft parameters and data is required. For example, main parameters are design range, cruise altitude and speed, cabin size and number of passengers. Since there are many different commercial transport aircraft configurations, two parametric baseline aircraft are defined, based on published data, handbooks and databases for existing transport aircraft to represent the majority of all aircraft. Commercial transport aircraft are often categorized according to their range in Short-Range (SR), Medium-Range (MR) and Long-Range (LR). Nevertheless, no clear definition or consistent standard for categorization could be found in literature. Table 4.1 shows the main parameters of the MR and LR baseline aircraft. Both baseline aircraft are typical twin-engine aircraft configurations. The MR baseline aircraft represents a typical transport aircraft comparable to a Boeing 737-800 and an Airbus A320-200. The LR baseline aircraft is comparable to a Boeing 777-300ER or an Airbus A350-1000.

[73] ATAX was developed in MATLAB® (R2017a) using object-oriented programming and parallel computing to enable fast calculation times. The used version for this thesis is ATAX v2.11.

Table 4.1 Main parameters of the medium-range (MR) and long-range (LR) baseline aircraft.

Parameter	MR	LR	Unit	*Parameter*	MR	LR	Unit
General				*Wing*			
Crew [a]	2/4	2/10	–	*Span*	34.8	63.9	m
Capacity [b]	189/184/162	550/442/370	–	*Area (ref.)*	124	440	m
Length	38.5	73.8	m	*Sweep*	25	33	°
Height	12.2	17.8	m	*Aspect ratio*	9.6	8.8	–
Mass				*Engine (2)*			
MTOM	76390	329770	kg	*Number*	2	2	-
MLM	65220	242150	kg	*Thrust*	130	484	kN

[a] *Number of crew members: Cockpit/Cabin*
[b] *Number of PAX: 1-class (max) / 2-class / 3-class*

A comprehensive overview of each baseline aircraft is given in the appendix *A.4 Baseline Aircraft and Mission Models.*

4.2 Flight Mission Model

Flight missions of commercial transport aircraft are characterized by specific performance data (e.g. altitude and speed), aircraft-specific data (e.g. configuration and masses), official regulations and environmental conditions (Gillet *et al.*, 2010). A typical mission profile can be described by an altitude and speed profile as a function of time (Simsic, 1991). Furthermore, the speed V of the aircraft is defined as a function of the altitude h. In this thesis, it is assumed that the Indicated Air Speed (IAS) is equal to the Calibrated Air Speed (CAS). To calculate the True Air Speed (TAS), the compressibility of the air and the air density are considered. The TAS constitutes the basis for all calculations in context with the Mach number, see Equation (4.1).

$$V_{TAS} = Ma \cdot \sqrt{\gamma \cdot R_{spec} \cdot T_{\infty}} \tag{4.1}$$

The parameter γ represents the heat capacity ratio of the air and R_{spec} stands for the specific gas constant of air. The temperature T_{∞} describes the ambient air temperature. For simplification, no wind conditions are assumed, so that the ground speed is equal to the TAS. In low altitudes, the speed is typically given by the CAS. According to (Nuic, 2004, p. C-12), the conversion from CAS to TAS is done with Equation (4.2).

$$V_{TAS}(h) = \sqrt{\frac{2\gamma}{\gamma-1} \cdot \frac{p(h)}{\rho(h)} \left\{ \left[1 + \frac{p_{0,ISA}}{p(h)} \left(1 + \frac{\gamma-1}{2\gamma} \cdot \frac{\rho_{0,ISA}}{p_{0,ISA}} \cdot V_{CAS}^2 \right)^{\frac{\gamma}{\gamma-1}} - 1 \right]^{\frac{\gamma-1}{\gamma}} - 1 \right\}} \tag{4.2}$$

Both, the air density $\rho(h)$ and air pressure $p(h)$ are dependent from the flight altitude h. The parameters $\rho_{0,ISA}$ and $p_{0,ISA}$ represent the conditions on Mean Sea Level (MSL). In general, a flight mission of commercial transport aircraft can be divided into the following main phases: *Taxi-out*, *Take-off*, *Climb*, *Cruise*, *Descent*, *Approach*, *Landing*, and *Taxi-in*, see Figure 4.1. The flight phase

loiter for holding is optional and not considered within this study. The corresponding parameters for the defined baseline MR/LR aircraft, are given in the appendix *A.4 Baseline Aircraft and Mission Models.*

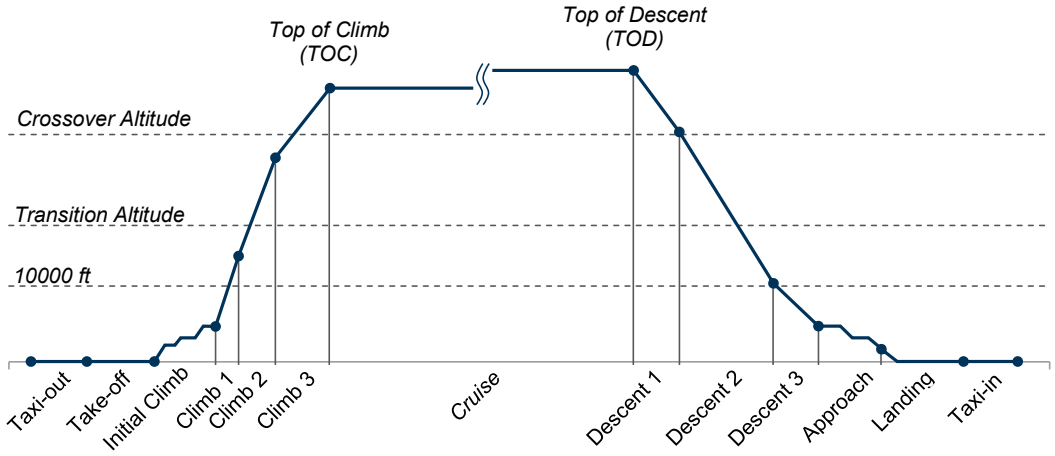

Figure 4.1 Overview of the phases and altitude profile of a typical mission of commercial transport aircraft (Lampl *et al.*, 2017b, p. 3).

In the following, the main characteristics and definitions of the individual phases of a typical flight mission of commercial transport aircraft are described:

Taxi-out. The Taxi-out phase begins with the engine start-up, followed by the push-back and taxi-out, and ends with the positioning of the aircraft on the runway. At standard conditions, the taxi speed is between 15-20 kt (Nuic, 2004, p. C-33; Chakraborty *et al.*, 2016, p. 16). The time accounting for this phase is 11 minutes [74].

Take-off. The Take-off phase starts with the beginning of acceleration on the runway and ends with reaching 35 ft over ground (obstacle height). Furthermore, it is assumed that the take-off speed is equal to the speed at the beginning of the climb (V_2).

Climb. The Climb phase comprises the whole climbing process until reaching cruise altitude. It is divided in Initial Climb and Climb 1, 2, and 3, that differ in the rate of climb, taken from the Aircraft Performance Database (Eurocontrol, 2017). According to Gillet et al. (2010, p. 5), three phases of acceleration are made during Initial Climb, where the speed V_2 increases by 10 kt, 30 kt and 60 kt (CAS). The next acceleration is attempted after reaching 10000 ft. This altitude limits the maximum allowed speed of 250 kt (CAS) under FL100[75]. After reaching the transition altitude at 18000 ft, the TAS and Mach number continuously increase until Top of Climb (TOC) altitude and cruise speed (Ma) is reached.

[74] The taxi-in times are based on averaged data for the period summer/winter 2012-2013 of the most relevant airports with minimum 500 flights in this period (Data from www.eurocontrol.int).

[75] According to *§91.111 Aircraft Speed* (CFR Part 91 – General Operating and Flight Rules) of the Federal Aviation Administration (FAA) (2019): *"Unless otherwise authorized by the Administrator, no person may operate an aircraft below 10,000 feet MSL at an indicated airspeed of more than 250 knots."*

Cruise. The Cruise represents the longest phase of the flight mission, regarding to range and time. Typical cruise altitudes for the baseline aircraft are 40000 ft (MR) and 42000 ft (LR). The maximum cruise speed is limited by the maximum operating Mach number Ma_{MO}. According to recorded flight data typical Mach numbers for the baseline aircraft are in the range of 0.78 – 0.82 (MR) and 0.84 – 0.88 (LR) (Rustenburg *et al.*, 2002, p. A-6; Tipps *et al.*, 2006, p. C-6). Due to high fuel consumption during cruise and thus a decrease of the overall aircraft weight, a step-climb or continuous cruise-climb can be selected, in addition to the level cruise at constant altitude.

Descent. The Descent phase begins at Top of Descent (TOD) altitude after the cruise. The air speeds during descent can be defined by a given air speed profile. The speed (Ma) remains constant until the crossover altitude is reached, which is fixed at 30000 ft. After falling below, the crossover altitude, the speed is kept constant at 300 kt (CAS). Similar to the climb phase, the speed has to be reduced to 250 kt (CAS), while reaching 10000 ft. The following rates of descent are defined according to the advisory circular of the Federal Aviation Administration (FAA) (2011, p. 3 in Appendix 1). For simplification, it is assumed that the approach angle is constant during descent and is set to 3° as a default value.

Approach. The start of the Approach is defined by the Initial Approach Fix (IAF) point, which marks the beginning of the approach at the altitude of 4000 ft. After reaching the Final Approach Fix (FAF), the final approach begins. Deceleration phases during the approach are defined at the IAF and FAF. The *Landing* phase begins with the threshold crossing at 100 ft and is followed by the touchdown at defined touchdown speeds.

Taxi-in. The following taxi with a typical speed between 15-20 kt lasts about 5 minutes[76] to reach the final parking position.

All the presented speeds or altitudes are typical parameters of the baseline aircraft missions and implemented in the mission model – however, all mission parameters can be modified in the model to generate several speed and altitude profiles. The ambient conditions (temperature, pressure and density) are modeled on the basis of the International Standard Atmosphere (ISA)[77]. The input of optional temperature deviations enables the modelling of hot or cold days. The implementation of the mission model and the integration into ATAX is presented in section *4.5 Tool Implementation.*

4.3 Aircraft System Models

For estimating the secondary power demand and the fuel consumption of aircraft systems within early aircraft design phases, two different approaches are applied. On the one hand, simplified physical models with defined input parameters and system constraints are developed. On the other hand, semi-empirical approaches or data found in published literature are used for power

[76] The taxi-out times are based on averaged data for the period summer/winter 2012-2013 of the most relevant airports with minimum 500 flights in this period (Data from www.eurocontrol.int).

[77] According to Johnson *et al.* (2002), the International Standard Atmosphere (ISO 2533:1975), the ICAO Standard Atmosphere and the U.S. Standard Atmosphere 1976 are identical in the altitude range from 0km up to 32km.

requirement estimations. The aircraft power system can be divided into primary power for generating thrust and into secondary power to supply the onboard distributed aircraft systems, see Figure 4.2. To estimate the secondary power requirements independently from the power system architectures, the generation and distribution system is not part of the aircraft system models.

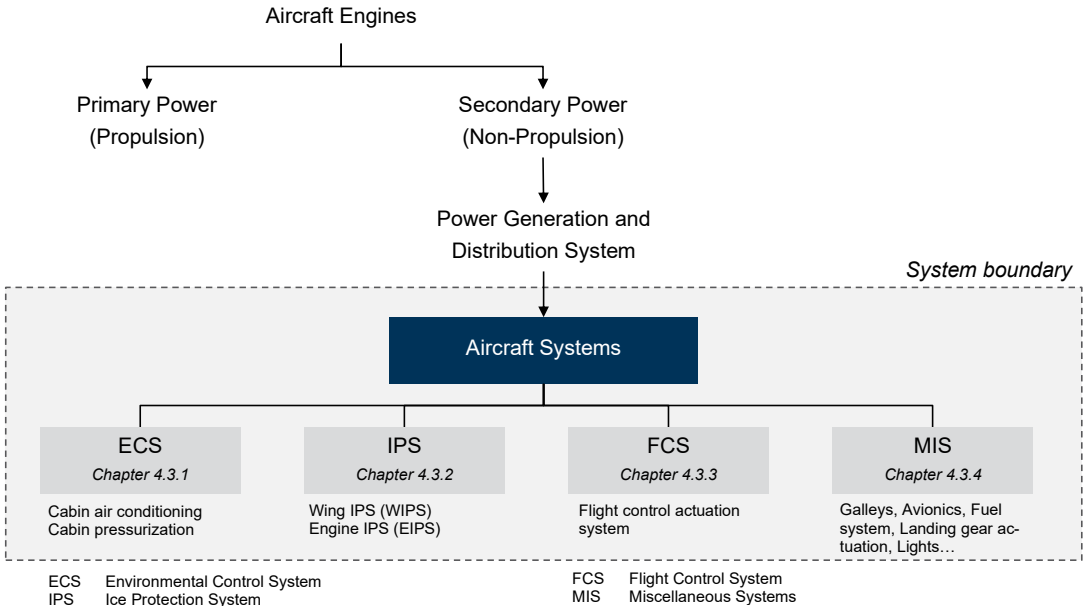

Figure 4.2 Overview of the aircraft system models and the defined system boundary for secondary power requirement estimations (Lampl *et al.*, 2017b, p. 4).

Simplified system models are used for the three most important aircraft systems, regarding secondary power consumption or criticality: The Environmental Control System (ECS), the Ice Protection System (IPS), and the Flight Control System (FCS). On basis of aircraft-level functions, major functions at system level are derived and used to develop the aircraft system models. As mentioned in the background chapter, a main advantage of this functional-analysis approach is that the power requirements can be calculated independently from system architectures and system technologies. The power requirements of the remaining, miscellaneous systems (MIS), e.g. galleys, avionics, and fuel systems, are mainly based on empirical methods or existing data from literature. The implementation of the aircraft systems models and the corresponding data models are described in section *4.5 Tool Implementation.*

4.3.1 Environmental Control System

The main functions of the Environmental Control System (ECS) are cabin air conditioning and cabin pressurization to provide a comfortable cabin environment for crew and passengers during the whole flight mission. Consequently, the ECS can be divided into an Air Conditioning System (ACS) and a cabin pressurization system. To meet the requirements in the early aircraft design phase a simplified pneumatic and electrical ECS model is developed. As the cabin pressurization is achieved by simply controlling the outflow of the cabin via a cabin outflow valve, the overall ECS model focuses on the main power consuming ACS.

Air Conditioning System. The schematic models of the ACS with corresponding mass flow rates and heat flow rates is illustrated in Figure 4.3. The pneumatic ACS is supplied by the engine bleed air system, including the pre-cooler heat exchanger which provides a constant temperature of the bleed air. The bleed air is generally drawn off from the intermediate pressure compressor or the high pressure compressor of the engine, regulated by valves and pre-coolers (Wild, 1990, pp. 40–41). Accordingly, it is assumed that the temperature and the pressure of the bleed air supply is constant throughout the mission – regardless of the engine speed[78]. The electrical ACS *(no-bleed architecture*) uses ram air and electrical Cabin Air Compressors (CAC) to generate the required compressed air and temperature. Again, it is assumed that the air temperature T_{CAC} is constant and requires no down regulation after the CAC, before entering the Air Conditioning Pack (ACP) (Sinnet, 2007, p. 6). Nevertheless, for the bleed-less architecture the temperature T_{ram} of the ram air supply changes with flight altitude and speed of the aircraft.

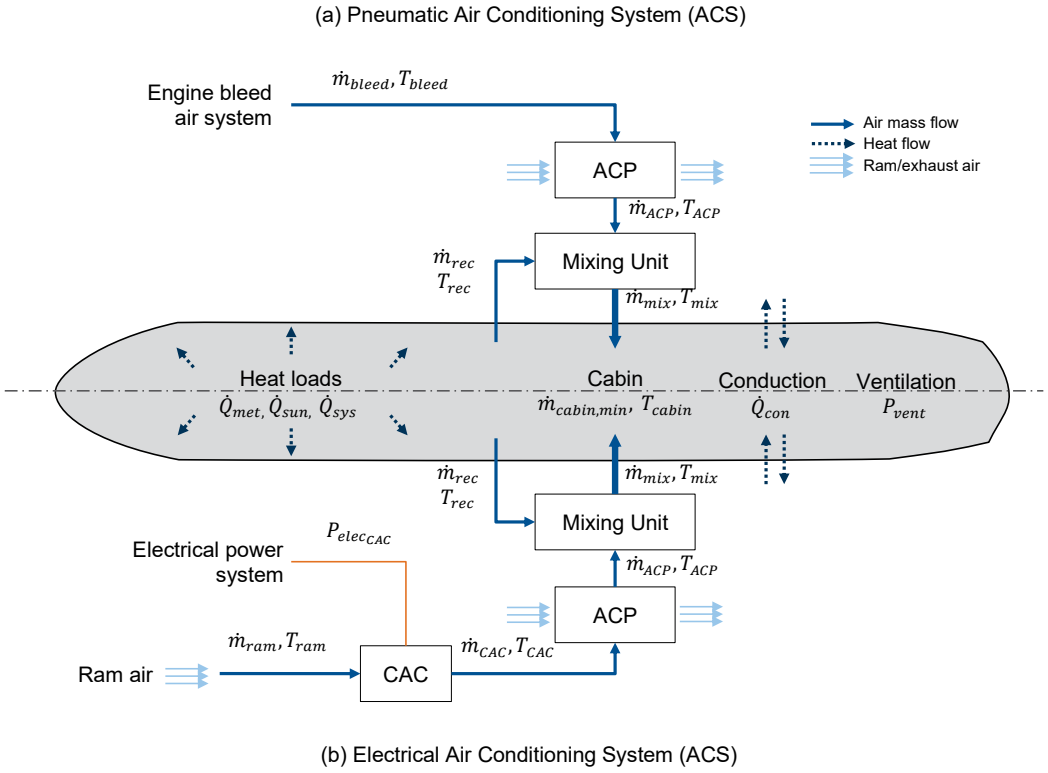

Figure 4.3 Simplified models of a pneumatic (top) and an electrical (bottom) Air Conditioning System (ACS) (Lampl *et al.*, 2017b, p. 5).

[78] This simplification requires following assumptions: In general, the bleed air pressure and temperature right behind the compressor valve and before the pre-cooler are depending on the engine speed (number of revolutions) and the compressor stage. Here, it is assumed that the pre-cooler is exactly varying the amount of required fan air to keep the bleed air conditions (pressure and temperature) after the pre-cooler constant. The efficiency of the pre-cooler heat exchanger is assigned to the engine bleed air system.

According to data found in literature, typical bleed air temperatures are in the range of $T_{bleed} = 180°C - 204\,°C$ (Moir and Seabridge, 2008, p. 387; Chakraborty, 2015, p. 181) and compressor air temperature is $T_{CAC} \approx 95\,°C$ (Moir and Seabridge, 2008, p. 387) before entering the ACP. The ACP consists of an air cycle machine and a heat exchanger using ram air to cool the hot pressurized air (Wild, 1990, pp. 41–42). Nevertheless, for this simplified ECS model both, the CAC and the ACP, are assumed as a *black box* with characteristic efficiencies η_{CAC} and η_{ACP}.

Within the mixing unit, which is assumed as lossless, recirculated cabin air is mixed with the conditioned supply air from the ACP and directed to the cabin by overhead distribution nozzles. The recirculated mass flow rate $\dot{m}_{rec}$ provides about 40-50% of the cabin air flow rate $\dot{m}_{cabin}$ (Tagge *et al.*, 1985, p. 41; Lammering, 2014, p. 39; Chakraborty, 2015, p. 245). The recirculation factor f_{rec} is initially set to 0.5 (50%) and can vary during the flight mission. Furthermore, it is assumed that the temperatures T_{ACP}, T_{rec} and T_{mix} are equal to the required cabin air temperature T_{cabin}. It is assumed that the cabin temperature is constant and homogenous inside the cabin. A hot air manifold with trim air (low pressure, high temperature) to adjust the temperature in different cabin zones is not considered.

The overall required power for the ACS P_{ACS} can be calculated with Equation (4.3), as the sum of all heat flow rates into and from the cabin (see Figure 4.3).

$$P_{ACS} \overset{\text{def}}{=} \sum \frac{dQ_i}{dt} = \dot{Q}_{cabin} = \dot{Q}_{con} + \dot{Q}_{met} + \dot{Q}_{sys} + \dot{Q}_{sun} \tag{4.3}$$

The total heat flow rate results from different heat loads and from the heat transfer between the cabin and the environment. Further equations and parameters required for each heat load are shown in *A.5 Aircraft System Model* (cf. Table A.10).

The supply requirements for air conditioning (index with ACS) of the pneumatic and electrical ECS can be calculated by using Equation (4.4), where η_{ACP} represents the efficiency of the ACP and c_p the specific heat capacity of air.

$$\dot{m}_{bleed/ram_{ACS}} = \dot{m}_{ACP_{ACS}} = \frac{P_{ACS}}{\eta_{ACP} \cdot c_p \cdot (T_{bleed/ram} - T_{ACP})} \tag{4.4}$$

Besides air conditioning requirements, the fresh air requirement for crew and passengers must be fulfilled. The Federal Aviation Administration (FAA) (2019) specified in the FAR 25.831 that the minimum fresh air $\dot{m}_{fresh}$ provided by the ventilation system must be at least 0.55 lbs/min (*minimum*) per occupant. According to Lammering (2014, p. 42), further values of 0.75 lbs/min (*standard*) and 1.0 lbs/min (*comfort*) are common. Following this, the mixed air mass flow rate $\dot{m}_{mix}$ can be calculated to verify if the fresh air requirements are met. If the mass flow rate for air conditioning is too low, corrected supply mass flow rates are calculated, see Equations (4.5) and (4.6).

$$\dot{m}_{mix_{ACS}} = \dot{m}_{ACP_{ACS}} + f_{rec} \cdot \dot{m}_{fresh} \tag{4.5}$$

$$\dot{m}_{bleed/ram} = \dot{m}_{ACP} = \begin{cases} \dot{m}_{bleed/ram_{ACS}} + (\dot{m}_{fresh} - \dot{m}_{mix_{ACS}}), & \dot{m}_{mix_{ACS}} < \dot{m}_{fresh} \\ \dot{m}_{bleed/ram_{ACS}} & , \quad \dot{m}_{mix_{ACS}} \geq \dot{m}_{fresh} \end{cases} \tag{4.6}$$

The resulting amount of bleed air $\dot{m}_{bleed}$ represents the power requirements for the pneumatic ECS. The electrical power requirements for the CAC are calculated using Equation (4.7).

$$P_{elec_{CAC}} = \frac{\dot{m}_{CAC} \cdot c_p \cdot (T_{CAC} - T_{ram})}{\eta_{CAC}} \qquad with \quad \dot{m}_{CAC} = \dot{m}_{ACP} = \dot{m}_{ram} \tag{4.7}$$

Additionally, for both the pneumatic and electrical ECS, the power for ventilation P_{vent} must be considered. Here, the electrical power for cabin ventilation is estimated with 135 W per occupant (Steinke, 2010, p. 28).

Cabin Pressurization System. Another important function of the ECS is cabin pressurization. A typical cabin altitude (pressure) schedule of transport aircraft is shown in Figure 4.4. The cabin pressurization is achieved by controlling the outflow of the cabin via controlled outflow valves. In this thesis, the required power for the electrical controlled outflow valves is neglected, as it is considerably less than the power requirements for air conditioning and ventilation. Nevertheless, for the sake of completeness, the ECS model calculates the cabin altitudes, considering two different modes of pressurization. In the isobaric mode, the cabin altitude (pressure) is controlled to a predetermined value. When the maximum differential pressure is reached, the mode is automatically switched to the constant differential mode. In this mode, the difference between cabin pressure and ambient air pressure is kept constant.

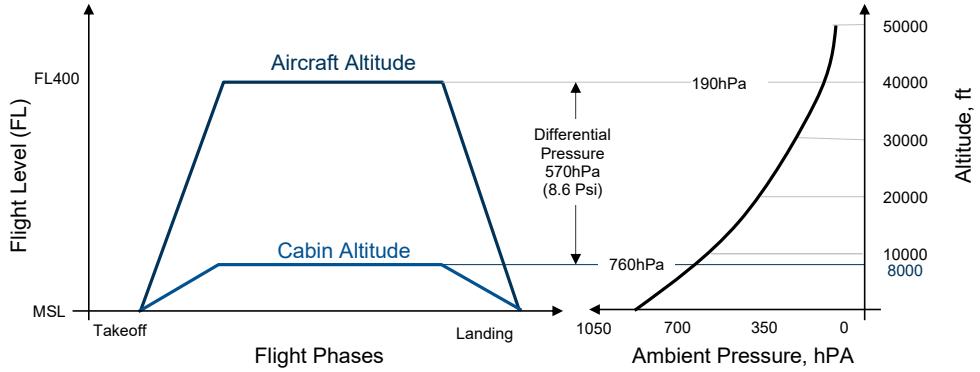

Figure 4.4 Typical cabin pressure altitude profile of a commercial transport aircraft, based on Moir and Seabridge (2008, p. 285).

According to the regulations, the maximum allowed cabin pressure altitude is 8000 ft. This altitude is a good compromise between the passenger's health and comfort and the aircraft structure weight, which would increase with a higher pressure difference between cabin and the environment (Hocking, 2005, p. 8). Typical values for the maximum or nominal differential pressure are in the range of 8.6 psi (Tagge *et al.*, 1985, p. 41) to 8.9 psi (Moir and Seabridge, 2008, p. 285). The

cabin pressure rate of change during climb and descent is therefore limited: The cabin altitude should not increase at more than 500 ft/min (climb) and should not decrease at more than 300 ft/min (descent), as the adaption during re-pressurization of the cabin is more difficult for the people (Hocking, 2005, p. 9).

4.3.2 Ice Protection System

The Ice Protection System (IPS) has the main function to avoid ice formation or ice accumulations at aerodynamically sensitive areas such as wing leading edges and engine cowlings at the inlet (Moir and Seabridge, 2008, p. 248). Furthermore, air data probes, cockpit windows, antennas and valves are heated to prevent icing and thus malfunctions or failures. In general, hot air or electrical heating elements are used for anti-icing or de-icing (Wild, 1990, p. 55). The two main IPS power consumers are the Engine Ice Protection System (EIPS) and Wing Ice Protection System (WIPS). EIPS is generally supplied by bleed air, even for MEA architectures like the B787. In general, there are two possible architectures for the WIPS, see Figure 4.5. The pneumatic WIPS is supplied by the engine bleed air systems, where the leading-edge devices are heated by hot engine bleed air over so-called piccolo tubes. The electro-thermal WIPS is supplied by the electrical power system. Therefore, attached heating mats inside the leading-edge devices provide the required heating for anti-icing or de-icing.

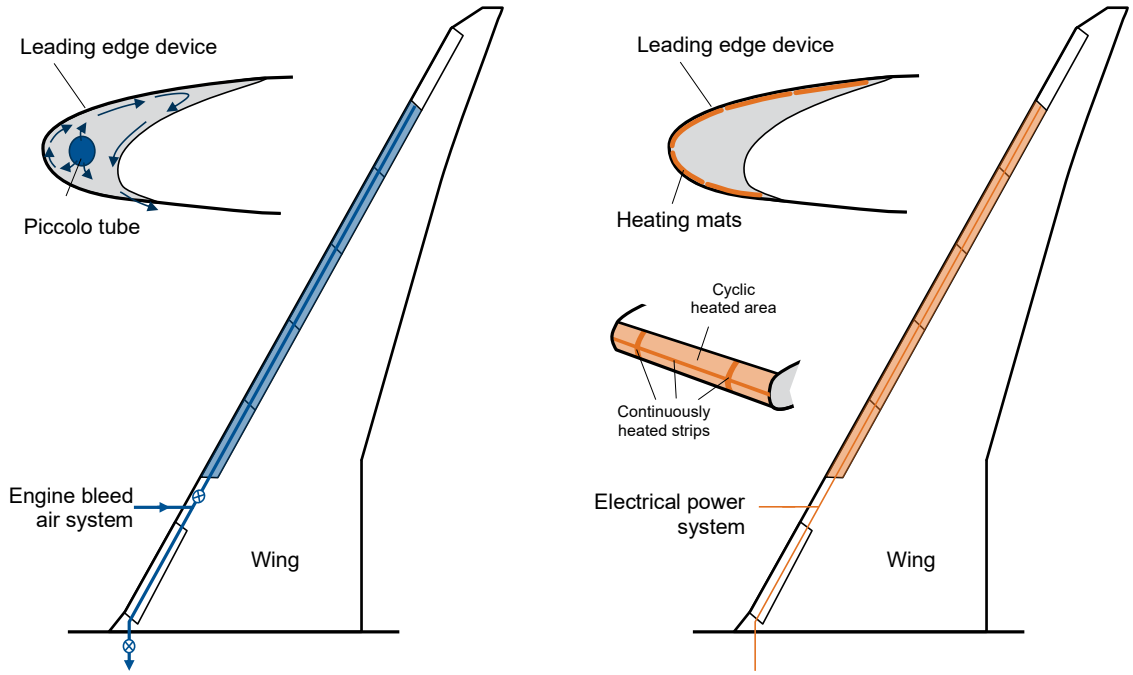

Figure 4.5 Simplified models of the Wing Ice Protection System (WIPS) with pneumatic power supply (left) and electrical power supply (right) (based on Chakraborty *et al.* (2016, p. 161) and Lammering (2014, p. 44)).

Sherif *et al.* (1997) published a semi-empirical method for the local heat transfer and ice accretion on aircraft wings, where the local heat transfer is influenced by energy added or removed to the surface in form of different heat flux densities (cf. Figure A.7). Based on this method, the total heat flux $\dot{q}_{total}$ can be calculated using Equation (4.8).

$$\dot{q}_{total} = \dot{q}_{conv} + \dot{q}_{sens} + \dot{q}_{evap} - \dot{q}_{kin} \tag{4.8}$$

The convectional heat flux $\dot{q}_{conv}$ describes the cooling of the surface due to air flow. The sensible heating $\dot{q}_{sens}$ is the heat flux required to heat the impinging water droplets to the desired surface temperature. Evaporation at wing or engine cowling and the corresponding heat losses are considered over the heat flux $\dot{q}_{evap}$. Furthermore, $\dot{q}_{kin}$ represents the kinetic heating. The corresponding calculations are given in the appendix (see *A.5 Aircraft System Models*). The required bleed air mass flow for a pneumatic IPS results from Equation (4.9), where A_{prot} is the area of the surface to protect, and $T_{surface}$ is the desired temperature of the protected surface. T_{bleed} is the temperature of the bleed air supply and $\eta_{bleed_{IPS}}$ is the overall heat transfer efficiency for the pneumatic IPS, that is assumed to be approximately 0.65 (Liscouët-Hanke, 2008, p. 87).

$$\dot{m}_{bleed} = \frac{\dot{q}_{total} \cdot A_{prot}}{\eta_{bleed_{IPS}} \cdot c_p \cdot (T_{bleed} - T_{surface})} \tag{4.9}$$

To calculate the power for the electrical IPS two further steps are required. In the first step, the resulting heat flux $\dot{q}_{total_{elec}}$ of the electrical IPS can be calculated using Equation (4.10). The parting strips are continuously heated (see Figure 4.5) for anti-icing considering the parting strip area ratio f_{ps}, that is about 20% (Chakraborty, 2015, p. 163) of $A_{prot,IPS}$. The factor f_{cyc} of the cyclic heat flux term is assumed to be 0.05 (Meier and Scholz, 2010, p. 7), which describes the ratio of heating time to the cycling time. The heat flux $\dot{q}_{cyc}$ for de-icing of the cyclic heated area is estimated with Equation (4.11) (Chakraborty, 2015, p. 162).

$$\dot{q}_{total_{elec}} = \dot{q}_{total} \cdot f_{ps} + \dot{q}_{cyc} \cdot f_{cyc} \tag{4.10}$$

$$\dot{q}_{cyc} = \frac{\rho_{ice} \cdot l_{ice}}{t_{heat}} \cdot (c_{ice} \cdot (T_{ref} - T_{\infty}) + L_f) \tag{4.11}$$

Therefore, it is assumed that a thin layer of ice l_{ice} of 0.5 mm is intermittently melted and heated to the desired surface temperature, and L_f is the latent heat that arises during evaporation of water. In a second step, the electrical power requirements P_{WIPS} can be calculated, see Equation (4.12). A typical value of electrical IPS efficiency $\eta_{elec_{IPS}}$ is 0.7 (Chakraborty, 2015, p. 133).

$$P_{WIPS} = \frac{\dot{q}_{total_{elec}} \cdot A_{prot}}{\eta_{elec_{IPS}}} \tag{4.12}$$

The estimated electrical power for the heating of other system (e.g. cockpit window heating, air data probes) are based on values published by Roskam (1989): 6 kW during take-off and climb, 7.5 kW during cruise and again 6 kW during descent and landing.

Icing Envelopes (System Activity). The IPS is active if the aircraft operates in icing conditions where the formation of super-cooled water is very likely. These icing conditions are defined as a standard by the FAA and EASA and can be used for the design of the IPS (Jeck, 2002). According to the FAA, different icing design envelopes are considered for the wing ice protection and for engine ice protection. Generally, *Continuous Maximum Atmospheric Icing Conditions* are applied to airframe ice protection (e.g. wings) and *Intermittent Maximum Atmospheric Icing Conditions* are applied to engine ice protection and sensors (Jeck, 2002, p. 1). The continuous icing conditions represent stratus clouds with large horizontal extent with small to medium Liquid Water Content (LWC) and appear for a relatively long time. In contrast to that, the intermittent maximum conditions appear for a relatively short time, but with higher LWC, which is typical for cumulus clouds with small horizontal extent.

Based on these considerations, the activity schedule for the IPS is defined by icing design envelope, which are characterized by ambient temperature vs. pressure altitude. If the aircraft is within the icing conditions the WIPS or EIPS are activated, respectively. For both, a standard median volume diameter of the water droplets of 20 µm is assumed (Jeck, 2002, p. 6), but the parameters can vary in the implemented tool.

4.3.3 Flight Control System

The power requirements of the Flight Control System (FCS) strongly depends on the aerodynamic forces acting on the flight control surfaces (Lammering, 2014, p. 53). Consequently, the initial power estimations can be done independent from the chosen actuation technology. The power requirements P_{cs} for the actuation of flight control surfaces – e.g. ailerons, rudder and elevators – are estimated over the surface loads in form of hinge moments M_{hinge}, which are required for the desired deflection rates $\dot{\gamma}_{cs}$, see Equation (4.13).

$$P_{cs} = M_{hinge} \cdot \dot{\gamma}_{cs} \tag{4.13}$$

The hinge moment is proportional to the dynamic pressure $\frac{\rho_\infty}{2} \cdot V_{TAS}^2$, the surface area A_{cs}, the average surface chord $\bar{c}_{CS}$, and the hinge moment coefficient $C_{hinge,CS}$, see Equation (4.14) and Equation (4.15) (Chakraborty *et al.*, 2015). To consider compressible effects at speeds, the coefficients $C_{hinge,\alpha}, C_{hinge,\gamma}$ are divided by the Prandtl-Glauert factor $\beta = \sqrt{1 - Ma^2}$. The angle of attack α and the deflection angle γ are dependent on the mission flight phases. The deflection rates $\dot{\gamma}_{CS}$ of the control surfaces are calculated by normalized maximum deflection angles $\hat{\delta}_+/\hat{\delta}_-$ and the related Cycles Per Second (CPS)[79] for each phase of the mission, see Table 4.2.

[79] One CPS describes the deflection of a control surface and its return to zero position within one second.

$$M_{hinge} = \frac{\rho_\infty}{2} \cdot V_{TAS}^2 \cdot A_{cs} \cdot \bar{c}_{cs} \cdot C_{hinge,cs} \tag{4.14}$$

$$C_{hinge,cs} = C_{hinge,0} + C_{hinge,\alpha} \cdot \alpha + C_{hinge,\gamma} \cdot \gamma \tag{4.15}$$

The resulting power is calculated with Equation (4.16), using the actuation efficiency $\eta_{Actuator}$.

$$P_{hyd/elec_{CS}} = \frac{P_{cs}}{\eta_{actuator}} \tag{4.16}$$

Table 4.2 Typical Characteristics of control surface deflections and related Cycles Per Second (CPS) for each mission phase (based on Simsic (1991) and Chakraborty (2015)).

Mission Phase	Activity	Aileron	Elevator	Rudder	Spoiler
	CPS	$\hat{\delta}_+/\hat{\delta}_-$	$\hat{\delta}_+/\hat{\delta}_-$	$\hat{\delta}_+/\hat{\delta}_-$	$\hat{\delta}$
Taxi-out [a]	0.00	0.00/−0.00	0.00/−0.00	0.00/−0.00	0.00
Take-off	0.40	0.12/−0.12	0.20/−0.20	0.20/−0.20	0.12
Initial climb	0.40	0.12/−0.12	0.20/−0.20	0.20/−0.20	0.12
Climb 1-3	0.40	0.12/−0.12	0.20/−0.20	0.20/−0.20	0.12
Cruise [b]	0.20	0.12/−0.12	0.20/−0.20	0.20/−0.20	0.12
Descent 1-3	0.30	0.12/−0.12	0.20/−0.20	0.20/−0.20	0.12
Initial Approach	0.30	0.12/−0.12	0.20/−0.20	0.20/−0.20	0.12
Final Approach	0.40	0.32/−0.40	0.50/−0.50	0.50/−0.50	0.30
Landing	0.40	0.32/−0.40	0.50/−0.50	0.50/−0.50	0.40
Taxi-in	0.00	0.00/−0.00	0.00/−0.00	0.00/−0.00	0.00

[a] *All controls free and correct checks are not considered*
[b] *Assumption: No turbulence during cruise*

The hinge moments of high-lift devices cannot be determined only with geometry data of the leading and trailing edge devices, but also require knowledge of the kinematics of the associated mechanism. Thus for a first estimation, the power requirements for the high-lift system actuation is based on an empirical approach (Chakraborty, 2015). In this work, the author relates the installed PCU power to the maximum take-off mass $MTOM$ of existing commercial transport aircraft to establish following Equation (4.17).

$$P_{PCU} = 1196.9 \cdot \left(\frac{MTOM}{1000}\right)^{0.5551} \tag{4.17}$$

The result represents the total power for both PCUs for the leading edge and trailing edge devices, and shows good accordance to power data presented in the work of Lammering (2014).

Finally, the required hydraulic power for the PCU can be calculated by using Equation (4.18), where η_{PCU} is the PCU efficiency.

$$P_{hyd_{PCU}} = \frac{P_{PCU}}{\eta_{PCU}} \tag{4.18}$$

If other types of flight control device configurations or actuation systems (cf. 2.3.4 Advanced Technologies and Concepts) are examined, power requirement data or simplified system models (including activity schedules) are required, respectively.

4.3.4 Miscellaneous Systems

All remaining systems with considerable power requirements which cannot be assigned to the ECS, IPS or FCS, are defined under miscellaneous systems (MIS). For each system, differentiated activity schedules can be defined.

Table 4.3 Overview of the electrical power requirements of Miscellaneous Systems (MIS).

System	Power Assumptions	Unit	Activity Schedule
Avionics	8000	W	All phases
Fuel system	0.136	W/kg	All phases (Reference: MTOM)
Galley	250	W/pax	Initial Climb, Climb 1-3, Cruise
Cabin lights	40	W/m	All phases (Reference: Cabin length)
In-flight entertainment	50	W/pax	All phases
Aircraft lights			
Position	500	W	All phases
Navigation	50	W	All phases
Beacon	200	W	All phases
Taxi	750	W	Taxi
Landing	4000	W	Taxi, Take-off, Initial Climb, Approach, Landing
Logo	500	W	Take-off, Initial Climb, Approach, Landing

In addition, the hydraulic power requirements for retraction and deployment of the landing gear is estimated by Equation (4.19), using the hydraulic power of the PCU as a reference.

$$P_{hyd_{LG}} = 1.53 \cdot P_{hyd_{PCU}} \tag{4.19}$$

This estimation is based on the hydraulic power requirements from flight test data of an Airbus A320 presented in the work of Lammering (2014, p. 26). For simplification, it is assumed that the power demand for retraction and extension of the landing gear is equal.

4.4 Thrust and Fuel Consumption

The overall fuel consumption is a good indicator for the overall efficiency of transport aircraft. To calculate the fuel consumption, following main data are required: Aircraft performance, flight mission, engine thrust and power offtakes. The aircraft performance can be described by the basic flight mechanics and aerodynamic characteristics of the aircraft (cf. *2.2 Aircraft Aerodynamics and Performance*). Dependent on the flight altitude and speed (*flight phase*), the required thrust can be determined for each step of the mission under consideration. The thrust requirements, in addition to the secondary engine power offtakes, enable the calculation of the total fuel flow in each mission step, and consequently the total fuel consumption of the aircraft can be determined.

4.4.1 Specific Fuel Consumption

The overall fuel consumption is made up of the resulting fuel consumption for the thrust and the resulting fuel consumption for the secondary power offtakes (cf. Figure 4.2). Accordingly, the overall Specific Fuel Consumption (SFC) can be divided into three different parts, see Equation (4.20). The main and basic SFC share is due to the engine thrust and is defined as SFC_{basic}. In addition, SFC_{shaft} and SFC_{bleed} considers the SFC due to engine power offtakes (shaft and bleed air power). The corresponding fuel flow $\dot{m}_{fuel}$ is calculated with Equation (4.21).

$$SFC = SFC_{basic} + SFC_{shaft} + SFC_{bleed} \tag{4.20}$$

$$\dot{m}_{fuel} = SFC \cdot T = (SFC_{basic} + SFC_{shaft} + SFC_{bleed}) \cdot T \tag{4.21}$$

The calculation of the required thrust T is described in the following section *4.4.2 Engine Thrust and Power Offtakes*. At this point, it is assumed (in contrast to reality) that all engines have the same thrust setting and consequently an equal share in total thrust. This means that all engines on the aircraft have the same thrust settings and thus the same fuel consumption. In addition, the engine power offtakes (loads) are also equally distributed among the installed engines.

Engine Thrust (Basic). To calculate SFC_{basic}, a method based on Torenbeek (1982, pp. 563–569) is applied, where following assumptions are made:

- The thrust is referred to fully expanded conditions (ideal thrust)
- The fuel mass flow is neglected relative to the engine air mass flow
- Constant specific heat ratio $\gamma = 1.4$
- Unmixed fan and exhaust (engine core) flow
- Engine power offtakes are ignored

The main required parameters for this method are Bypass Ratio (BPR), Turbine Entry Temperature (TET), the Overall Pressure Ratio (OPR) in addition to compressor, turbine, and nozzle efficiencies. BPR, TET and OPR are typical parameters to define a turbofan engine and the level of engine technology.

The first step of this method is to calculate the so-called gas generator function G, which describes the process within the engine core, see Equation (4.22).

$$G = \left(\Phi - \frac{\kappa}{\eta_c}\right) \cdot \left[1 - \frac{1.01}{\eta_G{}^{\frac{\gamma-1}{\gamma}} \cdot (\kappa + \mu) \cdot (1 - \frac{\kappa}{\Phi \cdot \eta_c \cdot \eta_t})}\right] \tag{4.22}$$

Where:

Φ	Normalized Turbine Entry Temperature (TET)	η_G	Gas generator efficiency (intake stagnation pressure ratio)
κ	Temperature function of the compression process	η_c	Engine compressor efficiency (isentropic)
μ	Ratio of stagnation to static temperature (ambient air)	η_t	Engine turbine efficiency (isentropic)

The characteristic non-dimensional TET Φ is depedend on the maximum TET $T_{TET,max}$ of the engine, and the characteristics of actual flight phase (thrust setting and ambient temperature), which are considered in the parameter k_{TET}, see Equation (4.23).

$$\Phi = \frac{T_{TET,max} \cdot k_{TET}}{T_\infty} \tag{4.23}$$

The characteristic temperature function of the compression process κ is defined with following Equations (4.24) and (4.25), where the parameter μ represents the ratio of the stagnation temperature to the ambient air temperature.

$$\kappa = \mu \cdot (OPR^{\frac{\gamma-1}{\gamma}} - 1) \tag{4.24}$$

$$\mu = 1 + \left(\frac{\gamma - 1}{2} \cdot Ma^2\right) \tag{4.25}$$

According to Scholz *et al.* (2013, p. 173), the gas generator efficiency η_G, including the engine inlet efficiency η_{inlet}, are calculated with Equations (4.26) and (4.27). In addition, a typical inlet pressure loss of $\frac{\Delta p}{p} \approx 0.02$ can be assumed.

$$\eta_G = 1 - \frac{\frac{\gamma}{2} \cdot Ma^2 \cdot (1 - \eta_{inlet})}{1 + \frac{\gamma - 1}{2} \cdot Ma^2} \tag{4.26}$$

$$\eta_{inlet} = 1 - (1.3 + 0.25 \cdot BPR) \cdot \frac{\Delta p}{p} \tag{4.27}$$

Finally, the SFC_{basic} and the corresponding fuel flow $\dot{m}_{fuel,basic}$ can be determined, see Equations (4.28)[80] and (4.29). As mentioned above, the secondary power fuel consumption is not taken into

[80] The factor of $2.01 \cdot 10^{-5}$ converts the results to SI-Units: $\frac{kg/s}{N}$ $(= \frac{g/s}{kN})$.

account in the calculation of SFC_{basic}. For this reason, the SFC due to engine power offtakes has to be calculated separately.

$$SFC_{basic} = \frac{2.01 \cdot 10^{-5} \cdot \sqrt{\theta} \cdot \left(\Phi - \mu - \frac{\kappa}{\eta_c}\right)}{\sqrt{5 \cdot \eta_n \cdot \left(1 + \eta_t \cdot \eta_f \cdot BPR\right) \cdot \left(G + \frac{\gamma - 1}{2} \cdot Ma^2 \cdot \frac{\eta_{inlet}}{\eta_t \cdot \eta_f} \cdot BPR\right)} - (1 + BPR) \cdot Ma} \tag{4.28}$$

$$\dot{m}_{fuel,basic} = SFC_{basic} \cdot T \tag{4.29}$$

Where:

θ	Relative ambient temperature $\theta = T_\infty / T_{0,ISA}$	G	Gas generator (engine core) function
Φ	Normalized Turbine Entry Temperature (TET)	η_n	Nozzle efficiency (isentropic)
κ	Temperature function of the compression process	η_c	Engine compressor efficiency (isentropic)
μ	Ratio of stagnation to static temperature (ambient air)	η_t	Engine turbine efficiency (isentropic)
BPR	Bypass Ratio	η_f	Engine fan efficiency (isentropic)
Ma	Mach number	η_{inlet}	Engine inlet efficiency (isentropic)

Shaft Power Offtakes. To calculate the SFC due to engine shaft power offtakes, two different methods have been found in literature, which are applicable in early aircraft design phases. The first method uses a constant shaft power coefficient k_p to calculate SFC_{shaft}, see Equation (4.30). The engine shaft power coefficient $k_{p,1}$ is determined on the basis of the data from different transport aircraft engines (Scholz, 1996, p. 163). This linear regression with a constant shaft power coefficient $k_{p,1}$ is a good approximation and can be used for preliminary estimations.

$$SFC_{shaft} = SFC_{basic} \cdot k_{p,1} \cdot \frac{P_{shaft}}{T_{max,rated}} \qquad with\ k_{p,1} = 0.0094\,\frac{N}{W} \tag{4.30}$$

Where:

SFC_{basic}	Specific fuel consumption due to engine thrust	P_{shaft}	Shaft power offtakes due to secondary power requirements
$k_{p,1}$	Constant shaft power coefficient in $\frac{N}{W}$ (Method 1)	$T_{max,rated}$	Maximum rated engine thrust at Mean Sea Level (MSL)

An alternative and more sophisticated approach uses a variable engine shaft power coefficient k_p. According to Scholz *et al.* (2013), k_p is generally not constant throughout the flight envelope of an aircraft. Consequently, they suggest a variable engine shaft power coefficient $k_{p,2}$, which depends on altitude h and Mach number Ma of the aircraft, see Equation (4.32) (Scholz *et al.*, 2013, p. 183). The calculation of the SFC_{shaft} is similar to the first method, but instead of the rated maximum take-off thrust, the actual thrust T is used, see Equation (4.31).

$$SFC_{shaft} = SFC_{basic} \cdot k_{p,2} \cdot \frac{P_{shaft}}{T} \tag{4.31}$$

$$k_{p,2} = 0.0057 + 4.6 \cdot 10^{-8} \cdot h - 0.0106 \cdot Ma - 4.44 \cdot 10^{-13} \cdot h^2 + 1.85 \cdot 10^{-7} \cdot h \cdot Ma + 0.0049 \cdot Ma^2 \tag{4.32}$$

Where:

SFC_{basic}	Specific fuel consumption due to engine thrust	P_{shaft}	Shaft power offtakes due to secondary power requirements
$k_{p,2}$	Variable shaft power coefficient in $\frac{N}{W}$ (Method 2)	T	Engine thrust

Independent of which calculation method is used, the corresponding fuel flow $\dot{m}_{fuel,shaft}$ is calculated with Equation (4.33). The required shaft power P_{shaft} is calculated with Equation (4.49) (cf. *4.4.2 Engine Thrust and Power Offtakes*).

$$\dot{m}_{fuel,shaft} = SFC_{shaft} \cdot T \tag{4.33}$$

Bleed Air. The SFC due to engine bleed air is calculated with Equation (4.34) (Method 1) or Equation (4.35) (Method 2). According to Scholz (Scholz), Method 1, which is based on the SAE AIR1168, shows good approximations within preliminary aircraft design. To calculate SFC_{bleed}, the coefficient $k_{b,1}$ and the bleed air requirements $\dot{m}_{bleed}$ are required in addition to the turbine entry temperature T_{TET} and thrust T.

$$SFC_{bleed} = k_{b,1} \cdot T_{TET} \cdot \frac{\dot{m}_{bleed}}{T} \qquad with\ k_{b,1} = 3.015 \cdot 10^{-5}\ \frac{1}{K} \tag{4.34}$$

Ahlefelder (2006) presents another method, which uses the overall pressure ratio OPR of the engine instead of the turbine entry temperature T_{TET}. The bleed-air parameter $k_{b,2}$ is defined differently in this case, where the relative enthalpy of the bleed-air is taken into account[81]. This results in the alternate Equation (4.35) and a different bleed-air coefficient $k_{b,2}$. Finally, the fuel flow $\dot{m}_{fuel,bleed}$ is calculated as usual, see Equation (4.36).

$$SFC_{bleed} = k_{b,2} \cdot OPR^{0.475} \cdot \frac{\dot{m}_{bleed}}{T} \qquad with\ k_{b,2} = 4.99 \cdot 10^{-3} \tag{4.35}$$

$$\dot{m}_{fuel,bleed} = SFC_{bleed} \cdot T \tag{4.36}$$

4.4.2 Engine Thrust and Power Offtakes

The above described methods to calculate the SFC requires the total thrust and engine power offtakes of the aircraft. The calculation of the engine thrust for each mission step[82] has to be done iteratively, as the aircraft mass changes over time, and thus also the aerodynamic characteristics and the required thrust of the aircraft (cf. Footnote 86).

Engine Thrust. To have a starting point for further iteration, the initial specific thrust requirements have to be estimated. This enables further calculations of the aerodynamic coefficients of the aircraft for each mission step. For this reason, a simplified engine model is used for the initial estimation of the thrust T, see Equation (4.37). Once the initial thrust is determined, the thrust iteration (*inner loop*) and fuel iteration (*outer loop*) can start (cf. Figure 4.7).

[81] Ahlefelder (2006) uses the relative enthalpy values of two already existing engines of a typical medium range aircraft. The considered engines are the CFM 56-5 (Boeing 737) and IAE V2500 (Airbus A320). Then a mean value is calculated from the relative enthalpies of both engines. Using this mean value, the engines were simulated in a simulation software (GastTurb® 8.0) to determine the bleed air parameters.

[82] A *step* is defined by altitude, speed and environmental conditions (e.g. temperature, air density…)

$$T = n_{eng} \cdot T_{max,rated} \cdot \left(\frac{V_{TAS}}{V_{ref}}\right)^{n_V} \cdot \left(\frac{\rho}{\rho_{ref}}\right)^{n_\rho} \cdot \left(\frac{n}{n_{ref}}\right)^{3.5} \tag{4.37}$$

Where:

n_{eng}	Number of installed engines	ρ	Air density (aircraft altitude)
$T_{max,rated}$	Maximum rated engine thrust at Mean Sea Level (MSL)	ρ_{ref}	Reference air density (Standard: $\rho_0 = 1.225\ kg/m^3$)
V_{TAS}	Aircraft speed (True Air Speed (TAS))	n_ρ	Engine altitude dependence (parameter)
V_{ref}	Reference speed	$\frac{n}{n_{ref}}$	Engine (spool) speed ratio
n_v	Engine speed dependence (parameter)		

The aerodynamic characteristics[83] of the aircraft, which are dependent on the mission steps and aircraft mass, can now be calculated. The time-based mass reduction due to the fuel flow leads to changes in the required lift and the corresponding drag of the aircraft. This again results in new thrust requirements, which in turn leads to changes in the overall SFC or fuel flow, respectively. Hence, to estimate the required thrust, the overall aircraft drag has to be calculated (cf. Equation (2.11)). According to Equation (2.6), the corresponding drag coefficient is generally divided into zero-lift drag and the (lift-depended) induced drag ($C_D = C_{D0} + k{C_L}^2$).

Howe (2010, pp. 145–150) presents a method to calculate the zero-lift drag coefficient, which is applicable in early aircraft design phases. In a first step, the clean zero-lift drag $C_{D0,clean}$ has to be calculated, see Equations (4.38) and (4.39)[84] (Howe, 2010, pp. 145–150). Afterwards, changes of the zero-lift drag due to varying aircraft configurations (e.g. extended landing gear and flaps) have to be considered (cf. Equation (2.8)). According to Howe (2010, p. 150) typical zero-lift drag increments due to landing gear extension of commercial transport aircraft is $\Delta C_{D0,LG} = 0.03$.

$$C_{D0,clean} = 0.005 \cdot \left(1 - \frac{2 \cdot c_{lam}}{R_{wet}}\right) \cdot \tau_{wing} \cdot \left[1 - 0.2 \cdot Ma + 0.12 \cdot \left(\frac{Ma \cdot \sqrt{\cos \varphi_{1/4}}}{f_{af} - {}^{t}/_{c}}\right)^{20}\right] \cdot R_{wet} \cdot f_{ac} \cdot {S_{ref}}^{-0.1} \tag{4.38}$$

$$\tau_{wing} = \left(\frac{R_{wet} - 2}{R_{wet}}\right) + \frac{1.9}{R_{wet}} \cdot \left[1 + 0.526 \cdot \left(\frac{{}^{t}/_{c}}{0.25}\right)^{3}\right] \tag{4.39}$$

Where:

c_{lam}	Fraction of wing chord with laminar flow	f_{af}	Airfoil design factor (Howe, 2010, p. 118)
R_{wet}	Effective overall wetted area to the reference area	${}^{t}/_{c}$	Wing thickness-to-chord ratio
τ_{wing}	Correction factor of the wing thickness	f_{ac}	Aircraft type factor (Howe, 2010, p. 149)
Ma	Mach number	S_{ref}	Wing reference area
$\varphi_{1/4}$	Wing sweep at 25% chord		

[83] The governing equations of the aerodynamic characteristics and performance of the aircraft are given in the background section (cf. *2.2.1 Aerodynamic Forces and Moments* and *2.2.2 Aircraft Stability and Flight Mechanics*).

[84] According to Howe (2010), the equations to calculate the drag coefficients are applicable for subsonic and transonic aircraft with moderate to high-aspect ratio wings ($\Lambda > 5$).

To estimate the typical zero-lift drag increments for extended flaps in take-off (TO) or landing (LD) configuration, following Equations (4.40) and (4.41) are used (Howe, 2010, pp. 149–150), where f_{flap} is a flap drag factor[85] and Λ the aspect ratio of the wing. The resulting zero-lift drag coefficient is often referred to as *effective* zero-lift drag coefficient $C_{D0,eff}$.

$$\Delta C_{D0,flaps,T0} = \frac{0.03 \cdot f_{flap} - 0.004}{\Lambda^{0.33}} \tag{4.40}$$

$$\Delta C_{D0,flaps,LD} = \frac{0.15 \cdot f_{flap}}{\Lambda^{0.33}} \tag{4.41}$$

To determine the lift-depended or induced drag C_{Di}, the lift coefficient C_L and the induced drag factor k are required. The lift coefficient can be calculated with following Equations (4.42), considering the actual aircraft weight mg and the aircraft speed, which is represented by the dynamic pressure q_∞. The flight path angle γ is calculated with Equation (4.43), where $\frac{dh}{dt}$ defines the climb or decent rate and V_{TAS} the speed of the aircraft.

$$C_L = \frac{m \cdot g \cdot \cos\,\gamma}{q_\infty \cdot S_{ref}} \tag{4.42}$$

$$\gamma = \arcsin\left(\frac{\frac{dh}{dt}}{V_{TAS}}\right) \tag{4.43}$$

According to Equation (2.7), the Oswald efficiency e is required to calculate the induced drag factor k. In addition to the dependence on the wing geometry (e.g. aspect ratio, taper ratio, wing sweep), there is also a dependence on the Mach number, and thus a dependence on the mission steps. Based on the Howe calculation method, the following formula can be extracted to determine the Oswald efficiency e, see Equations (4.44) and (4.45).

$$e = \left\{(1 + 0.12 \cdot Ma^2) \cdot \left[1 + \frac{0.142 + f_\lambda \cdot \Lambda \cdot \left(10 \cdot {}^{t}/_{c}\right)^{0.33}}{\left(\cos \varphi_{1/4}\right)^2} + \frac{0.1}{(4+\Lambda)^{0.8}}\right]\right\}^{-1} \tag{4.44}$$

$$f_\lambda = 0.005 \cdot [1 + 1.5 \cdot (\lambda - 0.6)^2] \tag{4.45}$$

Where:

Ma	Mach number	Λ	Wing aspect ratio (wing)
f_λ	Taper ratio factor	$\varphi_{1/4}$	Wing sweep at 25% chord
λ	Wing taper ratio (wing)		

[85] According to Howe (2010), typical values for f_{Flap} are 1.0 for single slotted flaps (SSF) and 1.2 for double slotted flaps (DSF).

The above presented approach enables the calculation of the drag coefficients and hence the overall aircraft drag for each mission step. In addition, an increase or decrease in overall or zero-lift drag, due to additional flight control functions (according to their activity schedule), have to be considered at this point, see Equation (4.46).

$$C_D = C_{D0,eff} + k \cdot {C_L}^2 + \Delta C_{D,FCS} \tag{4.46}$$

Finally, the overall aircraft drag can be calculated and the require thrust T can be determined, see Equations (4.47) and (4.48). In addition, for the calculation of the thrust, it has to be distinguished between different phases of the aircraft (e.g. during acceleration phases).

$$D = \frac{1}{2} \cdot \rho_\infty \cdot {V_\infty}^2 \cdot C_D \cdot S_{ref} \tag{4.47}$$

$$T = \begin{cases} D + m \cdot g \cdot \sin(\gamma) & ,Constant\ speed\ (\bar{a} = 0) \\ D + m \cdot g \cdot \sin(\gamma) + m \cdot \bar{a} & ,Acceleration\ or\ \text{deceleration}\ (\bar{a} \neq 0) \\ T_{max,rated} \cdot n_{eng} & ,Takeoff \\ T_{max,rated} \cdot n_{eng} \cdot f_{idle} & ,Taxi\ (ground\ phases) \end{cases} \tag{4.48}$$

It is assumed, that the thrust during take-off is the maximum rated thrust. Furthermore, the required thrust during taxi is assumed to be idle thrust, which is estimated to be in the range of 3-4% ($f_{idle} = 0.03 - 0.04$) of the maximum rated engine thrust $T_{max,rated}$.

Engine Power Offtakes. The last parameters required to calculate the overall aircraft fuel consumption, are the engine shaft power and engine bleed air requirements. Based on the secondary power requirements, which are provided by the *Aircraft System Models* (cf. *4.3*). The total shaft power requirements result from the electrical and hydraulic shaft power, see Equations (4.49) – (4.51). In order to calculate the electrical and hydraulic shaft power, the respective efficiencies of the power generation ($\eta_{gen,elec}$, $\eta_{pump,hyd}$) and the power distribution systems ($\eta_{dist,elec}$, $\eta_{dist,hyd}$) must also be taken into account.

$$P_{shaft} = P_{shaft,elec} + P_{shaft,hyd} \tag{4.49}$$

$$P_{shaft,elec} = \frac{P_{elec}}{\eta_{gen,elec} \cdot \eta_{dist,elec}} \tag{4.50}$$

$$P_{shaft,hydr} = \frac{P_{hyd}}{\eta_{pmp,hyd} \cdot \eta_{dist,hyd}} \tag{4.51}$$

Where:

P_{elec}	Total electrical power requirements (aircraft systems)	P_{hydr}	Total hydraulic power requirements (aircraft systems)
$\eta_{gen,elec}$	Efficiency of the electrical power generation system	$\eta_{pmp,hyd}$	Efficiency of the hydraulic power generation system (pump)
$\eta_{dist,elec}$	Efficiency of the electrical power distribution system	$\eta_{dist,hyd}$	Efficiency of the hydraulic power distribution system

4.5 Tool Implementation

The simulation environment for the aircraft performance and technology analysis, is implemented in MATLAB® and is named ATAX (Aircraft System Technology Analysis Tool). ATAX considers the aircraft characteristics, different aircraft systems and engine technologies in addition to mission data to calculate the overall and specific fuel consumption of the aircraft. Moreover, the fuel consumption of each aircraft system can be determined in each step of the flight mission. For the easy setup of run cases and parameter studies, a Graphical User Interface (GUI) was developed (cf. Figure 4.6). However, the tool (and all the functions) can also be used without GUI and thus integrated into scripts or other tools. In the following, a brief overview of the calculation procedure and the data model of the implemented tool are given.

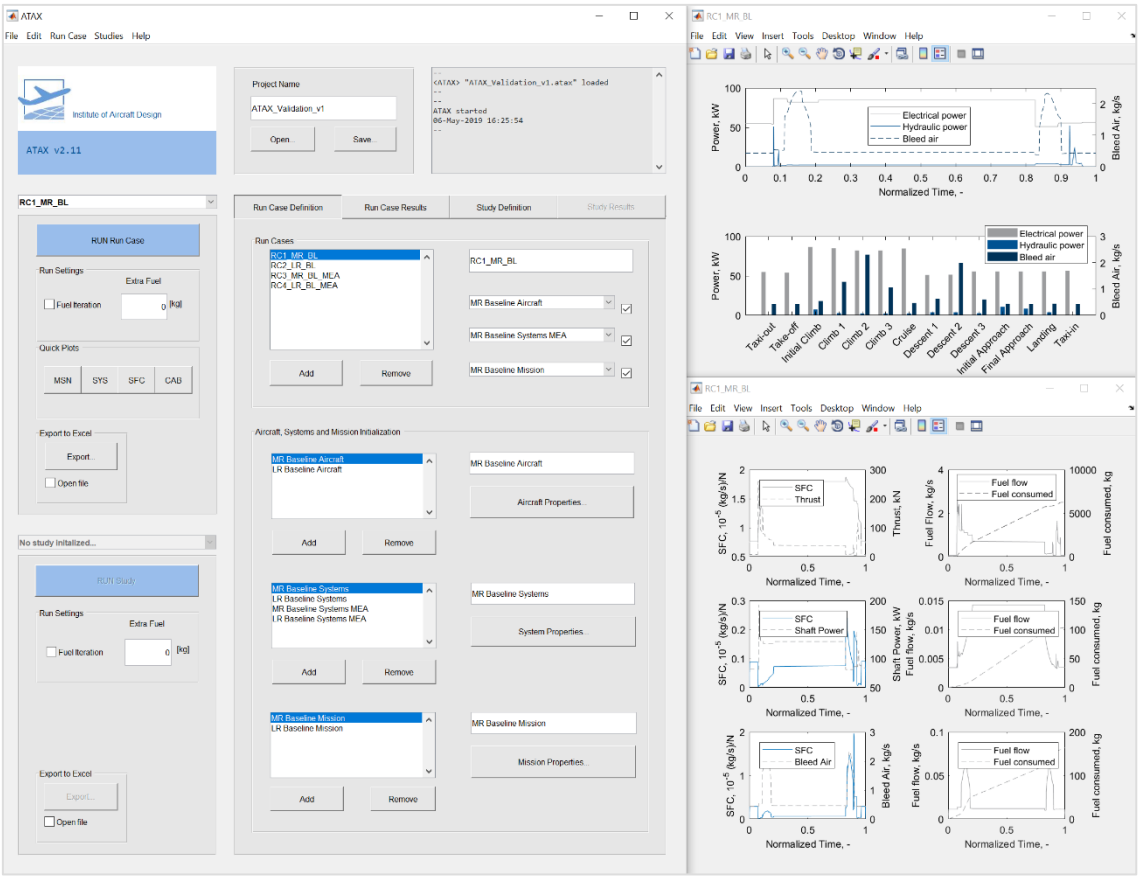

Figure 4.6 Overview of the main user interface (left) and exemplary result plots (right) of the Aircraft System Technology Analysis Tool (ATAX).

4.5.1 Calculation Procedure

The tool is implemented in MATLAB® and uses an object-oriented programmed data model (cf. *4.5.2 Data Model*). Simplified, the calculation procedure within the tool can be described in three essential steps (see Figure 4.7): *Run Case Setup*, *Engine Power Offtakes*, *Fuel and Thrust Iteration.*

Run Case Setup. The first step describes the initialization of one or multiple run case(s), before the calculation can begin. A run case consists of an aircraft configuration, aircraft systems and a defined mission: The aircraft configuration describes the main aircraft properties, which includes

general aircraft data (e.g. weight and utilization), geometry definitions (e.g. wetted area, wing and fuselage), and propulsion and power generation system data. The considered aircraft systems within ATAX are ECS, IPS, FCS and MIS as illustrated in Figure 4.2. For all aircraft systems, individual duty cycles or activity schedules are defined or determined, dependent on the function(s), flight phase, altitudes or, in the case of the IPS, icing conditions. The parameterized mission describes a typical altitude and speed profile, which can be modified and adapted at will. It is generally divided into 14 flight phases, which are further divided into steps (cf. Figure 4.1). Once all run cases are initialized, the calculation of the run cases can begin.

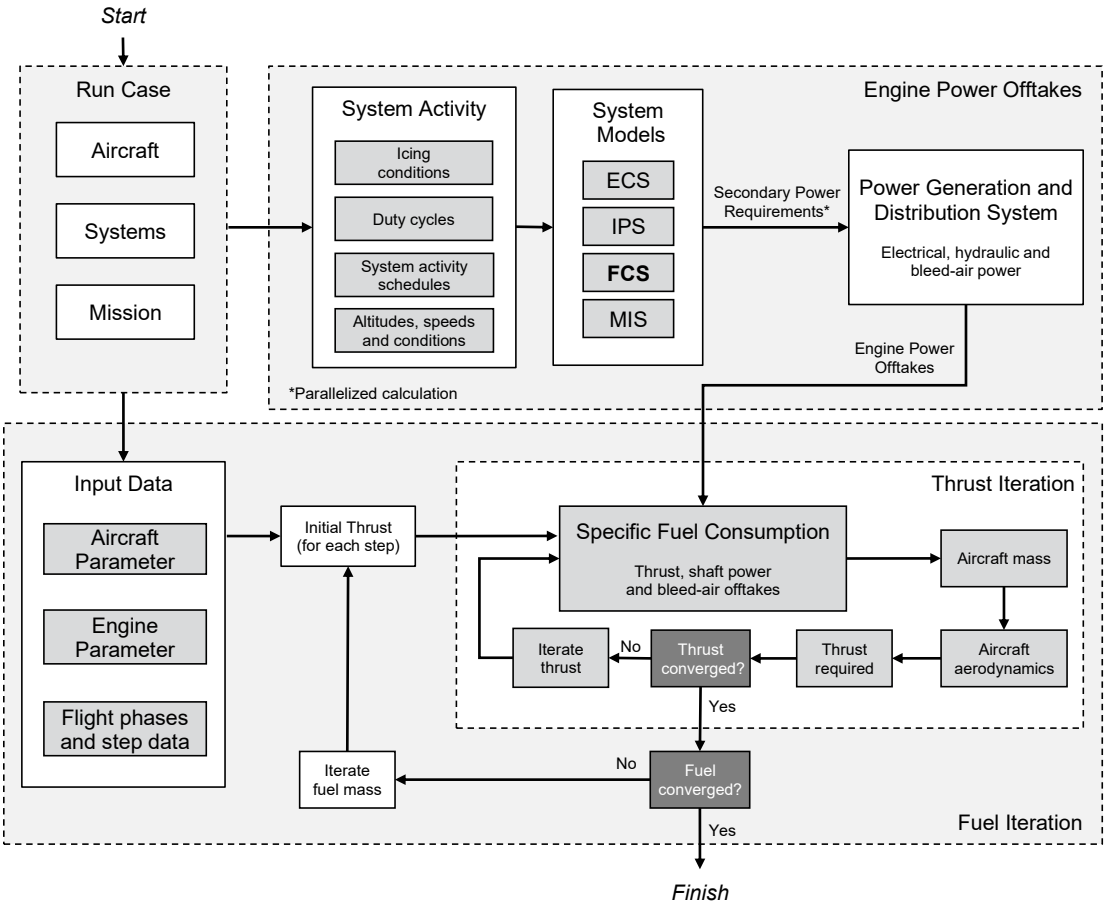

Figure 4.7 Top-level schematic of the calculation procedure of the implemented Aircraft System Technology Analysis Tool (ATAX).

Engine Power Offtakes. The procedure starts with the calculation of the secondary power requirements of the aircraft systems on board. These power requirements depend on the aircraft configuration (geometry, utilization, propulsion and power systems), aircraft system technologies and functions in addition to the altitude and airspeed. With the aforementioned aircraft system models (cf. *4.3*), the secondary power requirements, in form of electrical, hydraulic and pneumatic power requirements, can be determined for each step of the mission. This part of the calculation procedure is implemented in a parallelized manner to speed up the calculation time. Finally, taking into account the efficiency of the individual power generation and distribution systems, the actual engine power offtakes can be determined.

Fuel and Thrust Iteration. After the engine power offtakes are calculated, the fuel and thrust iteration is started[86]. The required engine thrust is dependent on the actual aircraft characteristics and the flight phase the aircraft is in. Hence, the thrust for each step of the flight mission has to be iteratively determined (*inner loop*). This is also true for the overall aircraft fuel iteration (*outer loop*). Once the thrust has converged in each step of the mission, the overall fuel convergence can be checked and iteratively modified if required, and the thrust iterations start all over again. This fuel and thrust iteration are schematically illustrated in Figure 4.7.

4.5.2 Data Model

As mentioned above, the data model has an object-oriented structure to enable a flexible and modular use of the tool. In the following, the general structure of the data model is presented. Once the tool is started, an *ATAX* object (project) is created, which consists of the following main objects, see Figure 4.8[87]:

- *ATAXinit:* This object contains all initialized *Aircraft, System* and *Mission* objects, which are defined within the ATAX project.
- *ATAXrun:* In this object, all *run cases* of the ATAX project are defined and stored. A run case can be composed arbitrarily from all initialized objects *Aircraft, System* and *Mission*. In addition, a *Results* object stores all results after a calculation is finished.
- *ATAXstudy:* This object consists of a baseline *run case* in addition to a single or multiple study *run case(s)*, which are automatically created if a parameter study is set up. After the parameter study is finished, all results are stored in the dedicated *Results* object of the study run cases.

At the top of the data model is the *ATAX* object (project) with its properties, consisting of parameters and further objects. The modular character of the data model can be shown using the *ATAXrun* object as an example (highlighted in Figure 4.8). This object is not only used for the definition of a single run case but also for the setup of a parameter study (*ATAXstudy*). That also applies to the objects *Aircraft (AC), Systems (SYS),* and *Mission (MSN)*, which are used for the initialization and the definition of the run cases. This modular structure enables a simple compilation, analysis and evaluation of different aircraft configurations, system technologies and flight missions. Furthermore, the ATAX project or single aircraft, systems and mission settings can be saved and loaded.

[86] The aircraft has a time-based mass change (reduction) due to the fuel consumption of the engines. This reduction in overall aircraft mass in turn reduces the required lift, and thus leads to lower aerodynamic drag (cf. Equation (2.6)). With the change in aircraft drag, the required thrust also changes and thus also the fuel consumption. Therefore, the solution of a differential equation is necessary. One solution of this differential equation is the well-known *Breguet equation*. However, if one or more flight parameters are changed during cruise flight (e.g. changes in aircraft configuration or system activity), this equation is merely a more or less accurate approximation. Consequently, an iterative solution was chosen.

[87] A comprehensive overview of the data model and its structure is given in *A.6 Data Model Structures and User Interfaces*.

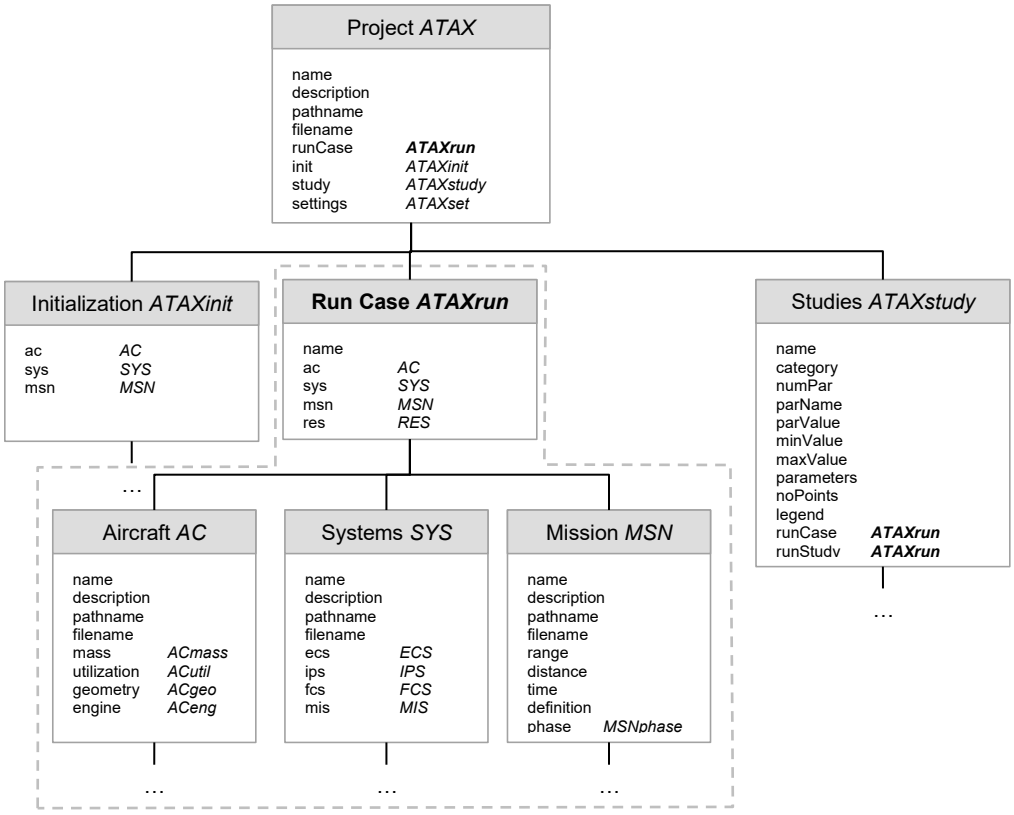

Figure 4.8 Simplified overview of the data model structure within the Aircraft System Technology Analysis Tool (ATAX).

The results are stored within the project and can be exported to Excel® worksheets. Furthermore, the tool provides several functions to display, compare, and analyze the results of single or multiple run cases. Besides the results of the power requirements, (specific) fuel consumption, or fuel flow for each step of the mission, time-averaged (mean) values and maximum (peak) values for each flight phase can be displayed.

4.6 Tool Validation

The overall objective of this section is to validate the developed Aircraft System Technology Analysis Tool (ATAX, v2.11) and check the results for plausibility. This includes the validation of the implemented data models, the aircraft performance models, and aircraft system models. Furthermore, the correct links between the models and the functions within the calculation procedure are tested. Therefore, the MR and LR baseline aircraft models are used (cf. section *4.1*). Furthermore, a conventional and more-electric configuration for each baseline aircraft are implemented and a total of four run cases result, see Table 4.4. The conventional aircraft configurations consist of a bleed-air powered ECS and IPS in addition to a hydraulic FCS actuation system. The remaining systems are electrical, with exception of the landing gear and high-lift control actuation systems (hydraulic). In contrast, all main aircraft systems of the more-electric configuration are electrical.

Table 4.4 Overview of the defined run cases for the tool validation.

Run Case	Baseline Aircraft	Configuration	ECS	WIPS	EIPS	FCS	LGA	MIS
1, 2	MR, LR	Conventional	P	P	P	H	H	E
3, 4	MR, LR	More Electric	E	E	P	E	E	E

ECS Environmental Control System
WIPS Wing Ice Protection System
EIPS Engine Ice Protection System
FCS Flight Control System (Actuation)
LGA Landing Gear Actuation
MIS Miscellaneous Systems
E Electrically powered
H Hydraulically powered
P Pneumatically powered (bleed air)

In a first step, the generation of the parameterized mission is tested, to validate the correct compilation of the altitude and speed profile from the mission input parameters. Afterwards, the run cases can be defined, and the calculation procedure started. For all run cases, an extra fuel of 5000 kg is considered and the calculation mode is set to *fuel iteration* (cf. section *4.5.1*). In addition, it is assumed the aerodynamic characteristics for the conventional and more-electric aircraft is identical and that no additional FCS functions are activated during the flight mission.

4.6.1 Mission Results

To generate a flight mission for commercial transport aircraft, various input parameters are required. The main parameters are range, cruise speed and profile, reference altitudes, characteristic speeds, typical climb and descent rates, ISA conditions and step size. Once all input parameters are initialized, the mission with defined altitude and speed profiles are generated[88]. For the tool validation, two typical flight missions are generated, see Figure 4.9. Both flight missions are performed at standard ISA conditions with take-off and landing at MSL. The standard altitude step size for the phases *Climb, Descent* and *Approach* is set to 500 ft. For the MR mission, a cruise phase at constant level (32000 ft) at Mach 0.81 is defined.

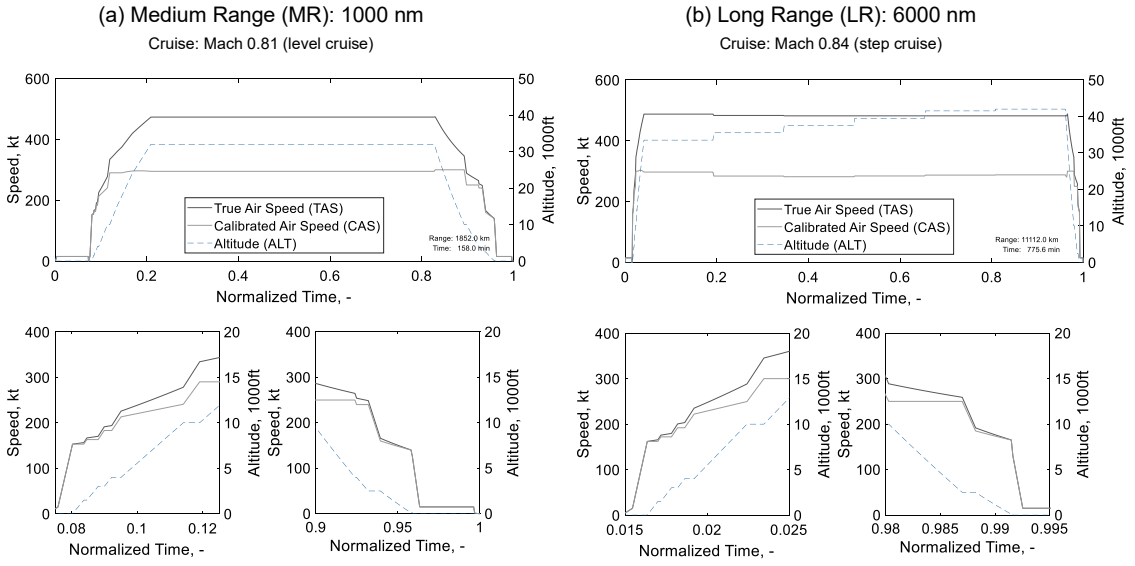

Figure 4.9 Altitude and speed profiles of two different flight missions with different ranges and cruise characteristics of commercial transport aircraft.

[88] A detailed overview of an exemplary flight mission with typical speed and altitude profiles is shown in Figure A.5.

In contrast, the LR mission shows a step-cruise profile at Mach 0.84 starting at 33500 ft (TOC) and ending at 42000 ft (TOD). The defined step climb interval during cruise is set to typical 2000 ft. The range of the MR mission is 1000 nm and of the LR mission is 6000 nm. Both generated flight missions are used for the following validation of the conventional and more-electric aircraft configuration.

4.6.2 Calculation Results

The calculation results are divided into the following three categories: secondary power requirements, specific fuel consumption, and fuel flow. For the sake of clarity, the validation results of the long-range (LR) baseline aircraft are presented in the appendix *A.5 Aircraft System Models*.

Secondary Power Requirements. Figure 4.10 gives an overview of the secondary power requirements of the conventional and more-electric aircraft configuration. The power requirements – in form of electrical, hydraulic and bleed-air power – over the normalized mission time are shown in the top diagramm, whereas the time-averaged power requirements for each flight phase are shown in the diagram below. More detailed results regarding the secondary power requirements of the main aircraft systems are illustrated in Figure 4.11.

The results of the conventional baseline aircraft show a mainly constant electrical power demand of about 100 kW for the mean time of the flight mission (climb and cruise), see Figure 4.10a and Figure 4.11a. In contrast, the hydraulic power requirements are significantly lower (approx. 3 kW during cruise). Nevertheless, due to actuation of the landing gear and high-lift system (PCU), two narrow peaks can be observed during the phases *Initial Climb* and *Climb 1* or *Initial Approach* and *Final Approach*, respectively. The main bleed-air power requirements result from the ECS (air conditioning system) and IPS (wing and engine IPS). During climb and descent phases two peaks of bleed-air demand can be observed: With increasing altitude and decreasing temperature, the aircraft reaches the icing condition envelopes of the EIPS and WIPS, and the systems are activated. Similar behavior is observed for the descent phase. The aircraft leaves the icing condition envelopes again at higher altitudes, thus no IPS is activated during cruise.

Almost all aircraft systems of the more-electric baseline aircraft are electrically powered[89], which is also clearly visible in the temporal course of the secondary power requirements, see Figure 4.10b and Figure 4.11b. In contrast to the conventional configuration, the electrical power requirements during cruise have doubled to approx. 200 kW. In addition, multiple peaks – two *narrow* and one *wide* – can be observed during climb and descent phases. The *wide peak* results from the power requirements of the electrical WIPS, once the aircraft enters the icing condition envelope (analogue to the conventional aircraft). The *narrow peaks* result again from the (now electrical) actuation of the landing gear and high-lift system. Nevertheless, the biggest share of electrical power demand in each flight phase results from the electrically powered ECS (cf. Figure 4.11b).

[89] The Engine Ice Protection System (EIPS) is still supplied by the locally available bleed air (cf. section 4.3.2).

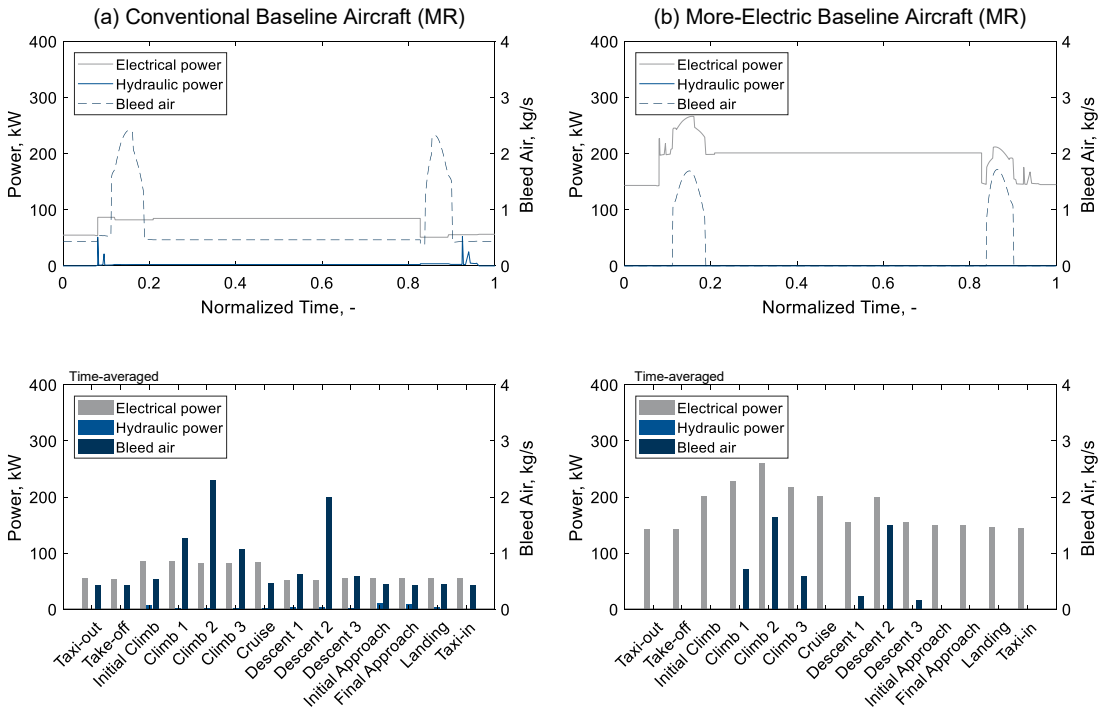

Figure 4.10 Overview of the secondary power requirements of the conventional (left) and more-electric (right) medium-range baseline aircraft.

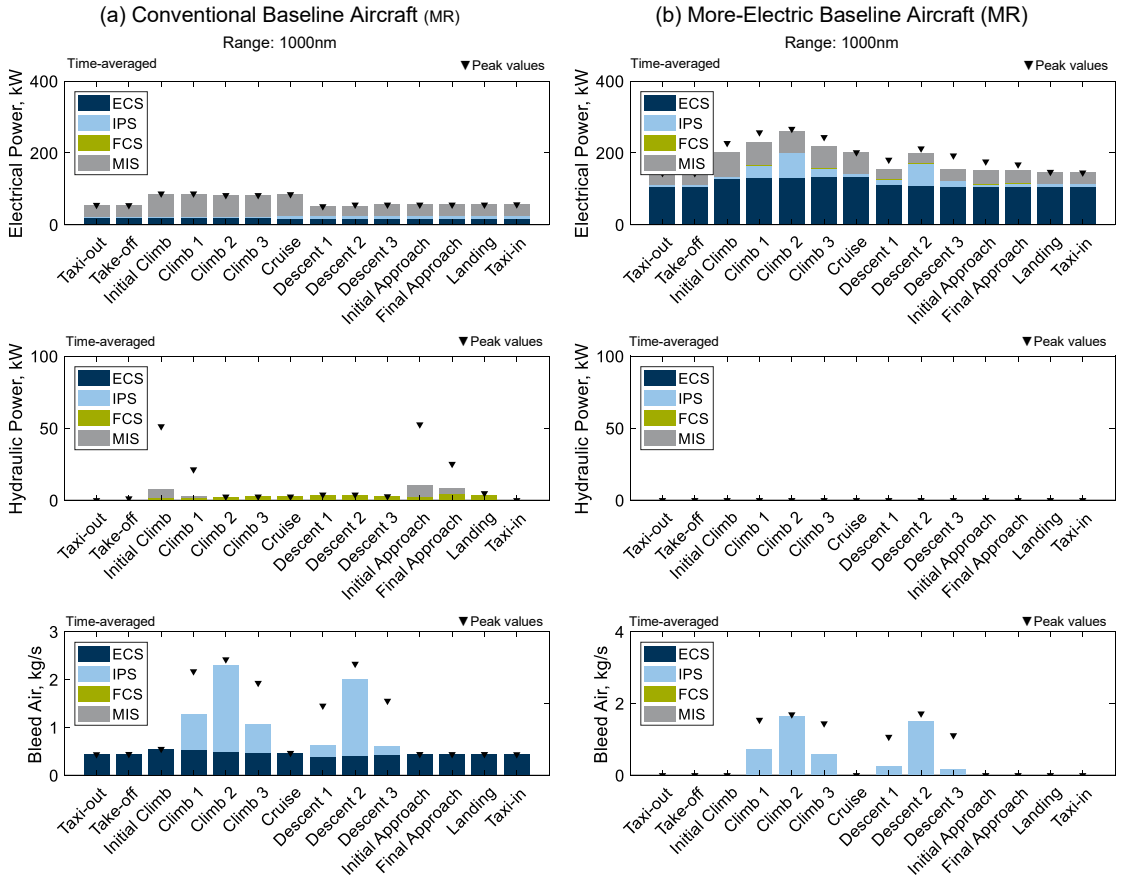

Figure 4.11 Details of the secondary power requirements of the conventional (left) and more-electric (right) medium-range baseline aircraft.

Specific Fuel Consumption and Fuel Flow. Figure 4.12 shows the SFC and the thrust of the aircraft over the normalized mission time (top). Moreover, the time-averaged and peak values for each flight phase are depicted in addition to the, the SFC shares of thrust, shaft power offtakes and bleed air. During cruise it can be observed that the SFC is almost constant, whereas the thrust is slightly decreasing. In contrast, during take-off, climb, descend, and landing phases, the SFC is changing significantly due to the varying thrust. Since the same baseline aircraft is used[90], the thrust and SFC over time is almost identical for both the conventional and more-electric aircraft configuration (cf. Figure 4.12).

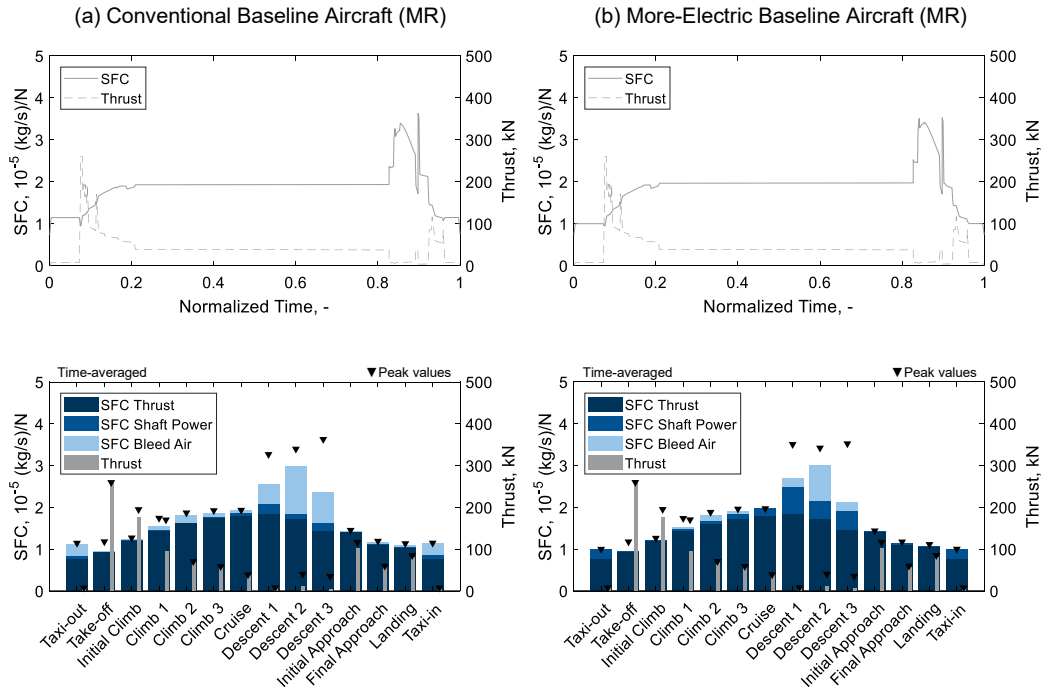

Figure 4.12 Overall specific Fuel Consumption (SFC) of the conventional (left) and more-electric (right) medium-range baseline aircraft.

However, a closer look at the SFC shares reveals clear differences between the conventional and more-electric configuration (cf. Figure 4.12 and Figure 4.13). On the one hand, the bleed-air shares of the SFC of all flight phases are higher for the conventional aircraft than for the more-electric aircraft. On the other hand, the more-electric aircraft shows higher SFC shares due to engine shaft power offtakes. The increase in SFC during the descent phases can be explained by the lower thrust requirements and the lower engine spool speeds, where the engine power offtakes are consequently more significant in terms of engine efficiency or SFC, respectively.

After the SFC is calculated, the fuel flow and the overall fuel consumption can be determined, see Figure 4.14. The profiles of the fuel flow and overall fuel consumption over time for both aircraft configurations are again very similar, as the dominating component of the fuel flow is still due to thrust generation.

[90] The conventional and more-electric aircraft have the same fuselage, wings, empennage and engines. Only the aircraft systems and system configurations are different.

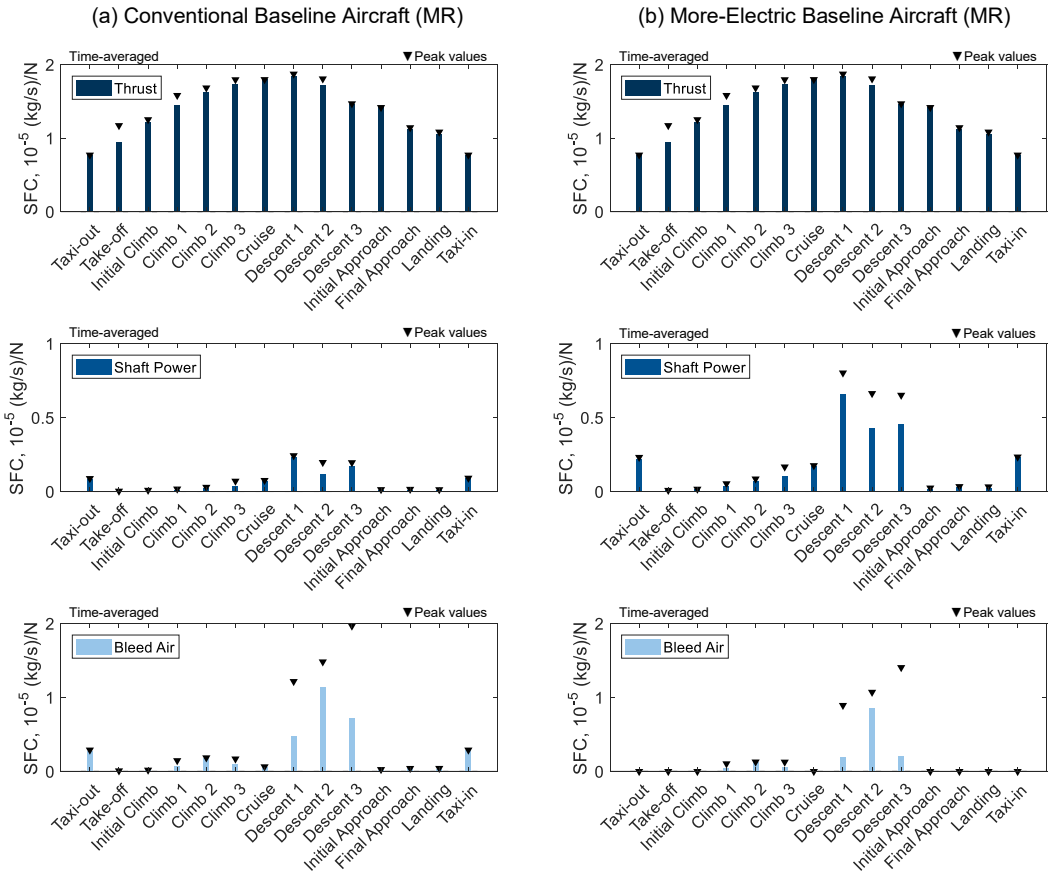

Figure 4.13 Details of the Specific Fuel Consumption (SFC) due to thrust, shaft power offtakes and bleed air of the conventional (left) and more-electric (right) medium-range baseline aircraft.

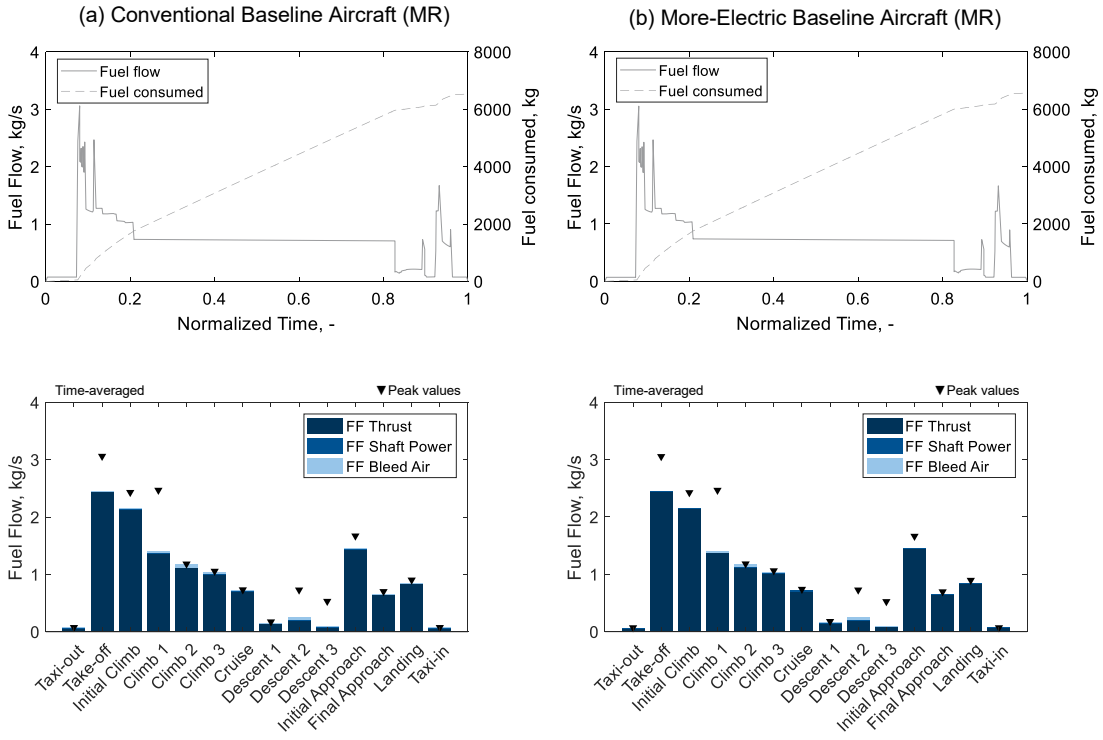

Figure 4.14 Overall fuel flow and fuel consumption of the conventional (left) and more-electric (right) medium-range baseline aircraft.

The highest fuel flows occur during *take-off* and *climb* phases, whereas the fuel flow during cruise is considerably lower. During the initial and final approach, the aircraft configurations have increased drag due to deployed high-lift devices and landing gears. Consequently, a higher thrust setting is required, and the fuel flow increases again (cf. Figure 4.14).

Summary. The implemented system models show realistic behavior depending on the flight mission, environmental conditions and their individual system activity schedules (cf. Liscouët-Hanke, 2008; Lammering, 2014; Chakraborty, 2015). The implemented methods to calculate SFC and fuel flow show suitable results and dependencies of the engine technologies used. However, it must be emphasized, that a real validation of the SFC and fuel flow modelling cannot be done due to the lack of existing and complete reference data. Nevertheless, the comparison of typical SFC and overall fuel consumption values of comparable transport aircraft[91] show that the results are highly plausible (Boeing, 2006, p. 5; Lammering, 2014, p. 116). In addition, a detailed analysis of the calculation procedure and the results confirmed that data model and the links between the data model and the calculation functions work as intended. Finally, it can be stated, that ATAX tool enables a comprehensive analysis, assessment and comparison of different aircraft concepts and aircraft systems technologies, even in early aircraft design phases.

[91] The compared aircraft are a Boeing 737-800 and an Airbus A320-200. The fuel consumption results of the Boeing 737-800 consider typical mission rules, 162 passengers and a cruise Mach number of 0.79 (Boeing, 2006, p.5). Lammering (2014) presents the results for an Airbus A320 reference aircraft – which is very similar to the A320-200– including typical mission phases, 150 passengers and a cruise Mach number of 0.78 (Lammering, 2014, p. 79).

5 Case Study

The overarching goal of this thesis is to develop a methodology for the integrated design of advanced flight control systems (configuration and architecture) and enable their comprehensive analysis and assessment at aircraft and system level. Furthermore, the presented approach is not only intended to implement parameter studies and tradeoffs of innovative concepts, but also to increase the available knowledge of the overall aircraft design and thus to provide a good basis for decision-making in early stages of aircraft design. The following case study demonstrates how this design approach and the integrated tools can be applied.

The chapter begins with a brief introduction of the case study, where the setup and approach are explained. Afterwards, the first part of the case study is presented where the focus is on the integrated design approach. In the second part, the advanced FCS concepts are analyzed at aircraft and system level. Finally, the findings and results of the case study are summarized including a critical review of the integrated design approach against the requirements of early aircraft design phases.

5.1 Setup and Approach

The case study is conducted according to the developed overall methodology (cf. Figure 3.1). The first part deals with the *integrated design* approach of advanced FCS. This includes the functional-driven design approach in addition to the subsequent advanced flight control system design. The second part presents the *analysis and assessment* of the advanced FCS using the simulation tool ATAX.

The baseline aircraft (cf. *Section 4.1*) is used as the starting point and additionally serve as a reference when evaluating the results, and hence is referred to as Reference Aircraft (RA). For the design of the aircraft with advanced FCS – hereinafter referred to as Concept Aircraft (CA) – two innovative system concepts are considered: The first concept refers to the Distributed System Architecture (DSA) for high-lift control systems and the associated integration of additional flight control functions. The second concept describes an Active Flow Control (AFC) system for local aerodynamic improvements at the trailing-edge flap of the high-lift control system (cf. Figure 2.22).

Distributed Electric-Drive System Architecture (DSA). The concept of the DSA for high-lift control systems is illustrated in Figure 5.1. This DSA concept has two drive stations for each inboard or outboard flap, which are connected via a local drive shaft. This ensures a synchronous deployment of both actuators. For each flap, only single-redundant brake and position sensors are required. In the case of a failure of one electric actuator, the other actuator can drive the flap in a degraded mode (Lampl *et al.*, 2017a, p. 7).

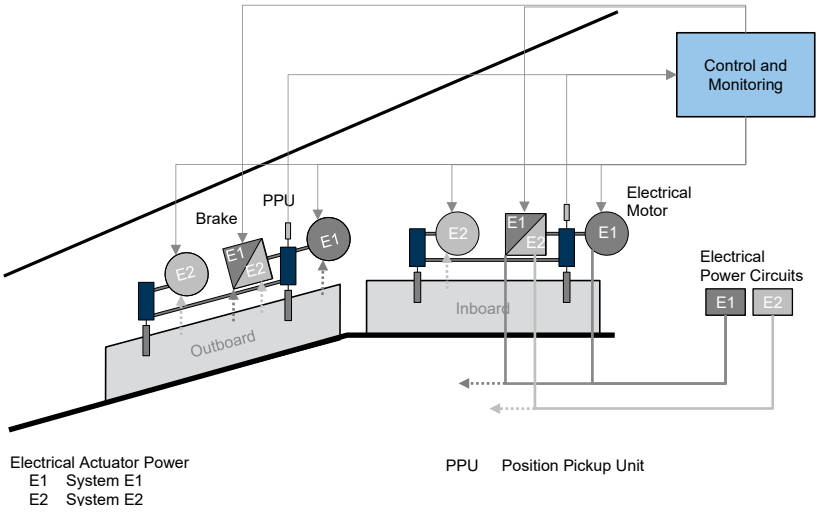

Figure 5.1 Schematics of the distributed electric-drive architecture for high-lift control systems.

This DSA concept for high-lift control systems, enables up to 30% weight savings and about 20% reduction in direct operating costs, compared to conventional architectures (cf. *2.3.4 Advanced Technologies and Concepts, p. 41*). In addition, due to the distributed architecture, the system concept provides the best prerequisites for integrating additional flight control functions (e.g. DFS).

Active Flow Control at the Trailing-Edge Flaps. The second innovative system concept in this study, is the application of AFC at the trailing-edge flaps. The aerodynamic improvements due to AFC enables size reductions of the trailing-edge flaps in chord direction (approx. 30%, inboard and outboard) and in spanwise direction (approx. 20%, outboard only), see Figure 5.2.

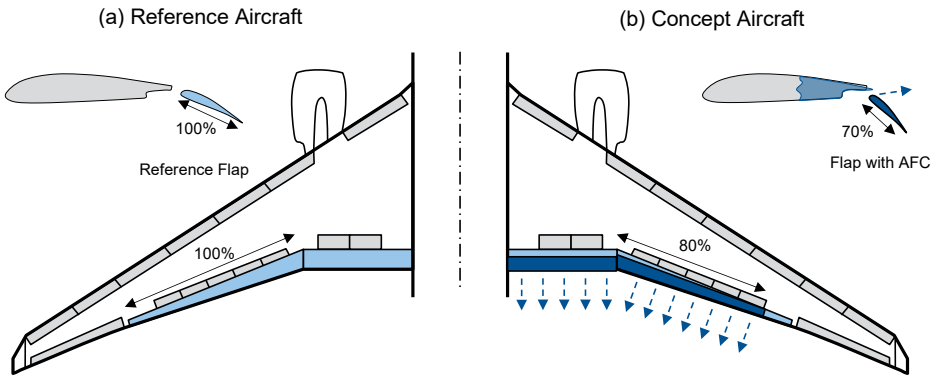

Figure 5.2 Reduced size of the trailing-edge flaps due to Active Flow Control (AFC).

The AFC is activated during the final approach and landing phases to gain the required extra lift. In addition, simplifications of the kinematics and support structure can be assumed. The two-staged AFC concepts is either powered by pressurized air from engine bleed-air or electrical compressors. Regardless of this, the weight benefit due to reduced flap size and simplified kinematics is higher than the weight of additional systems required for AFC (Meyer *et al.* (2014, p. 3), cf. *2.3.4 Advanced Technologies and Concepts, p. 39*).

Assumptions and Simplifications. To keep the case study within reasonable limits and to keep the focus on advanced FCS with additional flight control functions, following assumptions and simplifications are made:

- The empennage, including the horizontal and vertical tail with rudder and elevators, are identical for the RA and the CA.
- The flight missions for the RA and CA are identical.
- The aircraft engines, including the power generation and distribution systems are identical for the RA and CA (no resizing).
- The aircraft systems and their activity schedules are identical for the RA and CA, with exception of the FCS.

Simulation Environment. For this case study a commercial notebook was used, with the computing environment MATLAB® in version 2017a to run the developed tools AVLX (v1.0) and ATAX (v2.11). The tool can be compiled to a standalone executable file (application), which only requires the MATLAB Compiler Runtime to run the tool[92].

5.2 Integrated Design Approach

5.2.1 Functional-Driven Design

The first step of the integrated design is the *Functional-Driven Design Approach.* Based on the results of the requirements engineering, individual Multi-Domain Matrices (MDMs) are developed at aircraft, system and device level[93]. These three MDMs together form the so-called Functional MDM (FMDM) where different domains are considered depending on the level (cf. Figure 3.4 and Figure 3.5). To have a first impression, the MDM at device level is illustrated in Figure 5.3. The MDMs at aircraft and system level are shown in the appendix, see Figure A.2 and Figure A.3. The corresponding description of the type of relationships or effects are individually included for each matrix (see legends). In the following, specific parts of the FMDM are analyzed in more detail within the subsequent functional analyzes and synthesis.

[92] The MATLAB Compiler Runtime can be freely distributed together with the app or downloaded from the website: https://www.mathworks.com/products/compiler/matlab-runtime.html (accessed 26 October 2019).

[93] The results of the requirements engineering and the developed MDMs are partly based on the work of Daniel Sauterleute (2016, Ch. 5), a Master Thesis supervised by the author.

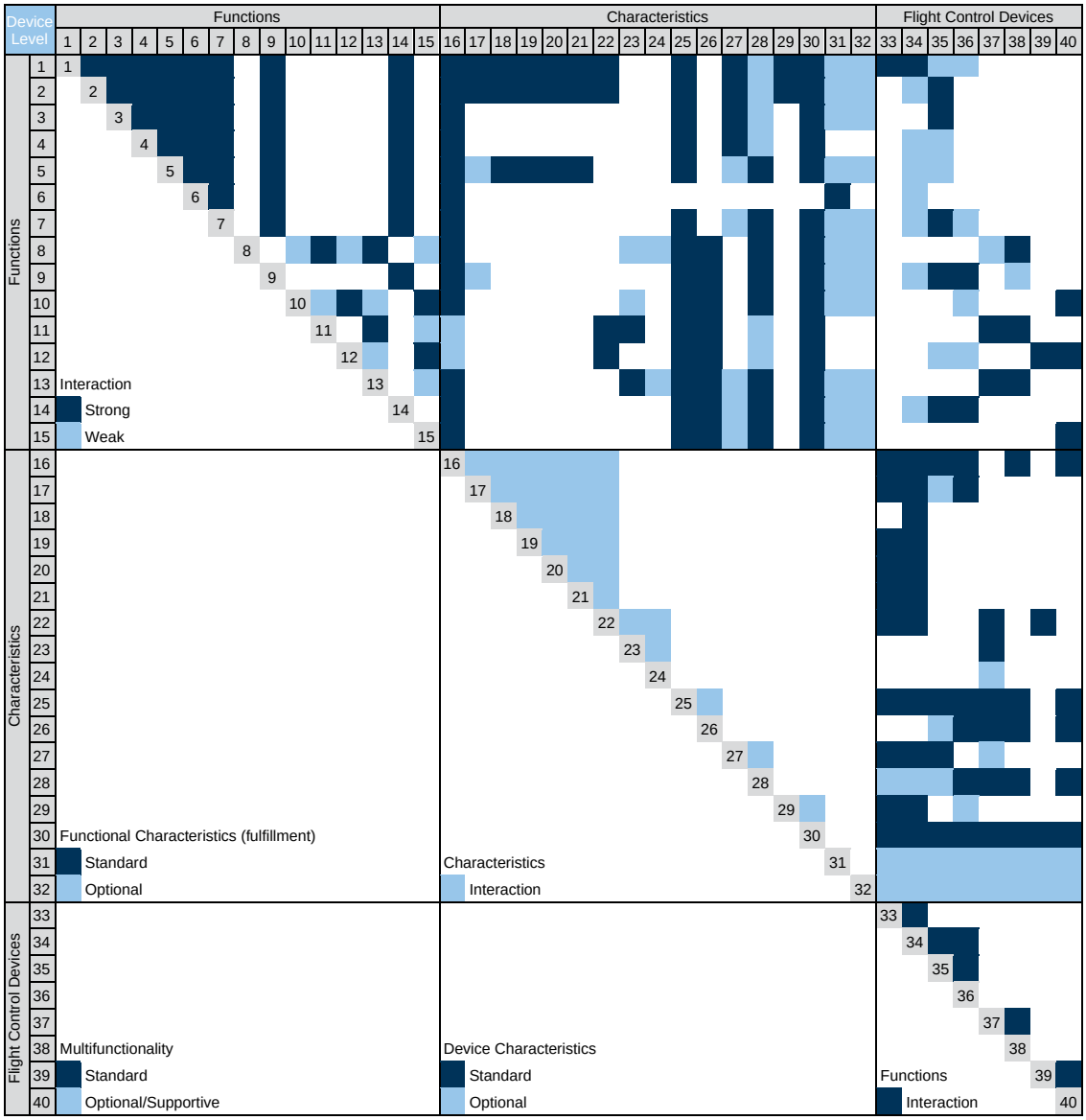

Functions

1 High-lift control
2 Airbrake
3 Lift dump
4 Cruise Variable Camber
5 Differential Flap Setting
6 Active Flow Control (Flap)
7 Active Load Control
8 Pitch Control
9 Roll Control
10 Yaw Control
11 Longitudinal stability control
12 Lateral/Directional stability control
13 Trim control lateral axis
14 Trim control longitudinal axis
15 Trim control vertical axis

Characteristics

16 Hinged
17 Drooped
18 Fowler
19 Dropped-Hinge
20 Linkage System
21 Link-Track System
22 Immovable (fixed)
23 Trimmable
24 Fully moveable
25 Positive deflection
26 Negative deflection
27 Stepwise deflection
28 Continuous deflection
29 System with gap
30 System without gap

(Characteristics continued)

31 Air jet (flow control)
32 Morphing

Devices

33 High-lift device (LE)
34 High-lift device (TE)
35 Spoiler
36 Aileron
37 Horizontal tail (THS)
38 Elevator
39 Vertical tail
40 Rudder

LE Leading Edge
TE Trailing Edge
THS Trimmable Horizontal Tail

Figure 5.3 Multifunctional Domain Matrix (MDM) results of the concept aircraft at device level.

Functional Analysis and Synthesis. In the interaction with the Functional MDM and with the MDM at device level, the design space of the functional allocation is explored. A distinction is made between *standard* and *optional* (or *supportive*) use of devices to fulfill corresponding functions. An optional or supportive allocation implies an unconventional or supportive use of the device in view of multifunctional solutions or integration of additional functions. The resulting design space of the functional allocation in the form of a graph is shown in Figure 5.4[94].

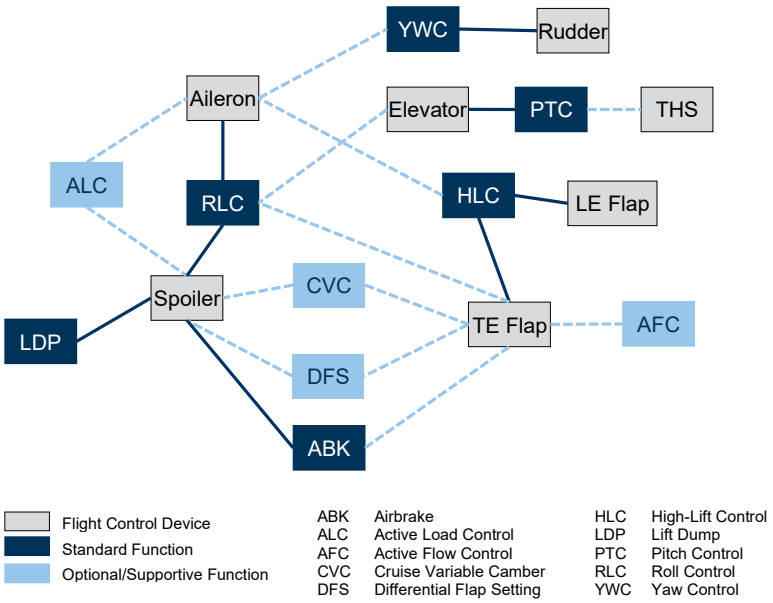

Figure 5.4 Schematic illustration of the functional allocation of the concept aircraft (simplified).

This illustration is equivalent in content to the Domain Mapping Matrix (DMM) "Functions x Flight Control Devices", which is part of the MDM at device level shown in Figure 5.3. In a next step, a cluster analysis of the DMM is conducted. For this purpose, the elements in the rows and columns are reordered to develop individual clusters or modules with certain characteristics, see Figure 5.5.

The following four modules (clusters) are defined:

(1) The first module describes the high-lift control (HLC) and the capability to adjust the lift distribution at the wing. In this module, the leading- and trailing-edge devices of the wing's high-lift system are naturally used for HLC. Furthermore, the trailing-edge device are used to implement the additional flight control functions CVC, DFS, and optionally AFC to adjust the overall lift distribution at the wing during certain flight phases. Additionally, the spoilers can be used to support certain functions (HLC, CVC, DFS) in order to locally improve the aerodynamic effects (e.g. gap control). Also, the ailerons can provide supportive functionality (e.g. flaperon).

[94] For the reason of clarity, trim and stability control functions are not shown in the figure.

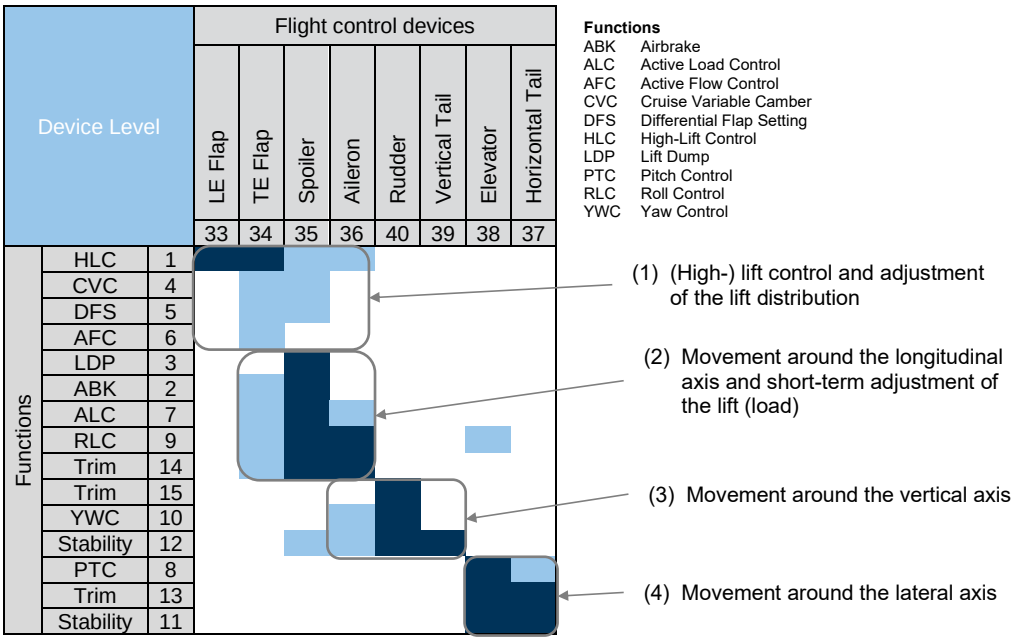

Figure 5.5 Cluster analysis results of the domain mapping matrix *Functions x Flight Control Devices* at device level (simplified).

(2) The second module refers to the longitudinal movement of the aircraft including the short-term adjustments of the lift distribution (or wing load). Essential control devices for fulfilling the corresponding flight control functions (LDP, ABK, ALC, RLC) are the ailerons and spoilers, but also the use of trailing-edge devices can be useful for configurational reasons.

(3) The functions trim control around the vertical axis, directional stability, and yaw control (YWC) are clustered in one module, which defines the movement around the vertical axis. These functions are fulfilled by the rudder(s) in addition to the vertical tail of the empennage. Moreover, there are possible interactions of the aileron or spoiler.

(4) The last module describes the movement around the lateral axis. These functions are provided by the elevator and the horizontal tail (e.g. THS)[95].

Based on the cluster analysis results, different solutions in form of flight control configurations are developed. Since the above cluster analysis of the DMM at the device level only provides the solution space for the functional allocation, further information and interactions at all levels are required to find and evaluate further alternative solutions. For this purpose, some information and relationships are already provided by the FMDM. The subsequent synthesis analysis identifies potentials, conflicts and synergies between different functions at aircraft, system, and device

[95] Just for illustration purposes, the optional use of the elevators is shown in Figure 5.5 (cf. row *9*, column *38*). If the elevators can be deflected differentially, they can also be used for RLC. Another example would be thrust vector control, which is standard for many military fighter aircraft, but not for commercial transport aircraft. Basically, however, differential thrust of the engines could be used for directional control or an immediate thrust change for pitch control. This was already successfully demonstrated at the A300 incident in Baghdad in November 2003.

level. This is required for the development and assessment of alternative solutions. The corresponding cluster analysis for the Design Structure Matrices (DSMs) *Functions* provides the following results at aircraft, system and device level:

At *aircraft level*, the interactions between the functions are analyzed from the flight-mechanical point of view. Here the term *impact* is used since a function can have certain impact on single or multiple functions. Following characteristic clusters are defined:

- *Take-off and landing* (low speed phase): This cluster results from the impact of the functions HLC AFC, and ABK on the remaining functions. For example, the deployment of the high-lift devices (with or without AFC) has a major impact on the controllability of the aircraft. From a flight-mechanical point of view, the HLC function interact with the control functions around the vertical, longitudinal and lateral axis.
- *Longitudinal movement* (all phases): This cluster includes the main function of PTC in addition to trim around the lateral axis and stability of the longitudinal movement. From a flight-mechanical point of view the longitudinal movement can be viewed independently of the lateral movement. The cluster is completed by the functions CVC, DFS and ALC.
- *Directional movement* (all phases): The directional movement is defined by RLC, YWC, trim around the longitudinal and vertical axis in addition to directional stability.

At *system level*, the separation of the functional effects at the wing from that at the empennage of the aircraft, becomes clear (from a system's point of view). This is characterized by the two clusters *Wing System* and *Empennage System*. The cluster *Wing System* includes all typical functions which are (mainly) fulfilled by flight control devices, which may have greater interferences or dependencies during system integration at the wing. For example, there are strong interdependencies between the functions high-lift control and roll control, regarding the available installation space of the control devices at wing trailing-edge. The *Empennage System* cluster can further be subdivided into control functions around the vertical axis (yaw control), and directional stability, and into control functions around the lateral axis (e.g. pitch control) and longitudinal stability.

The different interactions of functions at *device level* indicate the multifunctional use of certain flight control devices. The identification of these relationships takes place in close interaction with the DMM *Functions* x *Flight Control Devices*. Similar to the aircraft and system level, certain clusters can be identified for the DSM *Functions* at device level. These clusters are highlighted in Figure 5-7 c). According to the cluster analysis regarding the functional allocation (cf. DMM in Figure 5.5) following four clusters are identified:

- (High-) lift control and adjustment of the lift distribution
- Movement around the longitudinal axis and short-term adjustment of the lift
- Movement around the vertical axis
- Movement around the lateral axis

The first two clusters can be combined to form the module *Wing Flight Control System*, which is in focus of this case study. The remaining two clusters are dedicated to the *Empennage Flight Control System*.

The generation of alternative solutions is exemplarily demonstrated for the cluster *(High-) lift control and adjustment of the lift distribution*, which was determined with corresponding functions by the cluster analysis of the DMM (cf. Figure 5.5). Here, the different characteristics provided by the MDM at device level of the control devices are considered (cf. Figure 5.3). Moreover, the requirements, constraints and overall objectives at aircraft and system level are important. For the generation of different solutions for this cluster, different functions, control devices, characteristics and technologies are combined. However, obviously absurd solutions[96] should be filtered out. A selection of possible solutions for the cluster *(High-) lift control and adjustment of the lift distribution* is shown in Table 5.1.

Table 5.1 Overview of different configuration solutions for the cluster (*High-) lift control and adjustment of the lift distribution*.

ID	Functional allocation	Flight Control Device(s)	New Technologies	Comment
RA1	HLC	LE/TE Flaps, Aileron^{S}	-	Reference Aircraft (RA)
CA2	HLC HLC, DFS	LE Flaps, Aileron^{S} TE Flaps, Spoiler^{S}	DSA	Concept Aircraft 2
CA3	HLC HLC, DFS, CVC	LE Flaps, Aileron^{S} TE Flaps, Spoiler^{S}	DSA	Concept Aircraft 3
CA4	HLC HLC, DFS HLC, DFS, AFC	LE Flaps, Aileron^{S} Spoiler^{S} TE Flaps,	DSA, AFC	Concept Aircraft 4
CA5	HLC HLC, DFS, CVC HLC, DFS, CVC, AFC	LE Flaps, Aileron^{S} Spoiler^{S} TE Flaps	DSA, AFC	Concept Aircraft 5

^{S} Supportive

In the course of the synthesis analysis, these solution alternatives are evaluated for suitability. In the following only suitable or promising configurations will be investigated. The evaluation of the different solutions within the synthesis analysis is performed based on different characteristics at aircraft and system level. These characteristics are also largely reflected in the corresponding MDMs under the domain *Objectives* (cf. Figure A.2 and Figure A.3). According to this, the different configuration solutions can be evaluated[97], see Table 5.2.

[96] For example, a configuration with high-lift control devices only on one side and not on both sides of the wing.

[97] Basically, a Preliminary System Safety Analysis (PSSA) is required, to validate the found configurations. Nevertheless, to keep this study in reasonable limits, it is assumed that the configurations are feasible regarding the aircraft safety requirements. Accordingly, for this cases study, this activity is skipped. An illustrative example of an PSSA for different DSA concepts can be found in the work of Lampl *et al.* (2017a).

Table 5.2 Preliminary evaluation results of the different configuration solutions (selection).

	Characteristics	*Weighting*	RA	CA2	CA3	CA4	CA5
Aircraft Level	*Handling Qualities*	*3*	3	3	3	3	3
	Direct Operating Costs	*2*	1	2	3	3	3
	Environmental impact	*2*	1	2	2	2	3
	Direct Maintenance Costs	*2*	1	3	3	2	1
	System Cost	*1*	1	2	2	2	1
System Level	*Safety (system)*	*3*	3	3	3	3	3
	Complexity (system)	*2*	2	3	2	1	1
	Reconfiguration	*2*	1	2	2	2	2
	Multifunctionality	*2*	1	2	3	3	3
	Adaptiveness	*1*	1	2	3	2	2
	Power requirements	*2*	2	3	3	1	1
		Utility Value	29	**45**	**50**	41	40

The first concept in the table corresponds to the reference aircraft. The results of the concept aircraft indicate that CA2 and CA3 have the highest value according to the considered characteristics and applied metric (weighting). Configuration CA4 and CA5, which feature AFC, are evaluated slightly lower, due to the higher power requirements (pressurized air) during certain flight phases and the higher system complexity.

5.2.2 Advanced Flight Control System Design

According to the preliminary evaluation results of the different concepts, the design of the advanced flight control system can start with the configurational design. For this case study, it is assumed that the preliminary device allocation and sizing is complete (cf. Figure A.4a), based on the applied rules and guidelines of section *3.4.1 Preliminary Device Allocation and Sizing*. Based on this initial FCS design the aerodynamic modelling and analysis can start.

Aerodynamic Modelling and Analysis. To demonstrate the capability of the developed tool AVLX (cf. *Section 3.4.4*), the modelling of the DFS function shall serve as an example. Based on the initial design, the aerodynamic model can be developed, consisting of 13 surfaces and 6 control variables, which are assembled into the following groups:

- *Group 1:* The wing model consists of 5 surfaces for each side (left and right, duplicated). This enables the modelling of extended and deflected trailing-edge flaps (cf. 3.4.2). Furthermore, following control variables (devices) are integrated at the wing:
  - Inboard flap
  - Outboard flap
  - Aileron
- *Group 2:* The empennage consists of a horizontal stabilizer surface for each side (left and right, duplicated) and a vertical stabilizer. The control variables are defined as follows:
  - Trimmable Horizontal Stabilizer
  - Elevator
  - Rudder

The resulting aerodynamic model is displayed in Figure 5.6, where the wing model consists of 5 surfaces on each side (1 to 5, duplicated) and the empennage of the horizontal stabilizer (6, duplicated) and the vertical stabilizer (7). Based on the results of previously conducted parameter studies, a cosine distribution is selected for the spacing of the vortex in chord and spanwise direction.

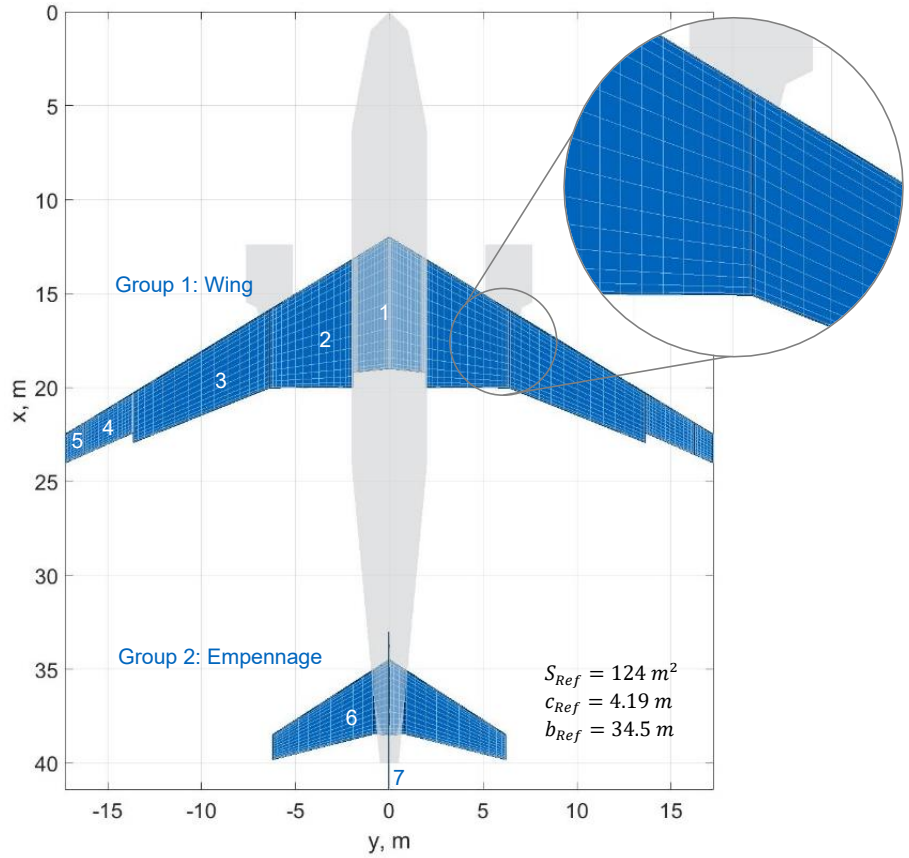

Figure 5.6 Aircraft model for the aerodynamic modelling of the Differential Flap Setting (DFS) function of the concept aircraft.

The operational point assumes that the aircraft is in trimmed and horizontal level flight, at a speed of $V_{TAS} = 165\ kt$ and a mass of $m_{AC} = 75000\ kg$. The trimming condition is defined in the calculation setup by setting the pitch moment coefficient $C_m = 0$ as a constraint of the THS control variable (deflection angle). For this study, six different run cases are defined to represent various DFS configurations.

The setup, calculation, and analysis were all done within the tool AVLX (v1.0). The total processing time[98] to calculate all six run cases was about 150 s, which is a reasonable value regarding larger parameter studies in early aircraft design phases.

[98] A pool with 4 CPUs (workers) of the computer (Intel® Core ™ i7-8550U CPU @ 1.80GHz, 16GB RAM) was used for parallel computation.

The results of the lift distribution over wingspan for various differential flap settings is shown in Figure 5.7a. With increasing DFS[99], the lift decreases in the outboard region and increases in the inboard region of the wing. However, the angle of attack slightly increases up to +4.6° (for the 30/05°) setting (cf. Figure 5.7a). Moreover, the maxima of the lift curves (or wing loads) are shifted towards the wing root, and hence decreases the overall wing bending moment. This decreasing effect of the bending moment is clearly shown in Figure 5.7b. Again, with increasing DFS, the peaks of the (local) wing bending moment is decreased. This is also true for the wing root bending moment, which is represented by the enclosed area under each curve. However, the DFS setting of 30°/10° shows the largest reduction of the wing root bending moment of 16% (cf. Figure 5.7b).

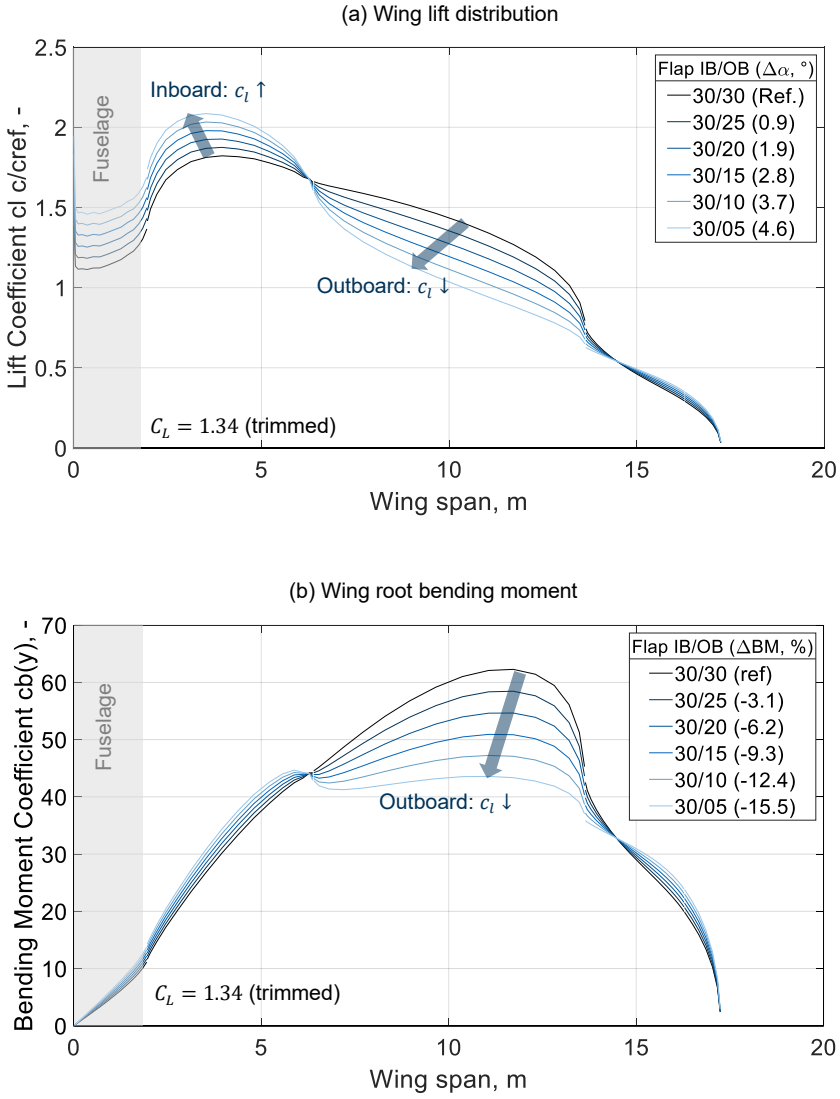

Figure 5.7 Lift distribution (left) and wing root bending moment results (right) for varying differential flap settings of the inboard (IB) and outboard (OB) trailing-edge flaps.

[99] In this context, increase means that the difference between the deflection angles of the IB and OB flaps becomes larger. This means that if the deflection angle of the IB flap remains constant at 30°, then the deflection angle of the OB flap decreases (here from 30° to 5°).

A helpful feature of the tool is the quick generation of 3D results to show the pressure distribution of each surface of the aircraft model. This enables to recognize aerodynamic effects of single or multiple control functions on different regions of the wing or other surfaces. Figure 5.10 shows the differential pressure distribution Δ*cp* of the wing in addition to the lift distribution (light-grey line) for various DFS configurations[100]. The dark-blue areas at the wing trailing edge – an area of high negative pressure - clearly indicate the deflected flaps at the IB and OB of the wing. With increasing DFS, this area at the outboard of the wing gets considerably smaller. Additionally, in comparison to the reference flap setting, the induced drag decreases up to -5.7% (30°/10°).

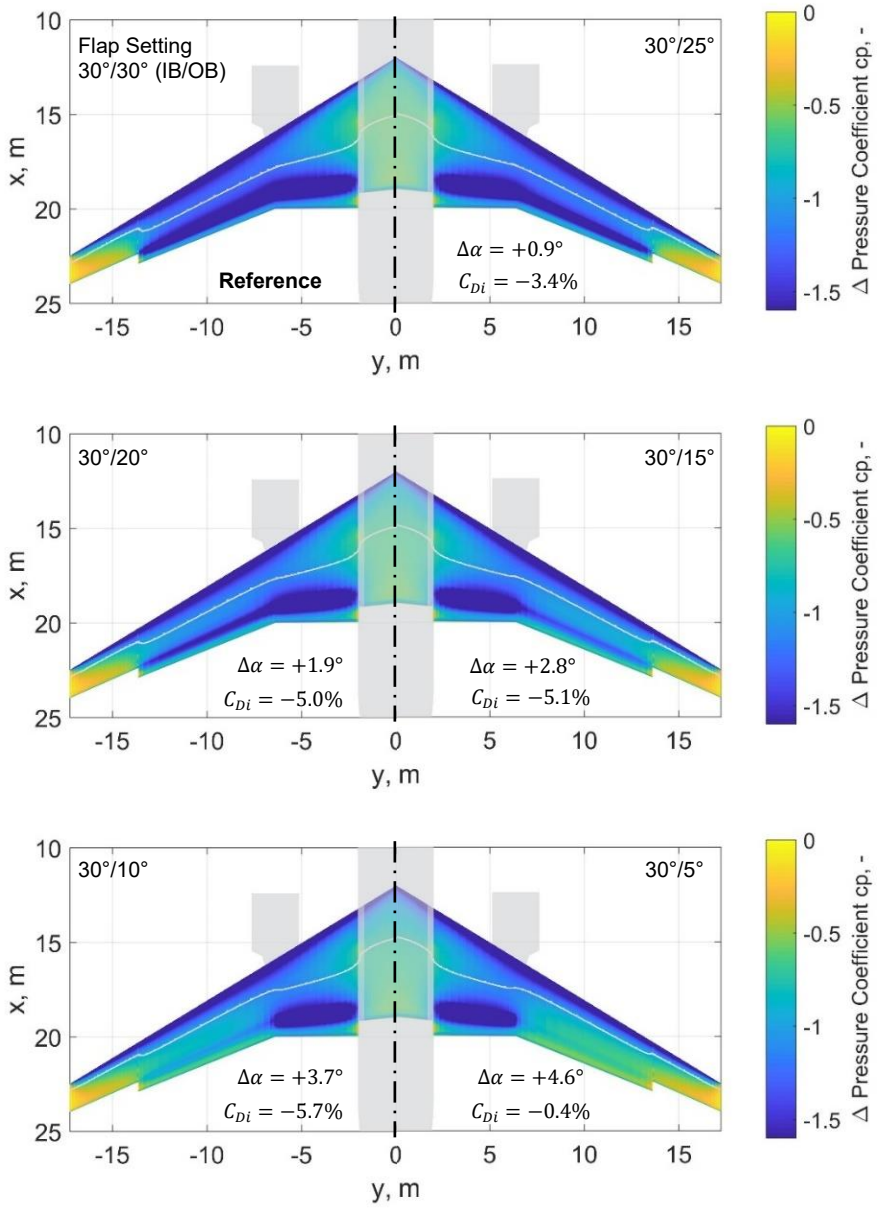

Figure 5.8 Pressure distribution for varying differential flap settings of the inboard (IB) and outboard (OB) trailing-edge flaps.

[100] AVLX provides additional parameters to display within the 3D plot: load vectors, the center of gravity and the resulting neutral point of the aircraft.

In addition to the aerodynamic parameters, hinge moments of all flight control devices are calculated, which may be used for a preliminary sizing of flight control actuators. The modelling of the CVC functions with AVLX is not suitable due to transonic effects, which cannot be reasonably represented by using VLM (cf. *Section 2.2.3, pp. 25)*.

Flight Control System Architecture. After the full flight control configuration is (iteratively) defined, the next step of the design method is the flight control system architecture design. Therefore, the design rules explained in section *3.5.1 Design Rules and Technological Constraints* are applied. Figure 5.9 illustrates the system architecture of the advanced FCS of CA2 and CA3. The RLC actuation architecture includes the ailerons and all outboard spoilers (left: 1-4, right: 7-10) on both wings. Whereas the HLC function is mainly provided by the slat and flap actuation system but is supported by slightly drooped ailerons. The CVC function (only available for CA3) is fulfilled by small deflections of the trailing-edge flaps, which again are supported by drooped spoilers for gap control[101]. The DFS function for wing load control is solely fulfilled by the trailing edge flaps and its actuation system (cf. Figure 5.1). In this case, it is of great advantage to have the DSA for the flap actuation system, instead of a traditional shaft transmission system (cf. Figure 2.23).

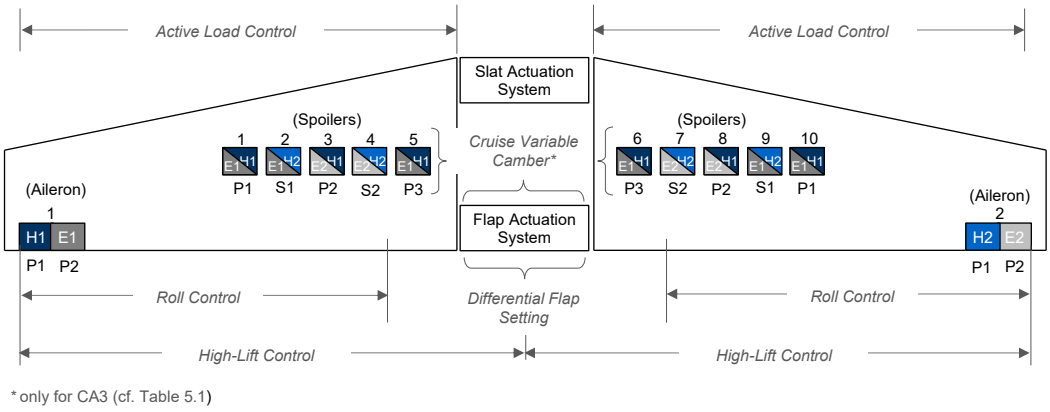

Figure 5.9 System architecture of the advanced flight control system with multifunctional flight control devices of the concept aircraft 2 and 3 (CA2 and CA3).

For the system architecture design of CA4 and CA5, which feature an AFC system, further design parameters have to be considered. For example, the AFC system with fluidic actuation at the trailing-edge flaps requires a pressurized air supply, which can be provided by the bleed-air system or by electrically powered compressors (cf. *2.3.4 Advanced Technologies and Concepts*, p. 39). Consequently, different actuation systems or available power supplies provide different design spaces, and hence different solutions.

Mass Estimation. In the next step, the mass estimation method (cf. *Section 3.6*) is applied. Figure 5.10 shows the results of the RA (left) in comparison to the CA3 (right). The largest share of the overall FCS mass is attributed to the high-lift control system (46% and 42%) at the wing. The total FCS results show that the FCS weight of the CA3 is $\Delta m_{FCS,CA3} \approx -103kg$ less than the FCS mass

[101] Small downward deflections of the spoiler can be used for the gap control between the trailing-edge of the wing and the leading-edge of the flap.

of the RA, due to the use of the DSA for the high-lift control system. Furthermore, the integration of the additional control function DFS enables an additional mass reduction of the wing structure (wing box) of approximately 500 kg (Recksiek, 2009, p. 53).

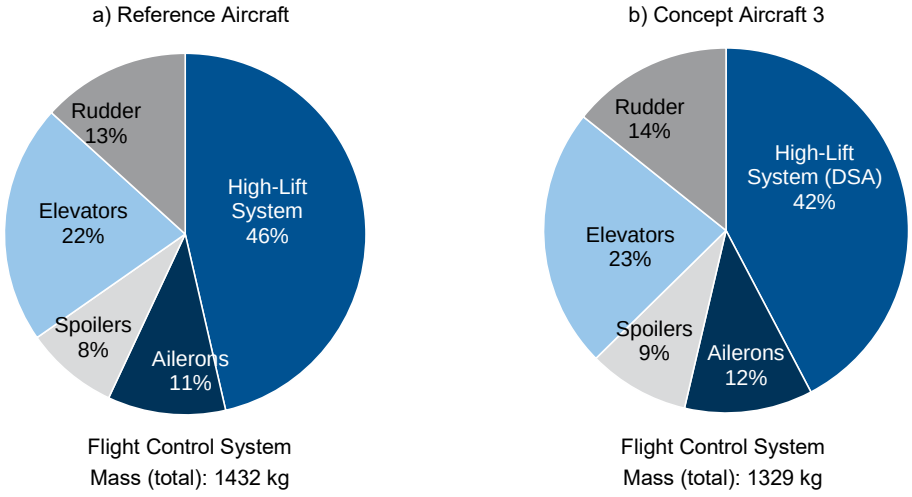

Figure 5.10 Overview of the flight control system mass shares of the reference aircraft (left) and concept aircraft 3 (right) with a distributed system architecture for the high-lift control system.

Additional weight savings can be expected for CA5. In Figure 5.11 the results of the flight control systems at the wings are presented, which enables a detailed and separated view of the high-lift control devices at the leading edge (LE) and trailing-edge (TE) of the wing. The overall weight reduction of the FCS is 205 kg ($\Delta m_{FCS,CA5} \approx -205kg$). This is mainly due to the use of AFC which allows to significantly reduce the size of the TE flaps. This results in an overall weight reduction of for the TE flaps of 163 kg ($\Delta m_{TE,flaps,CA5} \approx -163\ kg$), even though the integration of the AFC system adds weight. The corresponding wing planform and control surface models of RA and CA5 are shown in Figure 5.12.

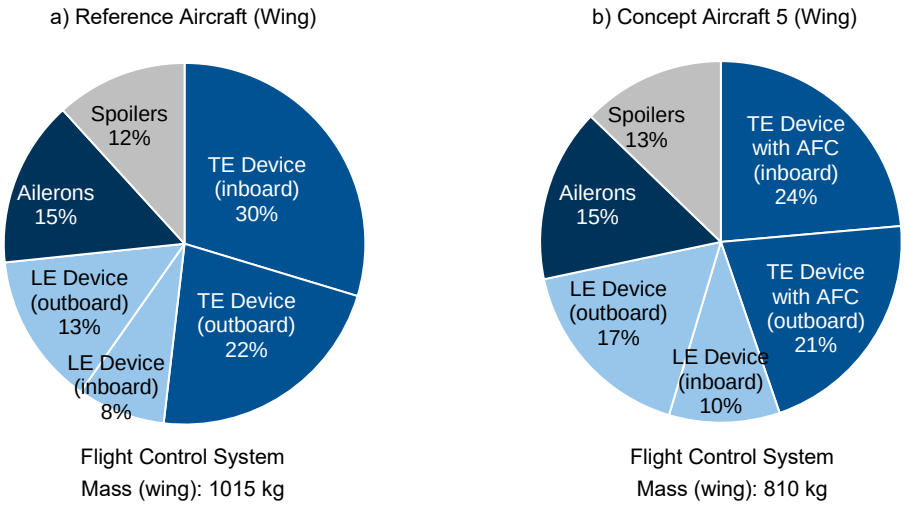

Figure 5.11 Overview of the flight control system mass shares at the wing: reference aircraft (left) and concept aircraft 5 (right).

The aileron span can be increased, as there is more space left at the TE of the wing due to the reduced (spanwise) size of the TE flaps. Furthermore, the ailerons can be divided into two ailerons of each side of the wing, see Figure 5.12b. Additionally, the aileron configuration of CA5 is slightly lighter than the configuration of the RA with weight savings of $\Delta m_{ailerons,CA5} \approx -25\ kg$.

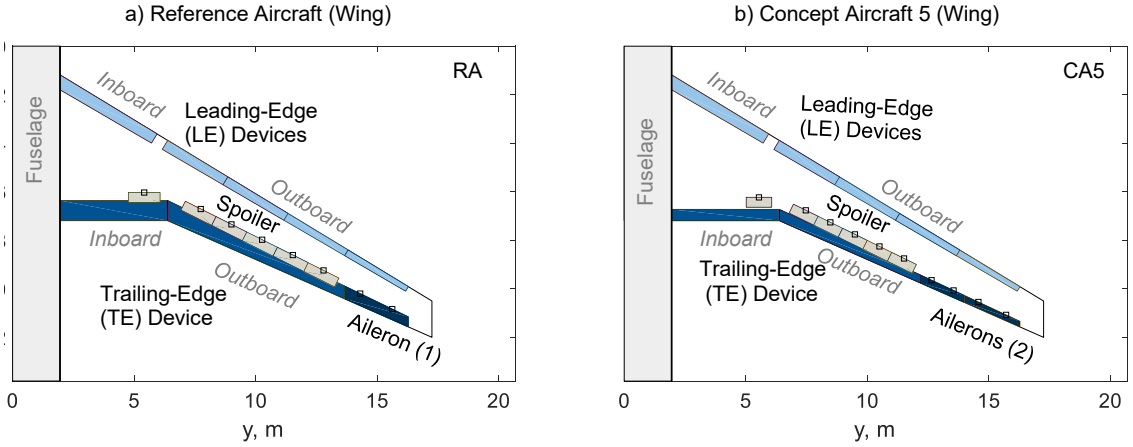

Figure 5.12 Wing planform and control surface model of the reference aircraft (left) and the concept aircraft 5 (right) with reduced size of the trailing-edge flaps and split ailerons at each wing.

5.3 Aircraft and System-Level Results

Based on the results of the integrated design, several run cases have been defined and calculated. The following section presents selected results regarding the relative fuel savings of the different concept aircraft configurations. In addition, some detailed results concerning the (specific) fuel consumption or secondary power requirements for selected flight phases are shown. The following Table 5.3 gives an overview of the defined aircraft (run cases). Furthermore, six different flight missions are defined, which are varying in range from 1000 km to 6000 km. Finally, a run case is defined for each aircraft and mission range, which resulting in a total of 24 run cases.

Table 5.3 Overview of the defined run cases for aircraft- and system-level analysis.

Aircraft (Run Case)	*ID*	ΔOEW	$\Delta Functions$	$\Delta Architecture$	Comment
Reference Aircraft	*RA*	0	-	-	Reference
Concept Aircraft 2	*CA2*	-1.43%	DFS	DSA	
Concept Aircraft 3	*CA3*	-1.43%	DFS, CVC	DSA	
Concept Aircraft 5	*CA5*	-1.67%	DFS, CVC, AFC	$DSA, AFC\ System$	Modification: Split ailerons

The *fuel iteration* option[102] was activated for the calculation procedure to get the actual amount of fuel required to successfully fulfill the flight mission. Afterwards, the (absolute) results for the individual calculated point (flight mission) were normalized to the results of the RA.

[102] In general, extra fuel at the end of the mission is required according to safety regulations. However, for this exemplary case study, the extra fuel is set to zero for all run cases.

5.3.1 Relative Fuel Savings

Figure 5.13 shows the relative fuel savings for CA2 and CA3. The bottom curve in the graph (CA2) shows the potential improvements due to the use of the DSA for the high-lift control system and one additional control function (DFS). The relative fuel savings are in the range of 0.43% (range: 1000 km) to 0.56% (6000 km). By adding the CVC function (CA3), the relative fuel savings increase to 0.64% (1000 km) up to 0.95% (6000 km). As expected, the relative fuel saving increases as the mission range increases. The two curves (CA2 and CA3) diverge with increasing mission ranges. This is due to the following effects: The effect of the wing mass reduction (DSA, DFS) is relatively smaller for greater ranges as the required fuel, and hence the overall aircraft take-off mass increases. In contrast, the effect of the CVC (aerodynamic improvements during cruise) increases for greater mission ranges, as the cruise phases gets relatively larger.

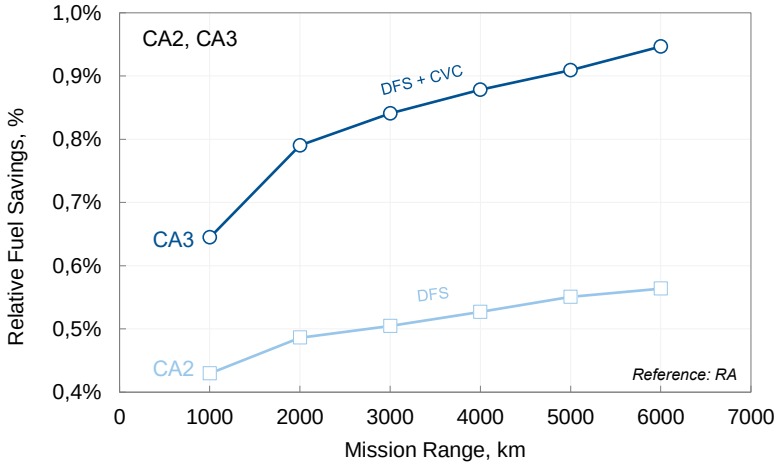

Figure 5.13 Relative fuel savings of the concept aircraft 2 and 3 (CA2, CA3) in relation to the reference aircraft (RA). (DFS: Differential Flap Setting, CVC: Cruise Variable Camber)

For the CA5, varying mass-flow rates (1.2, 2.2 and 3.2 kg/s) for the supply of the AFC system are considered, as there is yet no specific requirement defined, see Figure 5.14. To put the results into perspective, the fuel savings (light-grey area) of CA2 and CA3 are indicated.

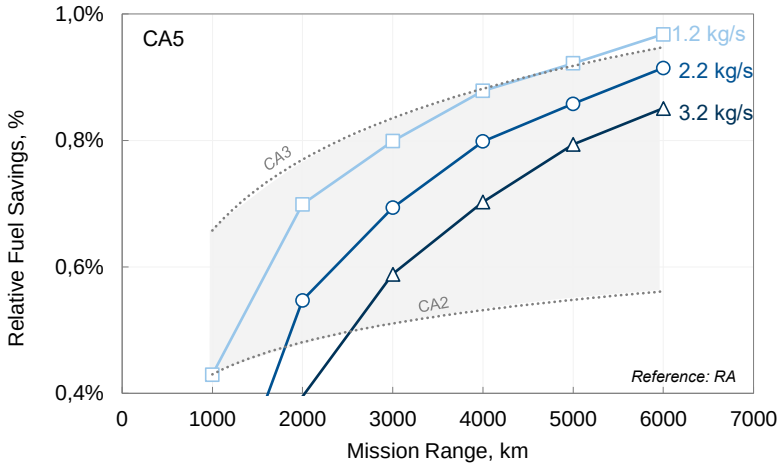

Figure 5.14 Relative fuel savings of the concept aircraft 5 (CA5) with varying mass flow rates for the active flow control system (AFC), in relation to the reference aircraft (RA).

The results show that the relative fuel savings are smaller for CA5 for low mission ranges (1000 and 2000km), compared to CA2 and CA3, but increases strongly with increasing mission range. For the considered mission range, only the CA5 with $\dot{m}_{AFC} = 1.2\ kg/s$ exceeds the relative fuel savings of CA2 and CA3 for the mission ranges equal or greater 5000 km (max. fuel savings of 0.97%). However, for CA5 with higher mass-flow rate requirements of the AFC system, the relative fuel savings decreased. According to the results, CA5 is, if at all, more suitable for greater mission ranges (long-range) transport aircraft. Furthermore, there is a high level of dependency on the AFC system requirements (e.g. mass-flow rates).

5.3.2 Fuel Consumption and Power Requirements

The relative fuel flow results of CA2 and CA3 in relation to the RA for a mission range of 3000 km are shown in Figure 5.15. Both results show that the fuel flow is relatively lower for the mean time (cruise phase) of the flight mission. In contrast to CA2, the results of CA3 (cf. Figure 5.15b) show that the relative difference of the relative *fuel consumed* increases with the duration of the cruise phase, leading to the divergence in the fuel-saving curves of the two concepts for increasing ranges (cf. Figure 5.13).

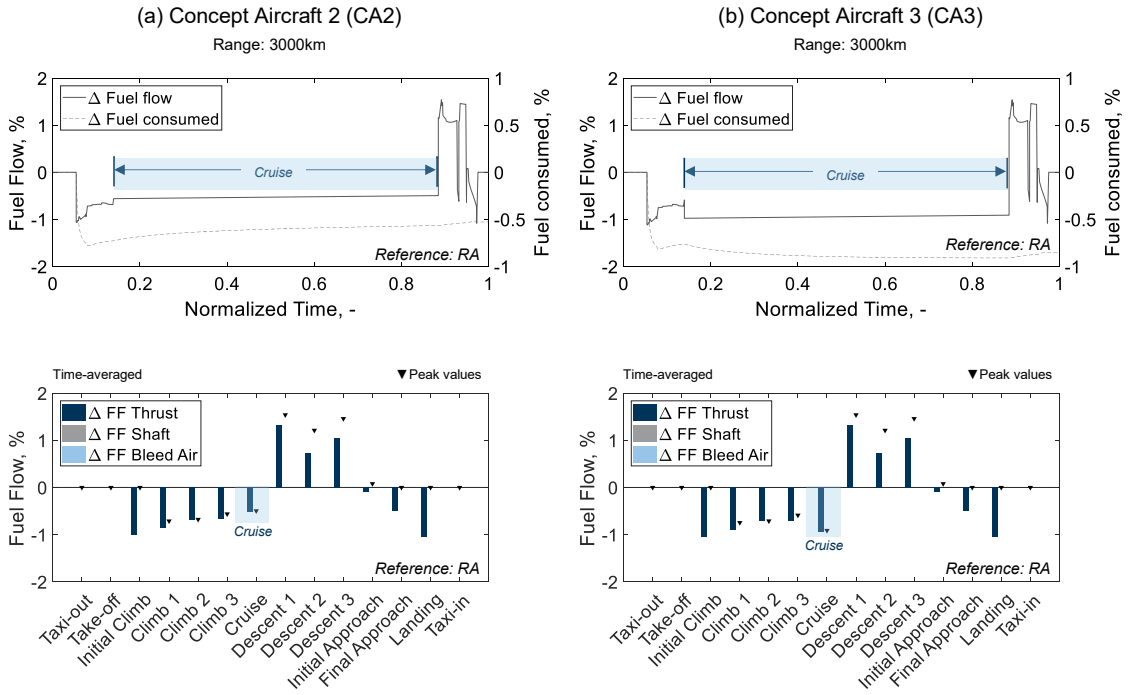

Figure 5.15 Relative fuel flow results of the concept aircraft 2 and 3 (CA2 and CA3) over the normalized time (top) and time-averaged values for each phase (bottom), for a mission range of 3000km.

Figure 5.16 shows the secondary power requirement results of the RA and the CA5 (absolute values). The AFC system of the CA5 requires a mass-flow rate of $\dot{m}_{AFC} = 2.2\ kg/s$ during the flight phases *initial approach*, *final approach* and *landing* (cf. Figure 5.16b). Consequently, the maximum required load for the bleed-air system is increased from 2.42 kg/s (RA) to 2.64 kg/s (CA5). For example, this result provides important input for further design and analysis of the operating points of the engine or bleed-air system.

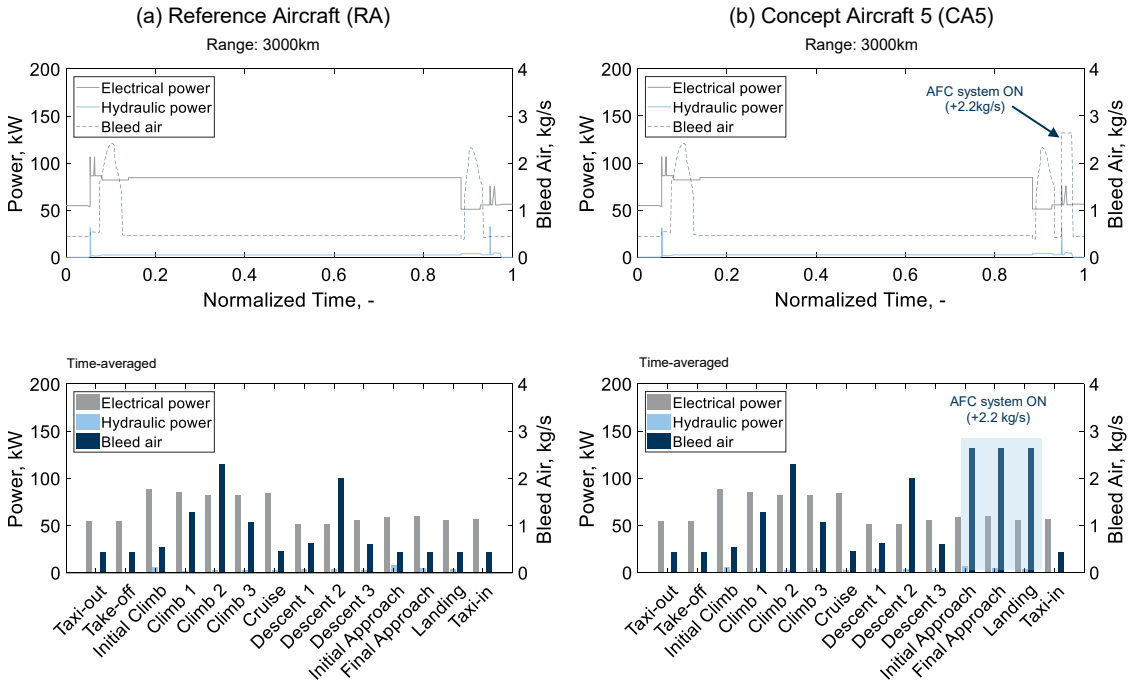

Figure 5.16 Secondary power requirements of the reference aircraft (left) and the concept aircraft 5 with Active Flow Control (AFC) activated during approach and landing phases (right).

As mentioned in the background section (cf. *Section 2.1.2)*, the engine technology regarding BPR and OPR has an impact on the engine power-offtakes (cf. Figure 2.4). In order to test this behavior, the RA and CA are equipped with a New Engine Option (NEO), featuring a turbofan with higher BPR and OPR. Figure 5.17 shows the corresponding results for CA5 (NEO) in addition to the results of CA2 and CA3 (light-grey area) in relation to the RA (NEO).

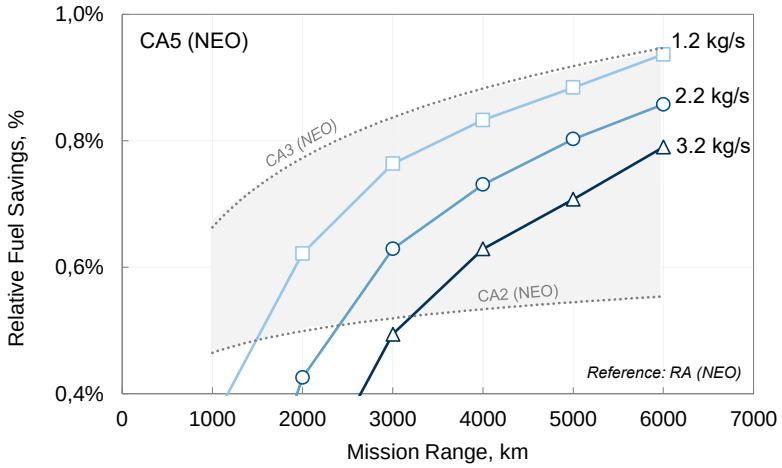

Figure 5.17 Relative fuel savings of the concept aircraft 5 (CA5) with New Engine Option (NEO) with higher bypass-ratio and varying mass flow rates for the Active Flow Control (AFC) system in relation to the reference aircraft (RA).

In comparison to the previous results, the relative fuel savings for all CA (NEO) are still in the similar range as the fuel savings of CA with the baseline engines (cf. Figure 5.14)[103]. However, one major difference is that all calculated points of CA5 (NEO) are below CA3 (NEO) for the considered mission ranges, even for CA5 (NEO) with low mass-flow rates (1.2 kg/s). The reason for this is the increasing fuel consumption for engine-power off-takes of high-BPR engines (cf. Figure 2.4), especially for engine bleed-air. Moreover, the results indicate that the increase in fuel consumption due to bleed-air is higher compared to shaft-power offtakes.

Summary. The fuel-savings results of all CA are mainly driven by the differences in the OEW compared to the RA (cf. Table 5.3). These differences in weight resulted directly from the chosen FCS architecture (e.g. DSA) or indirectly from the effects of additional flight control functions (e.g. DFS). Moreover, additional fuel savings resulted from aerodynamic improvements of additional flight control functions during certain flight phases (e.g. CVC, AFC). The results for the fuel savings in terms of percentage are within a plausible range compared to similar published studies (c.f. Liscouët-Hanke, 2008, p. 118; Chakraborty et al., 2015, p. 12). Another important aspect of the results is that clear (technological) dependencies and trends are correctly represented and visible. An overview of the relative fuel savings results for the ranges of 1000 km and 6000 km is shown in Table 5.4.

Table 5.4 Overview of the relative fuel savings for the Concept Aircraft (CA) compared to the reference Aircraft (RA) for selected mission ranges.

Concept Aircraft (CA)	Fuel Savings (Ref.: RA)		*Concept Aircraft (NEO)*	Fuel Savings (Ref.: RA (NEO))	
	1000 km	6000 km		1000 km	6000 km
CA2	0.43%	0.56%	*CA2 (NEO)*	0.47%	0.55%
CA3	0.64%	0.95%	*CA3 (NEO)*	0.65%	0.94%
CA5[1]	0.16%	0.92%	*CA5[1] (NEO)*	-0.12%	0.86%

[1] AFC System: +2.2kg/s *NEO New Engine Option*

In addition, for all calculated points shown in the graphs (cf. Figure 5.13 and Figure 5.14), secondary power requirements and (specific) fuel consumption data are available for each phase or step of the full flight mission. This enables further analysis regarding secondary power requirements or engine power-off takes, which are important to enable a holistic assessment of advantages and disadvantages of new system technologies and concepts in early aircraft design phases (cf. *2.1.1 Aircraft Configuration Design* and *2.1.2 Aircraft Systems*).

[103] However, the relative fuel savings between the baseline RA and RA (NEO) are of course significant (in the range of +5.8% to +9%), due to the more efficient engine (with higher BPR, OPR and TET compared to the baseline).

6 Conclusion

Advanced flight control systems combine the trends of gradual electrification (*more-electric aircraft, power-by-wire*) and the integration of additional flight control functions (*functional enhancement*) and show promising potential to improve the overall efficiency of the aircraft. The review of existing work indicated that there is a lack of enabling methodologies and tools for the design and analysis of advanced FCS during early aircraft design phases. This thesis contributes to close this gap and proposes an integrated design methodology in addition to a simulation environment to enable aircraft technology analysis and assessment. Within the scope of this work, all developed methods and tools are intended for the concept and preliminary design phase of commercial transport aircraft. The brief overview and key findings of the overall design methodology, including its methods, tools and the main results of the case study are summarized in this chapter.

At top level, the proposed methodology is divided into three main stages, consisting of the functional-driven design approach, the advanced flight control system design, and the technology analysis and assessment (cf. Figure 3.1). Based on this approach and the presented case study, the following key findings and achieved objectives can be summarized:

Functional-Driven Design Approach. The functional-driven design approach supports the transition from a knowledge-based to a functional-driven design of flight control systems. The approach comprises requirements engineering, the functional analysis and synthesis in addition to validation and evaluation activities. The core of this approach is the Functional Multiple Domain Matrix (FMDM), which is structured into matrices at aircraft, system and device level. Moreover, a function catalogue serves as a data basis, which describes all potential flight control functions and their characteristics and supports a differentiated view on each level. This functional-driven design approach enables the exploration of the available design space and the generation of alternative and multifunctional solutions for advanced FCS concepts. The application of this approach in the study revealed the following findings:

- The development and analysis of the FMDM provides a good overview on the multidisciplinary characteristics of flight control systems at different levels. Especially at system and device level, the cluster analysis serves as an effective tool.
- The functional-driven systematics of the approach proves to be promising for the design of advanced flight control system concept, enabling additional flight control functions while new technologies can be considered.

- The initial setup of the flight control function catalogue is very time consuming, as a lot of information at different levels are required. However, once a basic function catalogue is set up, the data of new technologies and concepts can be added, and the catalogue supports the functional-driven design approach. Furthermore, the catalogue can be seen as a growing data base and may be used in subsequent projects.
- The functional-driven design approach may be applied for retrofit studies, where selected delta MDM (as part of the overall FMDM) can be generated to identify possible improvements.

At this point it shall be emphasized again, that this functional-design approach gains the knowledge of the functional-driven design concept and its design space, considering all dependencies, synergies or conflicts at the different aircraft, system and device level.

Advanced Flight Control System Design. The next stage of the overall methodology composes the flight control configuration and the system architectural design, which is complemented by a parameterized mass estimation. The definition of the flight control configuration enables initial aerodynamic calculations. Afterwards, system architectures are designed, based on defined rules, technological assumptions, and distribution logics. Finally, the mass of the FCS is estimated, and the design can be analyzed, evaluated, or iteratively optimized (e.g. towards minimum mass). The application and analysis of the advanced FCS design method provide the following key findings:

- The aerodynamic modelling and analysis of the aircraft and additional flight control functions have been successfully demonstrated.
- Even though only one flight control function was modelled and analyzed in detail in the case study, the possibilities and the versatility of this approach, especially of the developed simulation tool are clearly visible. With this tool, a wide variety of control surface configurations can be created, calculated, and analyzed.
- The setup and parallelized computation of multiple run cases in AVLX proved to be helpful and enabled the execution of rapid parameter studies. Moreover, the integrated plot functions (2D and 3D) enable a quick presentation and analysis of the results.
- A preliminary design of advanced FCS architectures has been generated by applying the defined design rules and technological constraints. The distribution and assignment of the actuators, flight control computer, and power supply show good accordance to similar FCS architectures found in literature.
- The semi-empirical mass estimation for the FCS provide relatively good results for the fact that only very few input parameters are necessary. However, the absolute values must be considered carefully, and the use of differential values referring to a baseline is recommended.

Aircraft Technology Analysis and Assessment. A full aircraft technology analysis tool environment has been developed, with focus on the comprehensive and holistic analysis of advanced flight control configurations and system architectures. The developed tool ATAX considers the aircraft aerodynamics, aircraft systems, and the used engine technology to calculate secondary

power requirements, thrust, and finally the (specific) fuel consumption of the aircraft. Furthermore, the FCS model allows the setup of specific activity schedules including aerodynamic improvements to represent the advanced flight control configuration and system architecture in the best possible way. The key findings of the final step of the methodology can be summarized as follows:

- ATAX enables the setup, execution, and analysis of comprehensive parameter studies, while accuracy and computation time are still reasonable for early aircraft design phases.
- Besides the main aircraft system models (ECS, IPS, FCS, MIS) additional aircraft systems can be added, regardless of type of required power supply. Furthermore, the definition of individual activity schedules for each aircraft system enables the study of alternative, unconventional or off-design aircraft system settings.
- The tool provides separate shares of (specific) fuel consumption of the individual aircraft systems. This allows detailed and focused analyses of new technologies or system concepts for single or multiple flight phases.
- According to the overall results of case study, the implemented tool is suitable for the analysis and assessment of new system technologies in early aircraft design phases.
- The variety of results of different (system) parameters provided by the tool can be used for further design activities or analysis within the overall aircraft design process (e.g. sizing of the power generation and distribution system).

Recommendations and Outlook. Since the developed tools and the corresponding functions were programmed modularly and object-oriented, all calculations can also be set up and carried out by using scripts or using optimization algorithms, which were not covered in this work. The developed methods and tools are also suitable to be integrated into an overall aircraft design environment, including the integration of a superior and comprehensive aircraft data model. In addition, this step offers a good opportunity to integrate and apply the proposed methodology into an overall aircraft design process. Currently, the developed tools and methods are tailored for subsonic commercial transport aircraft only. Nevertheless, the general procedure and parts of the tools could also be applicable to supersonic or high-performance aircraft, but this would require some adjustments and extensions to the calculation tools. Considering the operational aspects of the flight control system and the flight control devices – especially with respect to certification and safety requirements (see *Appendix A.1*) – additional work has to be done. This includes, for example, the definition of a flight envelope for the baseline aircraft, and the aerodynamic modelling at specific operational points (limits). Furthermore, a more precise modelling of the flight control actuators or actuator systems could provide better (more accurate) secondary power and mass estimations. In order to be able to assess the (absolute) results even better, a validation of the tools with real aircraft and flight data is recommended. This allows the identification of inaccuracies in the presented approach, which can be taken into account when evaluating the results or provide a basis for further improvements of the developed models and tools.

Summarized, this work contributes to an integrated design and analysis of advanced FCS of commercial transport aircraft. The developed methods and tools provide a good compromise be-

tween accuracy of the results and computation time, to be applicable for conceptual and preliminary aircraft design phases (*cf. Figure 2.1*). Accordingly, early design studies considering advanced FCS concepts with new technologies or concepts can be performed, and hence their effects on the overall aircraft performance or efficiency can be holistically analyzed. Regardless of future aircraft concepts or available technologies, advanced flight control systems enable overall efficiency improvements and thus contribute to achieving the ambitious goals of the aviation industry to further reduce the global environmental impact (*Vision 2050*).

References

Ahlefelder, S. (2006), *Kraftstoffverbrauch durch Entnahme von Zapfluft und Wellenleistung von Strahltriebwerken*, Hamburg Aircraft Design and Systems Group (AERO), Department of Automotive and Aeronautical Engineering, Hamburg University of Applied Sciences.

Akoto, C.L., Bertram, O. and Schumann, H. (2017), "Generation of Potential System Architectures by Applying a Stochastic Clustering Algorithm in the High-Lift Actuation Preliminary Design Process", paper presented at International Dependency and Structure Modeling Conference, 11 - 13 September, Espoo, Finland, available at: https://elib.dlr.de/117340/1/2017_dsm_conference_Pre-Design_of_Actuation.pdf (accessed 8 January 2019).

Alduchov, O.A. and Eskridge, R.E. (1996), "Improved Magnus Form Approximation of Saturation Vapor Pressure", *Journal of Applied Meteorology*, Vol. 35 No. 4, pp. 601–609.

Anderson, J.D. (2011), *Fundamentals of aerodynamics, McGraw-Hill series in aeronautical and aerospace engineering,* 5th ed., McGraw-Hill, New York.

Anderson, R.D., Flora C. C., Nelson, M., Raymond, E.T. and Vincent, J.H. (1976), *Development of Weight and Cost Estimates for Lifting Surfaces with Active Controls, NASA Contractor Report*.

Bauer, C., Lagadec, K., Bès, C. and Mongeau, M. (2007), "Flight Control System Architecture Optimization for Fly-By-Wire Airliners", *Journal of Guidance, Control, and Dynamics*, Vol. 30 No. 4, pp. 1023–1029.

Bauer, M., Lohse, J., Haucke, F. and Nitsche, W. (2014), "High-Lift Performance Investigation of a Two-Element Configuration with a Two-Stage Actuator System", *AIAA Journal*, Vol. 52 No. 6, pp. 1307–1313.

Bennett, J.W., Mecrow, B.C., Jack, A.G. and Atkinson, D.J. (2010), "A Prototype Electrical Actuator for Aircraft Flaps", *IEEE Transactions on Industry Applications*, Vol. 46 No. 3, pp. 915–921.

Bennett, J.W., Mecrow, B.C., Jack, A.G., Atkinson, D.J., Sheldon, S., Cooper, B., Mason, G., Sewell, C. and Cudley, D. (2005), "A prototype electrical actuator for aircraft flaps and slats", in *EITC 2005, San Antonio, TX, USA*, National Taiwan University, Taipei, pp. 41–47.

Bertin, J.J. and Smith, M.L. (1994), *Aerodynamics for engineers,* 2. ed., 6. print, Prentice Hall, Englewood Cliffs, NJ.

Boeing (2006), "Boeing 737 Family Performance Summary", available at: https://web.archive.org/web/20140725005129/http://www.boeing.com/assets/pdf/commercial/startup/pdf/737ng_perf.pdf (accessed 18 October 2020).

Bossche, D. van den (2006), "The A380 Flight Control Electrohydrostatic Actuators, Achievements and Lessons Learnt", in International Council of the Aeronautical Sciences (ICAS) (Ed.), *25th Congress of the International Council of the Aeronautical Sciences, Hamburg, Germany, September 3-8*, International Council of Aeronautical Sciences (ICAS).

Botten, S.L., Whitley, C.R. and King, A.D. (2000), "Flight Control Actuation Technology for Next-Generation All-Electric Aircraft", *Technology Review Journal*, Millennium Issue Fall/Winter, pp. 55–68.

Bowes, G.M. (1974), "Aircraft Lift and Drag Prediction and Measurement", in Advisory Group for Aerospace Research and Development (AGARD) (Ed.), *Prediction Methods for Aircraft Aerodynamic Characteristics*, *AGARD Lecture Series*, 4-1 - 4-44.

Braslow, A.L. (1999), "History of Suction-Type Laminar-Flow Control with Emphasis on Flight Resrearch: Monographs in Aerospace History Number 13", available at: https://ntrs.nasa.gov/search.jsp?R=19990078750 (accessed 1 April 2019).

Brière, D. and Traverse, P. (1993), "AIRBUS A320/A330/A340 electrical flight controls - A family of fault-tolerant systems", in *FTCS-23 The Twenty-Third International Symposium on Fault-Tolerant Computing, Toulouse, France, 22-24 June 1993*, IEEE Comput. Soc. Press, pp. 616–623.

Brunet, V., Dandois, J. and Verbeke, C. (2013), "Recent Onera Flow Control Research on High-Lift Configurations", *Journal Aerospace Lab* 06-05, pp. 1–11.

Bunk, T. (2016), "Erweiterung eines aerodynamischen Berechnungstools zur Integration und Analyse von Hochauftriebsklappen im Flugzeugvorentwurf", Bachelor Thesis, Institute of Aircraft Design, Technical University of Munich (TUM), Munich, April 2016.

Cai, Y., Gao, Z., Chakraborty, I., Briceno, S. and Mavris, D. (2017), "Parametric Approach to Assessing Performance of High-Lift Device Active Flow Control Architectures", *Aerospace*, Vol. 4 No. 1, p. 6.

Chakraborty, I. (2015), "Subsystem Architecture Sizing and Analysis for Aircraft Conceptual Design", PhD Thesis, Daniel Guggenheim School of Aerospace Engineering, Georgia Institute of Technology, Atlanta, December 2015.

Chakraborty, I., Mavris, D.N., Emeneth, M. and Schneegans, A. (2015), "A methodology for vehicle and mission level comparison of More Electric Aircraft subsystem solutions. Application to the flight control actuation system", *Proceedings of the Institution of Mechanical Engineers, Part G: Journal of Aerospace Engineering*, Vol. 229 No. 6, pp. 1088–1102.

Chakraborty, I., Mavris, D.N., Emeneth, M. and Schneegans, A. (2016), "An integrated approach to vehicle and subsystem sizing and analysis for novel subsystem architectures", *Proceedings of the Institution of Mechanical Engineers, Part G: Journal of Aerospace Engineering*, Vol. 230 No. 3, pp. 496–514.

Ciobaca, V., Kühn, T., Rudnik, R., Bauer, M. and Gölling, B. (2011), *Active Flow Separation Control on a High-Lift Wing-Body Configuration: Part 2: The Pulsed Blowing Application, AIAA Applied Aerodynamics Conference*, Honolulu, Hawaii.

Ciobaca, V. and Wild, J. (2013), "An overview of Recent DLR Contributions on Active Flow-Separation Control Studies for High-Lift Configurations", *Journal Aerospace Lab* 06-12, pp. 1–11.

Concilio, A., Dimino, I., Lecce, L. and Pecora, R. (2018), *Morphing wing technologies: Large commercial aircraft and civil helicopters*, Butterworth-Heinemann, an imprint of Elsevier, Oxford, Cambridge, MA.

Criou, O. (2007), "A350 XWB Family and New Technologies", available at: http://hamburg.dglr.de/ (accessed 6 February 2019).

Cronin, M.J.J. (1990), "The all-electric aircraft", *IEE Review*, Vol. 36 No. 8, p. 309.

Cutts, S.J. (2002), "A collaborative approach to the More Electric Aircraft", in *International Conference on Power Electronics Machines and Drives, Bath, UK, 16-18 April 2002*, IEE, pp. 223–228.

Dam, C.P. van (2002), "The aerodynamic design of multi-element high-lift systems for transport airplanes", *Progress in Aerospace Sciences*, Vol. 38, pp. 101–144.

Dargel, G., Hansen, H., Wild, J., Streit, T., Rosemann, H. and Richter, K. (2002), *Aerodynamische Flügelauslegung mit multifunktionalen Steuerflächen, Deutscher Luft- und Raumfahrtkongress*, Stuttgart, Germany.

Dorbath, F., Nagel, B. and Gollnick, V. (2012), *A Knowledge Based Approach for Extended Physics-Based Wing Mass Estimation in Early Design Stages, International Congress of the Aeronautical Sciences,* 28th.

Drela, M. and Youngren, H. (2017a), "Athena Vortex Lattice (AVL). (Software)", available at: http://web.mit.edu/drela/Public/web/avl/ (accessed November 2017).

Drela, M. and Youngren, H. (2017b), "AVL 3.36 User Primer", available at: http://web.mit.edu/drela/Public/web/avl/avl_doc.txt (accessed 22 November 2018).

Eppinger, S.D. and Browning, T.R. (2012), *Design structure matrix methods and applications, Engineering systems*, MIT Press, Cambridge, MA, USA.

Eurocontrol (2017), "Aircraft Performance Database", available at: https://contentzone.eurocontrol.int/aircraftperformance (accessed 2 August 2016).

European Aviation Safety Agency (EASA) (2017), *Certification Specifications and Acceptable Means of Compliance for Large Aeroplanes CS-25: CS-25*.

European Aviation Safety Agency (EASA) (2018), *Certification Specifications and Acceptable Means of Compliance for Large Aeroplanes CS-25: CS-25 / Amendment 22*.

Faleiro, L. (2006), "Summary of the European Power Optimised Aircraft (POA) Project", in International Council of the Aeronautical Sciences (ICAS) (Ed.), *25th Congress of the International Council of the Aeronautical Sciences, Hamburg, Germany, September 3-8*, International Council of Aeronautical Sciences (ICAS).

Federal Aviation Administration (FAA) (2011), *Continuous Descent Final Approach,* Advisory Circular.

Federal Aviation Administration (FAA) (2019), *Federal Aviation Regulations (FAR) Part 25 - Airworthiness Standards: Transport Category Airplanes: FAR Part 25*.

Fujiwara, G. and Nguyen, N. (2015), "Adaptive Aeroelastic Wing Shape Optimization for High-Lift Configurations", paper presented at 33rd AIAA Applied Aerodynamics Conference, Dallas, TX.

Garriga, A.G., Govindaraju, P., Ponnusamy, S.S., Cimmino, N. and Mainini, L. (2017), "A modelling framework to support power architecture trade-off studies for More-Electric Aircraft", in Council of European Aerospace Societies (CEAS) (Ed.), *6th CEAS Air & Space Conference*, Bucharest, Romania.

Giannakakis, P., Laskaridis, P. and Pilidis, P. (2011), "Effects of Off-takes for Aircraft Secondary-Power Systems on Jet Engine Efficiency", *Journal of Propulsion and Power*, Vol. 27 No. 5, pp. 1024–1031.

Gillet, S., Nuic, A. and Mouillet, V. (2010), "Enhancement in realism of ATC simulations by improving aircraft behaviour models", Salt Lake City, UT, USA.

Goupil, P. (2011), "AIRBUS state of the art and practices on FDI and FTC in flight control system", *Control Engineering Practice*, Vol. 19 No. 6, pp. 524–539.

Graiff, M. (2016), "Development of a Tool for the Parametric Mass Estimation of Flight Control Systems in Preliminary Aircraft Design", Bachelor Thesis, Institute of Aircraft Design, Technical University of Munich (TUM), München, Germany, November, 2016.

Henke, R. (1999), ""A 320 HLF Fin" flight tests completed", *Air & Space Europe*, Vol. 1 No. 2, pp. 76–79.

Hilbig, R. and Wagner, H. (1984), "Variable Wing Camber Control for Civil Transport Aircraft", available at: https://www.icas.org/ICAS_ARCHIVE/ICAS1984/ICAS-84-5.2.1.pdf (accessed 25 March, 2019).

Hocking, M. (Ed.) (2005), *Air Quality in Airplane Cabins and Similar Enclosed Spaces, The Handbook of Environmental Chemistry*, Springer-Verlag, Berlin/Heidelberg.

Hoffman, A.C., Hansen, I.G., Beach, R.F., Plencner, R.M., Dengler, R.P., Jefferies, K.S. and Frye, R.J. (1985), *Advanced Secondary Power System for Transport Aircraft, NASA Technical Paper*.

Howe, D. (2010), *Aircraft conceptual design synthesis*, Professional Engineering Publishing, London.

Hunt, E.H., Reid, D.H., Space, D.R. and Tilton, F.E. (1995), "Commercial Airliner Environmental Control System. Engineering Aspects of Cabin Air Quality", in The Boeing Company (Ed.), *Aerospace Medical Association Annual Meeting*, Anaheim, California.

International Air Transport Association (IATA) (2013), "IATA Technology Roadmap", available at: https://www.iata.org/whatwedo/environment/Documents/technology-roadmap-2013.pdf (accessed 4 April 2019).

International Civil Aviation Organization (ICAO) (2010), *ICAO Environmental Report 2010: Aviation and Climate Change*, Montréal, Québec, Canada.

International Civil Aviation Organization (ICAO) (Ed.) (2013), *ICAO Environmental Report 2013: Aviation and Climate Change*.

International Civil Aviation Organization (ICAO) (Ed.) (2016), *ICAO Environmental Report 2016: On Board a Sustainable Future*, Montreal, QC, Canada.

Jeck, R.K. (2002), *Icing Design Envelopes (14 CFR Parts 25 and 29, Appendix C) Converted to a Distance-Based Format*, Washington, DC, USA.

Johnson, D.L., Roberts, B.C., Vaughan, W.W. and Parker, N.C. (2002), "Reference and Standard Atmosphere Models", in *10th Conference on Aviation, Range, and Aerospace Meteorology, Portland, Oregon, 13-16 May*, National Aeronautics and Space Administration, Portland, Oregon.

Jones, R.I. (1999), "The More Electric Aircraft. The past and the future?", in *IEE Colloquium. Electrical Machines and Systems for the More Electric Aircraft, London, UK, 9 Nov. 1999*, IEE, I/1-I/4.

Jones, R.I. (2005), "The more electric aircraft—assessing the benefits", *Proceedings of the Institution of Mechanical Engineers, Part G: Journal of Aerospace Engineering*, Vol. 216 No. 5, pp. 259–269.

Kiefner, B., Fokken, M., Schröder, K. and Quell, J. (2009), *Schlussbericht zum Technologievorhaben HICON Neue Konzepte für Hochauftriebskonfigurationen: IHK - Innovative Hochauftriebs-Konfigurationen*.

Kreitz, T., Bornholdt, R., Krings, M., Henning, K. and Thielecke, F. (2015), "Simulation-Driven Methodology for the Requirements Verification and Safety Assessment of Innovative Flight Control Systems", in *SAE 2015 AeroTech Congress & Exhibition, SEP. 22, 2015*, SAE International, Warrendale, PA, United States.

Lammering, T. (2014), "Integration of Aircraft Systems into Conceptual Design Synthesis", PhD Thesis, Institute of Aeronautics and Astronautics, RWTH Aachen, Aachen, May 2014.

Lammering, T. and Weber, G. (2013), "Liebherr State-of-the-Art Fly-By-Wire Flight Control System for Commercial Transport Aircraft", in Estorff, O. von and Thielecke, F. (Eds.), *Proceedings of the 4th International Workshop on Aircraft System Technologies: April 23-24, 2013, Hamburg, Germany*, *Berichte aus der Luft- und Raumfahrttechnik*, Shaker, Aachen, pp. 127–137.

Lampl, T. (2012), "Designing a System Test Rig for the Analysis of an Active Flow Control Concept Dedicated to Aircraft Flaps", Diploma Thesis, Institute of Aircraft Design, Technical University of Munich (TUM), Munich, Germany, December 2012.

Lampl, T. and Hornung, M. (2018), "An Integrated Design Approach for Advanced Flight Control Systems with Multifunctional Flight Control Devices", in *18th AIAA Aviation Technology, Integration, and Operations Conference, Atlanta, Georgia (USA), 25-29 June 2018*, American Institute of Aeronautics and Astronautics (AIAA).

Lampl, T., Königsberger, R. and Hornung, M. (2017a), "Design and Evaluation of Distributed Electric Drive Architectures for High-Lift Control Systems", paper presented at Deutscher Luft- und Raumfahrtkongress, 5-7 September, Munich, Germany.

Lampl, T., Muschkorgel, S. and Hornung, M. (2017b), "Parameterized Flight Mission for Secondary Power Requirement Estimations of Commercial Transport Aircraft", in *17th AIAA Aviation Technology, Integration, and Operations Conference, Denver, Colorado (USA), 5-9 June*, American Institute of Aeronautics and Astronautics (AIAA).

Lampl, T., Sauterleute, D. and Hornung, M. (2017c), "A Functional-Driven Design Approach for Advanced Flight Control Systems of Commercial Transport Aircraft", in Estorff, O. von and Thielecke, F. (Eds.), *Proceedings of the 6th International Workshop on Aircraft System Technologies: February 21-22, 2017, Hamburg, Germany*, *Berichte aus der Luft- und Raumfahrttechnik*, 1. Auflage, Shaker, Herzogenrath, pp. 3–12.

Lampl, T., Wolf, T. and Hornung, M. (2017d), "Preliminary Design of Advanced Flight Control System Architectures for Commercial Transport Aircraft", in Council of European Aerospace Societies (CEAS) (Ed.), *6th CEAS Air & Space Conference*, Bucharest, Romania.

Lampl, T., Wolf, T. and Hornung, M. (2019), "Preliminary design of advanced flight control system architectures for commercial transport aircraft", *CEAS Aeronautical Journal*, Vol. 10 No. 2, pp. 613–622.

Lengers, M. (2014), "Industrial Assessment of Overall Aircraft Driven Local Active Flow Control", in International Council of the Aeronautical Sciences (ICAS) (Ed.), *29th Congress of the International Council of the Aeronautical Sciences*, International Council of Aeronautical Sciences (ICAS), St. Petersburg, Russia.

Liscouët-Hanke, S. (2008), "A Model-Based Methodology for Integrated Preliminary Sizing and Analysis of Aircraft Power System Architectures", Dissertation, Institut National des Sciences Appliquée, Université Paul Sabatier, Toulouse, France, September 2008.

Maré, J.-C. and Fu, J. (2017), "Review on signal-by-wire and power-by-wire actuation for more electric aircraft", *Chinese Journal of Aeronautics*, Vol. 30 No. 3, pp. 857–870.

McLean, J.D., Crouch, J.D., Stoner, R.C., Sakurai, S., Seidel, G.E., Feifel, W.M. and Rush, H.M. (1999), *Study of the Application of Separation Control by Unsteady Excitation to Civil Transport Aircraft, NASA Contractor Report*, Seattle, Washington.

Meier, O. and Scholz, D. (2010), *A Handbook Method for the Estimation of Power Requirements for Electrical De-Icing Systems, Deutscher Luft- und Raumfahrtkongress*, Hamburg.

Meyer, M., Machunze, W. and Bauer, M. (2014), "Towards the Industrial Application of Active Flow Control in Civil Aircraft - An Active Highlift Flap", in *32nd AIAA Applied Aerodynamics Conference*, American Institute of Aeronautics and Astronautics (AIAA).

Moir, I. and Seabridge, A.G. (2008), *Aircraft systems: Mechanical, electrical, and avionics subsystems integration, Aerospace series,* 3rd ed., Wiley, Chichester, West Sussex, England, Hoboken, NJ.

Nguyen, N. (2010), *Elastically Shaped Future Air Vehicle Concept, NASA innovation Fund 2010 Project*, Moffet Field, California.

Nguyen, N., Kaul, U., Lebofsky, S., Chaparro, D. and Urnes, J. (2015), *Development of Variable Camber Continuous Trailing Edge Flap for Performance Adaptive Aeroelastic Wing, SAE Aero Tech Congress & Exhibition*, Seattle, Washington.

Nuic, A. (2004), *User Manual for the Base of Aircraft Data (BADA) - Revision 3.6*, Brétigny-sur-Orge.

Olson, E.D. (2015), "Semi-Empirical Prediction of Aircraft Low-Speed Aerodynamic Characteristics", Kissimmee, Florida.

Pantelakis, S., Kintscher, M., Wiedemann, M., Monner, H.P., Heintze, O. and Kühn, T. (2011), "Design of a smart leading edge device for low speed wind tunnel tests in the European project SADE", *International Journal of Structural Integrity*, Vol. 2 No. 4, pp. 383–405.

Petz, R. and Nitsche, W. (2004), *Active Separation Control on a High-Lift Configuration by a Periodically Pulsating Jet, International Congress of the Aeronautical Sciences,* 24th, Yokohama, Japan.

Platz, P. (1999), "Flächen- und Volumenberechnung charakteristischer Komponenten von Passagierflugzeugen", Hamburg, Germany, September 1999.

Randt, N.P. (2016), "Aircraft Technology Assessment Using Fleet-Level Metrics", PhD, Institute of Aircraft Design, Technical University of Munich (TUM), Munich, Germany, June 2016.

Raymond, E.T. and Chenoweth, C.C. (1993), *Aircraft flight control actuation system design*, Society of Automotive Engineers (SAE) International, Warrendale, PA.

Recksiek, M. (2009), "Advanced High Lift System Architecture with Distributed Electrical Flap Actuation", in Estorff, O. von (Ed.), *Proceedings of the 2nd International Workshop on Aircraft System Technologies: March 26 - 27, 2009, Hamburg, Germany*, *Berichte aus der Luft- und Raumfahrttechnik*, Shaker, Aachen, pp. 49–60.

Reckzeh, D. (2003), "Aerodynamic design of the high-lift-wing for a Megaliner aircraft", *Aerospace Science and Technology*, Vol. 7 No. 2, pp. 107–119.

Reckzeh, D. (2014), "Multifunctional Wing Moveables: Design of the A350XWB and the Way to Future Concepts", in International Council of the Aeronautical Sciences (ICAS) (Ed.), *29th Congress of the International Council of the Aeronautical Sciences*, International Council of Aeronautical Sciences (ICAS), St. Petersburg, Russia.

Richter, K. and Rosemann, H. (2012), "Steady Aerodynamics of Miniature Trailing-Edge Devices in Transonic Flows", *Journal of Aircraft*, Vol. 49 No. 3, pp. 898–910.

Rosero, J.A., Ortega, J.A., Aldabas, E. and Romeral, L. (2007), "Moving towards a more electric aircraft", *IEEE Aerospace and Electronic Systems Magazine*, Vol. 22 No. 3, pp. 3–9.

Roskam, J. (1989), *Airplane Design - Part IV: Layout Design of Landing Gear and Systems*, Lawrence, Kansas.

Rudolph, P.K.C. (1996), *High-Lift Systems on Commercial Subsonic Airliners, NASA Contractor Report*, Vol. 1996.

Rustenburg, J.W., Skinn, D.A. and Tipps, D.O. (2002), *Statistical Loads Data for the Airbus A-320 Aircraft in Commercial Operations*.

SAE ARP4754A (2010), *Guidelines for Development of Civil Aircraft and Systems,* Rev A, Society of Automotive Engineers (SAE) International, 400 Commonwealth Drive, Warrendale, PA, United States.

Sauterleute, D. (2016), "Funktionale Auslegung und Analyse von Flugsteuerungssystemen und Steuerflächen im Flugzeugvorentwurf", Master Thesis, Institute of Aircraft Design, Technical University of Munich (TUM), Munich, Germany, August 2016.

Schlichting, H. and Truckenbrodt, E.A. (1967), *Aerodynamik des Flugzeuges: Erster Band Grundlagen aus der Strömungsmechanik Aerodynamik des Tragflügels (Teil I),* Zweite neubearbeitete Auflage, Springer Berlin Heidelberg, Berlin, Heidelberg.

Schlottbohm, T., Lerch, M., Kupfer, C. and Thielecke, F. (2019), "More-Electrical Trailing Edge Concepts for Future Wing Moveables", in Estorff, O. von and Thielecke, F. (Eds.), *Proceedings of the 7th International Workshop on Aircraft System Technologies: February 19-20, 2019, Hamburg, Germany*, *Berichte aus der Luft- und Raumfahrttechnik*, 1. Auflage, Shaker, Herzogenrath, pp. 3–12.

Scholz, D. (1996), "CAE-Werkzeug zum Entwurf von Flugsteuerungs- und Hydrauliksystemen", Dissertation, 1996.

Scholz, D., Seresinhe, R., Staack, I. and Lawson, C. (2013), "Fuel Consumption due to Shaft Power Off-Takes From the Engine", in Estorff, O. von and Thielecke, F. (Eds.), *Proceedings of the 4th International Workshop on Aircraft System Technologies: April 23-24, 2013, Hamburg, Germany*, *Berichte aus der Luft- und Raumfahrttechnik*, Shaker, Aachen.

Schrage, D., Beltracchi, T., Berke, L., Dodd, A., Niedling, L. and Sobieski, J. (1991), *AIAA Technical Committee on MDO: White Paper on Current State of the Art*.

Seabridge, A.G. and Moir, I. (2013), *Design and development of aircraft systems, AIAA education series,* Second edition, John Wiley & Sons, Inc, Hoboken.

Sherif, S.A., Pasumarthi, N. and Bartlett, C.S. (1997), "A semi-empirical model for heat transfer and ice accretion on aircraft wings in supercooled clouds", *Cold Regions Science and Technology*, Vol. 26 No. 3, pp. 165–179.

Shmilovich, A. and Yadlin, Y. (2009), "Active Flow Control for Practical High-Lift Systems", *Journal of Aircraft*, Vol. 46 No. 4, pp. 1354–1364.

Simsic, C.J. (1991), "Electric actuation system duty cycles", in *NAECON '91: National aerospace and electronics conference: Papers, Dayton, OH, USA, 20-24 May 1991*, IEEE, pp. 540–545.

Sinnet, M. (2007), "787 No-Bleed Systems. Saving Fuel and Enhancing Operational Efficiencies", *AERO*, Vol. 9 No. 28, pp. 7–11.

Slingerland, R. and Zandstra, S. (2007), "Bleed Air versus Electric Power Off-takes from a Turbofan Gas Turbine over the Flight Cycle", paper presented at 7th AIAA ATIO Conf, 2nd CEIAT Int'l Conf on Innov and Integr in Aero Sciences,17th LTA Systems Tech Conf; followed by 2nd TEOS Forum, 18 September 2007 - 20 September 2007, Belfast, Northern Ireland.

Specht, E. (2005), "Der Mensch als wärmetechnisches System", available at: http://www.uni-magdeburg.de/isut/TV/Download/Der_Mensch_als_waermetechnisches_System.pdf (accessed 6 November 2018).

Steinke, T. (2010), "Entwicklung einer Methodik zur Modellierung und Analyse von Systemstrukturen im Flugzeugvorentwurf", Diploma Thesis, Institut für Luft- und Raumfahrt, RWTH Aachen, Aachen, Germany, November 2010.

Steward, D.V. (1981), *Systems and analysis and management: Structure, strategy, and design*, Petrocelli Books, New York.

Tagge, G.E., Irish, L.A. and Bailey, A.R. (1985), *Systems Study for an Integrated Digital/Electric Aircraft (IDEA), NASA Contractor Report*, Langley, Virgina.

Thebeau, R.E. (2001), "Knowledge Management of System Interfaces and Interactions for Product Development Processes", Master's Thesis, Massachusetts Institute of Technology (MIT), Cambridge, MA, USA, February 2001.

Thomas, J.L. and Nerney, B. (1976), "Aerodynamics of Arbitrary Wing Body Combinations with Vortex Lattice and Slender Body Theory", in American Institute of Aeronautics and Astronautics (AIAA) (Ed.), *14th AIAA Aerospace Sciences Meeting*, Washington, D.C.

Tipps, D.O., Skinn, D.A., Rustenburg, J.W., Jones, T. and Harris, D.A. (2006), *Statistical Loads Data for the Boeing 777-200 Aircraft in Commercial Operations*.

Torenbeek, E. (1982), *Synthesis of subsonic airplane design: An introduction to the preliminary design, of subsonic general aviation and transport aircraft, with emphasis on layout, aerodynamic design, propulsion, and performance*, Delft University Press; Nijhoff; Sold and distributed in the U.S. and Canada by Kluwer Boston, Delft, The Hague, Hingham, MA.

Torenbeek, E. (2013), *Advanced aircraft design: Conceptual design, analysis, and optimization of subsonic civil airplanes, Aerospace series*, John Wiley & Sons, Inc, Delft, Netherlands.

Torenbeek, E. (2014), *Flight Physics: Essentials of Aeronautical Disciplines and Technology, with Historical Notes*, Springer, Delft, Netherlands.

Traverse, P., Lacaze, I. and Souyris, J. (2004), "Airbus Fly-By-Wire. A Total Approach To Dependability", in Jacquart, R. (Ed.), *Building the Information Society*, *IFIP International Federation for Information Processing*, Vol. 156, Springer US, Boston, MA, pp. 191–212.

Velupillai, D. (1981), "British Aerospace 146 described", *Flight International* May 2, pp. 1243–1250.

Weimer, J.A. (1993), "Electrical power technology for the more electric aircraft", in *Digital Avionics Systems Conference, 1993. 12th DASC., AIAA/IEEE, Fort Worth, TX, USA, 25-28 Oct. 1993*, IEEE, pp. 445–450.

Wild, T.W. (1990), *Transport category aircraft systems, An IAP, Inc. training manual*, IAP, Inc, Casper, WY.

Appendix

A.1 Certification and Safety Requirements

A.2 Design Structure Matrix and Multiple Domain Matrix

A.3 Flight Control Function Catalogue

A.4 Baseline Aircraft and Mission Model

A.5 Aircraft System Model

A.6 Data Model Structures and User Interfaces

A.1 Certification and Safety Requirements

Certification Regulations CS-25

Commercial transport aircraft must comply with the respective certification regulations CS-25 published by the European Aviation Safety Agency (EASA) (European Aviation Safety Agency (EASA), 2017). The relevant paragraphs §25.671 to §25.703 regarding the flight control system can be found in subpart D. Furthermore, §25.1309 addresses the safety of any aircraft system and its impact at aircraft level. The objective of this paragraph (*Safety – Equipment, Systems and Installations*) is to ensure an acceptable safety level for installed aircraft systems on the aircraft. According to this, "*a logical and acceptable inverse relationship must exist between*" the average probability per flight hour and the severity of the failure condition, as shown in Table A.2.

Table A.1 Overview of the main paragraphs of the CS-25, which are specifically relevant for the development of flight control configurations and system architectures.

Requirements Category	CS-25	*Requirements Category*	CS-25
Flight Mechanics		**Structure**	
Performance (General)	25.101	*Flight Maneuvering Envelope*	25.333
- Stall Speed	25.103	*High-lift devices*	25.345
- Takeoff	25.105	*Speed control devices*	25.373
- Landing	25.125	*Control surface loads*	25.391
Controllability and Maneuverability	25.143	*Wing flaps*	25.457
- Longitudinal control	25.145	**Design and Construction**	
- Directional and lateral control	25.147	*Control surfaces*	25.651 ff.
Trim	25.161	*Control systems*	25.671 ff.
Stability	25.171	**Safety**	
- Static longitudinal stability	25.175	*Equipment, Systems and Installations*	25.1309
- Static directional and lateral stability	25.177		
- Dynamic stability	25.181		

Table A.2 Relationship between classification of failure conditions and probability for installed equipment and systems on the aircraft.

Failure Classification	Probability per Flight Hour	Effects on aircraft, passengers and crew
No	No probability	- No effects
Minor	Probable $< 10^{-3}$	- Flight reduction in functional capabilities or safety - Slight increase in crew workload - Physical discomfort for passengers
Major	Remote $< 10^{-5}$	- Significant reduction in functional capabilities, safety - Significant increase in workload or physical discomfort - Physical distress, possible injuries for passengers
Hazardous	Extremely Remote $< 10^{-7}$	- Large reduction in functional capabilities or safety - Physical distress or excessive workload of the flight crew - Serious or fatal injury of passengers or cabin crew
Catastrophic	Extremely Improbable $< 10^{-9}$	- Hull loss of the aircraft - Multiple fatalities - Fatalities

Table A.3 shows the exemplary results of the Functional Hazard Assessment (FHA) for advanced high-lift control systems with distributed electric drive architectures. The results of the FHA are taken from the author's publication *"Design and Evaluation of Distributed Electric Drive Architectures for High-Lift Control Systems"* (cf. Figure 2.23, p. 41).

Table A.3 Results of the Functional Hazard Assessment (FHA) of distributed electric drive architecture for high-lift control systems.

Functions	Failure Condition	Flight Phases	Effect of Failure	Classification
(1) High-lift control to provide augmented lift during take-off, approach, landing *(2) Multifunctional control to provide additional functions*	High-lift system runaway above max. flap extended speed	All phases	- Structural damage - Loss of control	Catastrophic
	High-lift system runaway below max. flap extended speed	Take-off, Landing	- Reduced flight performance - Deviation from flight path - Significant increase in workload	Hazardous
	High-lift system asymmetry on extension/retraction	Approach, Climb out	- Loss of control	Catastrophic
	Uncommanded retraction of high-lift system	Landing	- Increase of stall speed - Loss of control	Catastrophic
	Loss of extension capability of high-lift system	Landing	- Increase in landing distance - Increase in stall speed	Major
	Loss of retraction capability of high-lift system	Take-off, Climb out	- Reduction in climb performance - Reduced speed and range	Major
	Panel skew	Cruise, Landing	- Reduced aircraft performance - Increase in landing distance - Increase in stall speed	Major
	Multifunctional excessive asymmetry	All phases	- Loss of control	Catastrophic
(3) Position indication of the high-lift system	Loss of position indication	All phases	- Mission cancelation - Increase in landing distance - Increase in stall speed	Major
	Misleading position indication	Take-off, Landing	- Aircraft may approach stall regime without crew recognition	Hazardous

A.2 Design Structure Matrix and Multiple Domain Matrix

A MDM is based on the theory of the Design Structure Matrix (DSM), which was initially developed by Steward (1981) and advanced by Eppinger and Browning (2012). The DSM enables the modelling and analyzing of complex systems or processes. In general, the DSM is defined as a NxN matrix, where relations and interactions between the N elements of the system of the same domain are depicted, see Figure A.1a-b. An extension of the basic DSM is the Multiple Domain Matrix (MDM). The MDM includes several DSMs and corresponding Domain Mapping Matrices (DMM), which represent relations between elements of different domains, as illustrated in Figure A.1c.

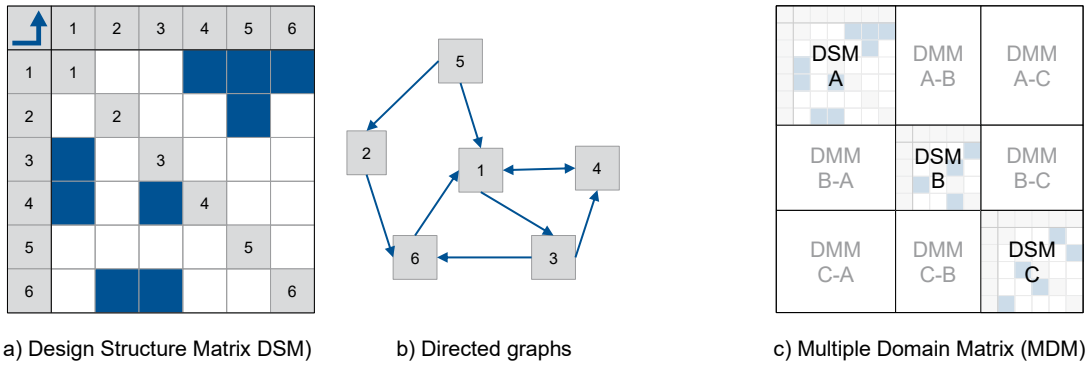

Figure A.1 Schematic of a Design Structure Matrix (DSM) (left) with derived directed graphs (middle) and a Multiple Domain Matrix (MDM) (right) (Lampl *et al.*, 2017c, p. 7).

For example, the following Figure A.2 and Figure A.3 show MDMs results of a concept aircraft at aircraft and system level (cf. *5 Case Study*).

MDM at Aircraft Level

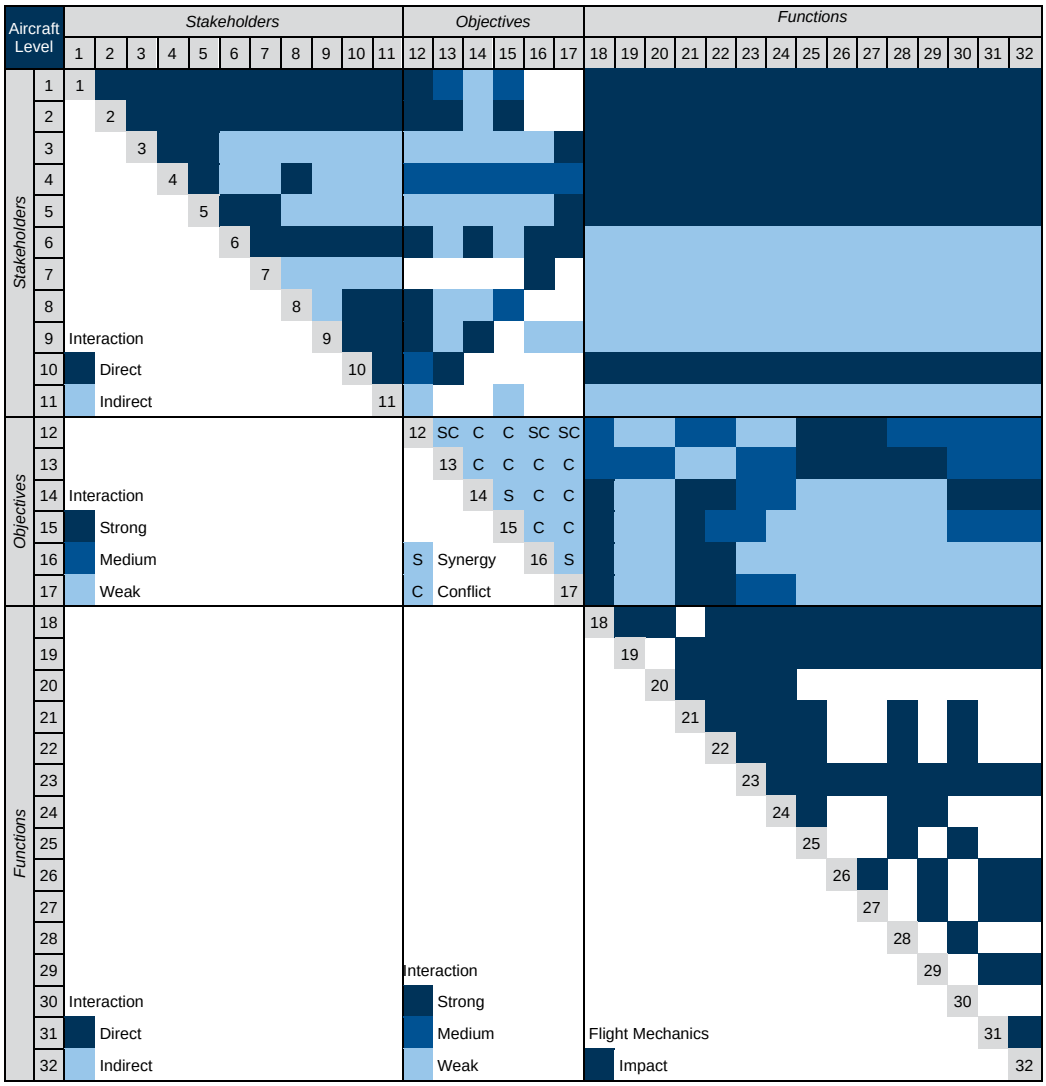

Stakeholder

1 Agencies (e.g. EASA, FAA)
2 Standards and Regulations
3 Suppliers
4 Research Institutes
5 Aircraft Manufacturer
6 Airlines and aircraft operator
7 MRO service provider
8 Air Traffic Management
9 Passengers
10 Flight Crew
11 Airport

Objectives

12 Safety
13 Handling Qualities
14 Direct Operating Costs
15 Environmental impact
16 Direct Maintenance Costs
17 System Cost

Functions

18 High-lift control
19 Airbrake
20 Lift dump
21 Cruise Variable Camber
22 Differential Flap Setting
23 Active Flow Control (Flap)
24 Active Load Control
25 Pitch Control
26 Roll Control
27 Yaw Control
28 Longitudinal stability control
29 Lateral/Directional stability control
30 Trim control around lateral axis
31 Trim control around longitudinal axis
32 Trim control around vertical axis

Figure A.2 Multifunctional Domain Matrix results (MDM) of the concept aircraft at aircraft level.

MDM at System Level

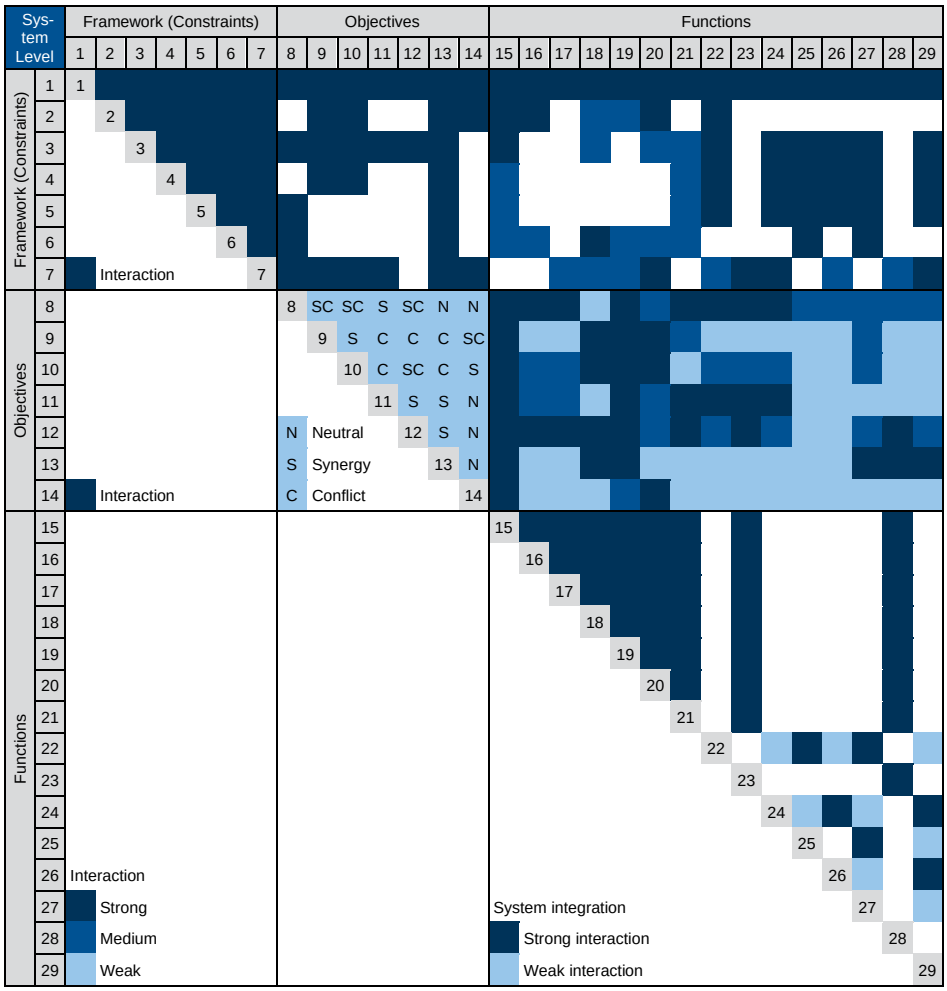

Framework (Constraints)

1 Wing design
2 Landing gear
3 Empennage
4 Fuselage
5 Center of Gravity
6 Neutral Point
7 Engines

Objectives

8 Safety (system)
9 Complexity (system)
10 Weight
11 Redundancy and Reconfiguration
12 Multifunctionality
13 Adaptiveness
14 Power requirements

Functions

15 High-lift control
16 Airbrake
17 Lift dump
18 Cruise Variable Camber
19 Differential Flap Setting
20 Active Flow Control (Flap)
21 Active Load Control
22 Pitch Control
23 Roll Control
24 Yaw Control
25 Longitudinal stability control
26 Lateral/Directional stability control
27 Trim control around lateral axis
28 Trim control around longitudinal axis
29 Trim control around vertical axis

Figure A.3 Multifunctional Domain Matrix (MDM) results of the concept aircraft at system level.

A.3 Flight Control Function Catalogue (Examples)

For the innovative and creative part of the methodology – the functional-driven design approach – it is recommended to set up a general flight control functions "catalogue" with the main requirements, classifications, constraints and potential use of new technologies or system concepts. To get an idea of such a catalogue, the flight control functions Roll Control (RLC) and High-Lift Control (HLC) are exemplary presented, see Table A.4 and Table A.5. Further examples of typical flight control functions are Active Load Control (ALC), Air Brake (ABK), or Lift Dump (LDP). Examples of additional flight control functions such as Differential Flap Setting (DFS) and Cruise Variable Camber (CVC) are shown in Table A.6 and Table A.7.

Table A.4 Roll control function within the function catalogue.

Flight Control Function	Roll Control (RLC)
Aircraft Level	
Requirements, Specifications	EASA CS 25.147, Flight critical, Handling Qualities: Control of the bank angle
Model, Objectives	Roll moment/rate is a function of: Surface deflection angle, deflection speed, surface area, surface lever-arm (with respect to the longitudinal axis), air speed, wing configuration
Parameter	Roll moment, Roll rate, Bank angle
Interactions	Yaw control, lateral stability, directional trim
System Level	
Conventional Configuration	Outboard wing: aileron(s), Inboard wing (thrust gate): High-speed Aileron (optional), Supportive: Spoiler
Integration, Constraints	Wing design (span, elasticity, space, rear spar, airfoil…), Winglets, high-lift system (trailing-edge), engine configuration
Redundancy, Reconfiguration	Different control surfaces (redundancy), segmented ailerons and spoilers, redundant actuators, power supply, flight control computers
Advanced Technologies	Flexible (morphing) wing, active flow control, tailerons, electric actuators
Device Level	
Control Devices	Ailerons, spoilers, flaperons, tailerons, fluidic actuators…
Deflection and Motion	Deflections up/down (ailerons), Asymmetric Deflection up (spoilers), Jet (fluidic actuators)
Aerodynamics, Aeromechanics	Control device effectiveness, aileron reversal, flow detachment
Multifunctionality	Active Load Control (maneuver, gust), support high-lift control, air brake, lift dump

Table A.5 High-lift control (HLC) function definition in the flight control function catalogue.

Flight Control Function	High-Lift Control (HLC)
Aircraft Level	
Requirements, Specifications	EASA CS-25: 25.105, 25.107, 25.109, 25.111, 25.113, 25.115, 25.117, 25.119, 25.121, 25.125, 25.701, Handling Qualities
Model, Objectives	Enable low speed phases for safe start and landing, steep climb-out, steep approach, minimum weight (low complexity), minimize start and landing distances
Parameter	Lift Coefficient, Drag Coefficient, Lift over Drag, Lift-off speed, touchdown speed, climb rate, angle of attack,
Interactions	Flight control, stability, trim
System Level	
Conventional Configuration	Leading-edge and trailing-edge control devices (slats/flaps), different positions (discrete)
Integration, Constraints	Wing design (span, elasticity, space, airfoil, wing sweep), winglets, front/rear spar (hinge line), ailerons, engines, landing gear, MTOM
Redundancy, Reconfiguration	Segmented high-lift control devices (inboard/outboard), redundant actuation and flight control computers, electronic rigging
Advanced Technologies	Flexible (morphing) structures, active flow control, distributed electric drive architecture
Device Level	
Control Devices	Leading-edge devices (Krueger-Flap, Slat, Droop nose) and trailing-edge devices (single-slotted flap, double slotted flap, fowler flap)
Deflection and Motion	Different kinematics: dropped hinge, linkage, track, fowler motion: translation, rotation
Aerodynamics, Aeromechanics	Pressure distribution (airfoil, wing), reduction of suction peaks, delay of flow detachment at the outer wing (to keep ailerons effective), boundary layer control
Multifunctionality	Cruise variable camber, differential flap setting (load alleviation)

Table A.6 Cruise Variable Camber (CVC) definition in the flight control function catalogue.

Flight Control Function	Cruise Variable Camber (CVC)
Aircraft Level	
Requirements, Specifications	EASA → CS 25.701
Model, Objectives	Increase the efficiency during cruise (drag reduction)
Parameter	Lift over drag, Drag, Wing camber
Interactions	Longitudinal Trim
System Level	
Configuration	Adjust the wing camber using the trailing-edge flaps and the spoilers (gap control)
Integration, Constraints	Wing design, high-lift control system design (actuation system architecture), spoiler design, simplified kinematics
Redundancy, Reconfiguration	Segmented high-lift control devices (inboard/outboard), redundant actuation and flight control computers, electronic rigging
Advanced Technologies	Flexible structures, shock bump device
Device Level	
Control Devices	Trailing-edge high-lift devices (flaps), spoiler
Deflection and Motion	Small deflections up/down (flaps), gap control (spoiler)
Aerodynamics, Aeromechanics	Drag, wave drag
Multifunctionality	High-lift control, active load control, differential flap setting

Table A.7 Differential Flap Setting (DFS) definition in the flight control function catalogue.

Flight Control Function	Differential Flap Setting (DFS)
Aircraft Level	
Requirements, Specifications	EASA → CS 25.701
Model, Objectives	Increase the efficiency during cruise (drag reduction)
Parameter	Lift over drag, Drag, Wing camber
Interactions	Longitudinal Trim
System Level	
Configuration	Adjust the wing camber using the trailing-edge flaps and the spoilers (gap control)
Integration, Constraints	Wing design, high-lift control system design (actuation system architecture), spoiler design, simplified kinematics
Redundancy, Reconfiguration	Segmented high-lift control devices (inboard/outboard), redundant actuation and flight control computers, electronic rigging
Advanced Technologies	Flexible structures, shock bump device
Device Level	
Control Devices	Trailing-edge high-lift devices (flaps), spoiler
Deflection and Motion	Small deflections up/down (flaps), gap control (spoiler)
Aerodynamics, Aeromechanics	Drag, wave drag
Multifunctionality	High-lift control, active load control, differential flap setting

A.4 Baseline Aircraft and Mission Models

Baseline Aircraft Models

Table A.8 provides the main parameters of the MR and LR baseline aircraft. The corresponding and conventional FCS configurations are shown in Figure A.4.

Table A.8 Main parameters of the medium-range (MR) and long-range (LR) baseline aircraft.

Parameter	MR	LR	Unit	Comment
General				
Crew	2/4	2/10	–	
Capacity	189/184/162	550/442/370	–	*1-class / 2-class / 3-class*
Length	38.5	73.8	m	
Height	12.2	17.8	m	
Fuselage Outer Diameter	3.9	6.1	m	
Mass and Fuel				
MTOM	76390	329770	kg	
MLM	65220	242150	kg	
OEM	42120	142665	kg	
Max. Fuel Capacity	25402	168642	ltr	
Wing				*See Figure A.4*
Span	34.8	63.9	m	
Area (ref.)	124	440	m	
Sweep	25	33	°	*At 25% chord line*
Aspect ratio	9.6	8.8	–	
Wetted area ratio	5.5	5.5	–	*Standard for transport aircraft*
Engine				
Number	2	2	–	
Type	Turbofan	Turbofan	–	
Rated Thrust	130	484	kN	
Bypass Ratio	6	7.1	–	
Overall Pressure Ratio	32	42	–	

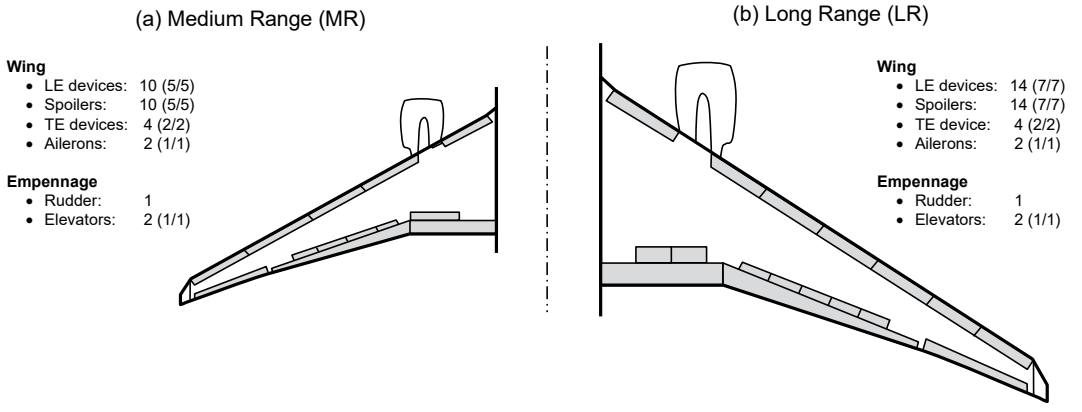

Figure A.4 Wing flight control configurations of the MR (left) and LR (right) baseline aircraft.

Baseline Mission Models

This section provides an overview and further details of the baseline mission model for the MR and LR baseline aircraft. The parameterized models should serve as basis to develop several missions for different transport aircraft models.

Table A.9 Mission altitude and speed data for the medium-range (MR) and long-range (LR) baseline aircraft (Lampl *et al.*, 2017b).

Flight Phase	Altitude, ft	Speed, kt, -			Climb Rate, ft/min	
Segment	MR/LR	MR	LR	CAS/TAS	MR	LR
Taxi-out						
Taxi	0	15	15	CAS	0	0
Take-off						
Acceleration	0	→ 153	→ 162	CAS	0	0
Lift-Off	0	153	162	CAS	2750	3000
Climb						
Initial Climb	→ 4000	183	192	CAS	2750	3000
Climb 1	→ 15000	→ 290	→ 300	CAS	2000	2400
Climb 2	→ 24000	↓	↓		1700	1800
Climb 3	→ TOC				1250	1450
Cruise						
Cruise Flight	→ TOD	0,81	0,84	Ma	0	0
Descent						
Descent 1	→ 30000	0,81	0,84	Ma	−2400	−2500
Descent 2	→ 10000	300	300	CAS	↓	↓
Descent 3	→ 4000	240	250	CAS		
Approach						
Initial Approach	→ 2500	240	250	CAS		
Final Approach	→ 1000	160	185	CAS		
Landing						
Threshold Crossing	100	140	165	CAS	↓	↓
Touchdown	→ 0	137	153	CAS	0	0
Deceleration	0	→ 15	→ 15	CAS	0	0
Taxi-in	0				0	0
Taxi	0	15	15	CAS	0	0

Take-off, Initial Climb and Climb

- Acceleration and lift-off with defined climb rate; Initial Climb to 4000 ft
- Climb 1-3 with different climb rates until reaching top of climb (TOC)

Descent, Approach and Landing

- Descent begins with top of descent (TOD); Assumption: constant flight path angle of 3°.
- Initial Approach Fix (IAF) at 4000 ft and Final Approach Fix (FAF) at 1000 ft
- Landing starts with the threshold crossing at 100 ft; touchdown at defined speed

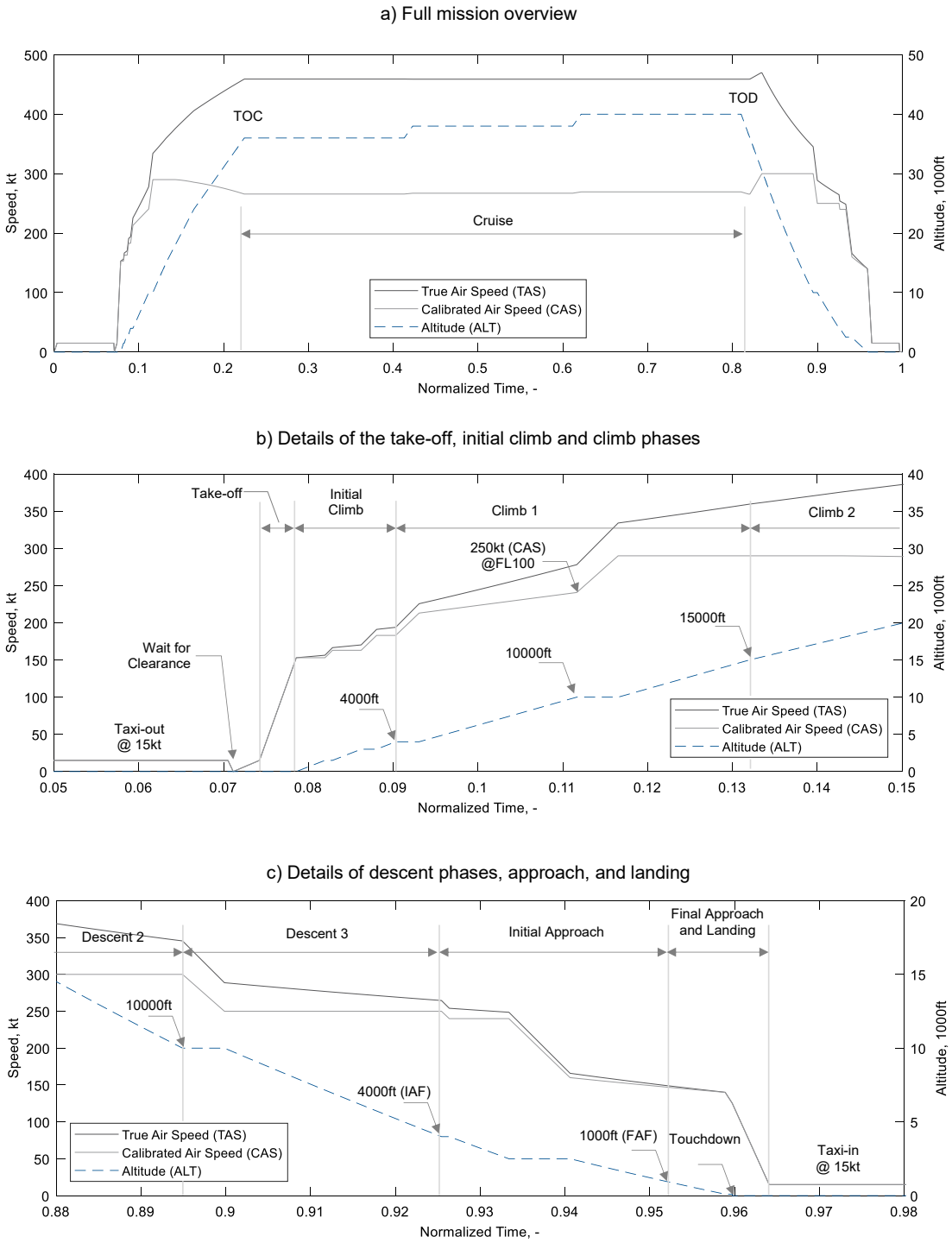

Figure A.5 Exemplary results and details of a typical flight mission of a commercial transport aircraft.

A.5 Aircraft System Models

This section provides further details and additional equations, which are required for the modelling of the aircraft systems (cf. *4.3 Aircraft System Models*).

Environmental Control System

The heat loads can be divided in heat dissipation by passengers and crew $\dot{Q}_{met}$ (*metabolism*), solar heating by the sun $\dot{Q}_{sun}$ and the heat loads by several electrical systems $\dot{Q}_{sys}$. The heat transfer between cabin and environment is considered by the conductional heat flow $\dot{Q}_{con}$. An overview of the different heat flow rates and corresponding equations are given in Table A.10.

Table A.10 Heat flow rate calculations of the Environmental Control System (ECS).

Heat flow	Equations	Notes
Metabolism	$\dot{Q}_{met} = \dot{Q}_{PAX} \cdot n_{PAX} + \dot{Q}_{crew} \cdot n_{crew}$	n_{PAX} Number of passengers n_{PAX} Number of crew members
Systems	$\dot{Q}_{sys} = \dot{Q}_{galleys} + \dot{Q}_{IFE} + \dot{Q}_{lights}$	
Sun (solar)	$\dot{Q}_{sun} = \dot{q}_{sun} \cdot A_{window} \cdot n_{window} \cdot f_{area}$	$\dot{q}_{sun} = 1367\ \frac{W}{m^2}$, Solar radiation f_{area} Window area factor
Conduction	$\dot{Q}_{con} = \frac{1}{R_{th}} \cdot (T_{skin} - T_{cabin})$	R_{th} Thermal resistance of the fuselage.

Metabolism. According to Specht (2005), the heat load due to metabolism mainly depends on the heaviness of work and the size of the body surface. Figure A.6 shows the typical heat dissipation of a human with a nominal size of 75 kg in dependence of the ambient air temperature and the heaviness of work. The vertical line shows the typical cabin air temperature of 24 °C (297.15 K). The values selected for the crew and passengers of the baseline aircraft are given in Table A.11.

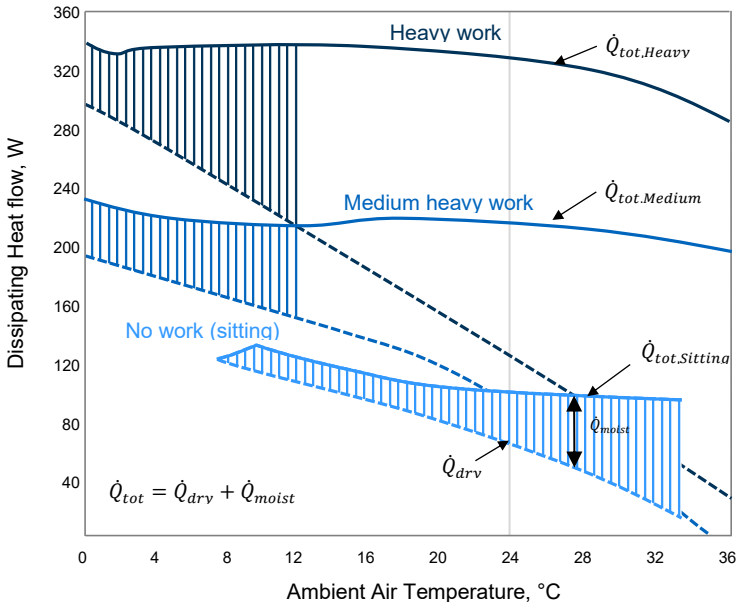

Figure A.6 Typical heat dissipation of a human (75 kg) sitting quietly (no work), working medium heavy and working heavy (Specht, 2005, p. 4).

Table A.11 Selected cabin heat load values due to metabolism of the baseline aircraft.

Heat Loads (Cabin)	Default Values	Notes
Metabolism		Values from Figure A.6
Passenger	$\dot{Q}_{PAX} = 70\ W/occ$	@ 24°C, no work (sitting), low moisture
Flight Crew	$\dot{Q}_{flight\_crew} = 100\ W/occ$	@ 24°C, medium heavy work, low moisture
Cabin Crew	$\dot{Q}_{cabin:crew} = 200\ W/occ$	@ 24°C, medium heavy work, medium moisture

Systems. Typical types of electrical cabin system which also contribute to the overall heat loads are the In-Flight Entertainment (IFE), the galleys and the cabin lights. Both, the IFE and cabin lights are assumed to be activated (switched on) during all phases of the flight mission. In contrast, the galleys are only activated during climb and cruise phases. The defined values for the baseline aircraft are listed in Table A.12.

Table A.12 Typical types and values of cabin system heat loads

Heat Loads (Cabin)	Default Values	Notes
Systems		All values: W per occurrence (number of passengers)
In-flight entertainment	$\dot{Q}_{IFE} = 27\ W/occ$	
Galleys	$\dot{Q}_{galleys} = 230\ W/occ$	
Cabin Lights	$\dot{Q}_{lighting} = 20\ W/occ$	

Ice Protection System

Based on the semi-empirical method of Sherif *et al.* (1997) the local heat transfer and ice accretion on the leading edge of an airfoil can be described by heat flux densities shown in Figure A.7.

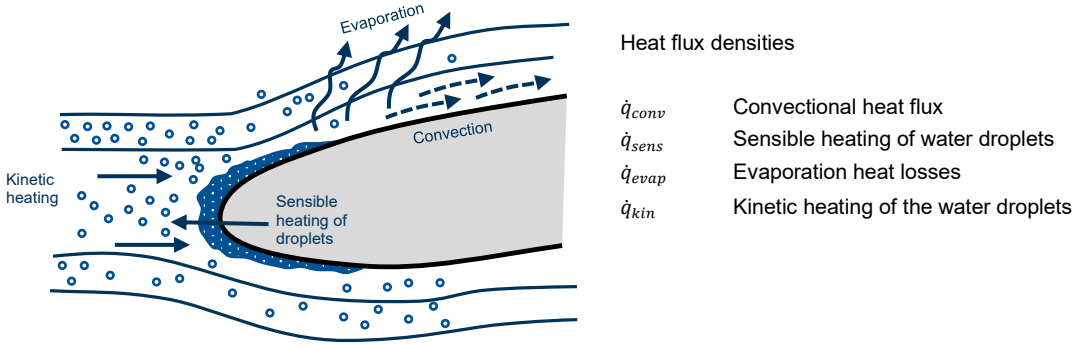

Figure A.7 Semi-empirical method for local heat transfer and ice accretion on the leading edge of an airfoil (Sherif *et al.*, 1997, p. 167).

Convection. Convection describes the cooling of the surface by the air flow around a surface. To calculate the convective heat flux density the temperature difference between the necessary surface temperature T_{surf} and the adiabatic wall temperature T_{aw} is required, in addition to the heat transfer coefficient h_{surf}, see Equation (A.1).

$$\dot{q}_{conv} = h_{surf} \cdot (T_{surf} - T_{aw}) \tag{A.1}$$

The local heat transfer coefficient of the surface depends on the Nusselt number Nu, which describes the ratio of convective to conductive heat transfer across the surface boundary, see Equations (A.2) and (A.3).

$$h_{surf} = Nu \frac{\lambda}{l_{ref}} \tag{A.2}$$

$$Nu = 0.0296 \cdot Re^{\frac{4}{5}} \cdot Pr^{\frac{1}{3}} \tag{A.3}$$

Where λ is the thermal conductivity of air and the l_{ref} characteristic length of the surface to protect. Furthermore, the Nusselt number Nu is a function of the Reynolds number Re and the Prandtl number Pr, which are calculated with Equations (A.4) and (A.5), respectively.

$$Re = \frac{\rho_\infty \cdot V_{TAS} \cdot l_{ref}}{\mu} \tag{A.4}$$

$$Pr = \frac{c_p \cdot \mu}{\lambda} \tag{A.5}$$

Where ρ_∞ is the air density, V_{TAS} the aircraft true air speed, μ the dynamic viscosity of air, and c_p is the specific heat capacity of air.

The adiabatic wall temperature is calculated with Equation (A.6), where T_∞ is the ambient temperature, κ is the adiabatic index of air and Ma the Mach number. f_{rec} is the temperature recovery factor and can be calculated with Equation (A.7) (Chakraborty, 2015, p. 141).

$$T_{aw} = T_\infty \cdot (1 + f_{rec} \frac{\kappa - 1}{2} Ma^2) \tag{A.6}$$

$$f_{rec} = 1 - 0.99 \cdot (1 - Pr^{0.5}) \tag{A.7}$$

Sensible Heating. The sensible heating represents the required heat flux density to heat the impinging water droplets which must be heated up to the desired surface temperature (Meier and Scholz, 2010). The sensible heat flux $\dot{q}_{sens}$ is calculated with Equation (A.8),

$$\dot{q}_{sens} = \dot{m}_{local} \cdot \{(T_{surf} - T_{aw}) \cdot [(1 - n) \cdot c_w + n \cdot c_i] + n \cdot L_f\} \tag{A.8}$$

where $\dot{m}_{local}$ is the local liquid water mass flow per unit area, n the so called freezing fraction of liquid water turning into ice, c_w and c_i are the specific heat coefficients of water and ice, and L_f is the required latent heat, as the ice must first become liquid. The freezing fraction n is calculated with Equation (A.9), where T_{ref} is the freezing point of water (273.15 K). The resulting local liquid water mass flow is $\dot{m}_{local}$ is calculated with Equation (A.10), and strongly depends on the local water content (ρ_{LWC}) and the water catch efficiency E_m.

$$n = \frac{c_w}{L_f} \cdot \left(T_{ref} - T_\infty\right) \tag{A.9}$$

$$\dot{m}_{local} = V_{TAS} \cdot \rho_{LWC} \cdot E_m \tag{A.10}$$

The *liquid water content* ρ_{LWC} is dependent on following parameters (Jeck, 2002): Droplet median volume diameter, ambient temperature, horizontal extent (intermittent or continuous). Therefore, the published data from the FAA of the distance-based format of the icing design envelope (Jeck, 2002) are integrated as a look-up table into the IPS model, to determine the liquid water content coefficient. The *water catch efficiency* E_m considers the fact that not all water droplets impinge the surface and is a function of aircraft speed, water droplet size and the surface geometry. An approximation of E_m, based on data from the standard AIR 1168/4, is given by Equation (A.11) (Meier and Scholz, 2010, p. 4). This approximation is true for a median droplet diameter of 20 µm and an altitude of 10000 ft; for other altitudes from 0-20000 ft the error is less than 10%.

$$E_m = 0.00324 \cdot \left(\frac{V_{TAS}}{t}\right)^{0.613} \tag{A.11}$$

Evaporation. The heat losses due to evaporation at wing or engine cowling are considered with Equation (A.12). For both IPS system architectures, pneumatic or electrical, it is assumed that the impinging water droplets completely evaporate. The latent heat for water evaporation is $L_e = 2257\ \frac{kJ}{kg}$. The corresponding mass flow $\dot{m}_{evap}$ is calculated in Equation (A.13), where RH is the relative humidity of the air, and $e_{w,\infty}$ and $e_{w,surf}$ are the saturation vapor pressures. To calculate the saturation vapor pressure dependent on the temperature T (in °C), the approximation of Alduchov and Eskridge (1996, p. 608) is used, see Equation (A.14).

$$\dot{q}_{evap} = \dot{m}_{evap} \cdot L_e \tag{A.12}$$

$$\dot{m}_{evap} = 0.7 \cdot h_{surf} \cdot \frac{RH \cdot e_{w,\infty} - e_{w,surf}}{\rho_\infty \cdot c_p} \tag{A.13}$$

$$e_w(T) = 6.1094 \cdot e^{\frac{17.265 \cdot T}{243.04 + T}} \tag{A.14}$$

Kinetic Heating. The last heat flux density considered is the kinetic heating of the accelerated and impinging water droplets, see Equation (A.15). The local liquid water mass flow is calculated the same as for the sensible heating (cf. Equation (A.10)).

$$\dot{q}_{kin} = \dot{m}_{local} \cdot \frac{V_{TAS}^2}{2} \tag{A.15}$$

Additional Validation Results of ATAX

This section shows additional results of the Long-Range (LR) baseline aircraft to validate the system models and the implemented tool (cf. section 4.6). Figure A.8 and Figure A.9 show the results of the secondary power requirements of the conventional and more-electric baseline aircraft. The results of the thrust, Specific Fuel Consumption (SFC), and fuel flow during are shown in Figure A.10, Figure A.11 and Figure A.12

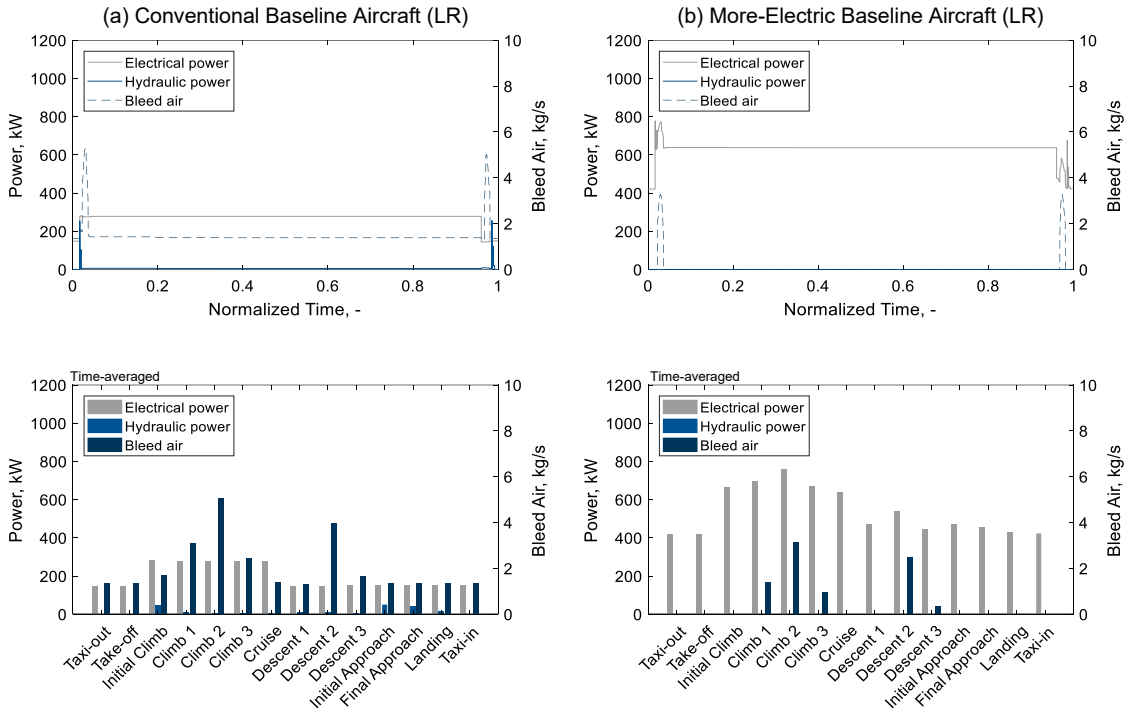

Figure A.8 Secondary power requirements of the conventional (left) and more-electric (right) long-range baseline aircraft.

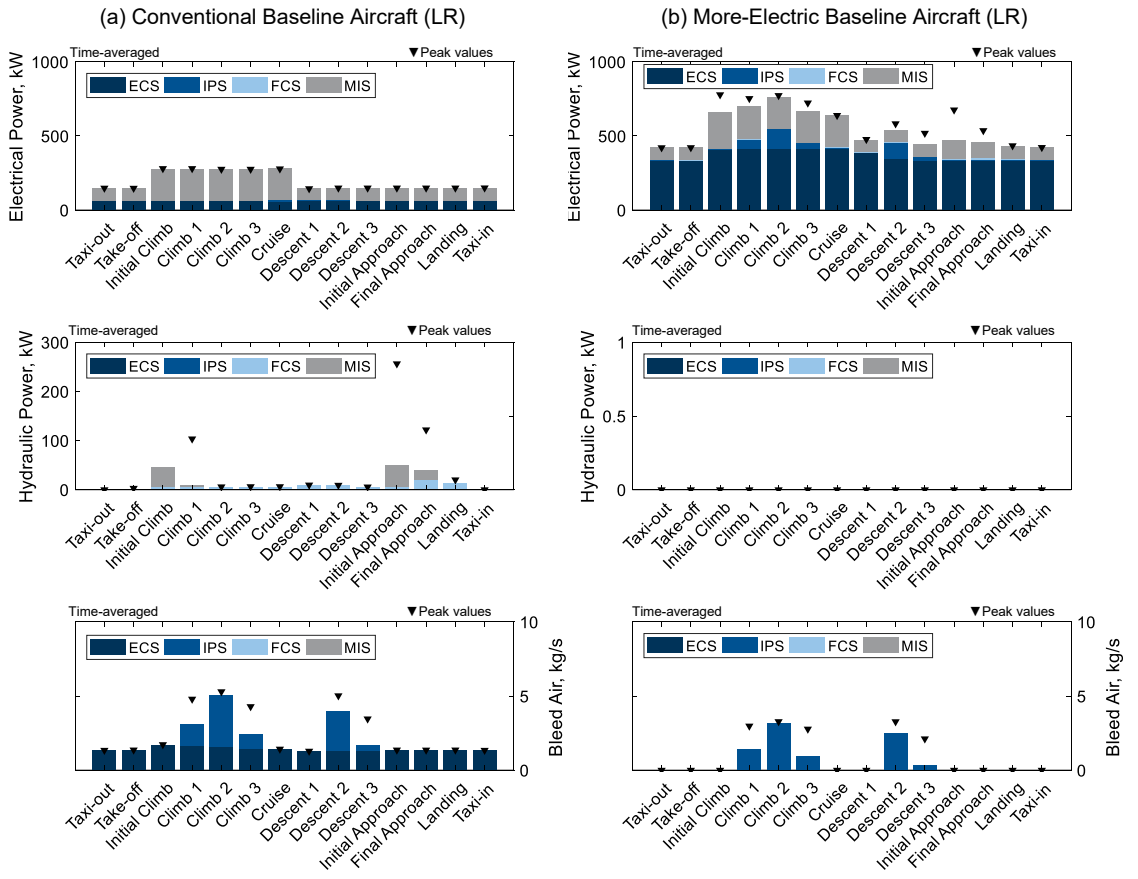

Figure A.9 Details of the secondary power requirements of the conventional (left) and more-electric (right) long-range baseline aircraft.

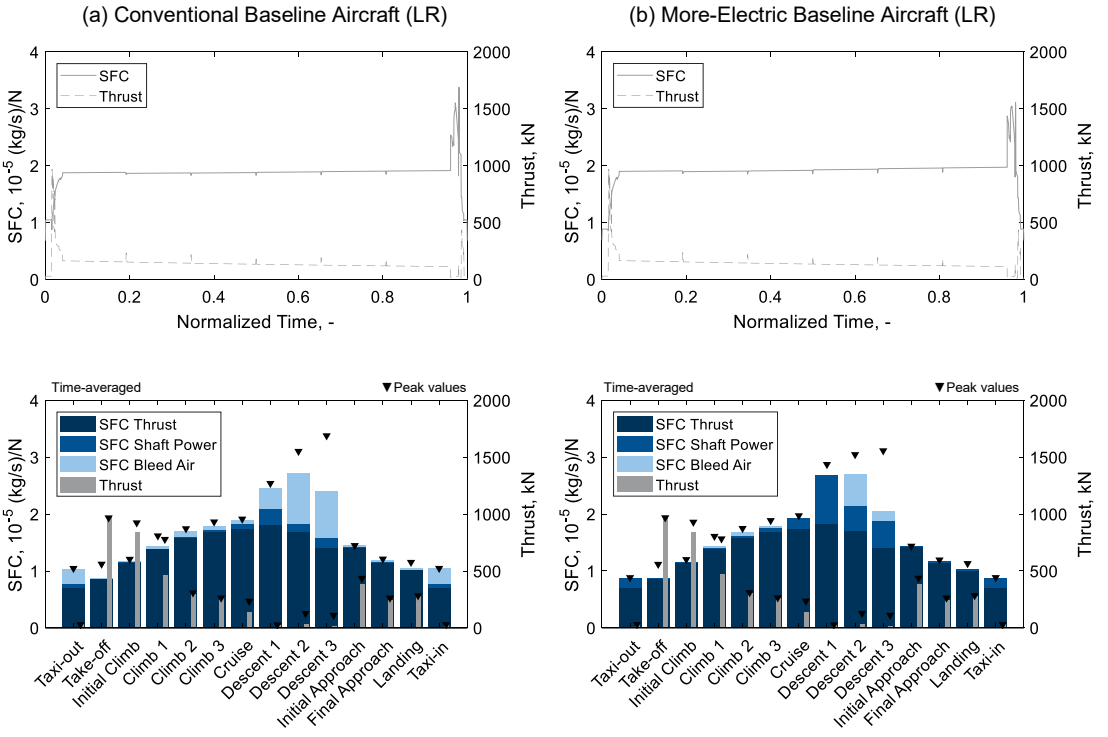

Figure A.10 Specific Fuel Consumption (SFC) of the conventional (left) and more-electric (right) long-range baseline aircraft.

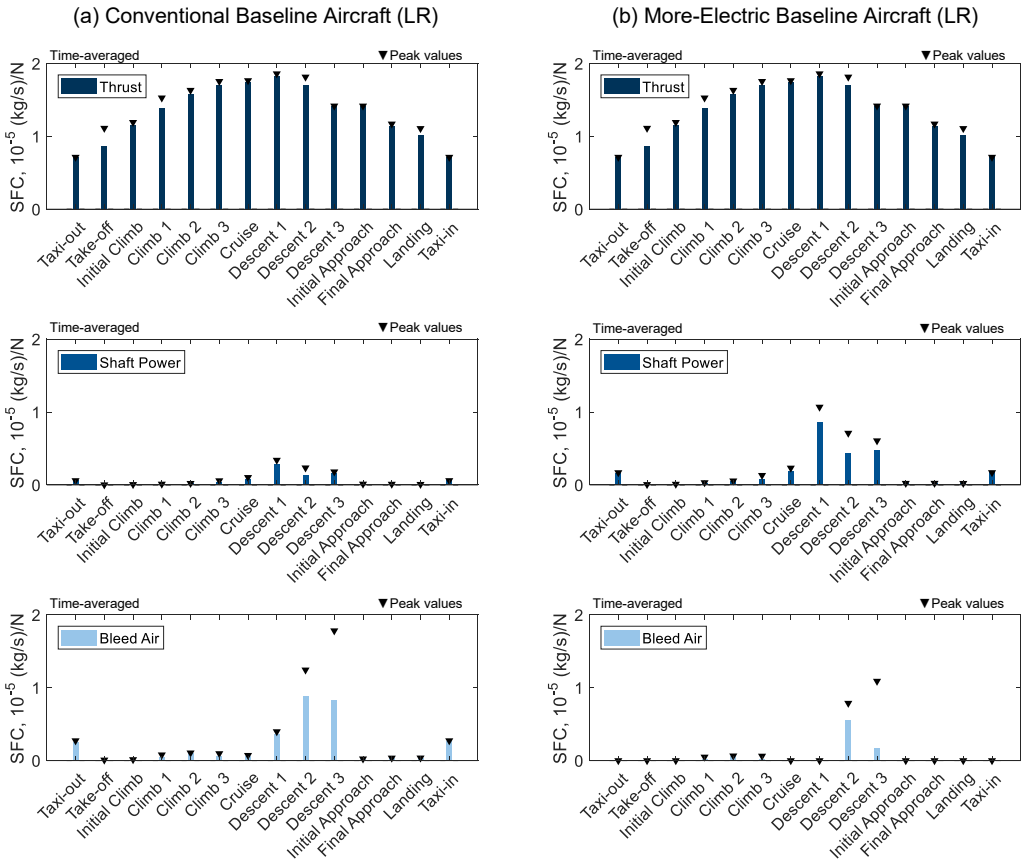

Figure A.11 Details of the Specific Fuel Consumption (SFC) due to thrust, shaft power offtakes and bleed-air of the conventional (left) and more-electric (right) long-range baseline aircraft.

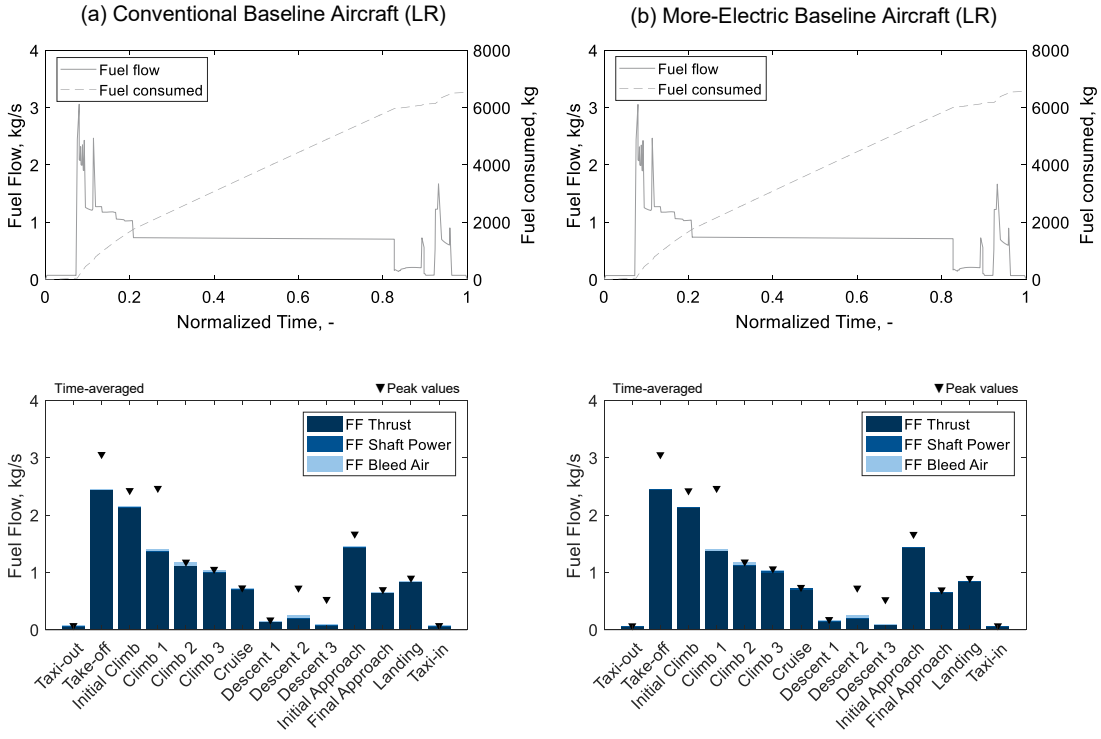

Figure A.12 Overall fuel flow and fuel consumption of the conventional (left) and more-electric (right) long-range baseline aircraft.

A.6 Data Model Structures and User Interfaces

The following section provides further details on the data model structures within the Aerodynamic Vortex Lattice Calculation and Analysis Tool (AVLX) and the Aircraft System Technology Analysis Tool (ATAX). The software environment used to develop and implement the tools for this work is MATLAB® in the version R2017a. It shall be noted, that for testing purposes, the properties of the medium range and long-range baseline aircraft can be loaded within the *Properties Windows* of ATAX and AVLX. The data are included in both tools by default. To load the baseline file, select *File* > *Load Baseline…* in the menu bar, or simply press *Ctrl+b.*

AVLX Data Structure

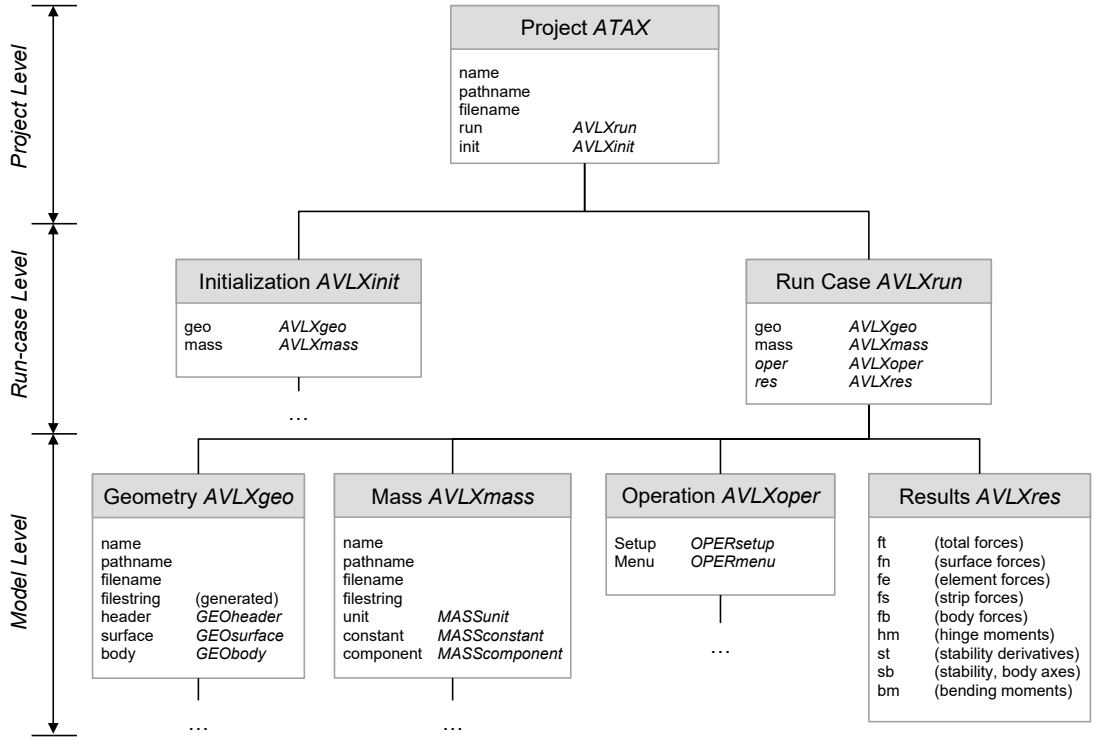

Figure A.13 Data model structure of the Aerodynamic Vortex Lattice Calculation and Analysis Tool (AVLX).

Figure A.14 and Figure A.15 show the main windows to define the geometry properties within AVLX. In the geometry property window, the user can select between the tab-pages *General, Surfaces, Bodies*, and *File.* With the first three tab-pages, the required geometry properties are defined, whereas the File tab shows the generated AVL file (this happens in the background). With a click on the *Initialize Geometry* button, the geometry is initialized and appears in the geometry list of the main window of AVLX (cf. Figure 3.11).

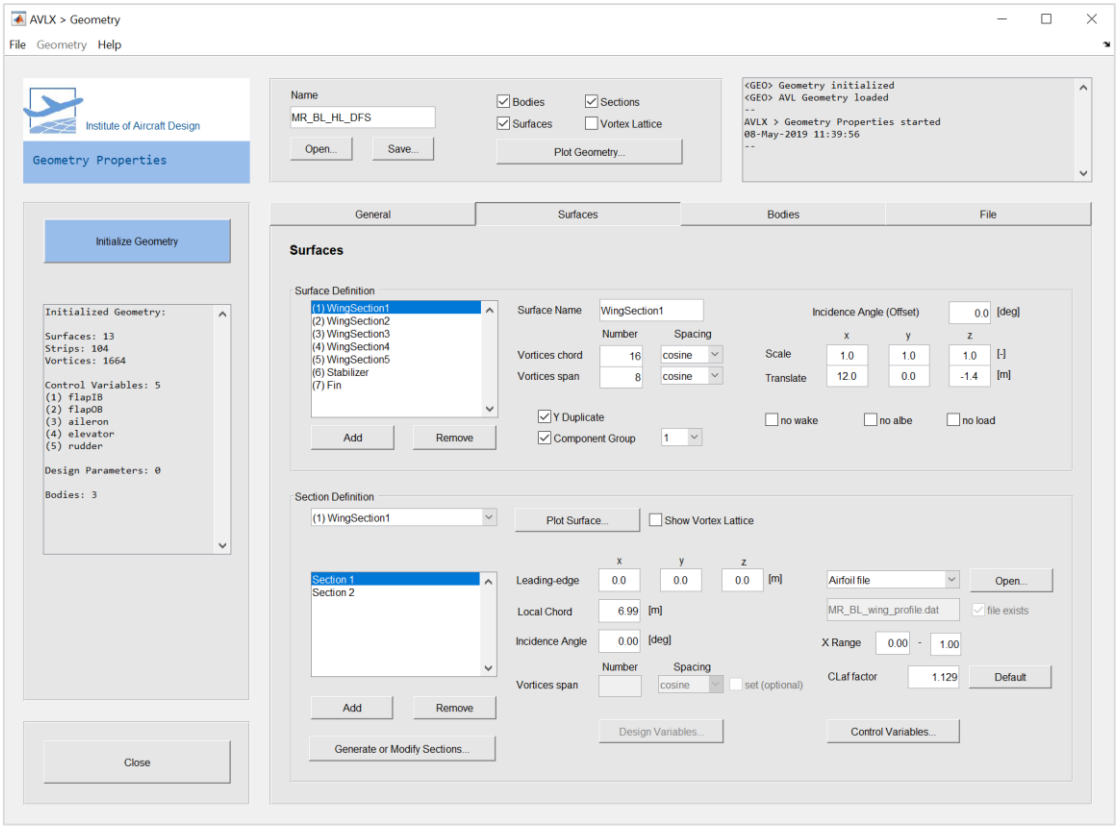

Figure A.14 Geometry properties window of the Aerodynamic Vortex Lattice Calculation and Analysis Tool (AVLX).

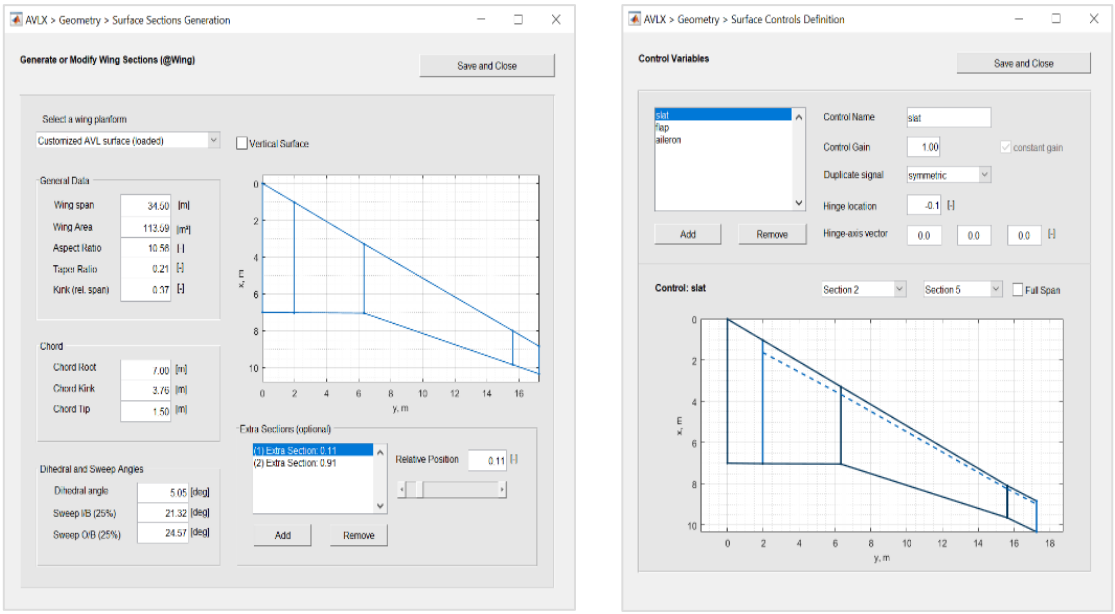

Figure A.15 Surface and section generation window (left) and the surface control definition (right) window of the Aerodynamic Vortex Lattice Calculation and Analysis Tool (AVLX).

ATAX Data Model Structure

Figure A.16 shows the top-level overview and basic principle of the ATAX data structure. At the top, there is the *ATAX* object at project level, which defines a project within the tool. Besides the general properties (e.g. name, description, filename), *ATAX* includes four additional objects at run-case level: *ATAXrun, ATAXinit, ATAXstudy, ATAXset*. At model level, the main objects define the aircraft model (*AC*), systems model (*SYS*), mission model (*MSN*). In addition, the results (*RES*) and the tool settings (*ATAXset*) are saved at this level.

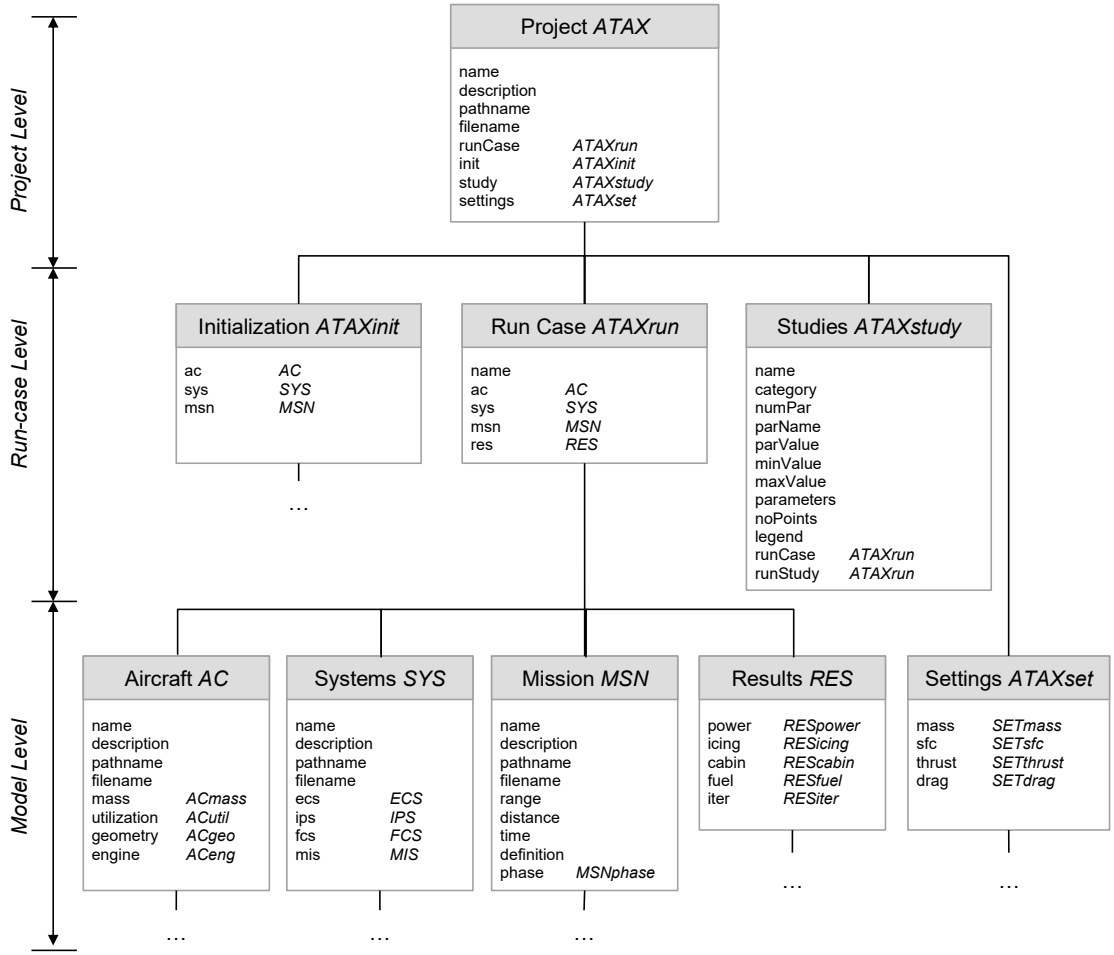

Figure A.16 Overview of the data model structure of the Aircraft System Technology Analysis Tool (ATAX).

In the following, further details of the data-model structure at model level, which are primarily relevant for the run-case definition, are presented. Figure A.17 shows the data structure of the mission model. The mission is primarily defined by the range and flight phases *(MSNphase*). The phase object is defined by the properties, time, distance and step (*MSNstep*). The step object contains all relevant data, such as speed and ISA conditions. The data model of the aircraft is illustrated in Figure A.18. It is further subdivided into the categories geometry (*ACgeo*), mass (*ACmass*), utilization (*ACutil*), and Engine (*ACeng*).

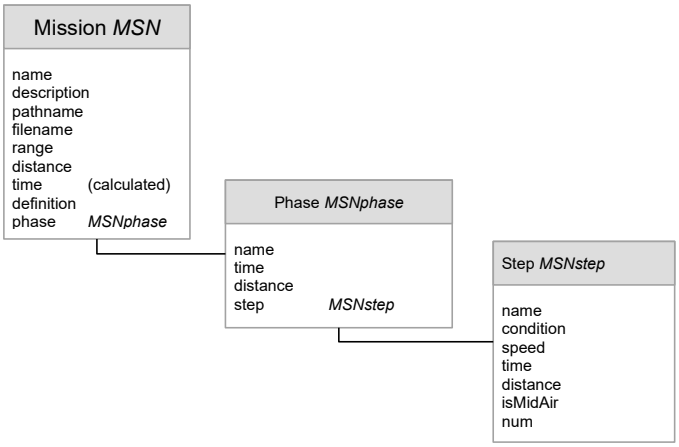

Figure A.17 Mission data model structure of the Aircraft System Technology Analysis Tool (ATAX).

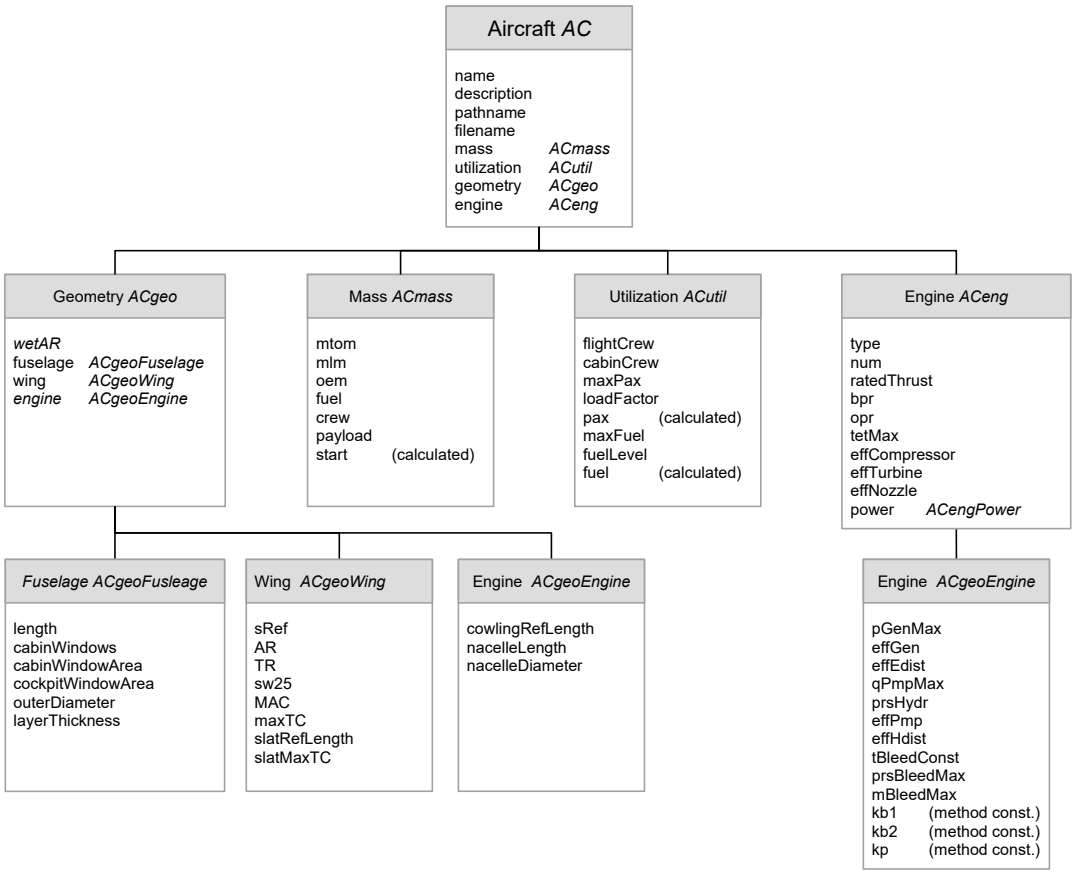

Figure A.18 Aircraft data model structure of the Aircraft System Technology Analysis Tool (ATAX).

The extensive data model structure of the systems is shown in Figure A.19. Since the focus in this work is on advanced FCS, the tree structure of the FCS is relatively complex, in comparison to the other systems. However, all required data should be available or can be determined by the presented overall methodology, even in early phases of aircraft design.

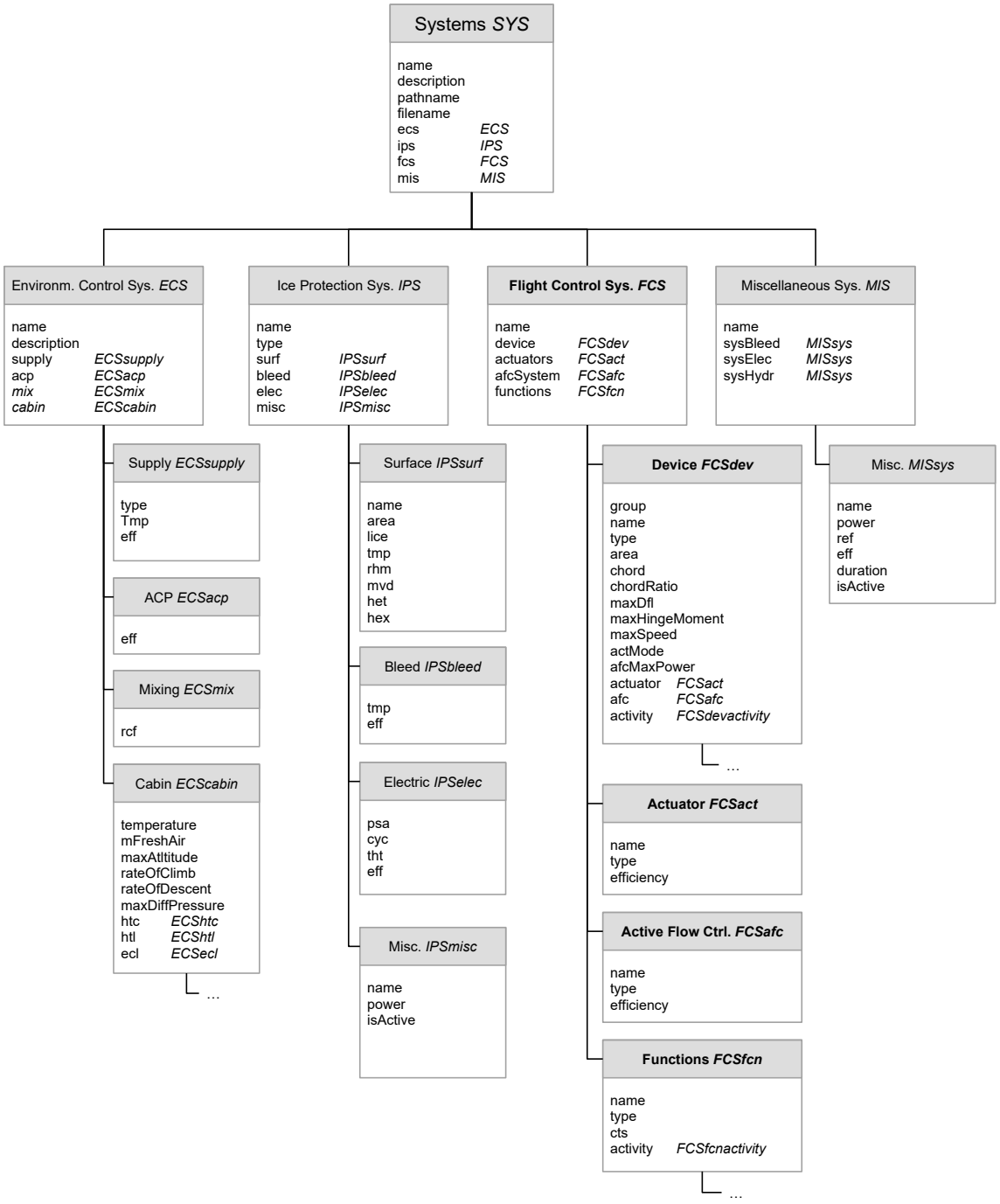

Figure A.19 Systems data model structure of the Aircraft System Technology Analysis Tool (ATAX).

Finally, single or multiple run case(s) can be defined by selecting the initialized mission, system and aircraft objects. If all required objects are arranged to a dedicated run case, the calculation procedure can start (cf. Figure 4.7). After the run-case calculation has finished, all relevant results are saved in the results object (*RES*), see Figure A.20. The results are further sub-divided into Power (*RESpower*), Fuel (*RESfuel*), Iteration (*RESiteration*), Icing (*RESicing*), and Cabin (*REScabin*).

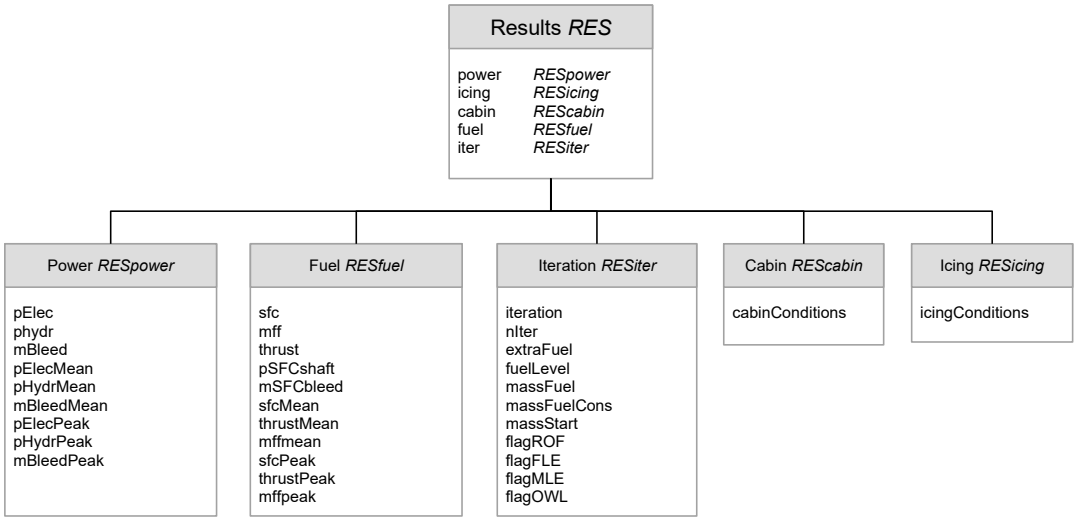

Figure A.20 Results data structure of the Aircraft System Technology Analysis Tool (ATAX).

Danksagung

Die vorliegende Arbeit entstand im Rahmen meiner Tätigkeit als wissenschaftlicher Mitarbeiter am Lehrstuhl für Luftfahrtsysteme an der Technischen Universität München. In dieser Zeit haben mich viele Personen begleitet, unterstützt und motiviert, denen ich sehr herzlich danken möchte.

Zuerst möchte ich mich bei meinem Doktorvater Prof. Dr.-Ing. Mirko Hornung bedanken. Für die Möglichkeit an seinem Lehrstuhl zu arbeiten, für die Unterstützung, die wertvollen Diskussionen und Gespräche, aber auch für den Freiraum und das geschenkte Vertrauen, um meine Ideen und Themen in dieser Zeit erfolgreich bearbeiten zu können. Mein besonderer Dank gilt auch Herrn Prof. Dr.-Ing. Frank Thielecke, der sich, ohne zu zögern bereit erklärt hat, die Rolle des Zweitgutachters und Prüfers bei meinem Promotionsvorhaben zu übernehmen. Außerdem möchte ich mich bei Herrn Prof. Dr.-Ing. Florian Holzapfel für die Übernahme des Prüfungsvorsitzes herzlichst bedanken.

An dieser Stelle möchte ich mich auch bei Herrn Dr.-Ing. Michael Meyer bedanken, der mich während meiner Diplomarbeitszeit bei Airbus Innovation Works in die interessante Welt der Luft- und Raumfahrtwissenschaften einführte und mich dadurch besonders zu meinem Promotionsvorhaben inspiriert hat.

Ein großer Dank gilt auch meinen Freunden, Kolleginnen und Kollegen am Lehrstuhl, die nicht nur für eine gute Arbeitsatmosphäre gesorgt haben, sondern mir auch jederzeit mit Rat und Tat zur Seite standen. Dabei möchte ich mich besonders bei Christoph, Anna, Jens, Felix, Korbinian, Lykos, Sebastian, Gilbert und Ekaterina bedanken. Ein herzlicher Dank gilt auch Frau Natalie Gulotta, die mich bei vielen organisatorischen und administrativen Tätigkeiten immer zuvorkommend unterstützt hat.

Danke auch an meine zahlreichen Studentinnen und Studenten, insbesondere an Timo Bunk, Mattia Graiff, Luca Litterst, Sandra Muschkorgel, Arul Sethuram, Daniel Sauterleute, Ralf Königsberger und Timo Wolf, die durch ihre Studien- und Abschlussarbeiten einen wertvollen Beitrag zu meiner Arbeit geleistet haben.

Der größte Dank gebührt meiner Familie: Ich danke meinen Eltern und meinen drei Brüdern, die immer an mich glauben und mich unterstützen; meiner wundervollen Frau Antonia, die immer für mich da ist und mich durch schwierige Phasen dieser Arbeit getragen hat, und meinen Kindern Emil, Luis und Paul, die mich zwar jeden Tag vor neue Herausforderungen stellen, mir aber auch immer wieder die schönsten Seiten des Lebens zeigen.

Wien, Dezember 2021

Publication List

The following list includes all technical paper and journal articles that were published during my time at the Institute of Aircraft Design at the Technical University of Munich.

Lampl, T., Sauterleute, D. and Hornung, M. (2017), "A Functional-Driven Design Approach for Advanced Flight Control Systems of Commercial Transport Aircraft", in Estorff, O. von and Thielecke, F. (Eds.), *Proceedings of the 6th International Workshop on Aircraft System Technologies: February 21-22, 2017, Hamburg, Germany*, *Berichte aus der Luft- und Raumfahrttechnik*, 1. Auflage, Shaker, Herzogenrath, pp. 3–12.

Lampl, T., Muschkorgel, S. and Hornung, M. (2017), "Parameterized Flight Mission for Secondary Power Requirement Estimations of Commercial Transport Aircraft", in *17th AIAA Aviation Technology, Integration, and Operations Conference, Denver, Colorado (USA), 5-9 June*, American Institute of Aeronautics and Astronautics (AIAA).

Lampl, T., Königsberger, R. and Hornung, M. (2017), "Design and Evaluation of Distributed Electric Drive Architectures for High-Lift Control Systems", in Deutsche Gesellschaft für Luft- und Raumfahrt (DGLR) (Ed.), *66. Deutsche Luft- und Raumfahrtkongress*, Munich, Germany.

Lampl, T., Wolf, T. and Hornung, M. (2017d), "Preliminary Design of Advanced Flight Control System Architectures for Commercial Transport Aircraft", in Council of European Aerospace Societies (CEAS) (Ed.), *6th CEAS Air & Space Conference*, Bucharest, Romania.

Lampl, T. and Hornung, M. (2018), "An Integrated Design Approach for Advanced Flight Control Systems with Multifunctional Flight Control Devices", in 18th AIAA Aviation Technology, Integration, and Operations Conference, Atlanta, Georgia (USA), 25-29 June 2018, American Institute of Aeronautics and Astronautics (AIAA).

Lampl, T., Wolf, T. and Hornung, M. (2019), "Preliminary design of advanced flight control system architectures for commercial transport aircraft", *CEAS Aeronautical Journal*, Vol. 10 No. 2, pp. 613–622.